

Regional Climate Projections

Coordinating Lead Authors:

Jens Hesselbjerg Christensen (Denmark), Bruce Hewitson (South Africa)

Lead Authors:

Aristita Busuioc (Romania), Anthony Chen (Jamaica), Xuejie Gao (China), Isaac Held (USA), Richard Jones (UK), Rupa Kumar Kolli (India), Won-Tae Kwon (Republic of Korea), René Laprise (Canada), Victor Magaña Rueda (Mexico), Linda Mearns (USA), Claudio Guillermo Menéndez (Argentina), Jouni Räisänen (Finland), Annette Rinke (Germany), Abdoulaye Sarr (Senegal), Penny Whetton (Australia)

Contributing Authors:

R. Arritt (USA), R. Benestad (Norway), M. Beniston (Switzerland), D. Bromwich (USA), D. Caya (Canada), J. Comiso (USA), R. de Elía (Canada, Argentina), K. Dethloff (Germany), S. Emori (Japan), J. Feddema (USA), R. Gerdes (Germany), J.F. González-Rouco (Spain), W. Gutowski (USA), I. Hanssen-Bauer (Norway), C. Jones (Canada), R. Katz (USA), A. Kitoh (Japan), R. Knutti (Switzerland), R. Leung (USA), J. Lowe (UK), A.H. Lynch (Australia), C. Matulla (Canada, Austria), K. McInnes (Australia), A.V. Mescherskaya (Russian Federation), A.B. Mullan (New Zealand), M. New (UK), M.H. Nokhandan (Iran), J.S. Pal (USA, Italy), D. Plummer (Canada), M. Rummukainen (Sweden, Finland), C. Schär (Switzerland), S. Somot (France), D.A. Stone (UK, Canada), R. Suppiah (Australia), M. Tadross (South Africa), C. Tebaldi (USA), W. Tennant (South Africa), M. Widmann (Germany, UK), R. Wilby (UK), B.L. Wyman (USA)

Review Editors:

Congbin Fu (China), Filippo Giorgi (Italy)

This chapter should be cited as:

Christensen, J.H., B. Hewitson, A. Busuioc, A. Chen, X. Gao, I. Held, R. Jones, R.K. Kolli, W.-T. Kwon, R. Laprise, V. Magaña Rueda, L. Mearns, C.G. Menéndez, J. Räisänen, A. Rinke, A. Sarr and P. Whetton, 2007: Regional Climate Projections. In: *Climate Change 2007: The Physical Science Basis. Contribution of Working Group I to the Fourth Assessment Report of the Intergovernmental Panel on Climate Change* [Solomon, S., D. Qin, M. Manning, Z. Chen, M. Marquis, K.B. Averyt, M. Tignor and H.L. Miller (eds.)]. Cambridge University Press, Cambridge, United Kingdom and New York, NY, USA.

Table of Contents

Executive Summary	849	11.7 Australia – New Zealand	896
11.1 Introduction	852	Box 11.4: Land Use and Land Cover Change Experiments Related to Climate Change	897
11.1.1 Summary of the Third Assessment Report.....	852	11.7.1 Key Processes	898
11.1.2 Introduction to Regional Projections	852	11.7.2 Skill of Models in Simulating Present Climate.....	898
Box 11.1: Summary of Regional Responses.....	858	11.7.3 Climate Projections.....	899
11.1.3 Some Unifying Themes.....	860	11.8 Polar Regions	902
11.2 Africa	866	11.8.1 Arctic.....	903
11.2.1 Key Processes	866	11.8.2 Antarctic.....	907
11.2.2 Skill of Models in Simulating Present and Past Climates.....	867	11.9 Small Islands	909
11.2.3 Climate Projections.....	867	11.9.1 Key Processes	910
11.3 Europe and the Mediterranean	872	11.9.2 Skill of Models in Simulating Present Climate.....	911
11.3.1 Key Processes	872	11.9.3 Temperature and Precipitation Projections.....	911
11.3.2 Skill of Models in Simulating Present Climate.....	872	11.9.4 Sea Level Rise	914
Box 11.2: The PRUDENCE Project.....	873	11.9.5 Tropical Cyclones.....	915
11.3.3 Climate Projections.....	873	Box 11.5: Coastal Zone Climate Change	916
11.4 Asia	879	11.10 Assessment of Regional Climate Projection Methods	918
11.4.1 Key Processes	879	11.10.1 Methods for Generating Regional Climate Information	918
11.4.2 Skill of Models in Simulating Present Climate.....	880	11.10.2 Quantifying Uncertainties	921
11.4.3 Climate Projections.....	881	Frequently Asked Question	
Box 11.3: Climatic Change in Mountain Regions	886	FAQ 11.1: Do Projected Changes in Climate Vary from Region to Region?	865
11.5 North America	887	References	926
11.5.1 Key Processes	887		
11.5.2 Skill of Models in Simulating Present Climate.....	888		
11.5.3 Climate Projections.....	889		
11.6 Central and South America	892		
11.6.1 Key Processes	892		
11.6.2 Skill of Models in Simulating Present Climate.....	893		
11.6.3 Climate Projections.....	894		
11.6.4 Extremes.....	896		

Supplementary Material

The following supplementary material is available on CD-ROM and in on-line versions of this report.

Supplementary Figures S11.1–S11.37

Supplementary Tables S1.1 and S1.2

Supplementary References

Executive Summary

Increasingly reliable regional climate change projections are now available for many regions of the world due to advances in modelling and understanding of the physical processes of the climate system. A number of important themes have emerged:

- Warming over many land areas is greater than global annual mean warming due to less water availability for evaporative cooling and a smaller thermal inertia as compared to the oceans.
- Warming generally increases the spatial variability of precipitation, contributing to a reduction of rainfall in the subtropics and an increase at higher latitudes and in parts of the tropics. The precise location of boundaries between regions of robust increase and decrease remains uncertain and this is commonly where Atmosphere-Ocean General Circulation Model (AOGCM) projections disagree.
- The poleward expansion of the subtropical highs, combined with the general tendency towards reductions in subtropical precipitation, creates especially robust projections of a reduction in precipitation at the poleward edges of the subtropics. Most of the regional projections of reductions in precipitation in the 21st century are associated with areas adjacent to these subtropical highs.
- There is a tendency for monsoonal circulations to result in increased precipitation due to enhanced moisture convergence, despite a tendency towards weakening of the monsoonal flows themselves. However, many aspects of tropical climatic responses remain uncertain.

Atmosphere-Ocean General Circulation Models remain the primary source of regional information on the range of possible future climates. A clearer picture of the robust aspects of regional climate change is emerging due to improvement in model resolution, the simulation of processes of importance for regional change and the expanding set of available simulations. Advances have been made in developing probabilistic information at regional scales from the AOGCM simulations, but these methods remain in the exploratory phase. There has been less development extending this to downscaled regional information. However, downscaling methods have matured since the Third Assessment Report (TAR; IPCC, 2001) and have been more widely applied, although only in some regions has large-scale coordination of multi-model downscaling of climate change simulations been achieved.

Regional climate change projections presented here are assessed drawing on information from four potential sources: AOGCM simulations; downscaling of AOGCM-simulated data using techniques to enhance regional detail; physical understanding of the processes governing regional responses; and recent historical climate change.

Previous chapters describe observed climate change on regional scales (Chapter 3) and compare global model simulations with these changes (Chapter 9). Comparisons of model simulations of temperature change with observations can be used to help constrain future regional temperature projections. Regional assessments of precipitation change rely primarily on convergence in both global and downscaling models along with physical insights. Where there is near unanimity among models with good supporting physical arguments, as is more typical for middle and higher latitudes, these factors encourage stronger statements as to the likelihood of a regional climate change. In some circumstances, physical insights alone clearly indicate the direction of future change.

The summary likelihood statements on projected regional climate are as follows:

- **Temperature projections:** These are comparable in magnitude to those of the TAR and confidence in the regional projections is now higher due to a larger number and variety of simulations, improved models, a better understanding of the role of model deficiencies and more detailed analyses of the results. Warming, often greater than the global mean, is *very likely* over all landmasses.
- **Precipitation projections:** Overall patterns of change are comparable to those of TAR, with greater confidence in the projections for some regions. Model agreement is seen over more and larger regions. For some regions, there are grounds for stating that the projected precipitation changes are *likely* or *very likely*. For other regions, confidence in the projected change remains weak.
- **Extremes:** There has been a large increase in the available analyses of changes in extremes. This allows for a more comprehensive assessment for most regions. The general findings are in line with the assessment made in TAR and now have a higher level of confidence derived from multiple sources of information. The most notable improvements in confidence relate to the regional statements concerning heat waves, heavy precipitation and droughts. Despite these advances, specific analyses of models are not available for some regions, which is reflected in the robust statements on extremes. In particular, projections concerning extreme events in the tropics remain uncertain. The difficulty in projecting the distribution of tropical cyclones adds to this uncertainty. Changes in extra-tropical cyclones are dependent on details of regional atmospheric circulation response, some of which remain uncertain.

The following summarises the robust findings of the projected regional change over the 21st century. Supporting narratives are provided in Sections 11.2 to 11.9. These changes are assessed as *likely* to *very likely* taking into account the uncertainties in climate sensitivity and emission trajectories (in the Special Report on Emission Scenarios (SRES) B1/A1B/B2 scenario range) discussed in earlier chapters.

All land regions:

It is *very likely* that all land regions will warm in the 21st century.

Africa:

Warming is *very likely* to be larger than the global annual mean warming throughout the continent and in all seasons, with drier subtropical regions warming more than the moister tropics. Annual rainfall is *likely* to decrease in much of Mediterranean Africa and the northern Sahara, with a greater likelihood of decreasing rainfall as the Mediterranean coast is approached. Rainfall in southern Africa is *likely* to decrease in much of the winter rainfall region and western margins. There is *likely* to be an increase in annual mean rainfall in East Africa. It is unclear how rainfall in the Sahel, the Guinean Coast and the southern Sahara will evolve.

Mediterranean and Europe:

Annual mean temperatures in Europe are *likely* to increase more than the global mean. Seasonally, the largest warming is *likely* to be in northern Europe in winter and in the Mediterranean area in summer. Minimum winter temperatures are *likely* to increase more than the average in northern Europe. Maximum summer temperatures are *likely* to increase more than the average in southern and central Europe. Annual precipitation is *very likely* to increase in most of northern Europe and decrease in most of the Mediterranean area. In central Europe, precipitation is *likely* to increase in winter but decrease in summer. Extremes of daily precipitation are *very likely* to increase in northern Europe. The annual number of precipitation days is *very likely* to decrease in the Mediterranean area. Risk of summer drought is *likely* to increase in central Europe and in the Mediterranean area. The duration of the snow season is *very likely* to shorten, and snow depth is *likely* to decrease in most of Europe.

Asia:

Warming is *likely* to be well above the global mean in central Asia, the Tibetan Plateau and northern Asia, above the global mean in eastern Asia and South Asia, and similar to the global mean in Southeast Asia. Precipitation in boreal winter is *very likely* to increase in northern Asia and the Tibetan Plateau, and *likely* to increase in eastern Asia and the southern parts of Southeast Asia. Precipitation in summer is *likely* to increase in northern Asia, East Asia, South Asia and most of Southeast Asia, but is *likely* to decrease in central Asia. It is *very likely* that heat waves/hot spells in summer will be of longer duration, more intense and more frequent in East Asia. Fewer very cold days are *very likely* in East Asia and South Asia. There is *very likely* to be an increase in the frequency of intense precipitation events in parts of South Asia, and in East Asia. Extreme rainfall and winds associated with tropical cyclones are *likely* to increase in East Asia, Southeast Asia and South Asia.

North America:

The annual mean warming is *likely* to exceed the global mean warming in most areas. Seasonally, warming is *likely* to be largest in winter in northern regions and in summer in the southwest. Minimum winter temperatures are *likely* to increase more than the average in northern North America. Maximum summer temperatures are *likely* to increase more than the average in the southwest. Annual mean precipitation is *very likely* to increase in Canada and the northeast USA, and *likely* to decrease in the southwest. In southern Canada, precipitation is *likely* to increase in winter and spring but decrease in summer. Snow season length and snow depth are *very likely* to decrease in most of North America except in the northernmost part of Canada where maximum snow depth is *likely* to increase.

Central and South America:

The annual mean warming is *likely* to be similar to the global mean warming in southern South America but larger than the global mean warming in the rest of the area. Annual precipitation is *likely* to decrease in most of Central America and in the southern Andes, although changes in atmospheric circulation may induce large local variability in precipitation response in mountainous areas. Winter precipitation in Tierra del Fuego and summer precipitation in south-eastern South America is *likely* to increase. It is uncertain how annual and seasonal mean rainfall will change over northern South America, including the Amazon forest. However, there is qualitative consistency among the simulations in some areas (rainfall increasing in Ecuador and northern Peru, and decreasing at the northern tip of the continent and in southern northeast Brazil).

Australia and New Zealand:

Warming is *likely* to be larger than that of the surrounding oceans, but comparable to the global mean. The warming is less in the south, especially in winter, with the warming in the South Island of New Zealand *likely* to remain less than the global mean. Precipitation is *likely* to decrease in southern Australia in winter and spring. Precipitation is *very likely* to decrease in south-western Australia in winter. Precipitation is *likely* to increase in the west of the South Island of New Zealand. Changes in rainfall in northern and central Australia are uncertain. Increased mean wind speed is *likely* across the South Island of New Zealand, particularly in winter. Increased frequency of extreme high daily temperatures in Australia and New Zealand, and a decrease in the frequency of cold extremes is *very likely*. Extremes of daily precipitation are *very likely* to increase, except possibly in areas of significant decrease in mean rainfall (southern Australia in winter and spring). Increased risk of drought in southern areas of Australia is *likely*.

Polar regions:

The Arctic is *very likely* to warm during this century more than the global mean. Warming is projected to be largest in winter and smallest in summer. Annual arctic precipitation is *very likely* to increase. It is *very likely* that the relative precipitation increase will be largest in winter and smallest in summer. Arctic sea ice is *very likely* to decrease in its extent and thickness. It is uncertain how the Arctic Ocean circulation will change. The Antarctic is *likely* to warm and the precipitation is *likely* to increase over the continent. It is uncertain to what extent the frequency of extreme temperature and precipitation events will change in the polar regions.

Small Islands:

Sea levels are *likely* to rise on average during the century around the small islands of the Caribbean Sea, Indian Ocean and northern and southern Pacific Oceans. The rise will *likely* not be geographically uniform but large deviations among models make regional estimates across the Caribbean, Indian and Pacific Oceans uncertain. All Caribbean, Indian Ocean and North and South Pacific islands are *very likely* to warm during this century. The warming is *likely* to be somewhat smaller than the global annual mean. Summer rainfall in the Caribbean is *likely* to decrease in the vicinity of the Greater Antilles but changes elsewhere and in winter are uncertain. Annual rainfall is *likely* to increase in the northern Indian Ocean with increases *likely* in the vicinity of the Seychelles in December, January and February, and in the vicinity of the Maldives in June, July and August, while decreases are *likely* in the vicinity of Mauritius in June, July and August. Annual rainfall is *likely* to increase in the equatorial Pacific, while decreases are projected by most models for just east of French Polynesia in December, January and February.

11.1 Introduction

Increasingly reliable regional climate change projections are now available for many regions of the world due to advances in modelling and understanding of the physical processes of the climate system. Atmosphere–Ocean General Circulation Models (AOGCMs) remain the foundation for projections while downscaling techniques now provide valuable additional detail. Atmosphere–Ocean General Circulation Models cannot provide information at scales finer than their computational grid (typically of the order of 200 km) and processes at the unresolved scales are important. Providing information at finer scales can be achieved through using high resolution in dynamical models or empirical statistical downscaling. Development of downscaling methodologies remains an important focus. Downscaled climate change projections tailored to specific needs are only now starting to become available.

11.1.1 Summary of the Third Assessment Report

The assessment of regional climate projections in the Third Assessment Report (TAR; Chapter 10 of IPCC, 2001) was largely restricted to General Circulation Model (GCM)-derived temperature with limited precipitation statements. The major assessment of temperature change was that it is very likely all land areas will warm more than the global average (with the exception of Southeast Asia and South America in June, July and August; JJA), with amplification at high latitudes. The changes in precipitation assessed to be likely were: an increase over northern mid-latitude regions in winter and over high-latitude regions in both winter and summer; in December, January and February (DJF), an increase in tropical Africa, little change in Southeast Asia, and a decrease in Central America; an increase or little change in JJA over South Asia and a decrease over Australia and the Mediterranean region. These projections were almost entirely based on analysis of nine coarse-resolution AOGCMs that had performed transient experiments for the 20th century with the specifications for the A2 and B2 emission scenarios. Chapter 10 of the TAR noted that studies with regional models indicate that changes at finer scales may be substantially different in magnitude from these large sub-continental findings.

Information available for assessment regarding climate variability and extremes at the regional scale was too sparse for it to be meaningfully drawn together in a systematic manner. However, some statements of a more generic nature were made. It was assessed that the variability of daily to interannual temperatures is likely to decrease in winter and increase in summer for mid-latitude Northern Hemisphere (NH) land areas, daily high temperature extremes are likely to increase and future increases in mean precipitation are very likely to lead to an increase in variability. In some specifically analysed regions, it was assessed that extreme precipitation may increase and there were indications that droughts or dry spells may increase in occurrence in Europe, North America and Australia.

11.1.2 Introduction to Regional Projections

Assessments of climate change projections are provided here on a region-by-region basis. The discussion is organised according to the same continental-scale regions used by Working Group II (WGII) in the Fourth Assessment Report (AR4) and in earlier assessments: Africa, Europe and Mediterranean, Asia, North America, Central and South America, Australia–New Zealand, Polar Regions and Small Islands. While the topics covered vary somewhat from region to region, each section includes a discussion of key processes of importance for climate change in that region, relevant aspects of model skill in simulating current climate, and projections of future regional climate change based on global models and downscaling techniques.

Each of these continental-scale regions encompasses a broad range of climates and is too large to be used as a basis for conveying quantitative regional climate change information. Therefore, each is subdivided into a number of sub-continental or oceanic regions. The sub-continental regions as defined in Table 11.1 are the framework for developing specific regional or sub-continental robust statements of projected change.

Area-averaged temperature and precipitation changes are presented from the coordinated set of climate model simulations archived at the Program for Climate Model Diagnosis and Intercomparison (PCMDI; subsequently called the multi-model data set or MMD). The regions are very close to those initially devised by Giorgi and Francesco (2000) with some minor modifications similar to those of Ruosteenoja et al. (2003). They have simple shapes and are no smaller than the horizontal scales on which current AOGCMs are useful for climate simulations (typically judged to be roughly 1,000 km).

These regional averages have some deficiencies for discussion of the AOGCM projections. In several instances, the simple definition of these boxes results in spatial averaging over regions in which precipitation is projected to increase and decrease. There are also sub-regions where the case can be made for a robust and physically plausible hydrological response, information about which is lost in the regional averages. Partially to help in discussing these features, this chapter also uses maps of temperature and precipitation responses, interpolated to a grid with 128 longitudes by 64 latitudes which is typical of many of the lower-resolution atmospheric models in the MMD.

In the regional discussion to follow, the starting points are temperature and precipitation. Changes in temperature are introduced in each continental section by plotting for each of the regions the evolution of the range of projected decadal mean change for the A1B scenario through the 21st century (simulations hereafter referred to as MMD-A1B). These are put into the context of observed changes in the 20th century by plotting the observed changes and how well the models reproduce these. This summary information is displayed for continental regions in Box 11.1, which also contains details of how the figures were constructed. The equivalent figures for the individual regions of each continental-scale region are displayed in the following sections. These are constructed in

the same way as Box 11.1, Figure 1. The 20th-century parts of these figures are also displayed in Section 9.4, where more details on their construction are provided. The discussion on precipitation provides a limited view of hydrological changes. Supplementary Material Figure S11.1 expands on this issue by comparing the annual mean responses in precipitation and in precipitation minus evaporation over the 21st century in the MMD-A1B projections. Over North America and Europe, for example, the region of drying in the sense of precipitation minus evaporation is shifted poleward compared to the region of reduced precipitation. A summary of the more significant hydrological cycle changes from the regional discussions is presented in Box 11.1.

Table 11.1 provides detailed information for each region generated from the MMD-A1B models focusing on the change in climate between the 1980 to 1999 period in the 20th-century integrations and the 2080 to 2099 period. The distribution of the annual and seasonal mean surface air temperature response and percentage change in precipitation are described by the median, the 25 and 75% values (half of the models lie between these two values) and the maximum and minimum values in the model ensemble. Information on model biases in these regional averages for the 1980 to 1999 simulations is provided in Supplementary Material Table S11.1 in a similar format. Maps of biases are referred to in some of the following and are included in the Supplementary Material as well. Data sources used in these comparisons are listed in the table and figure captions where these biases are displayed.

Most of the discussion focuses on the A1B scenario. The global mean near-surface temperature responses (between the period 1980 to 1999 of the 20th-century integrations and the period 2080 to 2099) in the ensemble mean of the MMD models are in the ratio 0.69:1:1.17 for the B1:A1B:A2 scenarios. The local temperature responses in nearly all regions closely follow the same ratio, as discussed in Chapter 10 and as illustrated in Supplementary Material Figures S11.2 to S11.4. Therefore, little is gained by repeating the discussion of the A1B scenario for the other scenarios. The ensemble mean local precipitation responses also approximately scale with the global mean temperature response, although not as precisely as the temperature itself. Given the substantial uncertainties in hydrological responses, the generally smaller signal/noise ratio and the similarities in the basic structure of the AOGCM precipitation responses in the different scenarios, a focus on A1B seems justified for the precipitation as well. The overall regional assessments, however, do rely on all available scenario information.

Given the dominantly linear response of the models, the 2080 to 2099 period allows the greatest clarity of the background climate change underlying the interannual and decadal variability. In the ensemble mean AOGCM projections there is no indication of abrupt climate change, nor does the literature on individual models provide any strong suggestions of robust nonlinearities. Some local temporal nonlinearities are to be expected, for example as the sea ice boundary retreats from a particular location in the Arctic. While the possibility

exists that changes of more abrupt character could happen, such as major ocean circulation or land surface/vegetation change, there is little basis to judge the plausibility of these factors (see Chapter 10). Therefore, this discussion is based on this linear picture.

Table 11.1 also provides some simple estimates of the signal-to-noise ratio. The signal is the change in 20-year means of seasonal or annual mean temperature or precipitation. The noise is an estimate of the internal variability of 20-year means of seasonal or annual mean temperature or precipitation, as generated by the models. The signal-to-noise ratio is converted into the time interval that is required before the signal is clearly discernible, assuming that the signal grows linearly over the century at the average rate in the ensemble mean A1B projection. ‘Clearly discernible’ is defined in this context as distinguishable with 95% confidence. As an example, the annual mean precipitation increase in northern Europe (NEU) (Table 11.1) is clearly discernible in these models after 45 years, meaning that the 20-year average from 2025 to 2044 will be greater than the 20-year mean over 1980 to 1999 with 95% confidence, accounting only for the internal variability in the models and no other sources of uncertainty. In contrast, the annual temperature response in Southeast Asia (SEA) rises above the noise by this measure after only 10 years, implying that the average temperature over the period 1990 to 2009 is clearly discernible in the models from the average over the control period 1980 to 1999. This measure is likely an overestimate of the time of emergence of the signal as compared to that obtained with more refined detection strategies (of the kind discussed in Chapter 9). This noise estimate is solely based on the models and must be treated with caution, but it would be wrong to assume that models always underestimate this internal variability. Some models overestimate and some underestimate the amplitude of the El Niño-Southern Oscillation (ENSO), for example, thereby over- or underestimating the most important source of interannual variability in the tropics. On the other hand, few models capture the range of decadal variability of rainfall in West Africa, for example (Hoerling, et al., 2006; Section 8.4).

Also included in Table 11.1 is an estimate of the probability of extremely warm, extremely wet and extremely dry seasons, for the A1B scenario and for the time period 2080 to 2099. An ‘extremely warm’ summer is defined as follows. Examining all of the summers simulated in a particular realisation of a model in the 1980 to 1999 control period, the warmest of these 20 summers can be computed as an estimate of the temperature of the warmest 5% of all summers in the control climate. The period 2080 to 2099 is then examined, and the fraction of the summers exceeding this warmth determined. This is referred to as the probability of extremely warm summers. The results are tabulated after averaging over models, and similarly for both extremely low and extremely high seasonal precipitation amounts. Values smaller (larger) than 5% indicate a decrease (increase) in the frequency of extremes. This follows the approach in Weisheimer and Palmer (2005) except that this chapter compares each model’s future with its own 20th century to help avoid distortions due to differing biases in the different

Table 11.1. Regional averages of temperature and precipitation projections from a set of 21 global models in the MMD for the A1B scenario. The mean temperature and precipitation responses are first averaged for each model over all available realisations of the 1980 to 1999 period from the 20th Century Climate in Coupled Models (20C3M) simulations and the 2080 to 2099 period of A1B. Computing the difference between these two periods, the table shows the minimum, maximum, median (50%), and 25 and 75% quartile values among the 21 models, for temperature (°C) and precipitation (%) change. Regions in which the middle half (25–75%) of this distribution is all of the same sign in the precipitation response are coloured light brown for decreasing and light blue for increasing precipitation. Signal-to-noise ratios for these 20-year mean responses is indicated by first computing a consensus standard deviation of 20-year means, using those models that have at least three realisations of the 20C3M simulations and using all 20-year periods in the 20th century. The signal is assumed to increase linearly in time, and the time required for the median signal to reach 2.83 ($2 \times \sqrt{2}$) times the standard deviation is displayed as an estimate of when this signal is significant at the 95% level. These estimates of the times for emergence of a clearly discernible signal are only shown for precipitation when the models are in general agreement on the sign of the response, as indicated by the colouring. The frequency (%) of extremely warm, wet and dry seasons, averaged over the models, is also presented, as described in Section 11.2.1. Values are only shown when at least 14 out of the 21 models agree on an increase (bold) or a decrease in the extremes. A value of 5% indicates no change, as this is the nominal value for the control period by construction. The regions are defined by rectangular latitude/longitude boxes and the coordinates of the bottom left-hand and top right-hand corners of these are given in degrees in the first column under the region acronym (see table notes for full names of regions). Information is provided for land areas contained in the boxes except for the Small Islands regions where sea areas are used and for Antarctica where both land and sea areas are used.

Region ^a	Season	Temperature Response (°C)						Precipitation Response (%)						Extreme Seasons (%)		
		Min	25	50	75	Max	T yrs	Min	25	50	75	Max	T yrs	Warm	Wet	Dry
AFRICA																
WAF	DJF	2.3	2.7	3.0	3.5	4.6	10	-16	-2	6	13	23		100	21	4
	MAM	1.7	2.8	3.5	3.6	4.8	10	-11	-7	-3	5	11		100		
12S,20W to 22N,18E	JJA	1.5	2.7	3.2	3.7	4.7	10	-18	-2	2	7	16		100	19	
	SON	1.9	2.5	3.3	3.7	4.7	10	-12	0	1	10	15		100	15	
	Annual	1.8	2.7	3.3	3.6	4.7	10	-9	-2	2	7	13		100	22	
EAF	DJF	2.0	2.6	3.1	3.4	4.2	10	-3	6	13	16	33	55	100	25	1
	MAM	1.7	2.7	3.2	3.5	4.5	10	-9	2	6	9	20	>100	100	15	4
12S,22E to 18N,52E	JJA	1.6	2.7	3.4	3.6	4.7	10	-18	-2	4	7	16		100		
	SON	1.9	2.6	3.1	3.6	4.3	10	-10	3	7	13	38	95	100	21	3
	Annual	1.8	2.5	3.2	3.4	4.3	10	-3	2	7	11	25	60	100	30	1
SAF	DJF	1.8	2.7	3.1	3.4	4.7	10	-6	-3	0	5	10		100	11	
	MAM	1.7	2.9	3.1	3.8	4.7	10	-25	-8	0	4	12		98		
35S,10E to 12S,52E	JJA	1.9	3.0	3.4	3.6	4.8	10	-43	-27	-23	-7	-3	70	100	1	23
	SON	2.1	3.0	3.7	4.0	5.0	10	-43	-20	-13	-8	3	90	100	1	20
	Annual	1.9	2.9	3.4	3.7	4.8	10	-12	-9	-4	2	6		100	4	13
SAH	DJF	2.4	2.9	3.2	3.5	5.0	15	-47	-31	-18	-12	31	>100	97		12
	MAM	2.3	3.3	3.6	3.8	5.2	10	-42	-37	-18	-10	13	>100	100	2	21
18N,20E to 30N,65E	JJA	2.6	3.6	4.1	4.4	5.8	10	-53	-28	-4	16	74		100		
	SON	2.8	3.4	3.7	4.3	5.4	10	-52	-15	6	23	64		100		
	Annual	2.6	3.2	3.6	4.0	5.4	10	-44	-24	-6	3	57		100		
EUROPE																
NEU	DJF	2.6	3.6	4.3	5.5	8.2	40	9	13	15	22	25	50	82	43	0
	MAM	2.1	2.4	3.1	4.3	5.3	35	0	8	12	15	21	60	79	28	2
48N,10W to 75N,40E	JJA	1.4	1.9	2.7	3.3	5.0	25	-21	-5	2	7	16		88	11	
	SON	1.9	2.6	2.9	4.2	5.4	30	-5	4	8	11	13	80	87	20	2
	Annual	2.3	2.7	3.2	4.5	5.3	25	0	6	9	11	16	45	96	48	2
SEM	DJF	1.7	2.5	2.6	3.3	4.6	25	-16	-10	-6	-1	6	>100	93	3	12
	MAM	2.0	3.0	3.2	3.5	4.5	20	-24	-17	-16	-8	-2	60	98	1	31
30N,10W to 48N,40E	JJA	2.7	3.7	4.1	5.0	6.5	15	-53	-35	-24	-14	-3	55	100	1	42
	SON	2.3	2.8	3.3	4.0	5.2	15	-29	-15	-12	-9	-2	90	100	1	21
	Annual	2.2	3.0	3.5	4.0	5.1	15	-27	-16	-12	-9	-4	45	100	0	46

Table 11.1 (continued)

Region ^a	Season	Temperature Response (°C)					Precipitation Response (%)						Extreme Seasons (%)			
		Min	25	50	75	Max	T yrs	Min	25	50	75	Max	T yrs	Warm	Wet	Dry
ASIA																
NAS	DJF	2.9	4.8	6.0	6.6	8.7	20	12	20	26	37	55	30	93	68	0
	MAM	2.0	2.9	3.7	5.0	6.8	25	2	16	18	24	26	30	89	66	1
50N,40E to 70N,180E	JJA	2.0	2.7	3.0	4.9	5.6	15	-1	6	9	12	16	40	100	51	2
	SON	2.8	3.6	4.8	5.8	6.9	15	7	15	17	19	29	30	99	65	0
	Annual	2.7	3.4	4.3	5.3	6.4	15	10	12	15	19	25	20	100	92	0
CAS	DJF	2.2	2.6	3.2	3.9	5.2	25	-11	0	4	9	22		84	8	
	MAM	2.3	3.1	3.9	4.5	4.9	20	-26	-14	-9	-4	3	>100	94		16
30N,40E to 50N,75E	JJA	2.7	3.7	4.1	4.9	5.7	10	-58	-28	-13	-4	21	>100	100	3	20
	SON	2.5	3.2	3.8	4.1	4.9	15	-18	-4	3	9	24		99		
	Annual	2.6	3.2	3.7	4.4	5.2	10	-18	-6	-3	2	6		100		12
TIB	DJF	2.8	3.7	4.1	4.9	6.9	20	1	12	19	26	36	45	95	40	0
	MAM	2.5	2.9	3.6	4.3	6.3	15	-3	4	10	14	34	70	96	34	2
30N,50E to 75N,100E	JJA	2.7	3.2	4.0	4.7	5.4	10	-11	0	4	10	28		100	24	
	SON	2.7	3.3	3.8	4.6	6.2	15	-8	-4	8	14	21		100	20	
	Annual	2.8	3.2	3.8	4.5	6.1	10	-1	2	10	13	28	45	100	46	1
EAS	DJF	2.1	3.1	3.6	4.4	5.4	20	-4	6	10	17	42	>100	96	18	2
	MAM	2.1	2.6	3.3	3.8	4.6	15	0	7	11	14	20	55	98	35	2
20N,100E to 50N,145E	JJA	1.9	2.5	3.0	3.9	5.0	10	-2	5	9	11	17	45	100	32	1
	SON	2.2	2.7	3.3	4.2	5.0	15	-13	-1	9	15	29		100	20	3
	Annual	2.3	2.8	3.3	4.1	4.9	10	2	4	9	14	20	40	100	47	1
SAS	DJF	2.7	3.2	3.6	3.9	4.8	10	-35	-9	-5	1	15		99		
	MAM	2.1	3.0	3.5	3.8	5.3	10	-30	-2	9	18	26		100	14	
5N,64E to 50N,100E	JJA	1.2	2.2	2.7	3.2	4.4	15	-3	4	11	16	23	45	96	32	1
	SON	2.0	2.5	3.1	3.5	4.4	10	-12	8	15	20	26	50	100	29	3
	Annual	2.0	2.7	3.3	3.6	4.7	10	-15	4	11	15	20	40	100	39	3
SEA	DJF	1.6	2.1	2.5	2.9	3.6	10	-4	3	6	10	12	80	99	23	2
	MAM	1.5	2.2	2.7	3.1	3.9	10	-4	2	7	9	17	75	100	27	1
11S,95E to 20N,115E	JJA	1.5	2.2	2.4	2.9	3.8	10	-3	3	7	9	17	70	100	24	2
	SON	1.6	2.2	2.4	2.9	3.6	10	-2	2	6	10	21	85	99	26	3
	Annual	1.5	2.2	2.5	3.0	3.7	10	-2	3	7	8	15	40	100	44	1
NORTH AMERICA																
ALA	DJF	4.4	5.6	6.3	7.5	11.0	30	6	20	28	34	56	40	80	39	0
	MAM	2.3	3.2	3.5	4.7	7.7	35	2	13	17	23	38	40	69	45	0
60N,170W to 72N,103W	JJA	1.3	1.8	2.4	3.8	5.7	25	1	8	14	20	30	45	86	51	1
	SON	2.3	3.6	4.5	5.3	7.4	25	6	14	19	31	36	40	86	51	0
	Annual	3.0	3.7	4.5	5.2	7.4	20	6	13	21	24	32	25	97	80	0
CGI	DJF	3.3	5.2	5.9	7.2	8.5	20	6	15	26	32	42	30	95	58	0
	MAM	2.4	3.2	3.8	4.6	7.2	20	4	13	17	20	34	35	94	49	1
50N,103W to 85N,10W	JJA	1.5	2.1	2.8	3.7	5.6	15	0	8	11	12	19	35	99	46	1
	SON	2.7	3.4	4.0	5.7	7.3	20	7	14	16	22	37	35	99	62	0
	Annual	2.8	3.5	4.3	5.0	7.1	15	8	12	15	20	31	25	100	90	0

Table 11.1 (continued)

Region ^a	Temperature Response (°C)							Precipitation Response (%)							Extreme Seasons (%)		
	Season	Min	25	50	75	Max	T yrs	Min	25	50	75	Max	T yrs	Warm	Wet	Dry	
NORTH AMERICA (continued)																	
WNA	DJF	1.6	3.1	3.6	4.4	5.8	25	-4	2	7	11	36	>100	80	18	3	
	MAM	1.5	2.4	3.1	3.4	6.0	20	-7	2	5	8	14	>100	87	14		
30N,50E to 75N,100E	JJA	2.3	3.2	3.8	4.7	5.7	10	-18	-10	-1	2	10		100	3		
	SON	2.0	2.8	3.1	4.5	5.3	20	-3	3	6	12	18	>100	95	17	2	
	Annual	2.1	2.9	3.4	4.1	5.7	15	-3	0	5	9	14	70	100	21	2	
CNA	DJF	2.0	2.9	3.5	4.2	6.1	30	-18	0	5	8	14		71	7		
	MAM	1.9	2.8	3.3	3.9	5.7	25	-17	2	7	12	17	>100	81	19	4	
30N,103W to 50N,85W	JJA	2.4	3.1	4.1	5.1	6.4	20	-31	-15	-3	4	20	>100	93		15	
	SON	2.4	3.0	3.5	4.6	5.8	20	-17	-4	4	11	24		91	11		
	Annual	2.3	3.0	3.5	4.4	5.8	15	-16	-3	3	7	15		98			
ENA	DJF	2.1	3.1	3.8	4.6	6.0	25	2	9	11	19	28	85	78	24		
	MAM	2.3	2.7	3.5	3.9	5.9	20	-4	7	12	16	23	60	86	23	2	
25N,85W to 50N,50W	JJA	2.1	2.6	3.3	4.3	5.4	15	-17	-3	1	6	13		98			
	SON	2.2	2.8	3.5	4.4	5.7	20	-7	4	7	11	17	>100	97	19		
	Annual	2.3	2.8	3.6	4.3	5.6	15	-3	5	7	10	15	55	100	29	1	
CENTRAL AND SOUTH AMERICA																	
CAM	DJF	1.4	2.2	2.6	3.5	4.6	15	-57	-18	-14	-9	0	>100	96	2	25	
	MAM	1.9	2.7	3.6	3.8	5.2	10	-46	-25	-16	-10	15	75	100	2	18	
10N,116W to 30N,83W	JJA	1.8	2.7	3.4	3.6	5.5	10	-44	-25	-9	-4	12	90	100		24	
	SON	2.0	2.7	3.2	3.7	4.6	10	-45	-10	-4	7	24		100		15	
	Annual	1.8	2.6	3.2	3.6	5.0	10	-48	-16	-9	-5	9	65	100	2	33	
AMZ	DJF	1.7	2.4	3.0	3.7	4.6	10	-13	0	4	11	17	>100	93	27	4	
	MAM	1.7	2.5	3.0	3.7	4.6	10	-13	-1	1	4	14		100	18		
20S,82W to 12N,34W	JJA	2.0	2.7	3.5	3.9	5.6	10	-38	-10	-3	2	13		100			
	SON	1.8	2.8	3.5	4.1	5.4	10	-35	-12	-2	8	21		100			
	Annual	1.8	2.6	3.3	3.7	5.1	10	-21	-3	0	6	14		100			
SSA	DJF	1.5	2.5	2.7	3.3	4.3	10	-16	-2	1	7	10		100			
	MAM	1.8	2.3	2.6	3.0	4.2	15	-11	-2	1	5	7		98	8		
56S,76W to 20S,40W	JJA	1.7	2.1	2.4	2.8	3.6	15	-20	-7	0	3	17		95			
	SON	1.8	2.2	2.7	3.2	4.0	15	-20	-12	1	6	11		99			
	Annual	1.7	2.3	2.5	3.1	3.9	10	-12	-1	3	5	7		100			
AUSTRALIA AND NEW ZEALAND																	
NAU	DJF	2.2	2.6	3.1	3.7	4.6	20	-20	-8	1	8	27		89			
	MAM	2.1	2.7	3.1	3.3	4.3	20	-24	-12	1	15	40		92		3	
30S,110E to 11S,155E	JJA	2.0	2.7	3.0	3.3	4.3	25	-54	-20	-14	3	26		94	3		
	SON	2.5	3.0	3.2	3.8	5.0	20	-58	-32	-12	2	20		98			
	Annual	2.2	2.8	3.0	3.5	4.5	15	-25	-8	-4	8	23		99			
SAU	DJF	2.0	2.4	2.7	3.2	4.2	20	-23	-12	-2	12	30		95			
	MAM	2.0	2.2	2.5	2.8	3.9	20	-31	-9	-5	13	32		90		6	
45S,110E to 30S,155E	JJA	1.7	2.0	2.3	2.5	3.5	15	-37	-20	-11	-4	9	>100	95		17	
	SON	2.0	2.6	2.8	3.0	4.1	20	-42	-27	-14	-5	4	>100	95		15	
	Annual	1.9	2.4	2.6	2.8	3.9	15	-27	-13	-4	3	12		100			

Table 11.1 (continued)

Region ^a	Season	Temperature Response (°C)				Precipitation Response (%)						Extreme Seasons (%)				
		Min	25	50	75	Max	T yrs	Min	25	50	75	Max	T yrs	Warm	Wet	Dry
POLAR REGIONS																
ARC ^b	DJF	4.3	6.0	6.9	8.4	11.4	15	11	19	26	29	39	25	100	90	0
	MAM	2.4	3.7	4.4	4.9	7.3	15	9	14	16	21	32	25	100	79	0
60N,180E to 90N,180W	JJA	1.2	1.6	2.1	3.0	5.3	15	4	10	14	17	20	25	100	85	0
	SON	2.9	4.8	6.0	7.2	8.9	15	9	17	21	26	35	20	100	96	0
	Annual	2.8	4.0	4.9	5.6	7.8	15	10	15	18	22	28	20	100	100	0
ANT ^c	DJF	0.8	2.2	2.6	2.8	4.6	20	-11	5	9	14	31	50	85	34	3
	MAM	1.3	2.2	2.6	3.3	5.3	20	1	8	12	19	40	40	88	54	0
90S,180E to 60S,180W	JJA	1.4	2.3	2.8	3.3	5.2	25	5	14	19	24	41	30	83	59	0
	SON	1.3	2.1	2.3	3.2	4.8	25	-2	9	12	18	36	45	79	42	1
	Annual	1.4	2.3	2.6	3.0	5.0	15	-2	9	14	17	35	25	99	81	1
SMALL ISLANDS																
CAR	DJF	1.4	1.8	2.1	2.4	3.2	10	-21	-11	-6	0	10		100	2	
	MAM	1.3	1.8	2.2	2.4	3.2	10	-28	-20	-13	-6	6	>100	100	3	18
10N,85W to 25N,60W	JJA	1.3	1.8	2.0	2.4	3.2	10	-57	-35	-20	-6	8	60	100	2	40
	SON	1.6	1.9	2.0	2.5	3.4	10	-38	-18	-6	1	19		100		22
	Annual	1.4	1.8	2.0	2.4	3.2	10	-39	-19	-12	-3	11	60	100	3	39
IND	DJF	1.4	2.0	2.1	2.4	3.8	10	-4	2	4	9	20	>100	100	19	1
	MAM	1.5	2.0	2.2	2.5	3.8	10	0	3	5	6	20	80	100	22	1
35S,50E to 17.5N,100E	JJA	1.4	1.9	2.1	2.4	3.7	10	-3	-1	3	5	20		100	17	
	SON	1.4	1.9	2.0	2.3	3.6	10	-5	2	4	7	21	>100	100	17	2
	Annual	1.4	1.9	2.1	2.4	3.7	10	-2	3	4	5	20	65	100	30	2
MED	DJF	1.5	2.0	2.3	2.7	4.2	25	-25	-16	-14	-10	-2	85	96	1	18
	MAM	1.5	2.1	2.4	2.7	3.7	20	-32	-23	-19	-16	-6	65	99	0	32
30N,5W to 45N,35E	JJA	2.0	2.6	3.1	3.7	4.7	15	-64	-34	-29	-20	-3	60	100	1	36
	SON	1.9	2.3	2.7	3.2	4.4	20	-33	-16	-10	-5	9	>100	99	2	21
	Annual	1.7	2.2	2.7	3.0	4.2	15	-30	-16	-15	-10	-6	45	100	0	50
TNE	DJF	1.4	1.9	2.1	2.3	3.3	10	-35	-8	-6	3	10	>100	100		
	MAM	1.5	1.9	2.0	2.2	3.1	15	-16	-7	-2	6	39	>100	100		
0,30W to 40N,10W	JJA	1.4	1.9	2.1	2.4	3.6	15	-8	-2	2	7	13	>100	100		
	SON	1.5	2.0	2.2	2.6	3.7	15	-16	-5	-1	3	9	>100	100		
	Annual	1.4	1.9	2.1	2.4	3.5	15	-7	-3	1	3	7	>100	100		
NPA	DJF	1.5	1.9	2.4	2.5	3.6	10	-5	1	3	6	17	>100	100	20	2
	MAM	1.4	1.9	2.3	2.5	3.5	10	-17	-1	1	3	17		100	14	
0,150E to 40N,120W	JJA	1.4	1.9	2.3	2.7	3.9	10	1	5	8	14	25	55	100	43	1
	SON	1.6	1.9	2.4	2.9	3.9	10	1	5	6	13	22	50	100	31	1
	Annual	1.5	1.9	2.3	2.6	3.7	10	0	3	5	10	19	60	100	35	1
SPA	DJF	1.4	1.7	1.8	2.1	3.2	10	-6	1	4	7	15	80	100	19	4
	MAM	1.4	1.8	1.9	2.1	3.2	10	-3	3	6	8	17	35	100	35	1
55S,150E to 0,80W	JJA	1.4	1.7	1.8	2.0	3.1	10	-2	1	3	5	12	70	100	27	3
	SON	1.4	1.6	1.8	2.0	3.0	10	-8	-2	2	4	5		100		
	Annual	1.4	1.7	1.8	2.0	3.1	10	-4	3	3	6	11	40	100	40	3

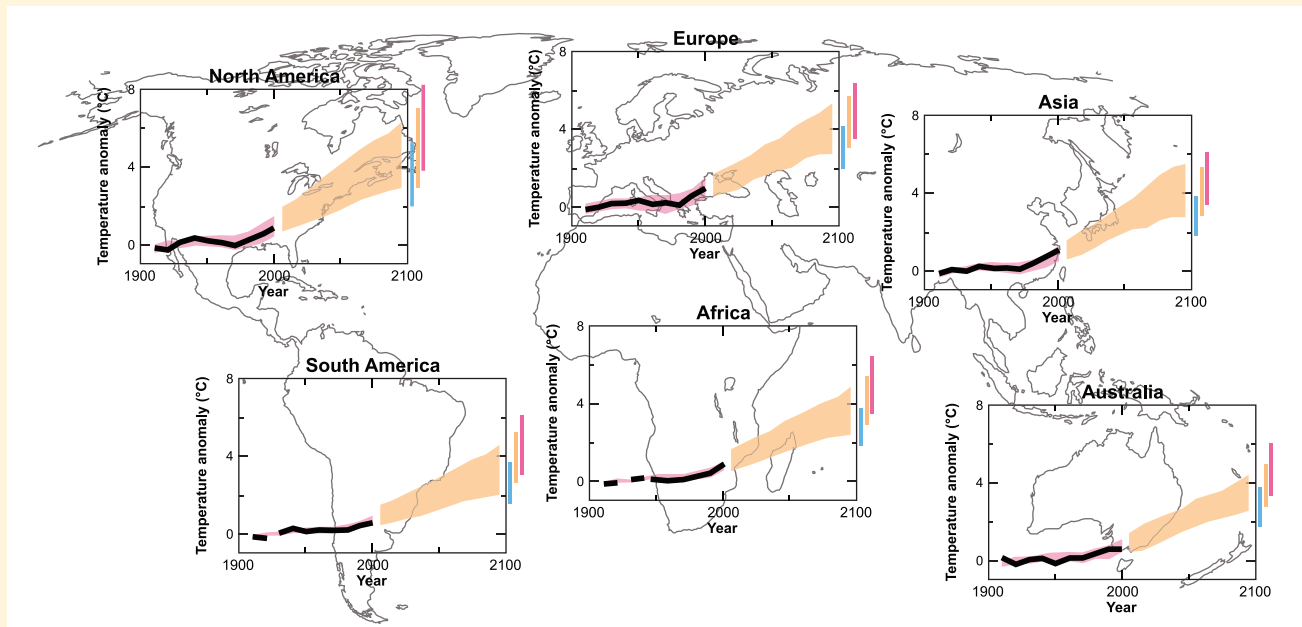
Notes: ^a Regions are: West Africa (WAF), East Africa (EAF), South Africa (SAF), Sahara (SAH), Northern Europe (NEU), Southern Europe and Mediterranean (SEM), Northern Asia (NAS), Central Asia (CAS), Tibetan Plateau (TIB), East Asia (EAS), South Asia (SAS), Southeast Asia (SEA), Alaska (ALA), East Canada, Greenland and Iceland (CGI), Western North America (WNA), Central North America (CNA), Eastern North America (ENA), Central America (CAM), Amazonia (AMZ), Southern South America (SSA), North Australia (NAU), South Australia (SAU), Arctic (ARC), Antarctic (ANT), Caribbean (CAR), Indian Ocean (IND), Mediterranean Basin (MED), Tropical Northeast Atlantic (TNE), North Pacific Ocean (NPA), and South Pacific Ocean (SPA).

^b land and ocean
^c land only

Box 11.1: Summary of Regional Responses

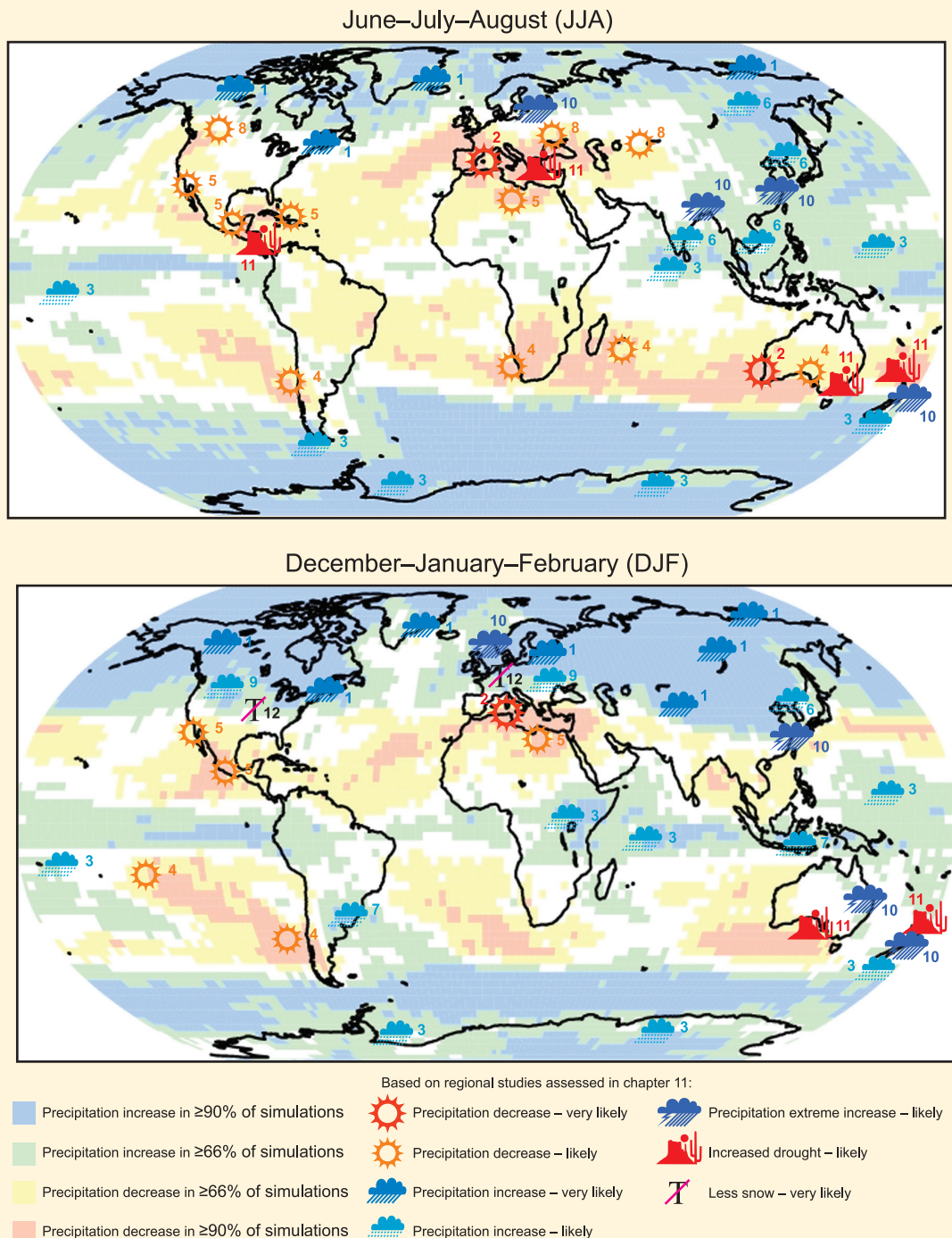
As an introduction to the more detailed regional analysis presented in this chapter, Box 11.1, Figure 1 illustrates how continental-scale warming is projected to evolve in the 21st century using the MMD models. This warming is also put into the context of the observed warming during the 20th century by comparing results from that subset of the models incorporating a representation of all known forcings with the observed evolution (see Section 9.4 for more details). Thus for the six continental regions, the figure displays: 1) the observed time series of the evolution of decadal averaged surface air temperature from 1906 to 2005 as an anomaly from the 1901 to 1950 average; 2) the range of the equivalent anomalies derived from 20th-century simulations by the MMD models that contain a full set of historical forcings; 3) the evolution of the range of this anomaly in MMD-A1B projections between 2000 and 2100; and 4) the range of the projected anomaly for the last decade of the 21st century for the B1, A1B, and A2 scenarios. For the observed part of these graphs, the decadal averages are centred on the decade boundaries (i.e., the last point is for 1996 to 2005), whereas for the future period they are centred on the decade mid-points (i.e., the first point is for 2001 to 2010). The width of the shading and the bars represents the 5 to 95% range of the model results. To construct the ranges, all simulations from the set of models involved were considered independent realisations of the possible evolution of the climate given the forcings applied. This involved 58 simulations from 14 models for the observed period and 47 simulations from 18 models for the future. Important in this representation is that the models' estimate of natural climate variability is included and thus the ranges include both the potential mitigating and amplifying effects of variability on the underlying signal. In contrast, the bars representing the range of projected change at the end of the century are constructed from ensemble mean changes from the models and thus provide a measure of the forced response. These bars were constructed from decadal mean anomalies from 21 models using A1B scenario forcings, from the 20 of these models that used the B1 forcings and the 17 that used the A2 forcings. The bars for the B1 and A2 scenarios were scaled to approximate ranges for the full set of models. The scaling factor for B1 was derived from the ratio between its range and the A1B range of the corresponding 20 models. The same procedure was used to obtain the A2 scaling factor. Only 18 models were used to display the ranges of projected temperature evolution as the control simulations for the other 3 had a drift of $>0.2^{\circ}\text{C}$ per century, which precludes clearly defining the decadal anomalies from these models. However, anomalies from all 21 models were included in calculating the bars in order to provide the fullest possible representation of projected changes in the MMD. Comparison of these different representations shows that the main messages from the MMD about projected continental temperature change are insensitive to the choices made. Finally, results are not shown here for Antarctica because the observational record is not long enough to provide the relevant information for the first part of the 20th century. Results of a similar nature to those shown here using the observations that are available are presented in Section 11.8. *(continued)*

Box 11.1, Figure 1. Temperature anomalies with respect to 1901 to 1950 for six continental-scale regions for 1906 to 2005 (black line) and as simulated (red envelope) by MMD models incorporating known forcings; and as projected for 2001 to 2100 by MMD models for the A1B scenario (orange envelope). The bars at the end of the orange envelope represent the range of projected changes for 2091 to 2100 for the B1 scenario (blue), the A1B scenario (orange) and the A2 scenario (red). The black line is dashed where observations are present for less than 50% of the area in the decade concerned. More details on the construction of these figures are given in Section 11.1.2.



Box 11.1, Figure 2 serves to illustrate some of the more significant hydrological changes, with the two panels corresponding to DJF and JJA. The backdrop to these figures is the fraction of the AOGCMs (out of the 21 considered for this purpose) that predict an increase in mean precipitation in that grid cell (using the A1B scenario and comparing the period 2080 to 2099 with the control period 1980 to 1999). Aspects of this pattern are examined more closely in the separate regional discussions.

Robust findings on regional climate change for mean and extreme precipitation, drought and snow are highlighted in the figure with further detail in the accompanying notes. (continued)



Box 11.1, Figure 2. Robust findings on regional climate change for mean and extreme precipitation, drought, and snow. This regional assessment is based upon AOGCM based studies, Regional Climate Models, statistical downscaling and process understanding. More detail on these findings may be found in the notes below, and their full description, including sources is given in the text. The background map indicates the degree of consistency between AR4 AOGCM simulations (21 simulations used) in the direction of simulated precipitation change.

- (1) Very likely annual mean increase in most of northern Europe and the Arctic (largest in cold season), Canada, and the North-East USA; and winter (DJF) mean increase in Northern Asia and the Tibetan Plateau.
- (2) Very likely annual mean decrease in most of the Mediterranean area, and winter (JJA) decrease in southwestern Australia.
- (3) Likely annual mean increase in tropical and East Africa, Northern Pacific, the northern Indian Ocean, the South Pacific (slight, mainly equatorial regions), the west of the South Island of New Zealand, Antarctica and winter (JJA) increase in Tierra del Fuego.
- (4) Likely annual mean decrease in and along the southern Andes, summer (DJF) decrease in eastern French Polynesia, winter (JJA) decrease for Southern Africa and in the vicinity of Mauritius, and winter and spring decrease in southern Australia.
- (5) Likely annual mean decrease in North Africa, northern Sahara, Central America (and in the vicinity of the Greater Antilles in JJA) and in South-West USA.
- (6) Likely summer (JJA) mean increase in Northern Asia, East Asia, South Asia and most of Southeast Asia, and likely winter (DJF) increase in East Asia.
- (7) Likely summer (DJF) mean increase in southern Southeast Asia and southeastern South America
- (8) Likely summer (JJA) mean decrease in Central Asia, Central Europe and Southern Canada.
- (9) Likely winter (DJF) mean increase in central Europe, and southern Canada
- (10) Likely increase in extremes of daily precipitation in northern Europe, South Asia, East Asia, Australia and New Zealand.
- (11) Likely increase in risk of drought in Australia and eastern New Zealand; the Mediterranean, central Europe (summer drought); in Central America (boreal spring and dry periods of the annual cycle).
- (12) Very likely decrease in snow season length and likely to very likely decrease in snow depth in most of Europe and North America.

models. The results are shown in Table 11.1 only when 14 out of the 21 models agree as to the sign of the change in frequency of extremes. For example, in Central North America (CNA), 15% of the summers in 2080 to 2099 in the A1B scenario are projected to be extremely dry, corresponding to a factor of three increase in the frequency of these events. In contrast, in many regions and seasons, the frequency of extreme warmth is 100%, implying that all seasons in 2080 to 2099 are warmer than the warmest season in 1980 to 1999, according to every model in this ensemble.

In each continental section, a figure is provided summarising the temperature and precipitation responses in the MMD-A1B projection for the last two decades of the 21st century. These figures portray a multi-model mean comprising individual models or model ensemble means where ensembles exist. Also shown is the simple statistic of the number of these models that show agreement in the sign of the precipitation change. The annual mean temperature and precipitation responses in each of the 21 separate AOGCMs are provided in Supplementary Material Figures S11.5 to 11.12 and S11.13 to 11.20, respectively.

Recent explorations of multi-model ensemble projections seek to develop probabilistic estimates of uncertainties and are provided in the Supplementary Material Table S11.2. This information is based on the approach of Tebaldi et al. (2004a,b; see also section 11.10.2).

11.1.3 Some Unifying Themes

The basic pattern of the projected warming as described in Chapter 10 is little changed from previous assessments. Examining the spread across the MMD models, temperature projections in many regions are strongly correlated with the global mean projections, with the most sensitive models in global mean temperature often the most sensitive locally. Differing treatments of regional processes and the dynamical interactions between a given region and the rest of the climate system are responsible for some spread. However, a substantial part of the spread in regional temperature projections is due to differences in the sum of the feedbacks that control transient climate sensitivity (see also Chapter 10).

The response of the hydrological cycle is controlled in part by fundamental consequences of warmer temperatures and the increase in water vapour in the atmosphere (Chapter 3). Water is transported horizontally by the atmosphere from regions of moisture divergence (particularly in the subtropics) to regions of convergence. Even if the circulation does not change, these transports will increase due to the increase in water vapour. The consequences of this increased moisture transport can be seen in the global response of precipitation, described in Chapter 10, where, on average, precipitation increases in the inter-tropical convergence zones, decreases in the subtropics, and increases in subpolar and polar regions. Over North America and Europe, the pattern of subpolar moistening and subtropical

drying dominates the 21st-century projections. This pattern is also described in Section 9.5.4, which assesses the extent to which this pattern is visible over land during the 20th century in precipitation observations and model simulations. Regions of large uncertainty often lie near the boundaries between these robust moistening and drying regions, with boundaries placed differently by each model.

High-resolution model results indicate that in regions with strong orographic forcing, some of these large-scale findings can be considerably altered locally. In some cases, this may result in changes in the opposite direction to the more general large-scale behaviour. In addition, large-area and grid-box average projections for precipitation are often very different from local changes within the area (Good and Lowe, 2006). These issues demonstrate the inadequacy of inferring the behaviour at fine scales from that of large-area averages.

Another important theme in the 21st-century projections is the poleward expansion of the subtropical highs, and the poleward displacement of the mid-latitude westerlies and associated storm tracks. This circulation response is often referred to as an enhanced positive phase of the Northern or Southern Annular Mode, or when focusing on the North Atlantic, the positive phase of the North Atlantic Oscillation (NAO). In regions without strong orographic forcing, superposition of the tendency towards subtropical drying and poleward expansion of the subtropical highs creates especially robust drying responses at the poleward boundaries of the five subtropical oceanic high centres in the South Indian, South Atlantic, South Pacific, North Atlantic and, less robustly, the North Pacific (where a tendency towards El-Niño like conditions in the Pacific in the models tends to counteract this expansion). Most of the regional projections of strong drying tendencies over land in the 21st century are immediately downstream of these centres (south-western Australia, the Western Cape Provinces of South Africa, the southern Andes, the Mediterranean and Mexico). The robustness of this large-scale circulation signal is discussed in Chapter 10, while Chapters 3, 8 and 9 describe the observed poleward shifts in the late 20th century and the ability of models to simulate these shifts.

The retreats of snow and ice cover are important for local climates. The difficulty of quantifying these effects in regions of substantial topographic relief is a significant limitation of global models (see Section 11.4.3.2, Box 11.3) and is improved with dynamical and statistical downscaling. The drying effect of an earlier spring snowmelt and, more generally, the earlier reduction in soil moisture (Manabe and Wetherald, 1987) is a continuing theme in discussion of summer continental climates.

The strong interactions between sea surface temperature gradients and tropical rainfall variability provides an important unifying theme for tropical climates. Models can differ in their projections of small changes in tropical ocean temperature gradients and in the simulation of the potentially large shifts in rainfall that are related to these oceanic changes. Chou and Neelin (2004) provide a guide to some of the complexity

involved in diagnosing and evaluating hydrological responses in the tropics. With a few exceptions, the spread in projections of hydrological changes is still too large to make strong statements about the future of tropical climates at regional scales (see also Section 10.3). Many AOGCMs project large tropical precipitation changes, so uncertainty as to the regional pattern of these changes should not be taken as evidence that these changes are likely to be small.

Assessments of the regional and sub-regional climate change projections have primarily been based on the AOGCM projections summarised in Table 11.1 and an analysis of the biases in the AOGCM simulations, regional downscaling studies available for some regions with either physical or statistical models or both, and reference to plausible physical mechanisms.

To assist the reader in placing the various regional assessments in a global context, Box 11.1 displays many of the detailed assessments documented in the following regional sections. Likewise, an overview of projected changes in various types of extreme weather statistics is summarised in Table 11.2, which contains information from the assessments within this chapter and from Chapter 10. Thus, the details of the assessment that lead to each individual statement can all be found in either Chapter 10, or the respective regional sections, and links for each statement are identifiable from Table 11.2.

Table 11.2. Projected changes in climate extremes. This table summarises key phenomena for which there is confidence in the direction of projected change based on the current scientific evidence. The included phenomena are those where confidence ranges between medium and very likely, and are listed with the notation of VL (very likely), L (likely), and M (medium confidence). maxTmax refers to the highest maximum temperature, maxTmin to the highest minimum temperature, minTmax to the lowest maximum temperature, and minTmin to the lowest minimum temperature. In addition to changes listed in the table, there are two phenomena of note for which there is little confidence. The issue of drying and associated risk of drought in the Sahel remains uncertain as discussed in Section 11.2.4.2. The change in mean duration of tropical cyclones cannot be assessed with confidence at this stage due to insufficient studies.

Temperature-Related Phenomena	
Change in phenomenon	Projected changes
Higher monthly absolute maximum of daily maximum temperatures (maxTmax) more hot / warm summer days	<p>VL (consistent across model projections) maxTmax increases at same rate as the mean or median¹ over northern Europe,² Australia and New Zealand³</p> <p>L (fairly consistent across models, but sensitivity to land surface treatment) maxTmax increases more than the median over southern and central Europe,⁴ and southwest USA⁵</p> <p>L (consistent with projected large increase in mean temperature) Large increase in probability of extreme warm seasons over most parts of the world⁶</p>
Longer duration, more intense, more frequent heat waves / hot spells in summer	<p>VL (consistent across model projections) Over almost all continents⁷, but particularly central Europe,⁸ western USA,⁹ East Asia¹⁰ and Korea¹¹</p>
Higher monthly absolute maximum of daily minimum temperatures (maxTmin); more warm and fewer cold nights	<p>VL (consistent with higher mean temperatures) Over most continents¹²</p>
Higher monthly absolute minimum of daily minimum temperatures (minTmin)	<p>VL (consistent across model projections) minTmin increases more than the mean in many mid- and high-latitude locations,¹³ particularly in winter over most of Europe except the southwest¹⁴</p>
Higher monthly absolute minimum of daily maximum temperatures (minTmax), fewer cold days	<p>L (consistent with warmer mean temperatures) minTmin increases more than the mean in some areas¹⁵</p>
Fewer frost days	<p>VL (consistent across model projections) Decrease in number of days with below-freezing temperatures everywhere¹⁶</p>
Fewer cold outbreaks; fewer, shorter, less intense cold spells / cold extremes in winter	<p>VL (consistent across model projections) Northern Europe, South Asia, East Asia¹⁷</p> <p>L (consistent with warmer mean temperatures) Most other regions¹⁸</p>
Reduced diurnal temperature range	<p>L (consistent across model projections) Over most continental regions, night temperatures increase faster than the day temperatures¹⁹</p>
Temperature variability on interannual and daily time scales	<p>L (general consensus across model projections) Reduced in winter over most of Europe²⁰ Increase in central Europe in summer²¹</p>

¹ Kharin and Zwiers (2005)

² §11.3.3.3, Supplementary Material Figure S11.23, PRUDENCE, Kjellström et al. (2007)

³ §11.7.3.5, CSIRO (2001)

⁴ §11.3.3.3, PRUDENCE, Kjellström et al. (2007)

⁵ §11.5.3.3, Bell et al. (2004),

⁶ Table 11.1

⁷ §11.3.3.3, Tebaldi et al. (2006), Meehl and Tebaldi (2004)

⁸ §11.5.3.3, Barnett et al. (2006), Clark et al. (2006), Tebaldi et al. (2006), Gregory and Mitchell (1995), Zwiers and Kharin (1998), Hegerl et al. (2004), Meehl and Tebaldi (2004)

⁹ §11.5.3.3, Bell et al. (2004), Leung et al. (2004)

¹⁰ §11.4.3.2, Gao et al. (2002)

¹¹ §11.4.3.2, Kwon et al. (2005), Boo et al. (2006)

¹² §11.3.3.2, §11.4.3.1

¹³ Kharin and Zwiers (2005)

¹⁴ §11.3.3.2, Fig. 11.3.3.3, PRUDENCE

¹⁵ §11.7.3.5, Whetton et al. (2002)

¹⁶ Tebaldi et al. (2006), Meehl and Tebaldi (2004), §11.3.3.2, PRUDENCE, §11.7.3.1, CSIRO (2001), Mullan et al. (2001b)

¹⁷ §11.3.3.2, PRUDENCE, Kjellström et al. (2007), §11.4.3.2, Gao et al. (2002), Rupa Kumar et al. (2006)

¹⁸ §11.1.3

¹⁹ §11.5.3.3, Bell et al. (2004), Leung et al. (2004), §11.4.3.2, Rupa Kumar et al. (2006), Mizuta et al. (2005)

²⁰ §11.3.3.2, Räisänen (2001), Räisänen and Alexandersson (2003), Giorgi and Bi (2005), Zwiers and Kharin (1998), Hegerl et al. (2004), Kjellström et al. (2007)

²¹ §11.3.3.2, PRUDENCE, Schär et al. (2004), Vidale et al. (2007)

Table 11.2. (continued)

Moisture-Related Phenomena	
Phenomenon	Projected changes
Intense precipitation events	<p>VL (consistent across model projections; empirical evidence, generally higher precipitation extremes in warmer climates) Much larger increase in the frequency than in the magnitude of precipitation extremes over most land areas in middle latitudes,²² particularly over northern Europe,²³ Australia and New Zealand²⁴ Large increase during the Indian summer monsoon season over Arabian Sea, tropical Indian Ocean, South Asia²⁵ Increase in summer over south China, Korea and Japan²⁶</p>
Intense precipitation events	<p>L (some inconsistencies across model projections) Increase over central Europe in winter²⁷ Increase associated with tropical cyclones over Southeast Asia, Japan²⁸ Uncertain Changes in summer over Mediterranean and central Europe²⁹ L decrease (consistent across model projections) Iberian Peninsula³⁰</p>
Wet days	<p>L (consistent across model projections) Increase in number of days at high latitudes in winter, and over northwest China³¹ Increase over the Inter-Tropical Convergence Zone³² Decrease in South Asia³³ and the Mediterranean area³⁴</p>
Dry spells (periods of consecutive dry days)	<p>VL (consistent across model projections) Increase in length and frequency over the Mediterranean area³⁵, southern areas of Australia, New Zealand³⁶ L (consistent across model projections) Increase in most subtropical areas³⁷ Little change over northern Europe³⁸</p>
Continental drying and associated risk of drought	<p>L (consistent across model projections; consistent change in precipitation minus evaporation, but sensitivity to formulation of land surface processes) Increased in summer over many mid-latitude continental interiors, e.g., central³⁹ and southern Europe, Mediterranean area,⁴⁰ in boreal spring and dry periods of the annual cycle over Central America⁴¹</p>

²² §11.3.3.4, Groisman et al. (2005), Kharin and Zwiers (2005), Hegerl et al. (2004), Semenov and Bengtsson (2002), Meehl et al. (2006)

²³ §11.3.3.4, Räisänen (2002), Giorgi and Bi (2005), Räisänen (2005)

²⁴ §11.1.3, §11.7.3.2, §11.3.3.4, Huntingford et al. (2003), Barnett et al. (2006), Frei et al. (2006), Hennessy et al. (1997), Whetton et al. (2002), Watterson and Dix (2003), Suppiah et al. (2004), McInnes et al. (2003), Hennessy et al. (2004b), Abbs (2004), Semenov and Bengtsson (2002)

²⁵ §11.4.3.2, May (2004a), Rupa Kumar et al. (2006)

²⁶ §11.4.3.2, Gao et al. (2002), Boo et al. (2006), Kimoto et al. (2005), Kitoh et al. (2005), Mizuta et al. (2005)

²⁷ §11.3.3.4, PRUDENCE, Frei et al. (2006), Christensen and Christensen (2003, 2004)

²⁸ §11.1.3, §11.4.3.2, Kimoto et al. (2005), Mizuta et al. (2005), Hasegawa and Emori (2005), Kanada et al. (2005)

²⁹ §11.3.3.4, PRUDENCE, Frei et al. (2006), Christensen and Christensen (2004), Tebaldi et al. (2006)

³⁰ §11.3.3.4, PRUDENCE, Frei et al. (2006)

³¹ §11.4.3.2, Gao et al. (2002), Hasegawa and Emori (2005)

³² Semenov and Bengtsson (2002)

³³ §11.4.3.2 Krishna Kumar et al. (2003)

³⁴ §11.3.3.4, Semenov and Bengtsson (2002), Voss et al. (2002); Räisänen et al. (2004); Frei et al. (2006)

³⁵ §11.3.3.4, Semenov and Bengtsson, 2002; Voss et al., 2002; Hegerl et al., 2004; Wehner, 2004; Kharin and Zwiers, 2005; Tebaldi et al., 2006

³⁶ §11.1.3, §11.7.3.2, §11.7.3.4, Whetton and Suppiah (2003), McInnes et al. (2003), Walsh et al. (2002), Hennessy et al. (2004c), Mullan et al. (2005)

³⁷ §11.1.3

³⁸ §11.3.3.4, Beniston et al. (2007), Tebaldi et al. (2006), Voss et al. (2002)

³⁹ §11.3.3.2, Rowell and Jones (2006)

⁴⁰ §11.1.3, §11.3.3.4, Voss et al. (2002)

⁴¹ §11.1.3

Table 11.2. (continued)

Tropical Cyclones (typhoons and hurricanes)	
Change in phenomenon	Projected changes
Increase in peak wind intensities	L (high-resolution Atmospheric GCM (AGCM) and embedded hurricane model projections) Over most tropical cyclone areas ⁴²
Increase in mean and peak precipitation intensities	L (high-resolution AGCM projections and embedded hurricane model projections) Over most tropical cyclone areas, ⁴³ South, ⁴⁴ East ⁴⁵ and southeast Asia ⁴⁶
Changes in frequency of occurrence	M (some high-resolution AGCM projections) Decrease in number of weak storms, increase in number of strong storms ⁴⁷ M (several climate model projections) Globally averaged decrease in number, but specific regional changes dependent on sea surface temperature change ⁴⁸ Possible increase over the North Atlantic ⁴⁹
Extratropical Cyclones	
Change in phenomenon	Projected changes
Changes in frequency and position	L (consistent in AOGCM projections) Decrease in the total number of extratropical cyclones ⁵⁰ Slight poleward shift of storm track and associated precipitation, particularly in winter ⁵¹
Change in storm intensity and winds	L (consistent in most AOGCM projections, but not explicitly analysed for all models) Increased number of intense cyclones ⁵² and associated strong winds, particularly in winter over the North Atlantic, ⁵³ central Europe ⁵⁴ and Southern Island of New Zealand ⁵⁵ More likely than not Increased windiness in northern Europe and reduced windiness in Mediterranean Europe ⁵⁶
Increased wave height	L (based on projected changes in extratropical storms) Increased occurrence of high waves in most mid-latitude areas analysed, particularly the North Sea ⁵⁷

⁴² Knutson and Tuleya (2004)⁴³ Knutson and Tuleya (2004)⁴⁴ §11.4.3.2, Unnikrishnan et al. (2006)⁴⁵ §11.3.4, Hasegawa and Emori (2005)⁴⁶ §11.3.4, Hasegawa and Emori (2005), Knutson and Tuleya (2004)⁴⁷ Oouchi et al. (2006)⁴⁸ Hasegawa and Emori (2005)⁴⁹ Sugi et al. (2002), Oouchi et al. (2006)⁵⁰ §11.3.3.6, Yin (2005), Lambert and Fyfe (2006), §11.3.3.5, Lionello et al. (2002), Leckebusch et al. (2006), Vérant (2004), Somot (2005)⁵¹ §11.1.3, Yin (2005), Lambert and Fyfe (2006)⁵² §11.1.2, §11.3.3.5, Yin (2005), Lambert and Fyfe (2006)⁵³ §11.3.3.5, Leckebusch and Ulbrich (2004)⁵⁴ §11.3.3.5, Zwiers and Kharin (1998), Knippertz et al. (2000), Leckebusch and Ulbrich (2004), Pryor et al. (2005a), Lionello et al. (2002), Leckebusch et al. (2006), Vérant (2004), Somot (2005)⁵⁵ §11.1.3, §11.7.3.7⁵⁶ §11.3.3.5, Lionello et al. (2002), Leckebusch et al. (2006), Vérant (2004), Somot (2005)⁵⁷ X.L. Wang et al. (2004)

Frequently Asked Question 11.1

Do Projected Changes in Climate Vary from Region to Region?

Climate varies from region to region. This variation is driven by the uneven distribution of solar heating, the individual responses of the atmosphere, oceans and land surface, the interactions between these, and the physical characteristics of the regions. The perturbations of the atmospheric constituents that lead to global changes affect certain aspects of these complex interactions. Some human-induced factors that affect climate ('forcings') are global in nature, while others differ from one region to another. For example, carbon dioxide, which causes warming, is distributed evenly around the globe, regardless of where the emissions originate, whereas sulphate aerosols (small particles) that offset some of the warming tend to be regional in their distribution. Furthermore, the response to forcings is partly governed by feedback processes that may operate in different regions from those in which the forcing is greatest. Thus, the projected changes in climate will also vary from region to region.

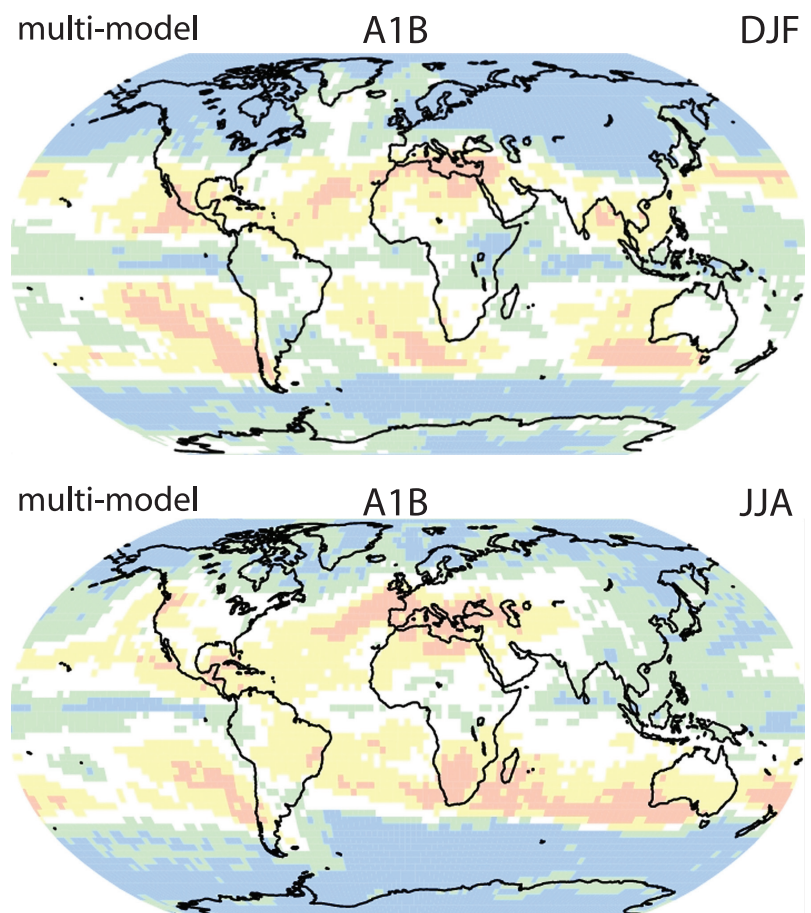
Latitude is a good starting point for considering how changes in climate will affect a region. For example, while warming is expected everywhere on Earth, the amount of projected warming generally increases from the tropics to the poles in the Northern Hemisphere. Precipitation is more complex, but also has some latitude-dependent features. At latitudes adjacent to the polar regions, precipitation is projected to increase, while decreases are projected in many regions adjacent to the tropics (see Figure 1). Increases in tropical precipitation are projected during rainy seasons (e.g., monsoons), and over the tropical Pacific in particular.

Location with respect to oceans and mountain ranges is also an important factor. Generally, the interiors of continents are projected to warm more than the coastal areas. Precipitation responses are especially sensitive not only to the continental geometry, but to the shape of nearby mountain ranges and wind flow direction. Monsoons, extratropical cyclones and hurricanes/typhoons are all influenced in different ways by these region-specific features.

Some of the most difficult aspects of understanding and projecting changes in regional climate relate to possible changes in the circulation of the atmosphere and oceans, and their patterns of variability. Although general statements covering a variety of regions with

qualitatively similar climates can be made in some cases, nearly every region is idiosyncratic in some ways. This is true whether it is the coastal zones surrounding the subtropical Mediterranean Sea, the extreme weather in the North American interior that depends on moisture transport from the Gulf of Mexico, or the interactions between vegetation distribution, oceanic temperatures and atmospheric circulation that help control the southern limit of the Sahara Desert.

While developing an understanding of the correct balance of global and regional factors remains a challenge, the understanding of these factors is steadily growing, increasing our confidence in regional projections.



FAQ 11.1, Figure 1. Blue and green areas on the map are by the end of the century projected to experience increases in precipitation, while areas in yellow and pink are projected to have decreases. The top panel shows projections for the period covering December, January and February, while the bottom panel shows projections for the period covering June, July and August.

11.2 Africa

Assessment of projected climate changes for Africa:

All of Africa is very likely to warm during this century. The warming is very likely to be larger than the global, annual mean warming throughout the continent and in all seasons, with drier subtropical regions warming more than the moister tropics.

Annual rainfall is likely to decrease in much of Mediterranean Africa and northern Sahara, with the likelihood of a decrease in rainfall increasing as the Mediterranean coast is approached. Rainfall in southern Africa is likely to decrease in much of the winter rainfall region and on western margins. There is likely to be an increase in annual mean rainfall in East Africa. It is uncertain how rainfall in the Sahel, the Guinean Coast and the southern Sahara will evolve in this century.

The MMD models have significant systematic errors in and around Africa (excessive rainfall in the south, southward displacement of the Atlantic Inter-Tropical Convergence Zone (ITCZ), insufficient upwelling off the West Coast) making it difficult to assess the consequences for climate projections. The absence of realistic variability in the Sahel in most 20th-century simulations casts some doubt on the reliability of coupled models in this region. Vegetation feedbacks and feedbacks from dust aerosol production are not included in the global models. Possible future land surface modification is also not taken into account in the projections. The extent to which current regional models can successfully downscale precipitation over Africa is unclear, and limitations of empirical downscaling results for Africa are not fully understood. There is insufficient information on which to assess possible changes in the spatial distribution and frequency of tropical cyclones affecting Africa.

11.2.1 Key Processes

The bulk of the African continent is tropical or subtropical with the central phenomenon being the seasonal migration of the tropical rain belts. Small shifts in the position of these rain belts result in large local changes in rainfall. There are also regions on the northern and southern boundaries of the continent with winter rainfall regimes governed by the passage of mid-latitude fronts, which are therefore sensitive to a poleward displacement of the storm tracks. This is evident from the correlation between South African rainfall and the Southern Annular Mode (Reason and Rouault, 2005) and between North African rainfall and the NAO (Lamb and Pepler, 1987). Troughs penetrating into the tropics from mid-latitudes also influence warm season rainfall, especially in southern Africa, and can contribute to a sensitivity of warm season rains to a displacement of the circulation (Todd and Washington, 1999). Any change in tropical cyclone

distribution and intensity will affect the southeast coastal regions, including Madagascar (Reason and Keibel, 2004).

The factors that determine the southern boundary of the Sahara and rainfall in the Sahel have attracted special interest because of the extended drought experienced by this region in the 1970s and 1980s. The field has moved steadily away from explanations for rainfall variations in this region as primarily due to land use changes and towards explanations based on changes in sea surface temperatures (SSTs). The early SST perturbation Atmospheric GCM (AGCM) experiments (Palmer, 1986; Rowell, et al., 1995) are reinforced by the results from the most recent models (Giannini et al., 2003; Lu and Delworth, 2005; Hoerling et al., 2006). The north-south inter-hemispheric gradient, with colder NH oceans conducive to an equatorward shift and/or a reduction in Sahel rainfall, is important. This has created interest in the possibility that aerosol cooling localised in the NH could dry the Sahel (Rotstayn and Lohmann, 2002; see also Section 9.5.4.3.1). However, temperatures over other oceanic regions, including the Mediterranean (Rowell, 2003), are also important.

In southern Africa, changing SSTs are also thought to be more important than changing land use patterns in controlling warm season rainfall variability and trends. Evidence has been presented for strong links with Indian Ocean temperatures (Hoerling et al., 2006). The warming of the troposphere over South Africa, possibly a consequence of warming of the Indo-Pacific, has been linked with the increase in days with stable inversion layers over southern Africa (Freiman and Tyson, 2000; Tadross et al., 2005a, 2006) in the late 20th century.

In addition to the importance of ocean temperatures, vegetation patterns help shape the climatic zones throughout much of Africa (e.g., Wang and Eltahir, 2000; Maynard and Royer, 2004a; Paeth and Henre, 2004; see also Section 11.7, Box 11.4). In the past, land surface changes have primarily acted as feedbacks generated by the underlying response to SST anomalies, and vegetation changes are thought to provide a positive feedback to climate change. The plausibility of this positive feedback is enhanced by recent work suggesting that land surface feedbacks may also play an important role in both intra-seasonal variability and rainy season onset in southern Africa (New et al., 2003; Anyah and Semazzi, 2004; Tadross et al., 2005a,b).

The MMD models prescribe vegetation cover; they would likely respond more strongly to large-scale forcing if they predicted vegetation, especially in semi-arid areas. The possibility of multiple stable modes of African climate due to vegetation-climate interactions has been raised, especially in the context of discussions of the very wet Sahara during the mid-Holocene 6 to 8 ka (Claussen et al., 1999; Foley et al., 2003). One implication is that centennial time-scale feedbacks associated with vegetation patterns may have the potential to make climate changes over Africa less reversible.

11.2.2 Skill of Models in Simulating Present and Past Climates

There are biases in the simulations of African climate that are systematic across the MMD models, with 90% of models overestimating precipitation in southern Africa, by more than 20% on average (and in some cases by as much as 80%) over a wide area often extending into equatorial Africa. The temperature biases over land are not considered large enough to directly affect the credibility of the model projections (see Supplementary Material Figure S11.21 and Table S11.1).

The ITCZ in the Atlantic is displaced equatorward in nearly all of these AOGCM simulations. Ocean temperatures are too warm by an average of 1°C to 2°C in the Gulf of Guinea and typically by 3°C off the southwest coast in the region of intense upwelling, which is clearly too weak in many models. In several of the models there is no West African monsoon as the summer rains fail to move from the Gulf onto land, but most of the models do have a monsoonal climate albeit with some distortion. Moderately realistic interannual variability of SSTs in the Gulf of Guinea and the associated dipolar rainfall variations in the Sahel and the Guinean Coast are, by the criteria of Cook and Vizy (2006), only present in 4 of the 18 models examined. Tennant (2003) describes biases in several AGCMs, such as the equatorward displacement of the mid-latitude jet in austral summer, a deficiency that persists in the most recent simulations (Chapter 8).

Despite these deficiencies, AGCMs can simulate the basic pattern of rainfall trends in the second half of the 20th century if given the observed SST evolution as boundary conditions, as described in the multi-model analysis of Hoerling et al. (2006) and the growing literature on the interannual variability and trends in individual models (e.g., Rowell et al., 1995; Bader and Latif, 2003; Giannini et al., 2003; Haarsma et al., 2005; Kamga et al., 2005; Lu and Delworth, 2005). However, there is less confidence in the ability of AOGCMs to generate interannual variability in the SSTs of the type known to affect African rainfall, as evidenced by the fact that very few AOGCMs produce droughts comparable in magnitude to the Sahel drought of the 1970s and 1980s (Hoerling et al., 2006). There are exceptions, but what distinguishes these from the bulk of the models is not understood.

The very wet Sahara 6 to 8 ka is thought to have been a response to the increased summer insolation due to changes in the Earth's orbital configuration. Modelling studies of this response provide background information on the quality of a model's African monsoon, but the processes controlling the response to changing seasonal insolation may be different from those controlling the response to increasing greenhouse gases. The fact that GCMs have difficulty in simulating the full magnitude of the mid-Holocene wet period, especially in the absence of vegetation feedbacks, may indicate a lack of sensitivity to other kinds of forcing (Jolly et al., 1996; Kutzbach et al., 1996).

Regional climate modelling has mostly focused on southern Africa, where the models generally improve on the climate

simulated by global models but also share some of the biases in the global models. For example, Engelbrecht et al. (2002) and Arnell et al. (2003) both simulate excessive rainfall in parts of southern Africa, reminiscent of the bias in the MMD. Hewitson et al. (2004) and Tadross et al. (2006) note strong sensitivity to the choice of convective parametrization, and to changes in soil moisture and vegetative cover (New et al., 2003; Tadross et al., 2005a), reinforcing the view (Rowell et al., 1995) that land surface feedbacks enhance regional climate sensitivity over Africa's semi-arid regions. Over West Africa, the number of Regional Climate Model (RCM) investigations is even more limited (Jenkins et al., 2002; Vizy and Cook, 2002). The quality of the 25-year simulation undertaken by Paeth et al. (2005) is encouraging, emphasizing the role of regional SSTs and changes in the land surface in forcing West African rainfall anomalies. Several recent AGCM time-slice simulations focusing on tropical Africa show good simulation of the rainy season (Coppola and Giorgi, 2005; Caminade et al., 2006; Oouchi et al., 2006).

Hewitson and Crane (2005) developed empirical downscaling for point-scale precipitation at sites spanning the continent, as well as a 0.1° resolution grid over South Africa. The downscaled precipitation forced by reanalysis data provides a close match to the historical climate record, including regions such as the eastern escarpment of the sub-continent that have proven difficult for RCMs.

11.2.3 Climate Projections

11.2.3.1 Mean Temperature

The differences in near-surface temperature between the years 2080 to 2099 and the years 1980 to 1999 in the MMD-A1B projections, averaged over the West African (WAF), East African (EAF), South African (SAF) and Saharan (SAH) sub-regions, are provided in Table 11.1, with the temporal evolution displayed in Figure 11.1. The Mediterranean coast is discussed together with southern Europe in Section 11.3. In all four regions and in all seasons, the median temperature increase lies between 3°C and 4°C, roughly 1.5 times the global mean response. Half of the models project warming within about 0.5°C of these median values. The distributions estimated by Tebaldi et al. (2004a,b; see also Supplementary Material Table S11.2) have a very similar half-width, but reduce the likelihood of the extreme high limit as compared to the raw quartiles in Table 11.1. There is a strong correlation across these AOGCMs between the global mean temperature response and the response in Africa. The signal-to-noise ratio is very large for these 20-year mean temperatures and 10 years is typically adequate to obtain a clearly discernible signal, as defined in Section 11.1.2. Regionally averaged temperatures averaged over the period 1990 to 2009 are clearly discernible from the 1980 to 1999 averages.

The upper panels in Figure 11.2 show the geographical structure of the ensemble-mean projected warming for the A1B scenario in more detail. Smaller values of projected warming, near 3°C, are found in equatorial and coastal areas and larger

values, above 4°C, in the western Sahara. The largest temperature responses in North Africa are projected to occur in JJA, while the largest responses in southern Africa occur in September, October and November (SON). But the seasonal structure in the temperature response over Africa is modest as compared to extratropical regions. The basic pattern of projected warming has been robust to changes in models since the TAR, as indicated by comparison with Hulme et al. (2001).

To date there is insufficient evidence from RCMs to modify the large-scale temperature projections from GCMs, although Tadross et al. (2005a) project changes in the A2 scenario for southern Africa that are lower than those in the forcing GCM and near the low end of the spread in the MMD models, likely due to a weaker drying tendency than in most of the global models.

11.2.3.2 Mean Precipitation

Figure 11.2 and Table 11.1 illustrate some of the robust aspects of the precipitation response over Africa in the MMD-A1B projections. The fractional changes in annual mean precipitation in each of the 21 models are provided in Supplementary Material Figure S11.13. With respect to the most robust features (drying in the Mediterranean and much of southern Africa, and increases in rainfall in East Africa), there is qualitative agreement with the results in Hulme et al. (2001) and Ruosteenoja et al. (2003), which summarise results from the models available at the time of the TAR.

The large-scale picture is one of drying in much of the subtropics and an increase (or little change) in precipitation in the tropics, increasing the rainfall gradients. This is a plausible hydrological response to a warmer atmosphere, a consequence of the increase in water vapour and the resulting increase in vapour transport in the atmosphere from regions of moisture divergence to regions of moisture convergence (see Chapter 9 and Section 11.2.1).

The drying along Africa's Mediterranean coast is a component of a larger-scale drying pattern surrounding the Mediterranean and is discussed further in the section on Europe (Section 11.3). A 20% drying in the annual mean is typical along the African Mediterranean coast in A1B by the end of the 21st century. Drying is seen throughout the year and is generated by nearly every MMD model. The drying signal in this composite

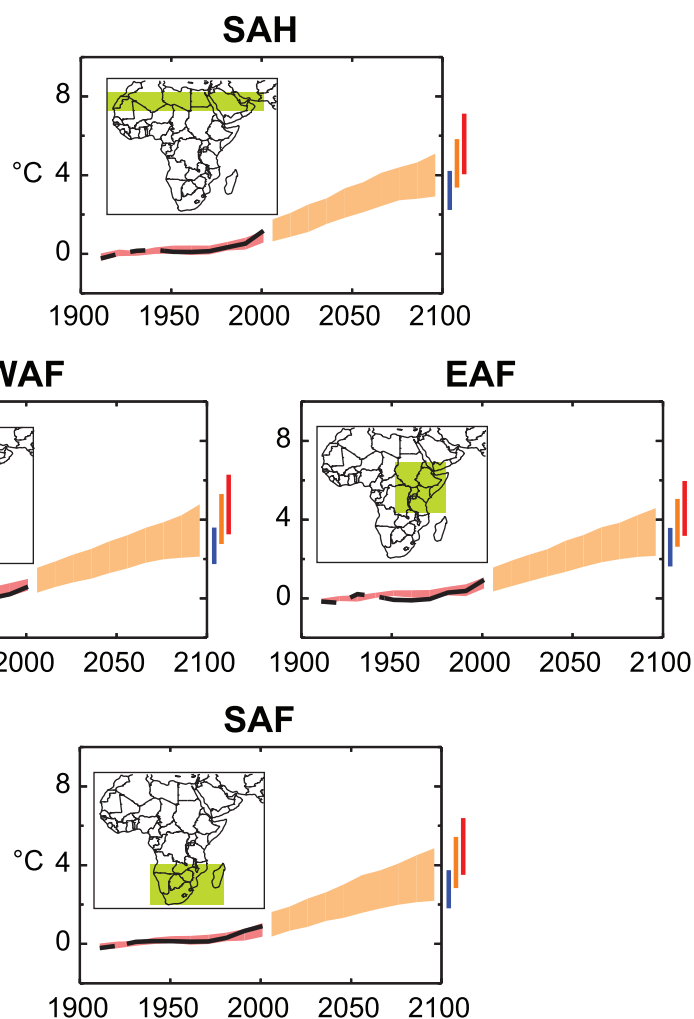


Figure 11.1. Temperature anomalies with respect to 1901 to 1950 for four African land regions for 1906 to 2005 (black line) and as simulated (red envelope) by MMD models incorporating known forcings; and as projected for 2001 to 2100 by MMD models for the A1B scenario (orange envelope). The bars at the end of the orange envelope represent the range of projected changes for 2091 to 2100 for the B1 scenario (blue), the A1B scenario (orange) and the A2 scenario (red). The black line is dashed where observations are present for less than 50% of the area in the decade concerned. More details on the construction of these figures are given in Box 11.1 and Section 11.1.2.

extends into the northern Sahara, and down the West Coast as far as 15°N. The processes involved include increased moisture divergence and a systematic poleward shift of the storm tracks affecting the winter rains, with positive feedback from decreasing soil moisture in summer (see Section 11.3).

In southern Africa, a similar set of processes produces drying that is especially robust in the extreme southwest in winter, a manifestation of a much broader-scale poleward shift in the circulation across the South Atlantic and Indian Oceans. However, the drying is subject to the caveat that strong orographic forcing may result in locally different changes (as discussed in Section 11.4.3.2, Box 11.3). With the exception of the winter rainfall region in the southwest, the robust drying in winter corresponds to the dry season over most of the sub-continent and does not contribute to the bulk of the annual mean

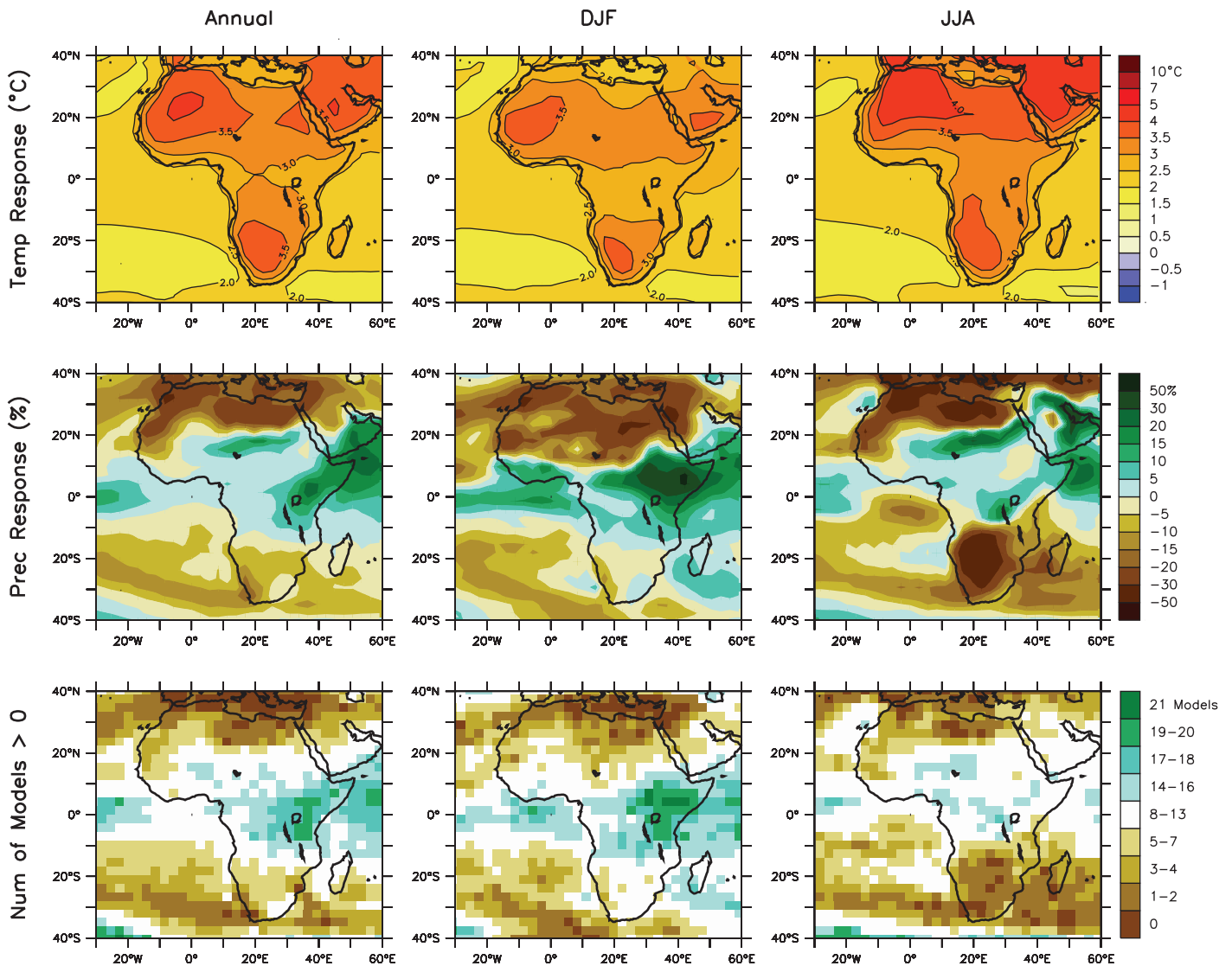


Figure 11.2. Temperature and precipitation changes over Africa from the MMD-A1B simulations. Top row: Annual mean, DJF and JJA temperature change between 1980 to 1999 and 2080 to 2099, averaged over 21 models. Middle row: same as top, but for fractional change in precipitation. Bottom row: number of models out of 21 that project increases in precipitation.

drying. More than half of the annual mean reduction occurs in the spring and is mirrored in some RCM simulations for this region (see below). To an extent, this can be thought of as a delay in the onset of the rainy season. This spring drying suppresses evaporation, contributing to the spring maximum in the temperature response.

The increase in rainfall in East Africa, extending into the Horn of Africa, is also robust across the ensemble of models, with 18 of 21 models projecting an increase in the core of this region, east of the Great Lakes. This East African increase is also evident in Hulme et al. (2001) and Ruosteenoja et al. (2003). The Guinean coastal rain belts and the Sahel do not show as robust a response. A straight average across the ensemble results in modest moistening in the Sahel with little change on the Guinean coast. The composite MMD simulations have a weak drying trend in the Sahel in the 20th century that does

not continue in the future projections (Biasutti and Giannini, 2006; Hoerling, et al., 2006), implying that the weak 20th-century drying trend in the composite 20th-century simulations is unlikely to be forced by greenhouse gases, but is more likely forced by aerosols, as in Rotstayn and Lohmann (2002), or a result of low-frequency internal variability of the climate.

Individual models generate large, but disparate, responses in the Sahel. Two outliers are GFDL/CM2.1, which projects very strong drying in the Sahel and throughout the Sahara, and MIROC3.2_midres, which shows a very strong trend towards increased rainfall in the same region (see Supplementary Figure S11.13; and see Table 8.1 for model descriptions). Cook and Vizy (2006) find moderately realistic interannual variability in the Gulf of Guinea and Sahel in both models. While the drying in the GFDL model is extreme within the ensemble, it generates a plausible simulation of 20th-century Sahel

rainfall trends (Held et al., 2005; Hoerling et al., 2006) and an empirical downscaling from AOGCMs (Hewitson and Crane, 2006) shows a similar response (see below). More research is needed to understand the variety of modelled precipitation responses in the Sahel and elsewhere in the tropics. Progress is being made in developing new methodologies for this purpose (e.g., Chou and Neelin, 2004; Lintner and Chiang, 2005; Chou et al., 2007), leading to better appreciation of the sources of model differences. Haarsma et al. (2005) describe a plausible mechanism associated with increasing land-ocean temperature contrast and decreasing surface pressures over the Sahara, which contributes to the increase in Sahel precipitation with warming in some models.

It has been argued (e.g., Paeth and Hense, 2004) that the partial amelioration of the Sahel drought since the 1990s may be a sign of a greenhouse-gas driven increase in rainfall,

providing support for those models that moisten the Sahel into the 21st century (e.g., Maynard et al., 2002; Haarsma et al., 2005; Kamga et al., 2005). However, it is premature to take this partial amelioration as evidence of a global warming signature, given the likely influence of internal variability on the inter-hemispheric SST gradients that influence Sahel rainfall, as well as the influence of aerosol variations.

Table 11.1 provides information on the spread of model-projected precipitation change in the four African sub-regions. The regions and seasons for which the central half (25 to 75%) of the projections are uniformly of one sign are: EAF where there is an increase in DJF, March, April and May (MAM), SON and in the annual mean; SAF where there is a decrease in austral winter and spring; and SAH where there is a decrease in boreal winter and spring. The Tebaldi et al. (2004a,b) Bayesian estimates (Supplementary Material Table S11.2)

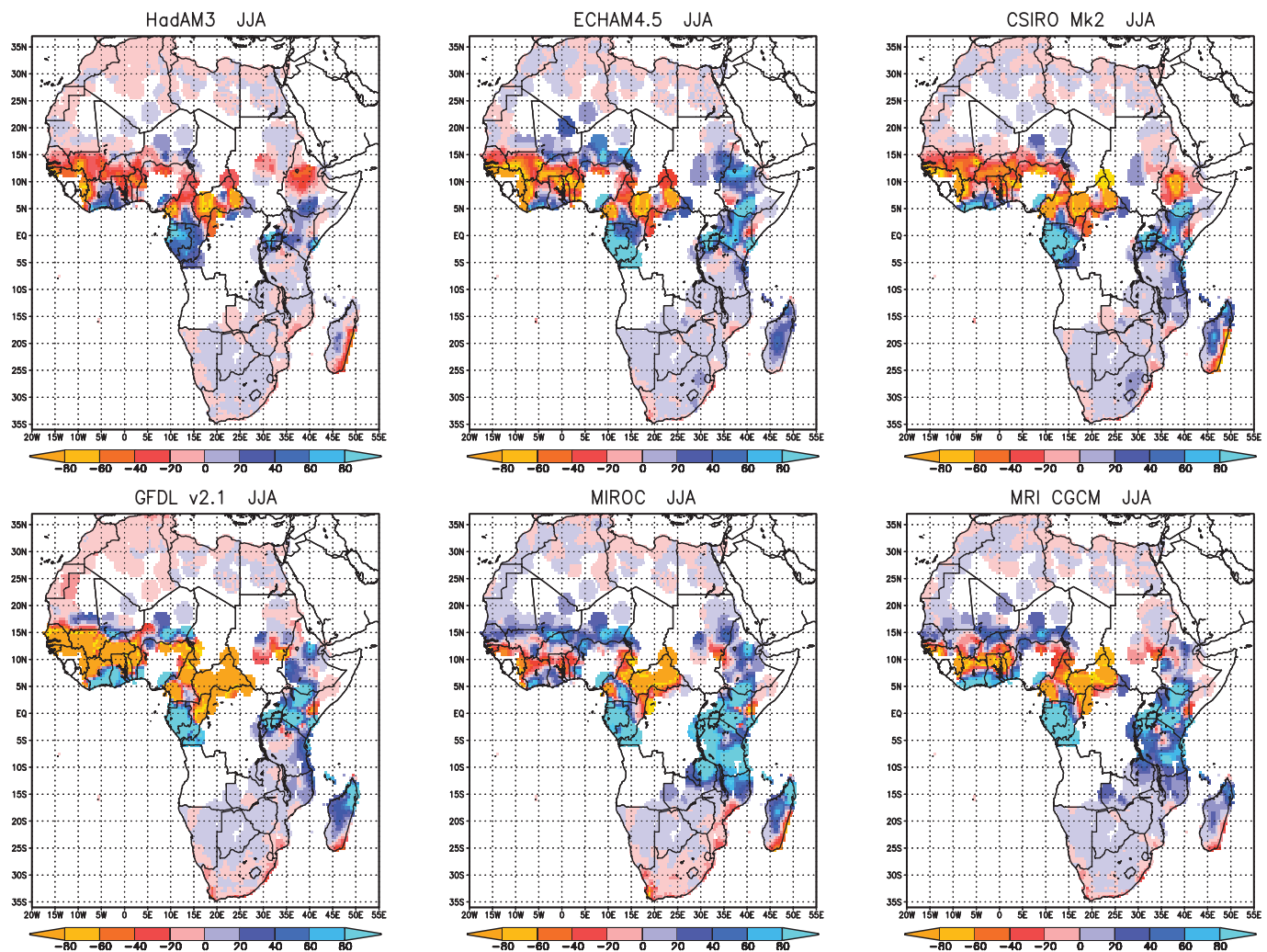


Figure 11.3. Anomaly of mean monthly precipitation (mm) using daily data empirically downscaled from six GCMs (ECHAM4.5, Hadley Centre Atmospheric Model (HadAM3), CSIRO Mk2, GFDL 2.1, MRI, MIROC; see Table 8.1 for descriptions of most of these models) to 858 station locations. The GCMs were forced by the SRES A2 scenario. Anomalies are for the future period (2070 to 2099 for the first three models, and 2080 to 2099 for the latter three models) minus a control 30-year period (from Hewitson and Crane, 2006).

do not change this distinction between robust and non-robust regions and seasons. The time required for emergence of a clearly discernible signal in these robust regions and seasons is typically 50 to 100 years, except in the Sahara where even longer times are required.

Land use change is a potential contributor to climate change in the 21st century (see also Section 11.7, Box 11.4). C.M. Taylor et al. (2002) project drying over the Sahel of 4% from 1996 to 2015 due to changing land use, but suggest that the potential exists for this contribution to grow substantially further into the century. Maynard and Royer (2004a) suggest that estimated land use change scenarios for the mid-21st century would have only a modest compensating effect on the greenhouse-gas induced moistening in their model. Neither of these studies includes a dynamic vegetation model.

Several climate change projections based on RCM simulations are available for southern Africa but are much scarcer for other regions. Tadross et al. (2005a) examine two RCMs, Providing Regional Impacts for Climate Studies (PRECIS) and Mesoscale Model version 5 (MM5), nested for southern Africa in a time-slice AGCM based in turn on lower-resolution Hadley Centre Coupled Model (HadCM3) coupled simulations for the Special Report on Emission Scenarios (SRES) A2 scenario. During the early summer season, October to December, both models predict drying over the tropical western side of the continent, responding to the increase in high-pressure systems entering from the west, with MM5 indicating that the drying extends further south and PRECIS further east. The drying in the west continues into late summer, but there are increases in total rainfall towards the east in January and February, a feature barely present in the ensemble mean of the MMD models. Results obtained by downscaling one global model must be assessed in the context of the variety of responses in southern Africa among the MMD models (Supplementary Material Figure S11.13).

Hewitson and Crane (2006) use empirical downscaling to provide projections for daily precipitation as a function of six GCM simulations. The degree of convergence in the downscaled results for the SRES A2 scenario near the end of the 21st century suggests more commonality in GCM-projected changes in daily circulation, on which the downscaling is based, than in the GCM precipitation responses. Figure 11.3 shows the response of mean JJA monthly total precipitation for station locations across Africa. The ensemble mean of these downscaling results shows increased precipitation in east Africa extending into southern Africa, especially in JJA, strong drying in the core Sahel in JJA with some coastal wetting, and moderate wetting in DJF. There is also drying along the Mediterranean coast, and, in most models, drying in the western portion of southern Africa. The downscaling also shows marked local-scale variation in the projected changes, for example, the contrasting changes in the west and east of Madagascar, and on the coastal and inland borders of the Sahel.

While this result is generally consistent with the underlying GCMs and the composite MMD projections, there is a tendency for greater Sahel drying than in the underlying GCMs, providing further rationale (alongside the large spread in model responses and poor coupled model performance in simulating droughts of the magnitude observed in the 20th century) for viewing with caution the projection for a modest increase in Sahel rainfall in the ensemble mean of the MMD models.

11.2.3.3 Extremes

Research on changes in extremes specific to Africa, in either models or observations, is limited. A general increase in the intensity of high-rainfall events, associated in part with the increase in atmospheric water vapour, is expected in Africa, as in other regions. Regional modelling and downscaling results (Tadross et al., 2005a) both support an increase in the rainfall intensity in southern Africa. In regions of mean drying, there is generally a proportionally larger decrease in the number of rain days, indicating compensation between intensity and frequency of rain. In the downscaling results of Hewitson and Crane (2006) and Tadross et al. (2005a), changes in the median precipitation event magnitude at the station scale do not always mirror the projected changes in seasonal totals.

There is little modelling guidance on possible changes in tropical cyclones affecting the southeast coast of Africa. Thermodynamic arguments for increases in precipitation rates and intensity of tropical storms (see Chapter 10) are applicable to these Indian Ocean storms as for other regions, but changes in frequency and spatial distribution remain uncertain. In a time-slice simulation with a 20-km resolution AGCM, Oouchi et al. (2006) obtain a significant reduction in the frequency of tropical storms in the Indian Ocean.

Using the definition of ‘extreme seasons’ given in Section 11.1.2, the probability of extremely warm, wet and dry seasons, as estimated by the MMD models, is provided in Table 11.1. As in most tropical regions, all seasons are extremely warm by the end of the 21st century, with very high confidence under the A1B scenario. Although the mean precipitation response in West Africa is less robust than in East Africa, the increase in the number of extremely wet seasons is comparable in both, increasing to roughly 20% (i.e., 1 in 5 of the seasons are extremely wet, as compared to 1 in 20 in the control period in the late 20th century). In southern Africa, the frequency of extremely dry austral winters and springs increases to roughly 20%, while the frequency of extremely wet austral summers doubles in this ensemble of models.

11.3 Europe and the Mediterranean

Assessments of projected climate change for Europe:

Annual mean temperatures in Europe are likely to increase more than the global mean. The warming in northern Europe is likely to be largest in winter and that in the Mediterranean area largest in summer. The lowest winter temperatures are likely to increase more than average winter temperature in northern Europe, and the highest summer temperatures are likely to increase more than average summer temperature in southern and central Europe.

Annual precipitation is very likely to increase in most of northern Europe and decrease in most of the Mediterranean area. In central Europe, precipitation is likely to increase in winter but decrease in summer. Extremes of daily precipitation are very likely to increase in northern Europe. The annual number of precipitation days is very likely to decrease in the Mediterranean area. The risk of summer drought is likely to increase in central Europe and in the Mediterranean area.

Confidence in future changes in windiness is relatively low, but it seems more likely than not that there will be an increase in average and extreme wind speeds in northern Europe.

The duration of the snow season is very likely to shorten in all of Europe, and snow depth is likely to decrease in at least most of Europe.

Although many features of the simulated climate change in Europe and the Mediterranean area are qualitatively consistent among models and qualitatively well understood in physical terms, substantial uncertainties remain. Simulated seasonal-mean temperature changes vary even at the sub-continental scale by a factor of two to three among the current generation of AOGCMs. Similarly, while agreeing on a large-scale increase in winter half-year precipitation in the northern parts of the area and a decrease in summer half-year precipitation in the southern parts of the area, models disagree on the magnitude and geographical details of precipitation change. These uncertainties reflect the sensitivity of the European climate change to the magnitude of the global warming and the changes in the atmospheric circulation and the Atlantic Meridional Overturning Circulation (MOC). Deficiencies in modelling the processes that regulate the local water and energy cycles in Europe also introduce uncertainty, for both the changes in mean conditions and extremes. Finally, the substantial natural variability of European climate is a major uncertainty, particularly for short-term climate projections in the area (e.g., Hulme et al., 1999).

11.3.1 Key Processes

In addition to global warming and its direct thermodynamic consequences such as increased water vapour transport from low to high latitudes (Section 11.1.3), several other factors may shape future climate changes in Europe and the Mediterranean area. Variations in the atmospheric circulation influence the European climate both on interannual and longer time scales. Recent examples include the central European heat wave in the summer 2003, characterised by a long period of anticyclonic weather (see Box 3.5), the severe cyclone-induced flooding in central Europe in August 2002 (see Box 3.6), and the strong warming of winters in northern Europe from the 1960s to 1990s that was affected by a trend toward a more positive phase of the NAO (Hurrell and van Loon, 1997; Räisänen and Alexandersson, 2003; Scaife et al., 2005). At fine geographical scales, the effects of atmospheric circulation are modified by topography, particularly in areas of complex terrain (Fernandez et al., 2003; Bojariu and Giorgi, 2005).

Europe, particularly its north-western parts, owes its relatively mild climate partly to the northward heat transport by the Atlantic MOC (e.g., Stouffer et al., 2006). Most models suggest increased greenhouse gas concentrations will lead to a weakening of the MOC (see Section 10.3), which will act to reduce the warming in Europe. However, in the light of present understanding, it is very unlikely to reverse the warming to cooling (see Section 11.3.3.1).

Local thermodynamic factors also affect the European climate and are potentially important for its future changes. In those parts of Europe that are presently snow-covered in winter, a decrease in snow cover is likely to induce a positive feedback, further amplifying the warming. In the Mediterranean region and at times in central Europe, feedbacks associated with the drying of the soil in summer are important even in the present climate. For example, they acted to exacerbate the heat wave of 2003 (Black et al., 2004; Fink et al., 2004).

11.3.2 Skill of Models in Simulating Present Climate

Atmosphere-Ocean General Circulation Models show a range of performance in simulating the climate in Europe and the Mediterranean area. Simulated temperatures in the MMD models vary on both sides of the observational estimates in summer but are mostly lower than observed in the winter half-year, particularly in northern Europe (Supplementary Material Table S11.1). Excluding one model that simulates extremely cold winters in northern Europe, the seasonal area mean temperature biases in the northern Europe region (NEU) vary from -5°C to 3°C and those in the southern Europe and Mediterranean region (SEM) from -5°C to 6°C , depending on model and season. The cold bias in northern Europe tends to increase towards the northeast, reaching -7°C in the ensemble mean in the northeast of European Russia in winter. This cold bias coincides with a north-south gradient in the winter mean sea level pressure that is weaker than observed, which implies

Box 11.2: The PRUDENCE Project

The Prediction of Regional scenarios and Uncertainties for Defining European Climate change risks and Effects (PRUDENCE) project involved more than 20 European research groups. The main objectives of the project were to provide dynamically downscaled high-resolution climate change scenarios for Europe at the end of the 21st century, and to explore the uncertainty in these projections. Four sources of uncertainty were studied: (i) sampling uncertainty due to the fact that model climate is estimated as an average over a finite number (30) of years, (ii) regional model uncertainty due to the fact that RCMs use different techniques to discretize the equations and to represent sub-grid effects, (iii) emission uncertainty due to choice of IPCC SRES emission scenario, and (iv) Boundary uncertainty due to the different boundary conditions obtained from different global climate models.

Each PRUDENCE experiment consisted of a control simulation representing the period 1961 to 1990 and a future scenario simulation representing 2071 to 2100. A large fraction of the simulations used the same boundary data (from the Hadley Centre Atmospheric Model (HadAM3H) for the A2 scenario) to provide a detailed understanding of the regional model uncertainty. Some simulations were also made for the B2 scenario, and by using driving data from two other GCMs and from different ensemble members from the same GCM. More details are provided in, for example, Christensen et al. (2007), Déqué et al. (2005) and <http://prudence.dmi.dk>.

weaker than observed westerly flow from the Atlantic Ocean to northern Europe in most models (Supplementary Material Figure S11.22).

Biases in simulated precipitation vary substantially with season and location. The average simulated precipitation in NEU exceeds that observed from autumn to spring (Supplementary Material Table S11.1), but the interpretation of the difference is complicated by the observational uncertainty associated with the undercatch of, in particular, solid precipitation (e.g., Adam and Lettenmaier, 2003). In summer, most models simulate too little precipitation, particularly in the eastern parts of the area. In SEM, the area and ensemble mean precipitation is close to observations.

Regional Climate Models capture the geographical variation of temperature and precipitation in Europe better than global models but tend to simulate conditions that are too dry and warm in southeastern Europe in summer, both when driven by analysed boundary conditions (Hagemann et al., 2004) and when driven by GCM data (e.g., Jacob et al., 2007). Most but not all RCMs also overestimate the interannual variability of summer temperatures in southern and central Europe (Jacob et al., 2007; Lenderink et al., 2007; Vidale et al., 2007). The excessive temperature variability coincides with excessive interannual variability in either shortwave radiation or evaporation, or

both (Lenderink et al., 2007). A need for improvement in the modelling of soil, boundary layer and cloud processes is implied. One of the key model parameters may be the depth of the hydrological soil reservoir, which appears to be too small in many RCMs (van den Hurk et al., 2005).

The ability of RCMs to simulate climate extremes in Europe has been addressed in several studies. In the Prediction of Regional scenarios and Uncertainties for Defining European Climate change risks and Effects (PRUDENCE) simulations (Box 11.2), the biases in the tails of the temperature distribution varied substantially between models but were generally larger than the biases in average temperatures (Kjellström et al., 2007). Inspection of the individual models showed similarity between the biases in daily and interannual variability, suggesting that similar mechanisms may be affecting both.

The magnitude of precipitation extremes in RCMs is model-dependent. In a comparison of the PRUDENCE RCMs, Frei et al. (2006) find that the area-mean five-year return values of one-day precipitation in the vicinity of the European Alps vary by up to a factor of two between the models. However, except for too-low extremes in the southern parts of the area in summer, the set of models as a whole showed no systematic tendency to over- or underestimate the magnitude of the extremes when compared with gridded observations. A similar level of skill has been found in other model verification studies made for European regions (e.g., Booij, 2002; Semmler and Jacob, 2004; Fowler et al., 2005; see also Frei et al., 2003).

Evidence of model skill in simulation of wind extremes is mixed. Weisse et al. (2005) find that an RCM simulated a very realistic wind climate over the North Sea, including the number and intensity of storms, when driven by analysed boundary conditions. However, most PRUDENCE RCMs, while quite realistic over sea, severely underestimate the occurrence of very high wind speeds over land and coastal areas (Rockel and Woth, 2007). Realistic frequencies of high wind speeds were only found in the two models that used a gust parametrization to mimic the large local and temporal variability of near-surface winds over land.

11.3.3 Climate Projections

11.3.3.1 Mean Temperature

The observed evolution of European temperatures in the 20th century, characterised by a warming trend modulated by multi-decadal variability, was well within the envelope of the MMD simulations (Figure 11.4).

In this century, the warming is projected to continue at a rate somewhat greater than its global mean, with the increase in 20-year mean temperatures (from its values in 1980 to 1999) becoming clearly discernible (as defined in Section 11.1.2) within a few decades. Under the A1B scenario, the simulated area and annual mean warming from 1980 to 1999 to 2080 to 2099 varies from 2.3°C to 5.3°C in NEU and from 2.2°C to 5.1°C in SEM. The warming in northern Europe is likely to be largest in winter and that in the Mediterranean area largest

in summer (Figure 11.5). Seasonal mean temperature changes typically vary by a factor of three among the MMD models (Table 11.1); however, the upper end of the range in NEU in DJF is reduced from 8.1°C to 6.7°C when one model with an extreme cold bias in present-day winter climate is excluded. Further details are given in Table 11.1 and Supplementary Material Figures S11.2 to S11.4.

Although changes in atmospheric circulation have a significant potential to affect temperature in Europe (e.g., Dorn et al., 2003), they are not the main cause of the projected warming (e.g., Rauthe and Paeth, 2004; Stephenson et al., 2006; van Ulden et al., 2007). A regression-based study using five of the MMD models (van Ulden and van Oldenborgh, 2006) indicated that in a region comprising mainly Germany, circulation changes enhanced the warming in most models in winter (due to an increase in westerly flow) and late summer (due to a decrease in westerly flow), but reduced the warming slightly in May and June. However, the circulation contribution to the simulated temperature changes (typically -1°C to 1.5°C depending on model and month) was generally much smaller than the total simulated warming in the late 21st century.

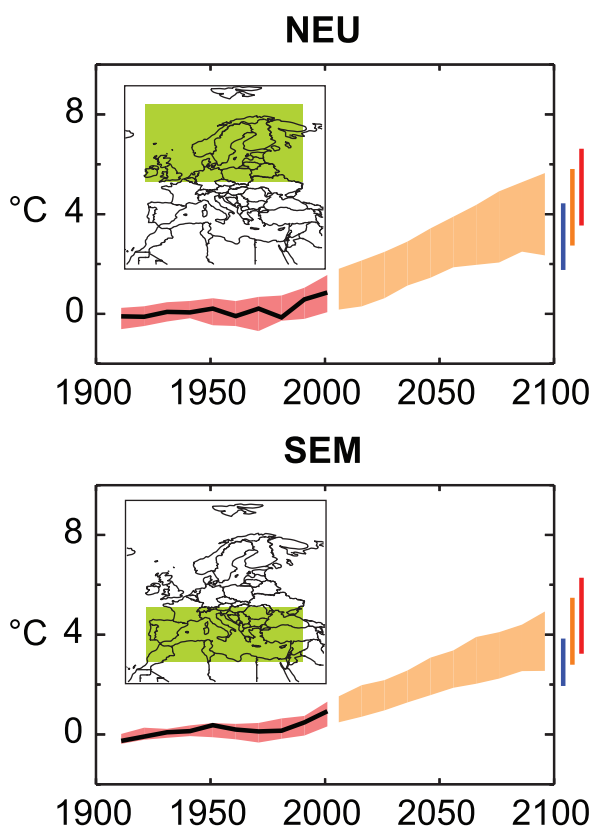


Figure 11.4. Temperature anomalies with respect to 1901 to 1950 for two Europe land regions for 1906 to 2005 (black line) and as simulated (red envelope) by MMD models incorporating known forcings; and as projected for 2001 to 2100 by MMD models for the A1B scenario (orange envelope). The bars at the end of the orange envelope represent the range of projected changes for 2091 to 2100 for the B1 scenario (blue), the A1B scenario (orange) and the A2 scenario (red). More details on the construction of these figures are given in Box 11.1 and Section 11.1.2.

Despite a decrease in the North Atlantic MOC in most models (see Section 10.3), all the MMD simulations show warming in Great Britain and continental Europe, as other climatic effects of increased greenhouse gases dominate over the changes in ocean circulation. The same holds for earlier simulations with increased greenhouse gas concentrations, except for a very few (Russell and Rind, 1999; Schaeffer et al., 2004) with slight cooling along the north-western coastlines of Europe but warming over the rest of the continent. The impact of MOC changes depends on the regional details of the change, being largest if ocean convection is suppressed at high latitudes where the sea ice feedback may amplify atmospheric cooling (Schaeffer et al., 2004). Sensitivity studies using AOGCMs with an artificial shutdown of the MOC and no changes in greenhouse gas concentrations typically show a 2°C to 4°C annual mean cooling in most of Europe, with larger cooling in the extreme north-western parts (e.g., Stouffer et al., 2006).

Statistical downscaling (SD) studies tend to show a large-scale warming similar to that of dynamical models but with finer-scale regional details affected by factors such as distance from the coast and altitude (e.g., Benestad, 2005; Hanssen-Bauer et al., 2005). Comparing RCM and SD projections for Norway downscaled from the same GCM, Hanssen-Bauer et al. (2003) found the largest differences between the two approaches in winter and/or spring at locations with frequent temperature inversions in the present climate. A larger warming at these locations in the SD projections was found, consistent with increased winter wind speed in the driving GCM and reduced snow cover, both of which suppress formation of ground inversions.

11.3.3.2 Mean Precipitation

A south-north contrast in precipitation changes across Europe is indicated by AOGCMs, with increases in the north and decreases in the south (Figure 11.5). The annual area-mean change from 1980 to 1999 to 2080 to 2099 in the MMD-A1B projections varies from 0 to 16% in NEU and from -4 to -27% in SEM (Table 11.1). The largest increases in northern and central Europe are simulated in winter. In summer, the NEU area mean changes vary in sign between models, although most models simulate increased (decreased) precipitation north (south) of about 55°N . In SEM, the most consistent and, in percentage terms, largest decreases, occur in summer, but the area mean precipitation in the other seasons also decreases in most or all models. More detailed statistics are given in Table 11.1. Increasing evaporation makes the simulated decreases in annual precipitation minus evaporation extend a few hundred kilometres further north in central Europe than the decreases in precipitation (Supplementary Material Figure S11.1).

Both circulation changes and thermodynamic factors appear to affect the simulated seasonal cycle of precipitation changes in Europe. Applying a regression method to five of the MMD simulations, van Ulden and van Oldenborgh (2006) found that in a region comprising mainly Germany, circulation changes played a major role in all seasons. In most models, increases

in winter precipitation were enhanced by increased westerly winds, with decreases in summer precipitation largely due to more easterly and anticyclonic flow. However, differences in the simulated circulation changes among the individual models were accompanied by large differences in precipitation change, particularly in summer. The residual precipitation change varied less with season and among models, being generally positive as expected from the increased moisture transport capacity of a warmer atmosphere. In a more detailed study of one model, HadAM3P, Rowell and Jones (2006) showed that decreases in summer precipitation in continental and southeastern Europe were mainly associated with thermodynamic factors. These included reduced relative humidity resulting from larger continental warming compared to surrounding sea areas and reduced soil moisture due mainly to spring warming causing earlier snowmelt. Given the confidence in the warming patterns

driving these changes, the reliability of the simulated drying was assessed as being high.

Changes in precipitation may vary substantially on relatively small horizontal scales, particularly in areas of complex topography. Details of these variations are sensitive to changes in the atmospheric circulation, as illustrated in Figure 11.6 for two PRUDENCE simulations that only differ with respect to the driving global model. In one, an increase in westerly flow from the Atlantic Ocean (caused by a large increase in the north-south pressure gradient) is accompanied by increases of up to 70% in annual precipitation over the Scandinavian mountains. In the other, with little change in the average pressure pattern, the increase is in the range of 0 to 20%. When compared with circulation changes in the more recent MMD simulations, these two cases fall in the opposite ends of the range. Most MMD models suggest an increased north-south pressure gradient

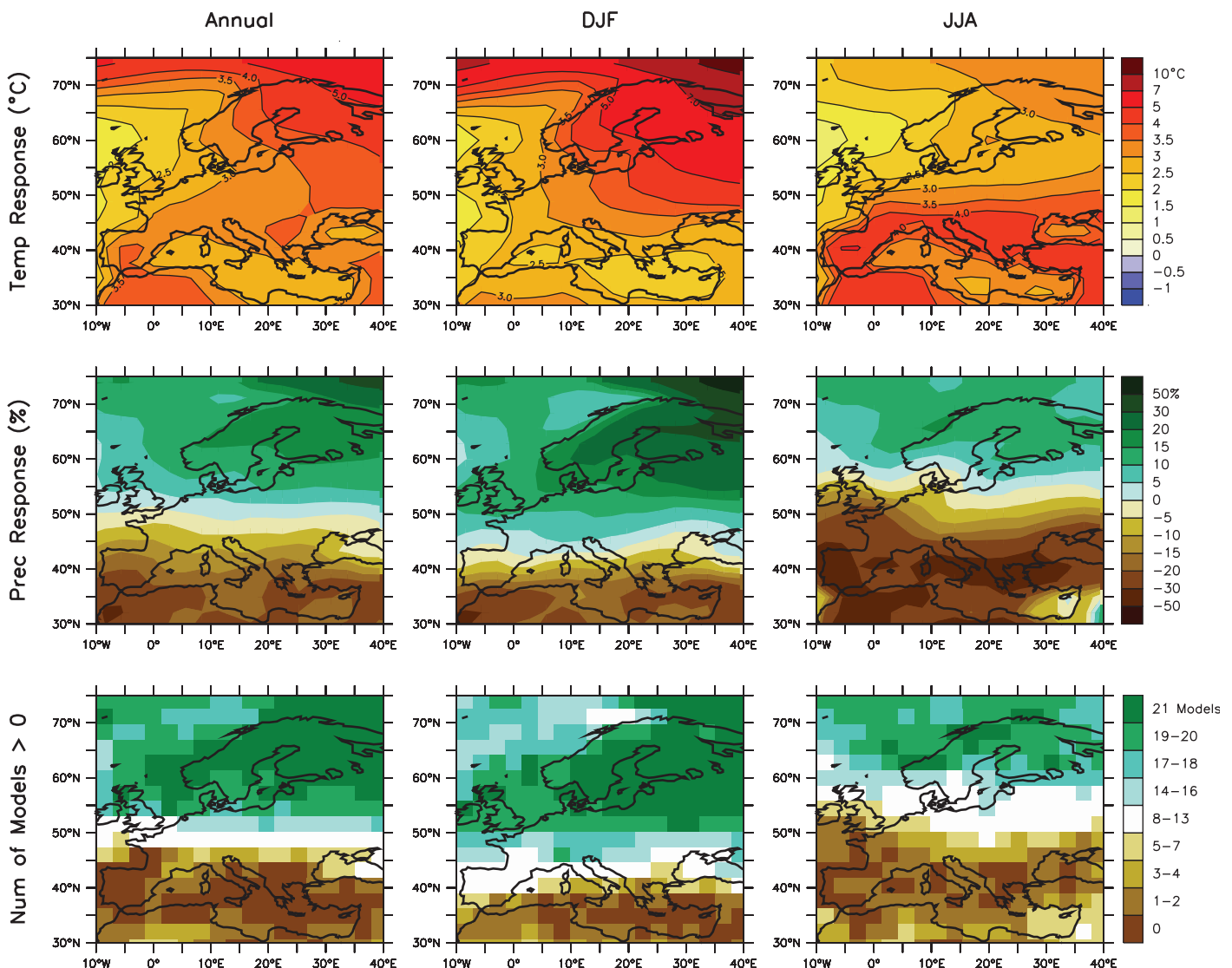


Figure 11.5. Temperature and precipitation changes over Europe from the MMD-A1B simulations. Top row: Annual mean, DJF and JJA temperature change between 1980 to 1999 and 2080 to 2099, averaged over 21 models. Middle row: same as top, but for fractional change in precipitation. Bottom row: number of models out of 21 that project increases in precipitation.

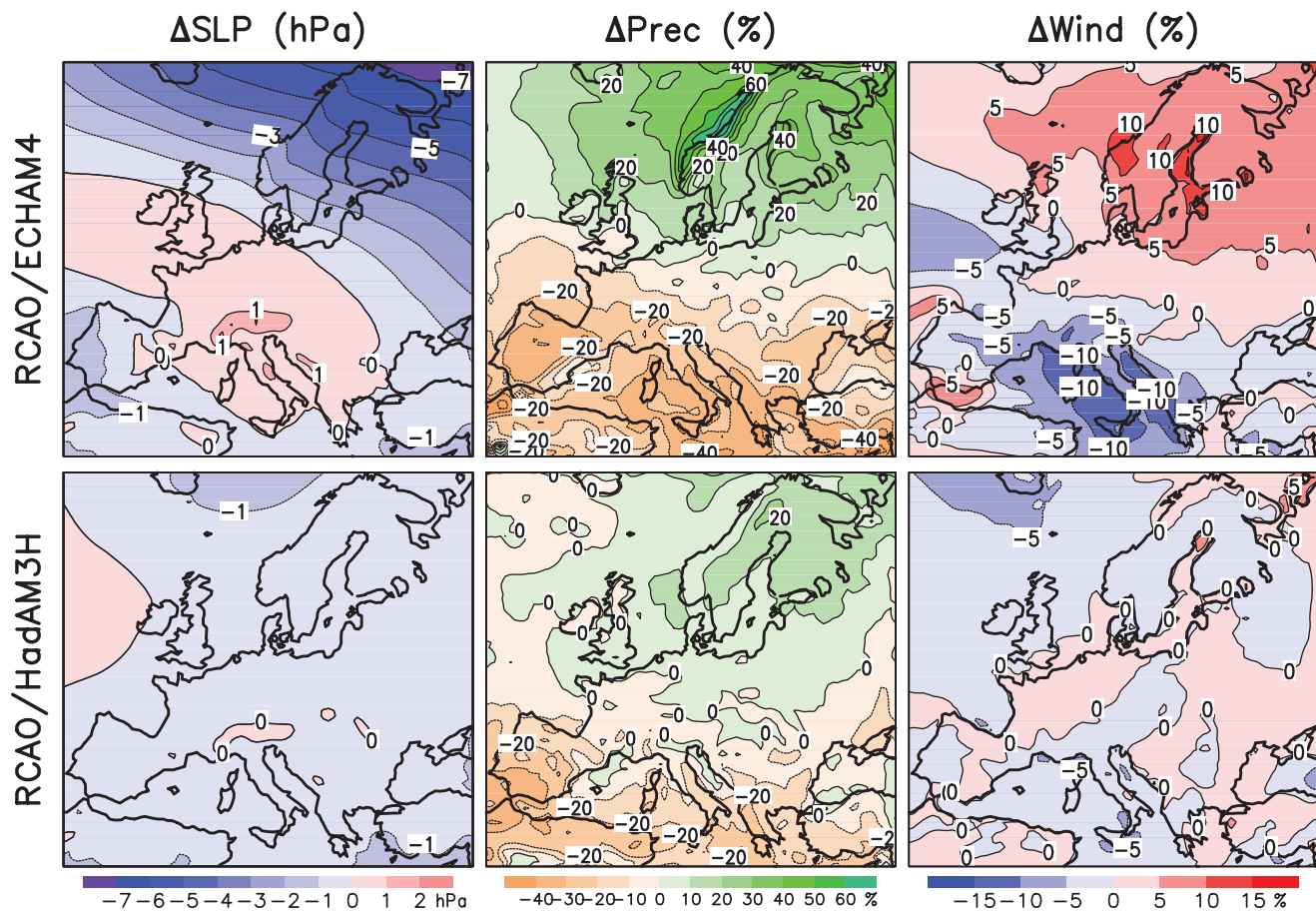


Figure 11.6. Simulated changes in annual mean sea level pressure (Δ SLP), precipitation (Δ Prec) and mean 10-m level wind speed (Δ Wind) from the years 1961 to 1990 to the years 2071 to 2100. The results are based on the SRES A2 scenario and were produced by the same RCM (Rossby Centre regional Atmosphere-Ocean model; RCO) using boundary data from two global models: ECHAM4/OPYC3 (top) and HadAM3H (bottom) (redrawn from Rummukainen et al., 2004).

across northern Europe, but the change is generally smaller than in the top row of Figure 11.6.

Projections of precipitation change in Europe based on SD tend to support the large-scale picture from dynamical models (e.g., Busuioc et al., 2001; Beckmann and Buishand, 2002; Hanssen-Bauer et al., 2003, 2005; Benestad, 2005; Busuioc et al., 2006), although variations between SD methods and the dependence on the GCM data sets used (see Section 11.10.1.3) make it difficult to draw quantitative conclusions. However, some SD studies have suggested a larger small-scale variability of precipitation changes than indicated by GCM and RCM results, particularly in areas of complex topography (Hellström et al., 2001).

The decrease in precipitation together with enhanced evaporation in spring and early summer is very likely to lead to reduced summer soil moisture in the Mediterranean region and parts of central Europe (Douville et al., 2002; Wang, 2005). In northern Europe, where increased precipitation competes with earlier snowmelt and increased evaporation, the MMD models disagree on whether summer soil moisture will increase or decrease (Wang, 2005).

11.3.3.3 Temperature Variability and Extremes

Based on both GCM (Giorgi and Bi, 2005; Rowell, 2005; Clark et al., 2006) and RCM simulations (Schär et al., 2004; Vidale et al., 2007), interannual temperature variability is likely to increase in summer in most areas. However, the magnitude of change is uncertain, even in central Europe where the evidence for increased variability is strongest. In some PRUDENCE simulations, interannual summer temperature variability in central Europe doubled between 1961 to 1990 and 2071 to 2100 under the A2 scenario, while other simulations showed almost no change (Vidale et al., 2007). Possible reasons for the increase in temperature variability are reduced soil moisture, which reduces the capability of evaporation to damp temperature variations, and increased land-sea contrast in average summer temperature (Rowell, 2005; Lenderink et al., 2007).

Simulated increases in summer temperature variability also extend to daily time scales. Kjellström et al. (2007) analyse the PRUDENCE simulations and find that the inter-model differences in the simulated temperature change increase towards the extreme ends of the distribution. However, a general increase in summer daily temperature variability is

evident, especially in southern and central parts of Europe, with the highest maximum temperatures increasing more than the median daily maximum temperature (Supplementary Material Figure S11.23). Similarly, Shkolnik et al. (2006) report a simulated increase in summer daily time-scale temperature variability in mid-latitude western Russia. These RCM results are supported by GCM studies of Hegerl et al. (2004), Meehl and Tebaldi (2004) and Clark et al. (2006).

In contrast with summer, models project reduced temperature variability in most of Europe in winter, both on interannual (Räisänen, 2001; Räisänen et al., 2003; Giorgi et al., 2004; Giorgi and Bi, 2005; Rowell, 2005) and daily time scales (Hegerl et al., 2004; Kjellström et al., 2007). In the PRUDENCE simulations, the lowest winter minimum temperatures increased more than the median minimum temperature especially in eastern, central and northern Europe, although the magnitude of this change was strongly model-dependent (Supplementary Material Figure S11.23). The geographical patterns of the change indicate a feedback from reduced snow cover, with a large warming of the cold extremes where snow retreats but a more moderate warming in the mostly snow-free south-western Europe (Rowell, 2005; Kjellström et al., 2007).

Along with the overall warming and changes in variability, heat waves are very likely to increase in frequency, intensity and duration (Barnett et al., 2006; Clark et al., 2006; Tebaldi et al., 2006). Conversely, the number of frost days is very likely to decrease (Tebaldi et al., 2006).

11.3.3.4 Precipitation Variability and Extremes

In northern Europe and in central Europe in winter, where time mean precipitation is simulated to increase, high extremes of precipitation are very likely to increase in magnitude and frequency. In the Mediterranean area and in central Europe in summer, where reduced mean precipitation is projected, extreme short-term precipitation may either increase (due to the increased water vapour content of a warmer atmosphere) or decrease (due to a decreased number of precipitation days, which if acting alone would also make heavy precipitation less common). These conclusions are based on several GCM (e.g., Semenov and Bengtsson, 2002; Voss et al., 2002; Hegerl et al., 2004; Wehner, 2004; Kharin and Zwiers, 2005; Tebaldi et al., 2006) and RCM (e.g., Jones and Reid, 2001; Räisänen and Joelsson, 2001; Booij, 2002; Christensen and Christensen, 2003, 2004; Pal et al., 2004; Räisänen et al., 2004; Sánchez et al., 2004; Ekström et al., 2005; Frei et al., 2006; Gao et al., 2006a; Shkolnik et al., 2006; Beniston et al., 2007) studies. However, there is still a lot of quantitative uncertainty in the changes in both mean and extreme precipitation.

Time scale also matters. Although there are some indications of increased interannual variability, particularly in summer precipitation (Räisänen, 2002; Giorgi and Bi, 2005; Rowell, 2005), changes in the magnitude of long-term (monthly to annual) extremes are expected to follow the changes in mean precipitation more closely than are those in short-term extremes (Räisänen, 2005). On the other hand, changes in the frequency

of extremes tend to increase with increasing time scale even when this is not the case for the changes in the magnitude of extremes (Barnett et al., 2006).

Figure 11.7 illustrates the possible characteristics of precipitation change. The eight models in this PRUDENCE study (Frei et al., 2006) projected an increase in mean precipitation in winter in both southern Scandinavia and central Europe, due to both increased wet day frequency and increased mean precipitation for the wet days. In summer, a decrease in the number of wet days led to a decrease in mean precipitation, particularly in central Europe. Changes in extreme short-term precipitation were broadly similar to the change in average wet-day precipitation in winter. In summer, extreme daily precipitation increased in most models despite the decrease in mean precipitation, although the magnitude of the change was highly model-dependent. However, this study only covered the uncertainties associated with the choice of the RCM, not those associated with the driving GCM and the emissions scenario.

Much larger changes are expected in the recurrence frequency of precipitation extremes than in the magnitude of extremes (Huntingford et al., 2003; Barnett et al., 2006; Frei et al., 2006). For example, Frei et al. (2006) estimate that, in Scandinavia under the A2 scenario, the highest five-day winter precipitation totals occurring once in 5 years in 2071 to 2100 would be similar to those presently occurring once in 8 to 18 years (the range reflects variation between the PRUDENCE models). In the MMD simulations, large increases occur in the frequencies of both high winter precipitation in northern Europe and low summer precipitation in southern Europe and the Mediterranean area (Table 11.1).

The risk of drought is likely to increase in southern and central Europe. Several model studies have indicated a decrease in the number of precipitation days (e.g., Semenov and Bengtsson, 2002; Voss et al., 2002; Räisänen et al., 2003, 2004; Frei et al., 2006) and an increase in the length of the longest dry spells in this area (Voss et al., 2002; Pal et al., 2004; Beniston et al., 2007; Gao et al., 2006a; Tebaldi et al., 2006). By contrast, the same studies do not suggest major changes in dry-spell length in northern Europe.

11.3.3.5 Wind Speed

Confidence in future changes in windiness in Europe remains relatively low. Several model studies (e.g., Zwiers and Kharin, 1998; Knippertz et al., 2000; Leckebusch and Ulbrich, 2004; Pryor et al., 2005a; van den Hurk et al., 2006) have suggested increased average and/or extreme wind speeds in northern and/or central Europe, but some studies point in the opposite direction (e.g., Pryor et al., 2005b). The changes in both average and extreme wind speeds may be seasonally variable, but the details of this variation appear to be model-dependent (e.g., Räisänen et al., 2004; Rockel and Woth, 2007).

A key factor is the change in the large-scale atmospheric circulation (Räisänen et al., 2004; Leckebusch et al., 2006). Simulations with an increased north-south pressure gradient across northern Europe (e.g., top row of Figure 11.6) tend to

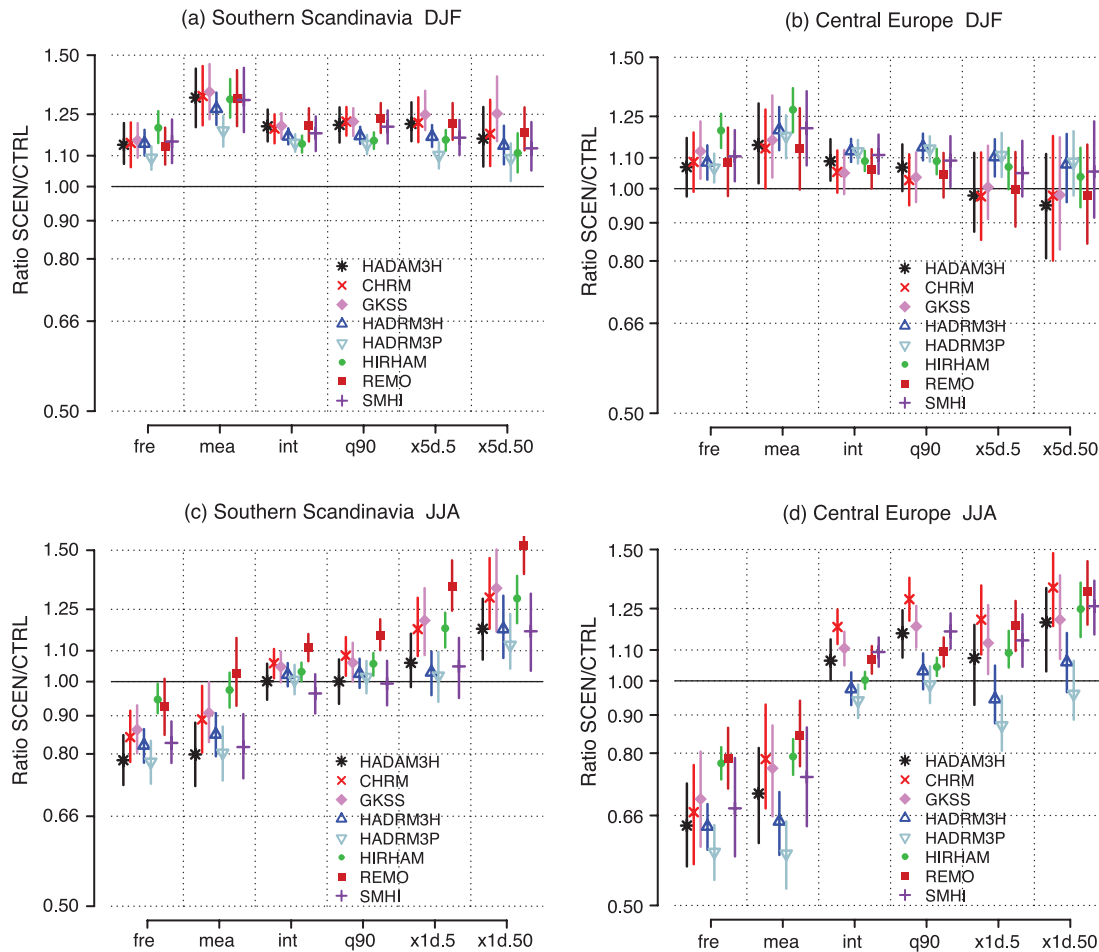


Figure 11.7. Changes (ratio 2071–2100 / 1961–1990 for the A2 scenario) in domain-mean precipitation diagnostics in the PRUDENCE simulations in southern Scandinavia (5°E–20°E, 55°N–62°N) and central Europe (5°E–15°E, 48°N–54°N) in winter (top) and in summer (bottom). *fre* = wet-day frequency; *mea* = mean seasonal precipitation; *int* = mean wet-day precipitation; *q90* = 90th percentile of wet-day precipitation; *x1d.5* and *x1d.50* = 5- and 50-year return values of one-day precipitation; *x5d.5* and *x5d.50* = 5- and 50-year return values of five-day precipitation. For each of the eight models, the vertical bar gives the 95% confidence interval associated with sampling uncertainty (re-drawn from Frei et al., 2006). Models are the Hadley Centre Atmospheric Model (HadAM3H), the Climate High Resolution Model (CHRM), the climate version of the ‘Lokalmmodell’ (CLM), the Hadley Centre Regional Model (HadRM3H and HadRM3P), the combination of the High-Resolution Limited Area Model (HIRLAM) and the European Centre Hamburg (ECHAM4) GCM (HIRHAM), the regional climate model REMO, and the Rossby Centre regional Atmosphere-Ocean model (RCAO).

indicate stronger winds in northern Europe, because of both the larger time-averaged pressure gradient and a northward shift in cyclone activity. Conversely, the northward shift in cyclone activity tends to reduce windiness in the Mediterranean area. On the other hand, simulations with little change in the pressure pattern tend to show only small changes in the mean wind speed (bottom row of Figure 11.6). Most of the MMD-projected pressure changes fall between the two PRUDENCE simulations shown in Figure 11.6, which suggests that the most likely outcome for windiness might be between these two cases.

Extreme wind speeds in Europe are mostly associated with strong winter cyclones (e.g., Leckebusch and Ullbrich, 2004), the occurrence of which is only indirectly related to the time-mean circulation. Nevertheless, models suggest a general similarity between the changes in average and extreme wind speeds (Knippertz et al., 2000; Räisänen et al., 2004). A caveat to this conclusion is that, even in most RCMs, the simulated

extremes of wind speed over land tend to be too low (see Section 11.3.2).

11.3.3.6 Mediterranean Cyclones

Several studies have suggested a decrease in the total number of cyclones in the Mediterranean Sea (Lionello et al., 2002; Vérant, 2004; Somot 2005; Leckebusch et al., 2006; Pinto et al., 2006; Ulbrich et al., 2006), but there is no agreement on whether the number of intense cyclones will increase or decrease (Lionello et al., 2002; Pinto et al., 2006).

11.3.3.7 Snow and Sea Ice

The overall warming is very likely to shorten the snow season in all of Europe. Snow depth is also likely to be reduced, at least in most areas, although increases in total winter precipitation may counteract the increased melting and decreased fraction of

solid precipitation associated with the warming. The changes may be large, including potentially a one-to-three month shortening of the snow season in northern Europe (Räisänen et al., 2003) and a 50 to 100% decrease in snow depth in most of Europe (Räisänen et al., 2003; Rowell, 2005) by the late 21st century. However, snow conditions in the coldest parts of Europe, such as northern Scandinavia and north-western Russia (Räisänen et al., 2003; Shkolnik et al., 2006) and the highest peaks of the Alps (Beniston et al., 2003) appear to be less sensitive to the temperature and precipitation changes projected for this century than those at lower latitudes and altitudes (see also Section 11.4.3.2, Box 11.3).

The Baltic Sea is likely to lose a large part of its seasonal ice cover during this century. Using a regional atmosphere-Baltic Sea model (Meier et al., 2004), the average winter maximum ice extent decreased by about 70% (60%) between 1961 to 1990 and 2071 to 2100 under the A2 (B2) scenario. The length of the ice season was projected to decrease by one to two months in northern parts and two to three months in the central parts. Comparable decreases in Baltic Sea ice cover were projected by earlier studies (Haapala et al., 2001; Meier, 2002).

11.4 Asia

Assessment of projected climate change for Asia:

All of Asia is very likely to warm during this century; the warming is likely to be well above the global mean in central Asia, the Tibetan Plateau and northern Asia, above the global mean in East and South Asia, and similar to the global mean in Southeast Asia. It is very likely that summer heat waves/hot spells in East Asia will be of longer duration, more intense, and more frequent. It is very likely that there will be fewer very cold days in East Asia and South Asia.

Boreal winter precipitation is very likely to increase in northern Asia and the Tibetan Plateau, and likely to increase in eastern Asia and the southern parts of Southeast Asia. Summer precipitation is likely to increase in northern Asia, East and South Asia and most of Southeast Asia, but it is likely to decrease in central Asia. An increase in the frequency of intense precipitation events in parts of South Asia, and in East Asia, is very likely.

Extreme rainfall and winds associated with tropical cyclones are likely to increase in East, Southeast and South Asia. Monsoonal flows and the tropical large-scale circulation are likely to be weakened.

While broad aspects of Asian climate change show consistency among AOGCM simulations, a number of sources of uncertainty remain. A lack of observational data in some areas limits model assessment. There has been little assessment of the projected changes in regional climatic means and extremes.

There are substantial inter-model differences in representing monsoon processes, and a lack of clarity over changes in ENSO further contributes to uncertainty about future regional monsoon and tropical cyclone behaviour. Consequently, quantitative estimates of projected precipitation change are difficult to obtain. It is likely that some local climate changes will vary significantly from regional trends due to the region's very complex topography and marine influences.

11.4.1 Key Processes

As monsoons are the dominant phenomena over much of Asia, the factors that influence the monsoonal flow and precipitation are of central importance for understanding climate change in this region. Precipitation is affected both by the strength of the monsoonal flows and the amount of water vapour transported. Monsoonal flows and the tropical large-scale circulation often weaken in global warming simulations (e.g., Knutson and Manabe, 1995). This arises out of an increase in dry static stability associated with the tropical warming in these models, and the reduction in adiabatic warming/cooling needed to balance a given amount of radiative cooling/condensational heating (e.g., Betts, 1998). But there is an emerging consensus that the effect of enhanced moisture convergence in a warmer, moister atmosphere dominates over any such weakening of the circulation, resulting in increased monsoonal precipitation (e.g., Douville et al., 2000; Giorgi et al., 2001a,b; Stephenson et al., 2001; Dairaku and Emori, 2006; Ueda et al., 2006).

There is an association of the phase of ENSO with the strength of the summer monsoons (Pant and Rupa Kumar, 1997), so changes in ENSO will have an impact on these monsoons. However, such an impact can be compounded by a change in the ENSO-South Asian monsoon connection under greenhouse gas warming (Krishna Kumar et al., 1999; Ashrit et al., 2001; Sarkar et al., 2004; see Section 3.7). Moreover, there is a link between Eurasian snow cover and the strength of the monsoon (see also Section 3.7), with the monsoon strengthening if snow cover retreats. Aerosols, particularly absorbing aerosols, further modify monsoonal precipitation (e.g., Ramanathan et al., 2005 for South Asia), as do modifications of vegetation cover (e.g., Chen et al., 2004 for East Asia). However, most emission scenarios suggest that future changes in regional climate are still likely to be dominated by increasing greenhouse gas forcing rather than changes in sulphate and absorbing aerosols, at least over the South Asian region.

For South Asia, the monsoon depressions and tropical cyclones generated over the Indian seas modulate the monsoon anomalies. For East Asia, the monsoonal circulations are strengthened by extratropical cyclones energised in the lee of the Tibetan Plateau and by the strong temperature gradient along the East Coast. The influence of ENSO on the position and strength of the subtropical high in the North Pacific influences both typhoons and other damaging heavy rainfall events, and has been implicated in observed inter-decadal variations in typhoon tracks (Ho et al., 2004). This suggests that the spatial structure of warming in the Pacific will be relevant for changes

in these features. The dynamics of the Meiyu-Changma-Baiu rains in the early summer, which derive from baroclinic disturbances strongly modified by latent heat release, remain poorly understood. While an increase in rainfall in the absence of circulation shifts is expected, relatively modest shifts or changes in timing can significantly affect East Chinese, Korean and Japanese climates.

Over central and Southeast Asia and the maritime continent, interannual rainfall variability is significantly affected by ENSO (e.g., McBride et al., 2003), particularly the June to November rainfall in southern and eastern parts of the Indonesian Archipelago, which is reduced in El Niño years (Aldrian and Susanto, 2003). Consequently, the pattern of ocean temperature change across the Pacific is of central importance to climate change in this region.

In central Asia, including the Tibetan Plateau, the temperature response is strongly influenced by changes in winter and spring snow cover, the isolation from maritime influences, and the spread of the larger winter arctic warming into the region. With regard to precipitation, a key issue is related to the moisture transport from the northwest by westerlies and polar fronts. How far the projected drying of the neighbouring Mediterranean penetrates into these regions is likely to be strongly dependent on accurate simulation of these moisture transport processes. The dynamics of climate change in the Tibetan Plateau are further complicated by the high altitude of this region and its complex topography with large elevation differences.

11.4.2 Skill of Models in Simulating Present Climate

Regional mean temperature and precipitation in the MMD models show biases when compared with observed climate (Supplementary Material Table S11.1). The multi-model mean shows a cold and wet bias in all regions and in most seasons, and the bias of the annual average temperature ranges from -2.5°C over the Tibetan Plateau (TIB) to -1.4°C over South Asia (SAS). For most regions, there is a 6°C to 7°C range in the biases from individual models with a reduced bias range in Southeast Asia (SEA) of 3.6°C . The median bias in precipitation is small (less than 10%) in Southeast Asia, South Asia, and Central Asia (CAS), larger in northern Asia and East Asia (NAS and EAS, around +23%), and very large in the Tibetan Plateau (+110%). Annual biases in individual models are in the range of -50 to $+60\%$ across all regions except the Tibetan Plateau, where some models simulate annual precipitation 2.5 times that observed and even larger seasonal biases occur in winter and spring. These global models clearly have significant problems over Tibet, due to the difficulty in simulating the effects of the dramatic topographic relief, as well as the distorted albedo feedbacks due to extensive snow cover. However, with only limited observations available, predominantly in valleys, large errors in temperature and significant underestimates of precipitation are likely.

South Asia

Over South Asia, the summer is dominated by the southwest monsoon, which spans the four months from June to September and dominates the seasonal cycles of the climatic parameters. While most models simulate the general migration of seasonal tropical rain, the observed maximum rainfall during the monsoon season along the west coast of India, the north Bay of Bengal and adjoining northeast India is poorly simulated by many models (Lal and Harasawa, 2001; Rupa Kumar and Ashrit, 2001; Rupa Kumar et al., 2002, 2003). This is likely linked to the coarse resolution of the models, as the heavy rainfall over these regions is generally associated with the steep orography. However, the simulated annual cycles in South Asian mean precipitation and surface air temperature are reasonably close to the observed (Supplementary Material Figure S11.24). The MMD models capture the general regional features of the monsoon, such as the low rainfall amounts coupled with high variability over northwest India. However, there has not yet been sufficient analysis of whether finer details of regional significance are simulated more adequately in the MMD models.

Recent work indicates that time-slice experiments using an AGCM with prescribed SSTs, as opposed to a fully coupled system, are not able to accurately capture the South Asian monsoon response (Douville, 2005). Thus, neglecting the short-term SST feedback and variability seems to have a significant impact on the projected monsoon response to global warming, complicating the regional downscaling problem. However, May (2004a) notes that the high-resolution (about 1.5 degrees) European Centre-Hamburg (ECHAM4) GCM simulates the variability and extremes of daily rainfall (intensity as well as frequency of wet days) in good agreement with the observations (Global Precipitation Climatology Project, Huffman et al., 2001).

Three-member ensembles of baseline simulations (1961–1990) from an RCM (PRECIS) at 50 km resolution have confirmed that significant improvements in the representation of regional processes over South Asia can be achieved (Rupa Kumar et al., 2006). For example, the steep gradients in monsoon precipitation with a maximum along the western coast of India are well represented in PRECIS.

East Asia

Simulated temperatures in most MMD models are too low in all seasons over East Asia; the mean cold bias is largest in winter and smallest in summer. Zhou and Yu (2006) show that over China, the models perform reasonably in simulating the dominant variations of the mean temperature over China, but not the spatial distributions. The annual precipitation over East Asia exceeds the observed estimates in almost all models and the rain band in the mid-latitudes is shifted northward in seasons other than summer. This bias in the placement of the rains in central China also occurred in earlier models (e.g., Zhou and Li, 2002; Gao et al., 2004). In winter, the area-mean precipitation is overestimated by more than 50% on average due to strengthening of the rain band associated with extratropical systems over South China. The bias and inter-model differences

in precipitation are smallest in summer but the northward shift of this rain band results in large discrepancies in summer rainfall distribution over Korea, Japan and adjacent seas.

Kusunoki et al. (2006) find that the simulation of the Meiyu-Changma-Baiu rains in the East Asian monsoon is improved substantially with increasing horizontal resolution. Confirming the importance of resolution, RCMs simulate more realistic climatic characteristics over East Asia than AOGCMs, whether driven by re-analyses or by AOGCMs (e.g., Ding et al., 2003; Oh et al., 2004; Fu et al., 2005; Zhang et al., 2005a, Ding et al., 2006; Sasaki et al., 2006b). Several studies reproduce the fine-scale climatology of small areas using a multiply nested RCM (Im et al., 2006) and a very-high resolution (5 km) RCM (Yasunaga et al., 2006). Gao et al. (2006b) report that simulated East Asia large-scale precipitation patterns are significantly affected by resolution, particularly during the mid- to late-monsoon months, when smaller-scale convective processes dominate.

Southeast Asia

The broad-scale spatial distribution of temperature and precipitation in DJF and JJA averaged across the MMD models compares well with observations. Rajendran et al. (2004) examine the simulation of current climate in the MRI coupled model (see Table 8.1 for model details). Large-scale features were well simulated, but errors in the timing of peak rainfall over Indochina were considered a major shortcoming. Collier et al. (2004) assess the performance of the CCSM3 model (see Table 8.1 for model details) in simulating tropical precipitation forced by observed SST. Simulation was good over the Maritime continent compared to the simulation for other tropical regions. B. Wang et al. (2004) assess the ability of 11 AGCMs in the Asian-Australian monsoon region simulation forced with observed SST variations. They found that the models' ability to simulate observed interannual rainfall variations was poorest in the Southeast Asian portion of the domain. Since current AOGCMs continue to have some significant shortcomings in representing ENSO variability (see Section 8.4), the difficulty of projecting changes in ENSO-related rainfall in this region is compounded.

Rainfall simulation across the region at finer scales has been examined in some studies. The Commonwealth Scientific and Industrial Research Organisation (CSIRO) stretched-grid Conformal-Cubic Atmospheric Model (CCAM) at 80-km resolution shows reasonable precipitation simulation in JJA, although Indochina tended to be drier than in the observations (McGregor and Nguyen, 2003). Aldrian et al. (2004a) conducted a number of simulations with the Max-Planck Institute (MPI) regional model for an Indonesian domain, forced by reanalyses and by the ECHAM4 GCM. The model was able to represent the spatial pattern of seasonal rainfall. It was found that a resolution of at least 50 km was required to simulate rainfall seasonality correctly over Sulawesi. The formulation of a coupled regional model improves regional rainfall simulation over the oceans (Aldrian et al., 2004b). Arakawa and Kitoh (2005) demonstrate an accurate simulation of the diurnal cycle of rainfall over Indonesia with an AGCM of 20-km horizontal resolution.

Central Asia and Tibet

Due to the complex topography and the associated mesoscale weather systems of the high-altitude and arid areas, GCMs typically perform poorly over the region. Importantly, the GCMs, and to a lesser extent RCMs, tend to overestimate the precipitation over arid and semi-arid areas in the north (e.g., Small et al., 1999; Gao et al., 2001; Elguindi and Giorgi, 2006).

Over Tibet, the few available RCM simulations generally exhibit improved performance in the simulation of present-day climate compared to GCMs (e.g., Gao et al., 2003a,b; Zhang et al., 2005b). For example, the GCM simulation of Gao et al. (2003a) overestimated the precipitation over the north-western Tibetan Plateau by a factor of five to six, while in an RCM nested in this model, the overestimate was less than a factor of two.

11.4.3 Climate Projections

11.4.3.1 Temperature

The temperature projections for the 21st century based on the MMD-A1B models (Figure 11.8 and Table 11.1) represent a strong warming over the 21st century. Warming is similar to the global mean warming in Southeast Asia (mean warming between 1980 to 1999 and 2080 to 2099 of 2.5°C). Warming greater than the global mean is projected for South Asia (3.3°C) and East Asia (3.3°C), and much more than the global mean in the continental interior of Asia (3.7°C in central Asia, 3.8°C in Tibet and 4.3°C in northern Asia). In four out of the six regions, the largest warming occurs in DJF, but in central Asia, the maximum occurs in JJA. In Southeast Asia, the warming is nearly the same throughout the year. Model-to-model variation in projected warming is typically about three-quarters of the mean warming (e.g., 2.0°C to 4.7°C for annual mean warming in South Asia). The 5 to 95% ranges based on Tebaldi et al. (2004a) suggest a slightly smaller uncertainty than the full range of the model results (Supplementary Material Table S11.2). Because the projected warming is large compared to the interannual temperature variability, a large majority of individual years and seasons in the late 21st century are likely to be extremely warm by present standards (Table 11.1). The projections of changes in mean temperature and, where available, temperature extremes, are discussed below in more detail for individual Asian regions.

South Asia

For the A1B scenario, the MMD-A1B models show a median increase of 3.3°C (see Table 11.1) in annual mean temperature by the end of the 21st century. The median warming varies seasonally from 2.7°C in JJA to 3.6°C in DJF, and is likely to increase northward in the area, particularly in winter, and from sea to land (Figure 11.9). Studies based on earlier AOGCM simulations (Douville et al., 2000; Lal and Harasawa, 2001; Lal et al., 2001; Rupa Kumar and Ashrit, 2001; Rupa Kumar et al., 2002, 2003; Ashrit et al., 2003; May, 2004b) support this picture. The tendency of the warming to be more pronounced in

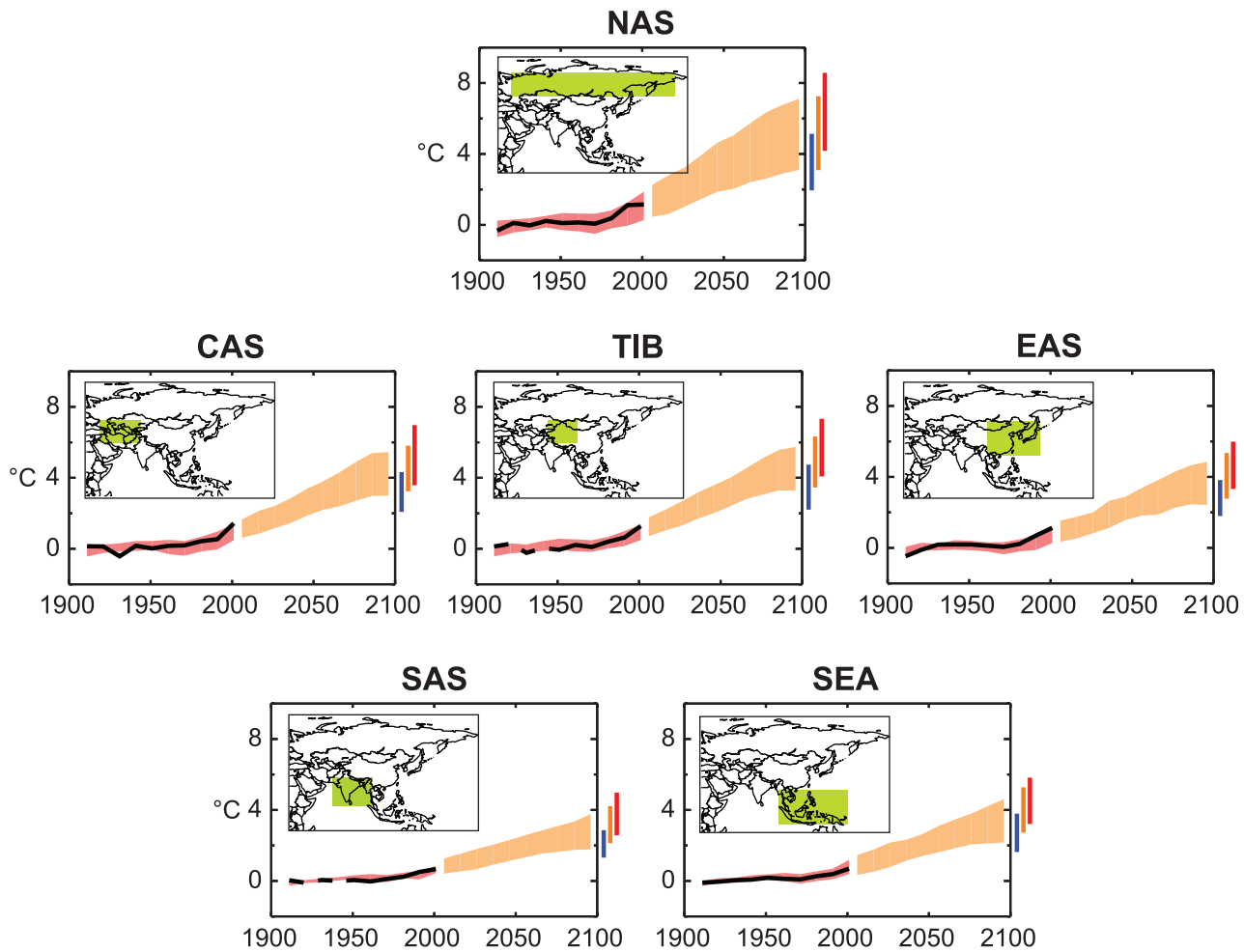


Figure 11.8. Temperature anomalies with respect to 1901 to 1950 for six Asian land regions for 1906 to 2005 (black line) and as simulated (red envelope) by MMD models incorporating known forcings; and as projected for 2001 to 2100 by MMD models for the A1B scenario (orange envelope). The bars at the end of the orange envelope represent the range of projected changes for 2091 to 2100 for the B1 scenario (blue), the A1B scenario (orange) and the A2 scenario (red). The black line is dashed where observations are present for less than 50% of the area in the decade concerned. More details on the construction of these figures are given in Box 11.1 and Section 11.1.2.

winter is also a conspicuous feature of the observed temperature trends over India (Rupa Kumar et al., 2002, 2003).

Downscaled projections using the Hadley Centre Regional Model (HadRM2) indicate future increases in extreme daily maximum and minimum temperatures throughout South Asia due to the increase in greenhouse gas concentrations. This projected increase is of the order of 2°C to 4°C in the mid-21st century under the IPCC Scenario IS92a in both minimum and maximum temperatures (Krishna Kumar et al., 2003). Results from a more recent RCM, PRECIS, indicate that the night temperatures increase faster than the day temperatures, with the implication that cold extremes are very likely to be less severe in the future (Rupa Kumar et al., 2006).

East Asia

The MMD-A1B models project a median warming of 3.3°C (Table 11.1) by the end of the 21st century, which varies seasonally from 3.0°C in JJA to 3.6°C in DJF. The warming tends to be largest in winter, especially in the northern inland area (Figure 11.9), but the area-mean difference from the other

seasons is not large. There is no obvious relationship between model bias and the magnitude of the warming. The spatial pattern of larger warming over northwest EAS (Figure 11.9) is very similar to the ensemble mean of pre-MMD models. Regional Climate Model simulations show mean temperature increases similar to those simulated by AOGCMs (Gao et al., 2001, 2002; Kwon et al., 2003; Jiang, 2005; Kurihara et al., 2005; Y.L. Xu et al., 2005).

Daily maximum and minimum temperatures are very likely to increase in East Asia, resulting in more severe warm but less severe cold extremes (Gao et al., 2002; Mizuta et al., 2005; Y.L. Xu et al., 2005; Boo et al., 2006). Mizuta et al. (2005) analyse temperature-based extreme indices over Japan with a 20-km mesh AGCM and find the changes in the indices to be basically those expected from the mean temperature increase, with changes in the distribution around the mean not playing a large role. Boo et al. (2005) report similar results for Korea. Gao et al. (2002) and Y.L. Xu et al. (2005) find a reduced diurnal temperature range in China and larger increases in daily minimum than maximum temperatures.

Southeast Asia

In the MMD-A1B simulations, the median warming for the region is 2.5°C by the end of the 21st century, with little seasonal variation (Table 11.1). Simulations by the CSIRO Division of Atmospheric Research Limited Area Model (DARLAM; McGregor et al., 1998) and more recently by the CSIRO stretched-grid model (McGregor and Dix, 2001) centred on the Indochina Peninsula (AIACC, 2004) at a resolution of 14 km have demonstrated the potential for significant local variation in warming, particularly the tendency for warming to be significantly stronger over the interior of the landmasses than over the surrounding coastal regions. A tendency for the warming to be stronger over Indochina and the larger landmasses of the archipelago is also visible in the MMD models (Figures 10.8 and 11.9). As in other regions, the magnitude of the warming depends on the forcing scenario.

Central Asia and Tibet

In the MMD-A1B simulations, central Asia warms by a median of 3.7°C, and Tibet by 3.8°C (Table 11.1) by the end of the 21st century. The seasonal variation in the simulated warming is modest. Findings from earlier multi-model studies (Zhao et al., 2002; Xu et al., 2003a,b; Meleshko et al., 2004; Y. Xu et al., 2005) are consistent with the MMD models' results.

An RCM study by Gao et al. (2003b) indicates greater warming over the Plateau compared to surrounding areas, with the largest warming at highest altitudes, for example, over the Himalayas (see also Box 11.3). The higher temperature increase over high-altitude areas can be explained by the decrease in surface albedo associated with the melting of snow and ice (Giorgi et al., 1997). This phenomenon is found to different extents in some, although not all, of the MMD models, and it is visible in the multi-model mean changes, particularly in the winter (Figure 11.9).

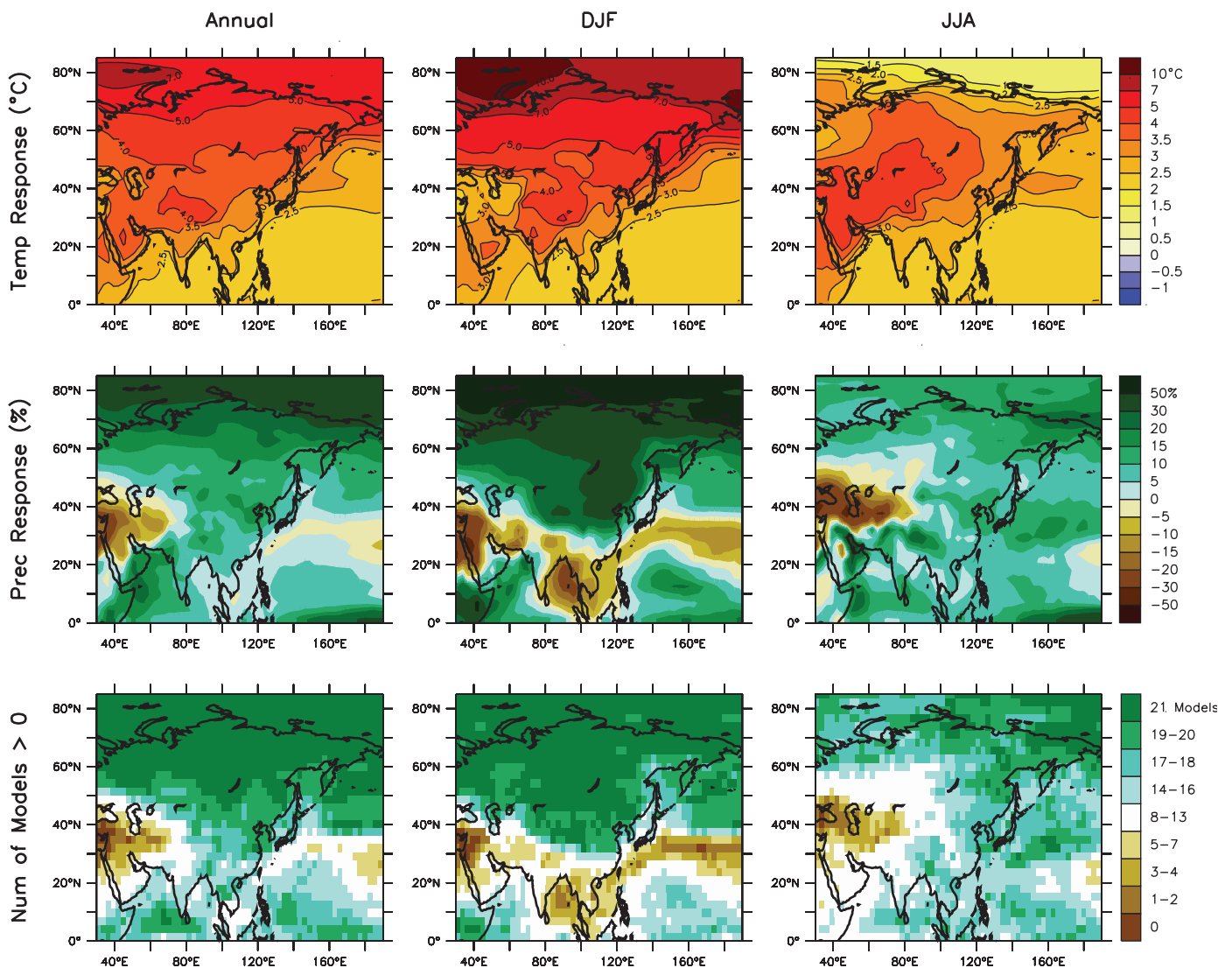


Figure 11.9. Temperature and precipitation changes over Asia from the MMD-A1B simulations. Top row: Annual mean, DJF and JJA temperature change between 1980 to 1999 and 2080 to 2099, averaged over 21 models. Middle row: same as top, but for fractional change in precipitation. Bottom row: number of models out of 21 that project increases in precipitation.

11.4.3.2 Precipitation and Associated Circulation Systems

The MMD models indicate an increase in annual precipitation in most of Asia during this century, the percentage increase being largest and most consistent among models in North and East Asia (Figure 11.9 and Table 11.1). The main exception is central Asia, particularly its western parts, where most models simulate reduced precipitation in the summer. Based on these simulations, sub-continental boreal winter precipitation is very likely to increase in northern Asia and the Tibetan Plateau, and likely to increase in eastern Asia. It is also likely to increase in the southern parts of Southeast Asia. Summer precipitation is likely to increase in North, South, Southeast and East Asia, but decrease in central Asia. Probability estimates from Tebaldi et al. (2004a; see Supplementary Material Table S11.2) support these judgments.

The projected decrease in mean precipitation in central Asia is accompanied by an increase in the frequency of very dry spring, summer and autumn seasons; conversely, in winter, where models project increases in the mean precipitation, very high precipitation becomes more common (Table 11.1). The projections of changes in mean precipitation and, where available, precipitation extremes, are discussed in more detail below for individual Asian regions. Where appropriate, the connection to changes in circulation systems that bring precipitation is also discussed. Smaller (slightly larger) changes are generally projected for the B1 (A2) scenario, but the inter-scenario differences are small compared with the inter-model differences.

South Asia

Most of the MMD-A1B models project a decrease in precipitation in DJF (the dry season), and an increase during the rest of the year. The median change is 11% by the end of the 21st century, and seasonally is -5% in DJF and 11% in JJA, with a large inter-model spread (Table 11.1). The probabilistic method of Tebaldi et al. (2004a) similarly shows a large spread, although only 3 of the 21 models project a decrease in annual precipitation. This qualitative agreement on increasing precipitation for most of the year is also supported by earlier AOGCM simulations (Lal and Harasawa, 2001; Lal et al., 2001; Rupa Kumar and Ashrit, 2001; Rupa Kumar et al., 2002, 2003; Ashrit et al., 2003; May, 2004b).

In a study with four GCMs, Douville et al. (2000) find a significant spread in the summer monsoon precipitation anomalies despite a general weakening of the monsoon circulation (see also May, 2004b). They conclude that the changes in atmospheric water content, precipitation and land surface hydrology under greenhouse forcing could be more important than the increase in the land-sea thermal gradient for the future evolution of monsoon precipitation. Stephenson et al. (2001) propose that the consequences of climate change could manifest in different ways in the physical and dynamical components of monsoon circulation. Douville et al. (2000) also argue that the weakening of the ENSO-monsoon correlation could be explained by a possible increase in precipitable water as a result of global

warming, rather than by an increased land-sea thermal gradient. However, model diagnostics using ECHAM4 to investigate this aspect indicate that both the above mechanisms can play a role in monsoon changes in a greenhouse-gas warming scenario. Ashrit et al. (2001) show that the monsoon deficiency due to El Niño might not be as severe, while the favourable impact of La Niña seems to remain unchanged. In a later study using the Centre National de Recherches Météorologiques (CNRM) GCM, Ashrit et al. (2003) find that the simulated ENSO-monsoon teleconnection shows a strong modulation on multi-decadal time scales, but no systematic change with increasing amounts of greenhouse gases.

Time-slice experiments with ECHAM4 indicate a general increase in the intensity of heavy rainfall events in the future, with large increases over the Arabian Sea and the tropical Indian Ocean, in northern Pakistan and northwest India, as well as in northeast India, Bangladesh and Myanmar (May, 2004a). The HadRM2 RCM shows an overall decrease by up to 15 days in the annual number of rainy days over a large part of South Asia, under the IS92a scenario in the 2050s, but with an increase in the precipitation intensity as well as extreme precipitation (Krishna Kumar et al., 2003). Simulations with the PRECIS RCM also project substantial increases in extreme precipitation over a large area, particularly over the west coast of India and west central India (Rupa Kumar et al., 2006). Dairaku and Emori (2006) show from a high-resolution AGCM simulation (about 1.5 degrees) that the increased extreme precipitation over land in South Asia would arise mainly from dynamic effects, that is, enhanced upward motion due to the northward shift of monsoon circulation.

Based on regional HadRM2 simulations, Unnikrishnan et al. (2006) report increases in the frequency as well as intensities of tropical cyclones in the 2050s under the IS92a scenario in the Bay of Bengal, which will cause more heavy precipitation in the surrounding coastal regions of South Asia, during both southwest and northeast monsoon seasons.

East Asia

The MMD-A1B models project an increase in precipitation in East Asia in all seasons. The median change at the end of the 21st century is +9% in the annual mean with little seasonal difference, and a large model spread in DJF (Table 11.1). In winter, this increase contrasts with a decrease in precipitation over the ocean to the southeast, where reduced precipitation corresponds well with increased mean sea level pressure. While the projections have good qualitative agreement, there remain large quantitative differences among the models, which is consistent with previous studies (e.g., Giorgi et al., 2001a; Hu et al., 2003; Min et al., 2004).

Based on the MMD models, Kimoto (2005) projects increased Meiyu-Changma-Baiu activity associated with the strengthening of anticyclonic cells to its south and north, and Kwon et al. (2005) show increased East Asia summer precipitation due to an enhanced monsoon circulation in the decaying phase of El Niño. A 20-km mesh AGCM simulation shows that Meiyu-Changma-Baiu rainfall increases over the Yangtze River valley,

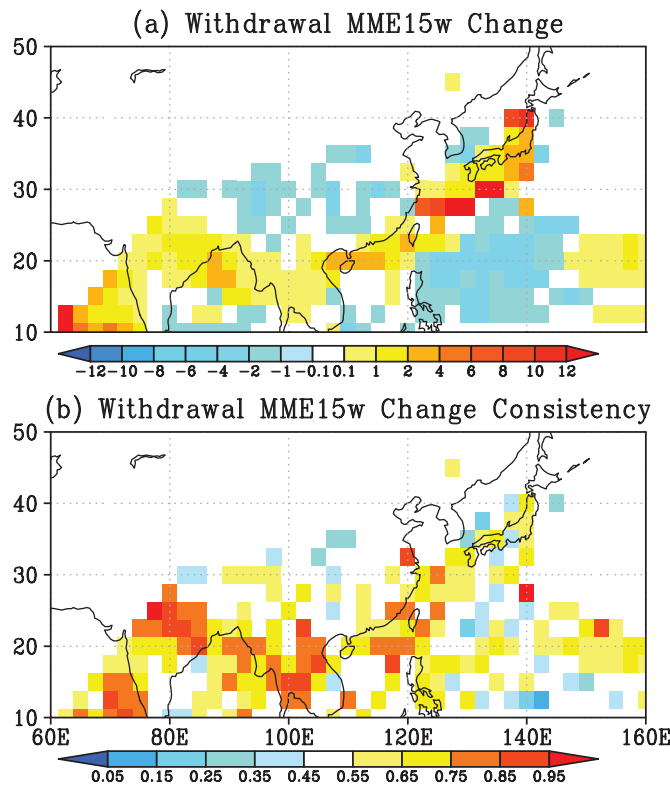


Figure 11.10. (a) The ensemble mean change in withdrawal date of the summer rainy season between the MMD-A1B projections in 2081 to 2100 as compared with the 1981 to 2000 period in the 20C3M simulations. A positive value indicates a later withdrawal date in the A1B scenario. Units are 5 days. (b) Fraction of the models projecting a positive difference in withdrawal date. (Kitoh and Uchiyama, 2006).

the East China Sea and western Japan, while rainfall decreases to the north of these areas mostly due to the lengthening of the Meiyu-Changma-Baiu (Kusunoki et al., 2006). Simulations by RCMs support the results from AOGCMs. For example, Kurihara et al. (2005) show an increase in precipitation over western Japan in summer.

Kitoh and Uchiyama (2006) investigated the onset and withdrawal times of the Asian summer rainfall season in 15 MMD simulations (Figure 11.10). They find a delay in early summer rain withdrawal over the region extending from Taiwan to the Ryukyu Islands to the south of Japan, but an earlier withdrawal over the Yangtze Basin, although the latter is not significant due to large inter-model variation. Changes in onset dates are smaller.

Yasunaga et al. (2006) used a 5-km mesh cloud-resolving RCM to investigate summer rainfall in Japan. They find no changes in June rainfall but increased July rainfall in a warmer climate. The increase in July can be attributed to the more frequent large-precipitation systems.

Intense precipitation events are very likely to increase in East Asia, consistent with the historical trend in this region (Fujibé et al., 2005; Zhai et al., 2005). Kanada et al. (2005) show, using a 5-km resolution RCM, that the confluence of disturbances from the Chinese continent and from the East China Sea would

often cause extremely heavy precipitation over Japan's Kyushu Island in July in a warmer climate. An increase in the frequency and intensity of heavy precipitation events also occurs in Korea in the long RCM simulation of Boo et al. (2006). Similarly based on RCM simulations, Y.L. Xu et al. (2005) report more extreme precipitation events over China. Gao et al. (2002) find a simulated increase in the number of rainy days in northwest China, and a decrease in rain days but an increase in days with heavy rain over South China. Kitoh et al. (2005) report similar results in South China from an AOGCM simulation.

Kimoto et al. (2005) suggest that the frequencies of non-precipitating and heavy (≥ 30 mm day⁻¹) rainfall days would increase significantly at the expense of relatively weak (1–20 mm day⁻¹) rainfall days in Japan. Mizuta et al. (2005) find significantly more days with heavy precipitation and stronger average precipitation intensity in western Japan and Hokkaido Island. Hasegawa and Emori (2005) show that daily precipitation associated with tropical cyclones over the western North Pacific would increase.

The previously noted weakening of the East Asian winter monsoon (e.g., Hu et al., 2000) is further confirmed by recent studies (e.g., Kimoto, 2005; Hori and Ueda, 2005).

Southeast Asia

Area-mean precipitation over Southeast Asia increases in most MMD model simulations, with a median change of about 7% in all seasons (Table 11.1), but the projected seasonal changes vary strongly within the region. The seasonal confidence intervals based on the methods of Tebaldi et al. (2004a,b) are similar for DJF and JJA (roughly –4% to 17%). The strongest and most consistent increases broadly follow the ITCZ, lying over northern Indonesia and Indochina in JJA, and over southern Indonesia and Papua New Guinea in DJF (Figure 11.9). Away from the ITCZ, precipitation decreases are often simulated. The pattern is broadly one of wet season rainfall increase and dry season decrease.

Earlier studies of precipitation change in the area in some cases have suggested a worse inter-model agreement than found for the MMD models. Both Giorgi et al. (2001a) and Ruosteenoja et al. (2003) find inconsistency in the simulated direction of precipitation change in the region, but a relatively narrow range of possible changes; similar results were found over an Indonesian domain by Boer and Faqih (2004). Compositing the projections from a range of earlier simulations forced by the IS92a scenario, Hulme and Sheard (1999a,b) find a pattern of rainfall increase across northern Indonesia and the Philippines, and decrease over the southern Indonesian archipelago. More recently, Boer and Faqih (2004) compared patterns of change across Indonesia from five AOGCMS and obtained highly contrasting results. They conclude that ‘no generalisation could be made on the impact of global warming on rainfall’ in the region.

The regional high-resolution simulations of McGregor et al. (1998), McGregor and Dix (2001) and AIACC (2004) have demonstrated the potential for significant local variation in projected precipitation change. The simulations showed

considerable regional detail in the simulated patterns of change, but little consistency across the three simulations. The authors related this result to significant deficiencies in the current-climate simulations of the models for this region.

Rainfall variability will be affected by changes in ENSO and its effect on monsoon variability, but this is not well understood (see Section 10.3). However, as Boer and Faqih (2004) note, those parts of Indonesia that experience a mean rainfall decrease are likely to also experience increases in drought risk. The region is also likely to share the general tendency for daily

extreme precipitation to become more intense under enhanced greenhouse conditions, particularly where the mean precipitation is projected to increase. This has been demonstrated in a range of global and regional studies (see Section 10.3), but needs explicit study for the Southeast Asian region.

The northern part of the Southeast Asian region will be affected by any change in tropical cyclone characteristics. As noted in Section 10.3, there is evidence in general of likely increases in tropical cyclone intensity, but less consistency about how occurrence will change (see also Walsh, 2004). The likely

Box 11.3: Climatic Change in Mountain Regions

Although mountains differ considerably from one region to another, one common feature is the complexity of their topography. Related characteristics include rapid and systematic changes in climatic parameters, in particular temperature and precipitation, over very short distances (Becker and Bugmann, 1997); greatly enhanced direct runoff and erosion; systematic variation of other climatic (e.g., radiation) and environmental (e.g., soil types) factors. In some mountain regions, it has been shown that temperature trends and anomalies have an elevation dependence (Giorgi et al., 1997), a feature that is not, however, systematically observed in all upland areas (e.g., Vuille and Bradley, 2000, for the Andes).

Few model simulations have attempted to directly address issues related specifically to future climatic change in mountain regions, primarily because the current spatial resolution of GCMs and even RCMs is generally too crude to adequately represent the topographic detail of most mountain regions and other climate-relevant features such as land cover that are important determinants in modulating climate in the mountains (Beniston et al., 2003). High-resolution RCM simulations (5-km and 1-km grid scales) are used for specific investigations of processes such as surface runoff, infiltration, evaporation and extreme events such as precipitation (Weisman et al., 1997; Walser and Schär, 2004; Kanada et al., 2005; Yasunaga et al., 2006) and damaging wind storms (Goyette et al., 2003), but these simulations are too costly to operate in a 'climate mode'. Because of the highly complex terrain, empirical and statistical downscaling techniques have often been seen as a very valuable tool to generate climate change information for mountainous regions (e.g., Benestad, 2005; Hanssen-Bauer et al., 2005).

Projections of changes in precipitation patterns in mountains are unreliable in most GCMs because the controls of topography on precipitation are not adequately represented. In addition, it is now recognised that the superimposed effects of natural modes of climatic variability such as ENSO or the NAO can perturb mean precipitation patterns on time scales ranging from seasons to decades (Beniston and Jungo, 2001). Even though there has been progress in reproducing some of these mechanisms in coupled ocean-atmosphere models (Osborn et al., 1999), deficiencies remain and prevent a good simulation of these large-scale modes of variability (see also Section 8.4). However, several studies indicate that the higher resolution of RCMs and GCMs can represent observed mesoscale patterns of the precipitation climate that are not resolved in coarse-resolution GCMs (Frei et al., 2003; Kanada et al., 2005; Schmidli et al., 2006; Yasunaga et al., 2006).

Snow and ice are, for many mountain ranges, a key component of the hydrological cycle, and the seasonal character and amount of runoff is closely linked to cryospheric processes. In temperate mountain regions, the snowpack is often close to its melting point, so that it may respond rapidly to minor changes in temperature. As warming increases in the future, regions where snowfall is the current norm will increasingly experience precipitation in the form of rain (e.g., Leung et al., 2004). For every degree celsius increase in temperature, the snow line will on average rise by about 150 m. Although the snow line is difficult to determine in the field, it is established that at lower elevations the snow line is very likely to rise by more than this simple average estimate (e.g., Martin et al., 1994; Vincent, 2002; Gerbaux et al., 2005; see also Section 4.2). Beniston et al. (2003) show that for a 4°C shift in mean winter temperatures in the European Alps, as projected by recent RCM simulations for climatic change in Europe under the A2 emissions scenario, snow duration is likely to be reduced by 50% at altitudes near 2,000 m and by 95% at levels below 1,000 m. Where some models predict an increase in winter precipitation, this increase does not compensate for the effect of changing temperature. Similar reductions in snow cover that will affect other mountain regions of the world will have a number of implications, in particular for early seasonal runoff (e.g., Beniston, 2003), and the triggering of the annual cycle of mountain vegetation (Cayan et al., 2001; Keller et al., 2005).

Because mountains are the source region for over 50% of the globe's rivers, the impacts of climatic change on mountain hydrology not only affect the mountains themselves but also populated lowland regions that depend on mountain water resources for domestic, agricultural, energy and industrial supply. Water resources for populated lowland regions are influenced by mountain climates and vegetation; shifts in intra-annual precipitation regimes could lead to critical water amounts resulting in greater flood or drought episodes (e.g., Barnett et al., 2005; Graham et al., 2007).

increase in intensity (precipitation and winds) is supported for the northwest Pacific (and other regions) by the recent modelling study of Knutson and Tuleya (2004). The high-resolution time-slice modelling experiment of Hasegawa and Emori (2005) also demonstrates an increase in tropical cyclone precipitation in the western North Pacific, but not an increase in tropical cyclone intensity. Wu and Wang (2004) examined possible changes in tracks in the northwest Pacific due to changes in steering flow in two Geophysical Fluid Dynamics Laboratory (GFDL) enhanced greenhouse gas experiments. Tracks moved more north-easterly, possibly reducing tropical cyclone frequency in the Southeast Asian region. Since most of the tropical cyclones form along the monsoon trough and are also influenced by ENSO, changes in the occurrence, intensity and characteristics of tropical cyclones and their interannual variability will be affected by changes in ENSO (see Section 10.3).

Central Asia and Tibet

Precipitation over central Asia increases in most MMD-A1B projections for DJF but decreases in the other seasons. The median change by the end of the 21st century is -3% in the annual mean, with $+4\%$ in DJF and -13% in JJA (the dry season) (Table 11.1). This seasonal variation in the changes is broadly consistent with the earlier multi-model study of Meleshko et al. (2004), although they find an increase in summer precipitation in the northern part of the area.

Over the Tibetan Plateau, all MMD-A1B models project increased precipitation in DJF (median 19%). Most but not all models also simulate increased precipitation in the other seasons (Table 11.1). Earlier studies both by AOGCMs and RCMs are consistent with these findings (Gao et al., 2003b; Y. Xu et al., 2003a,b, 2005).

11.5 North America

Assessment of projected climate change for North America:

All of North America is very likely to warm during this century, and the annual mean warming is likely to exceed the global mean warming in most areas. In northern regions, warming is likely to be largest in winter, and in the southwest USA largest in summer. The lowest winter temperatures are likely to increase more than the average winter temperature in northern North America, and the highest summer temperatures are likely to increase more than the average summer temperature in the southwest USA.

Annual mean precipitation is very likely to increase in Canada and the northeast USA, and likely to decrease in the southwest USA. In southern Canada, precipitation is likely to increase in winter and spring, but decrease in summer.

Snow season length and snow depth are very likely to decrease in most of North America, except in the northernmost part of Canada where maximum snow depth is likely to increase.

The uncertainties in regional climate changes over North America are strongly linked to the ability of AOGCMs to reproduce the dynamical features affecting the region (Chapter 10). Atmosphere-Ocean General Circulation Models exhibit large model-to-model differences in ENSO and NAO/Arctic Oscillation (AO) responses to climate changes. Changes in the Atlantic MOC are uncertain, and thus so is the magnitude of consequent reduced warming in the extreme north-eastern part of North America; cooling here cannot be totally excluded. The Hudson Bay and Canadian Archipelago are poorly resolved by AOGCMs, contributing to uncertainty in ocean circulation and sea ice changes and their influence on the climate of northern regions. Tropical cyclones are not resolved by the MMD models and inferred changes in the frequency, intensity and tracks of disturbances making landfall in southeast regions remain uncertain. At the coarse horizontal resolution of the MMD models, high-altitude terrain is poorly resolved, which likely results in an underestimation of warming associated with snow-albedo feedback at high elevations in western regions. Little is known about the dynamical consequences of the larger warming over land than over ocean, which may affect the northward displacement and intensification of the subtropical anticyclone off the West Coast. This could affect the subtropical North Pacific eastern boundary current, the offshore Ekman transport, the upwelling and its cooling effect on SST, the persistent marine stratus clouds and thus precipitation in the southwest USA.

The uncertainty associated with RCM projections of climate change over North America remains large despite the investments made in increasing horizontal resolution. All reported RCM projections were driven by earlier AOGCMs that exhibited larger biases than the MMD models. Coordinated ensemble RCM projections over North America are not yet available, making it difficult to compare results.

11.5.1 Key Processes

Central and northern regions of North America are under the influence of mid-latitude cyclones. Projections by AOGCMs (Chapter 10) generally indicate a slight poleward shift in storm tracks, an increase in the number of strong cyclones but a reduction in medium-strength cyclones over Canada and poleward of 70°N . Consequent with the projected warming, the atmospheric moisture transport and convergence is projected to increase, resulting in a widespread increase in annual precipitation over most of the continent except the south and south-western part of the USA and over Mexico.

The southwest region is very arid, under the general influence of a subtropical ridge of high pressure associated with the thermal contrast between land and adjacent ocean. The North American Monsoon System develops in early July (e.g., Higgins

and Mo, 1997); the prevailing winds over the Gulf of California undergo a seasonal reversal, from northerly in winter to southerly in summer, bringing a pronounced increase in rainfall over the southwest USA and ending the late spring wet period in the Great Plains (e.g., Bordoni et al., 2004). The projection of smaller warming over the Pacific Ocean than over the continent, and amplification and northward displacement of the subtropical anticyclone, is likely to induce a decrease in annual precipitation in the south-western USA and northern Mexico.

The Great Plains Low-Level Jet (LLJ) is a dynamical feature that transports considerable moisture from the Gulf of Mexico into the central USA, playing a critical role in the summer precipitation there. Several factors, including the land-sea thermal contrast, contribute to the strength of the moisture convergence during the night and early morning, resulting in prominent nocturnal maximum precipitation in the plains of the USA (such as Nebraska and Iowa; e.g., Augustine and Caracena, 1994). The projections of climate changes indicate an increased land-sea thermal contrast in summer, with anticipated repercussions on the LLJ.

Interannual variability over North America is connected to two large-scale oscillation patterns (see Chapter 3), ENSO and the NAO/AO. The MMD model projections indicate an intensification of the polar vortex and many models project a decrease in the arctic surface pressure, which contributes to an increase in the AO/NAO index; the uncertainty is large, however, due to the diverse responses of AOGCMs in simulating the Aleutian Low (Chapter 10). The MMD model projections indicate a shift towards mean El-Niño like conditions, with the eastern Pacific warming more than the western Pacific; there is a wide range of behaviour among the current models, with no clear indication of possible changes in the amplitude or period of El Niño (Chapter 10).

11.5.2 Skill of Models in Simulating Present Climate

Individual AOGCMs in the MMD vary in their ability to reproduce the observed patterns of pressure, surface air temperature and precipitation over North America (Chapter 8). The ensemble mean of MMD models reproduces very well the annual-mean mean sea level pressure distribution (Section 8.4). The maximum error is of the order of ± 2 hPa, with the simulated Aleutian Low pressure extending somewhat too far north, probably due to the inability of coarse-resolution models to adequately resolve the high topography of the Rocky Mountains that blocks incoming cyclones in the Gulf of Alaska. Conversely, the pressure trough over the Labrador Sea is not deep enough. The depth of the thermal low pressure over the southwest region in summer is somewhat excessive.

The MMD models simulate successfully the overall pattern of surface air temperature over North America, with reduced biases compared to those reported in the TAR. Ensemble-mean regional mean bias ranges from -4.5°C to 1.9°C for the 25th to 75th percentile range, and medians vary from -2.4°C to $+0.4^{\circ}\text{C}$ depending on region and season (Supplementary

Material Table S11.1). The ensemble mean of MMD models reproduces the overall distribution of annual mean precipitation (Supplementary Material Table S11.1), but almost all models overestimate precipitation for western and northern regions. The ensemble-mean regional mean precipitation bias medians vary from -16% to $+93\%$ depending on region and season. The ensemble-mean precipitation is excessive on the windward side of major mountain ranges, with the excess reaching 1 to 2 mm day⁻¹ over high terrain in the west of the continent.

Regional Climate Models are quite successful in reproducing the overall climate of North America when driven by reanalyses. Over a $10^{\circ} \times 10^{\circ}$ Southern Plains region, an ensemble of six RCMs in the North American Regional Climate Change Assessment Program (NARCCAP; Mearns et al., 2005) had 76% of all monthly temperature biases within $\pm 2^{\circ}\text{C}$ and 82% of all monthly precipitation biases within $\pm 50\%$, based on preliminary results for a single year. RCM simulations over North America exhibit rather high sensitivity to parameters such as domain size (e.g., Juang and Hong, 2001; Pan et al., 2001; Vannitsem and Chomé, 2005) and the intensity of large-scale nudging (providing large-scale information to the interior of the model domain, see e.g., von Storch et al., 2000; Miguez-Macho et al., 2004) if used. In general, RCMs are more skilful at reproducing cold-season temperature and precipitation (e.g., Pan et al., 2001; Han and Roads, 2004; Plummer et al., 2006) because the warm-season climate is more controlled by mesoscale and convective-scale precipitation events, which are harder to simulate (Giorgi et al., 2001a; Leung et al., 2003; Liang et al., 2004; Jiao and Caya, 2006). On the other hand, Gutowski et al. (2004) find that spatial patterns of monthly precipitation for the USA, when viewed as a whole rather than broken into individual regions, are better simulated in summer than winter. Several studies point to the large sensitivity of RCMs to parametrization of moist convection, including the vertical transport of moisture from the boundary layer (Chaboureaud et al., 2004; Jiao and Caya, 2006) and entrainment mixing between convective plumes and the local environment (Derbyshire et al., 2004). In a study of the simulation of the 1993 summer flood in the central USA by 13 RCMs, Anderson et al. (2003) find that all models produced a precipitation maximum that represented the flood, but most underestimated it to some degree, and 10 out of 13 of the models succeeded in reproducing the observed nocturnal maxima of precipitation. Leung et al. (2003) examined the 95th percentile of daily precipitation and find generally good agreement across many areas of the western USA.

A survey of recently published RCM current-climate simulations driven with AOGCMs data reveals that biases in surface air temperature and precipitation are two to three times larger than the simulations driven with reanalyses. The sensitivity of simulated surface air temperature to changing lateral boundary conditions from reanalyses to AOGCMs appears to be high in winter and low in summer (Han and Roads, 2004; Plummer et al., 2006). Most RCM simulations to date for North America have been made for time slices that are too short to properly sample natural variability. Some

RCMs have employed less than optimal formulations, such as outdated parametrizations (e.g., bucket land surface scheme), too few levels in the vertical (e.g., 14) or a too-low uppermost computational level (e.g., 100 hPa).

11.5.3 Climate Projections

11.5.3.1 Surface Air Temperature

The ensemble mean of the MMD models projects a generalised warming for the entire continent with the magnitude projected to increase almost linearly with time (Figure 11.11). On an annual-mean basis, projected surface air temperature warming varies from 2°C to 3°C along the western, southern and eastern continental edges (where at least 16 out of the 21 models project a warming in excess of 2°C) up to more than 5°C in the northern region (where 16 out of the 21 AOGCMs project a warming in excess of 4°C). This warming exceeds the spread among models by a factor of three to four over most of the continent. The warming in the USA is projected to exceed 2°C by nearly all the models, and to exceed 4°C by more than 5 AOGCMs out of 21. More regional and seasonal detail on ranges of projected warming is provided in Table 11.1 and Supplementary Table S11.2.

The largest warming is projected to occur in winter over northern parts of Alaska and Canada, reaching 10°C in the northernmost parts, due to the positive feedback from a reduced period of snow cover. The ensemble-mean northern warming varies from more than 7°C in winter (nearly all AOGCMs project a warming exceeding 4°C) to as little as 2°C in summer.

In summer, ensemble-mean projected warming ranges between 3°C and 5°C over most of the continent, with smaller values near the coasts. In western, central and eastern regions, the projected warming has less seasonal variation and is more modest, especially near the coast, consistent with less warming over the oceans. The warming could be larger in winter over elevated areas as a result of snow-albedo feedback, an effect that is poorly modelled by AOGCMs due to insufficient horizontal resolution (see also Box 11.3). In winter, the northern part of the eastern region is projected to warm most while coastal areas are projected to warm by only 2°C to 3°C.

The climate change response of RCMs is sometimes different from that of the driving AOGCM. This appears to be the result of a combination of factors, including the use of different parametrizations (convection and land surface processes are particularly important over North America in summer) and resolution (different resolution may lead to differing behaviour of the same parametrization). For example, Chen et al. (2003) find that two RCMs project larger temperature changes in summer than their driving AOGCM. In contrast, the projected warming of an RCM compared to its driving AOGCM was found to be 1.5°C less in the central USA (Pan et al., 2004; Liang et al., 2006), a region where observations have shown a cooling trend in recent decades. This resulted in an area of little warming that may have been due to a changing pattern of the LLJ frequency and associated moisture convergence. It is argued that the improved simulation of the LLJ in the RCM is made possible owing to its increased horizontal and vertical resolution. However, other RCMs with similar resolution do not produce the same response.

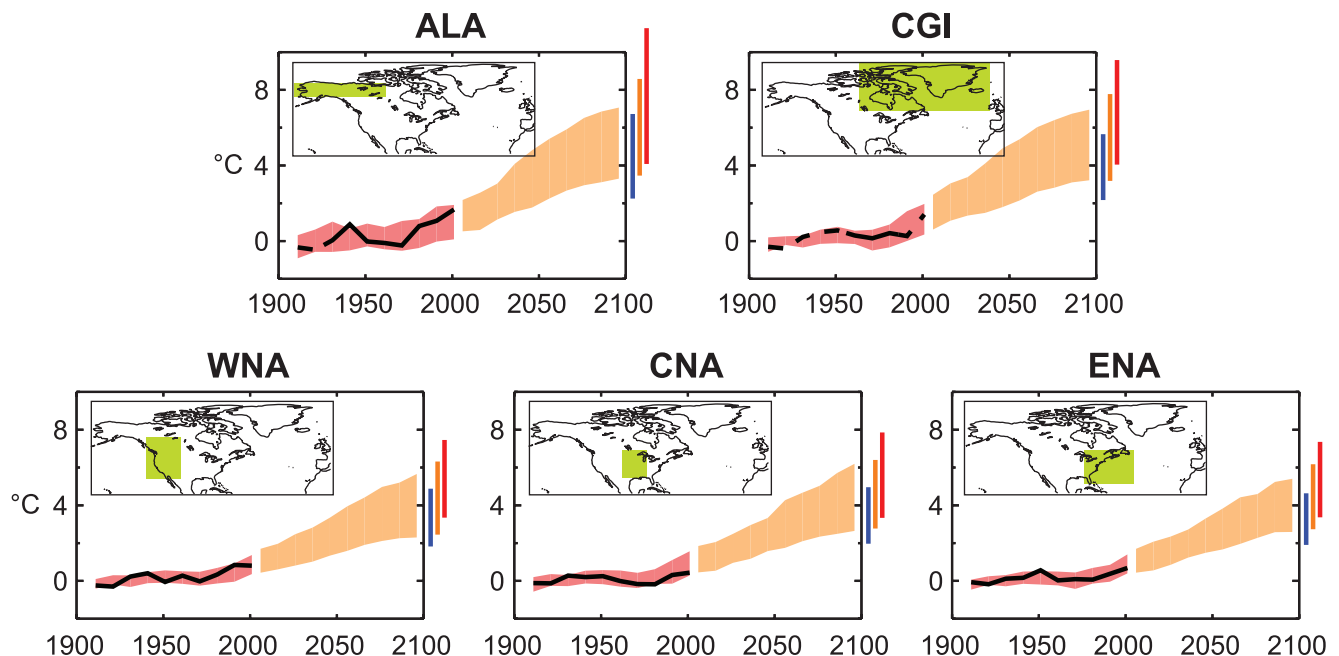


Figure 11.11. Temperature anomalies with respect to 1901 to 1950 for five North American land regions for 1906 to 2005 (black line) and as simulated (red envelope) by MMD models incorporating known forcings; and as projected for 2001 to 2100 by MMD models for the A1B scenario (orange envelope). The bars at the end of the orange envelope represent the range of projected changes for 2091 to 2100 for the B1 scenario (blue), the A1B scenario (orange) and the A2 scenario (red). The black line is dashed where observations are present for less than 50% of the area in the decade concerned. More details on the construction of these figures are given in Box 11.1 and Section 11.1.2.

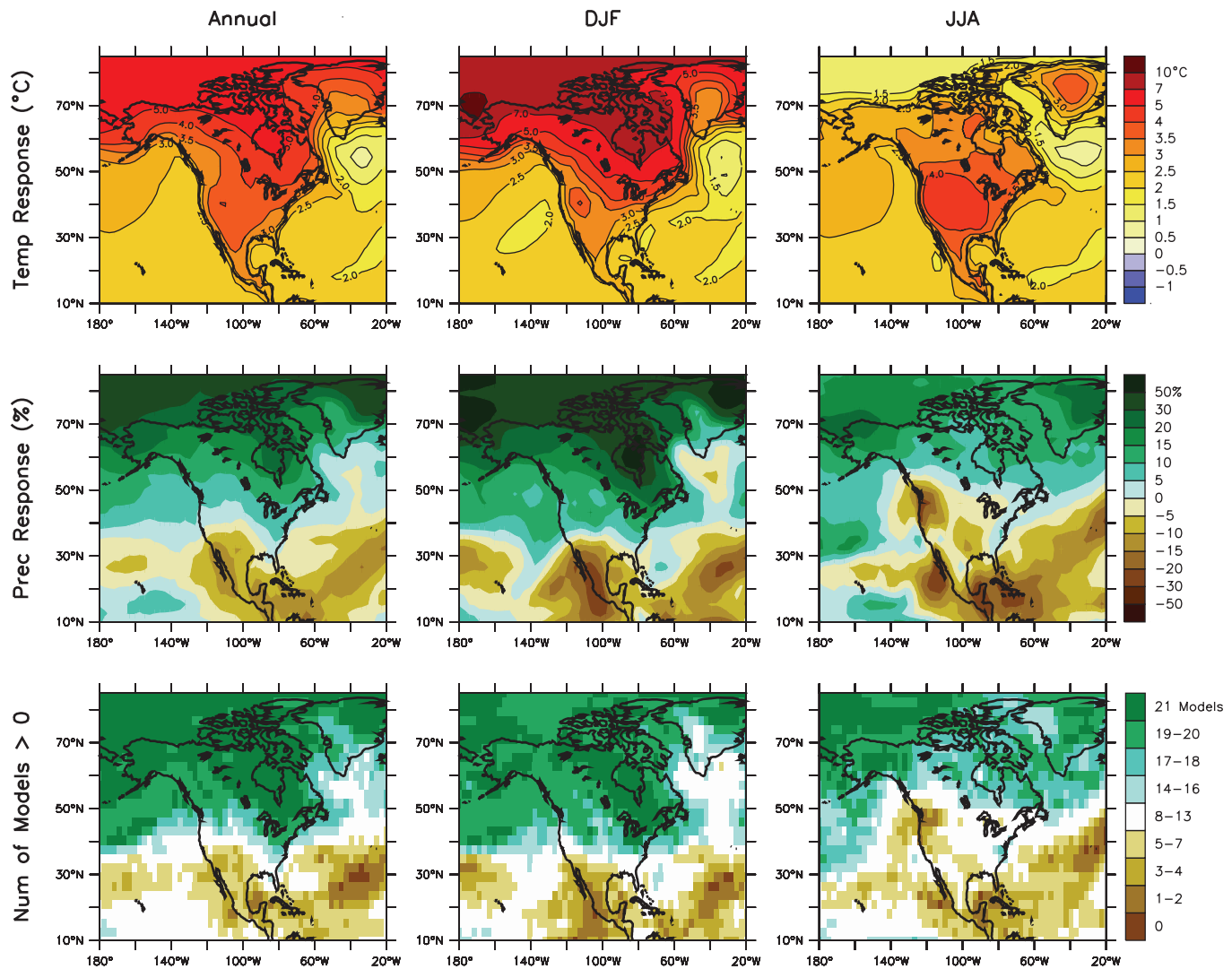


Figure 11.12. Temperature and precipitation changes over North America from the MMD-A1B simulations. Top row: Annual mean, DJF and JJA temperature change between 1980 to 1999 and 2080 to 2099, averaged over 21 models. Middle row: same as top, but for fractional change in precipitation. Bottom row: number of models out of 21 that project increases in precipitation.

11.5.3.2 Precipitation

As a consequence of the temperature dependence of the saturation vapour pressure in the atmosphere, the projected warming is expected to be accompanied by an increase in atmospheric moisture flux and its convergence/divergence intensity. This results in a general increase in precipitation over most of the continent except the most south-westerly part (Figure 11.12). The ensemble mean of MMD models projects an increase in annual mean precipitation in the north reaching +20%, which is twice the inter-model spread, so likely significant; the projected increase reaches as much as +30% in winter. Because the increased saturation vapour pressure can also yield greater evaporation, projected increases in annual precipitation are partially offset by increases in evaporation; regions in central North America may experience net surface drying as a result (see Supplementary Material Figure S11.1). See Table 11.1 and Supplementary Table S11.2 for more

regional and seasonal details, noting that regional averaging hides important north-south differences.

In keeping with the projected northward displacement of the westerlies and the intensification of the Aleutian Low (Section 11.5.3.3), northern region precipitation is projected to increase, by the largest amount in autumn and by the largest fraction in winter. Due to the increased precipitable water, the increase in precipitation amount is likely to be larger on the windward slopes of the mountains in the west with orographic precipitation. In western regions, modest changes in annual mean precipitation are projected, but the majority of AOGCMs indicate an increase in winter and a decrease in summer. Models show greater consensus on winter increases (ensemble mean maximum of 15%) to the north and on summer decreases (ensemble mean maximum of -20%) to the south. These decreases are consistent with enhanced subsidence and flow of drier air masses in the southwest USA and northern Mexico resulting from an amplification of the subtropical anticyclone

off the West Coast due to the land-sea contrast in warming (e.g., Mote and Mantua, 2002). However, this reduction is close to the inter-model spread so it contains large uncertainty, an assessment that is reinforced by the fact that some AOGCMs project an increase in precipitation.

In central and eastern regions, projections from the MMD models show the same characteristics as in the west, with greater consensus for winter increases to the north and summer decreases to the south. The line of zero change is oriented more or less west-to-east and moves north from winter to summer. The line of zero change is also projected to lie further to the north under SRES scenarios with larger greenhouse gas amounts. However, uncertainty around the projected changes is large and the changes do not scale well across different SRES scenarios.

Govindasamy (2003) finds that, averaged over the USA, the few existing time-slice simulations with high-resolution AGCM results do not significantly differ from those obtained with AOGCMs. Available RCM simulations provide little extra information on average changes. Some RCMs project precipitation changes of different sign, either locally (Chen et al., 2003) or over the entire continental USA (Han and Roads, 2004, where in summer the AOGCM generally produced a small increase and the RCM a substantial decrease). In contrast, Plummer et al. (2006) find only small differences in precipitation responses using two sets of physical parametrizations in their RCM, despite the fact that one corrected significant summer precipitation excess present in the other.

11.5.3.3 Temperature and Precipitation Extremes

Several RCM studies focused particularly on changes in extreme temperature events. Bell et al. (2004) examine changes in temperature extremes in their simulations centred on California. They find increases in extreme temperature events, both as distribution percentiles and threshold events, prolonged hot spells and increased diurnal temperature range. Leung et al. (2004) examine changes in extremes in their RCM simulations of the western USA; in general, they find increases in diurnal temperature range in six sub-regions of their domain in summer. Diffenbaugh et al. (2005) find that the frequency and magnitude of extreme temperature events changes dramatically under SRES A2, with increases in extreme hot events and a decrease in extreme cold events.

In a study of precipitation extremes over California, Bell et al. (2004) find that changes in precipitation exceeding the 95th percentile followed changes in mean precipitation, with decreases in heavy precipitation in most areas. Leung et al. (2004) find that extremes in precipitation during the cold season increase in the northern Rockies, the Cascades, the Sierra Nevada and British Columbia by up to 10% for 2040 to 2060, although mean precipitation was mostly reduced, in accord with earlier studies (Giorgi et al., 2001a). In a large river basin in the Pacific Northwest, increases in rainfall over snowfall and rain-on-snow events increased extreme runoff by 11%, which would contribute to more severe flooding. In their 25-km RCM

simulations covering the entire USA, Diffenbaugh et al. (2005) find widespread increases in extreme precipitation events under SRES A2, which they determine to be significant.

11.5.3.4 Atmospheric Circulation

In general, the projected climate changes over North America follow the overall features of those over the NH (Chapter 10). The MMD models project a northward displacement and strengthening of the mid-latitude westerly flow, most pronounced in autumn and winter. Surface pressure is projected to decrease in the north, with a northward displacement of the Aleutian low-pressure centre and a north-westward displacement of the Labrador Sea trough, and to decrease slightly in the south. The reductions in surface pressure in the north are projected to be strongest in winter, reaching -1.5 to -3 hPa, in part as a result of the warming of the continental arctic air mass. On an annual basis, the pressure decrease in the north exceeds the spread among models by a factor of 3 on an annual-mean basis and a factor of 1.5 in summer, so it is significant. The East Pacific subtropical anticyclone is projected to intensify in summer, particularly off the coast of California and Baja California, resulting in an increased air mass subsidence and drier airflow over south-western North America. The pressure increase (less than 0.5 hPa) is small compared to the spread among models, so this projection is rather uncertain.

11.5.3.5 Snowpack, Snowmelt and River Flow

The ensemble mean of the MMD models projects a general decrease in snow depth (Chapter 10) as a result of delayed autumn snowfall and earlier spring snowmelt. In some regions where winter precipitation is projected to increase, the increased snowfall can more than make up for the shorter snow season and yield increased snow accumulation. Snow depth increases are projected by some GCMs over some land around the Arctic Ocean (Figure S10.1) and by some RCMs in the northernmost part of the Northwest Territories (Figure 11.13). In principle a similar situation could arise at lower latitudes at high elevations in the Rocky Mountains, although most models project a widespread decrease of snow depth there (Kim et al., 2002; Snyder et al., 2003; Leung et al., 2004; see also Box 11.3).

Much SD research activity has focused on resolving future water resources in the complex terrain of the western USA. Studies typically point to a decline in winter snowpack and hastening of the onset of snowmelt caused by regional warming (Hayhoe et al., 2004; Salathé, 2005). Comparable trends towards increased annual mean river flows and earlier spring peak flows have also been projected by two SD techniques for the Saguenay watershed in northern Québec, Canada (Dibike and Coulibaly, 2005). Such changes in the flow regime also favour increased risk of winter flooding and lower summer soil moisture and river flows. However, differences in snowpack behaviour derived from AOGCMs depend critically on the realism of downscaled winter temperature variability and its

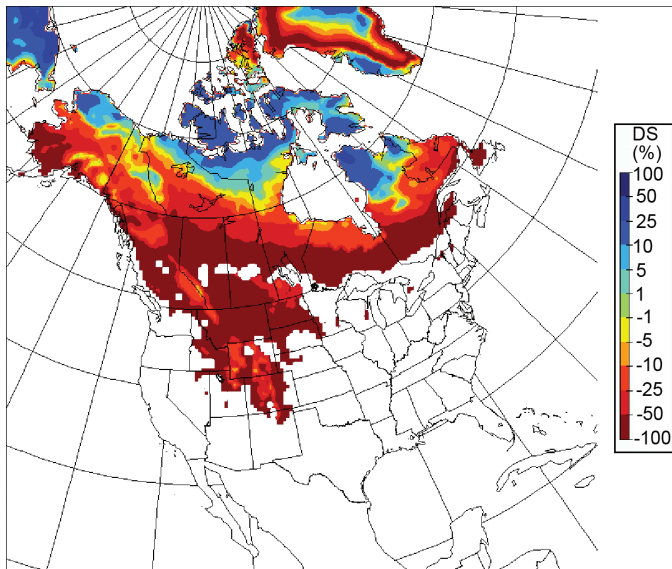


Figure 11.13. Percent snow depth changes in March (only calculated where climatological snow amounts exceed 5 mm of water equivalent), as projected by the Canadian Regional Climate Model (CRCM; Plummer et al., 2006), driven by the Canadian General Circulation Model (CGCM), for 2041 to 2070 under SRES A2 compared to 1961 to 1990.

interplay with precipitation and snowpack accumulation and melt (Salathé, 2005). Hayhoe et al. (2004) produced a standard set of statistically downscaled temperature and precipitation scenarios for California; under both the A1F1 and B1 scenarios, they find overall declines in snowpack.

11.6 Central and South America

Assessment of projected climate change for Central and South America:

All of Central and South America is very likely to warm during this century. The annual mean warming is likely to be similar to the global mean warming in southern South America but larger than the global mean warming in the rest of the area.

Annual precipitation is likely to decrease in most of Central America, with the relatively dry boreal spring becoming drier. Annual precipitation is likely to decrease in the southern Andes, with relative precipitation changes being largest in summer. A caveat at the local scale is that changes in atmospheric circulation may induce large local variability in precipitation changes in mountainous areas. Precipitation is likely to increase in Tierra del Fuego during winter and in south-eastern South America during summer.

It is uncertain how annual and seasonal mean rainfall will change over northern South America, including

the Amazon forest. In some regions, there is qualitative consistency among the simulations (rainfall increasing in Ecuador and northern Peru, and decreasing at the northern tip of the continent and in southern northeast Brazil).

The systematic errors in simulating current mean tropical climate and its variability (Section 8.6) and the large inter-model differences in future changes in El Niño amplitude (Section 10.3) preclude a conclusive assessment of the regional changes over large areas of Central and South America. Most MMD models are poor at reproducing the regional precipitation patterns in their control experiments and have a small signal-to-noise ratio, in particular over most of Amazonia (AMZ). The high and sharp Andes Mountains are unresolved in low-resolution models, affecting the assessment over much of the continent. As with all landmasses, the feedbacks from land use and land cover change are not well accommodated, and lend some degree of uncertainty. The potential for abrupt changes in biogeochemical systems in AMZ remains as a source of uncertainty (see Box 10.1). Large differences in the projected climate sensitivities in the climate models incorporating these processes and a lack of understanding of processes have been identified (Friedlingstein et al., 2003). Over Central America, tropical cyclones may become an additional source of uncertainty for regional scenarios of climate change, since the summer precipitation over this region may be affected by systematic changes in hurricane tracks and intensity.

11.6.1 Key Processes

Over much of Central and South America, changes in the intensity and location of tropical convection are the fundamental concern, but extratropical disturbances also play a role in Mexico's winter climate and throughout the year in southern South America. A continental barrier over Central America and along the Pacific coast in South America and the world's largest rainforest are unique geographical features that shape the climate in the area.

Climate over most of Mexico and Central America is characterised by a relatively dry winter and a well-defined rainy season from May through October (Magaña et al., 1999). The seasonal evolution of the rainy season is largely the result of air-sea interactions over the Americas' warm pools and the effects of topography over a dominant easterly flow, as well as the temporal evolution of the ITCZ. During the boreal winter, the atmospheric circulation over the Gulf of Mexico and the Caribbean Sea is dominated by the seasonal fluctuation of the Subtropical North Atlantic Anticyclone, with invasions of extratropical systems that affect mainly Mexico and the western portion of the Great Antilles.

A warm season precipitation maximum, associated with the South American Monsoon System (Vera et al., 2006), dominates the mean seasonal cycle of precipitation in tropical and subtropical latitudes over South America. Amazonia has had

increasing rainfall over the last 40 years, despite deforestation, due to global-scale water vapour convergence (Chen et al., 2001; see also Section 3.3). The future of the rainforest is not only of vital ecological importance, but also central to the future evolution of the global carbon cycle, and as a driver of regional climate change. The monsoon system is strongly influenced by ENSO (e.g., Lau and Zhou, 2003), and thus future changes in ENSO will induce complementary changes in the region. Displacements of the South Atlantic Convergence Zone have important regional impacts such as the large positive precipitation trend over the recent decades centred over southern Brazil (Liebmann et al., 2004). There are well-defined teleconnection patterns (the Pacific-South American modes, Mo and Nogués-Paegle, 2001) whose preferential excitation could help shape regional changes. The Mediterranean climate of much of Chile makes it sensitive to drying as a consequence of poleward expansion of the South Pacific subtropical high, in close analogy to other regions downstream of oceanic subtropical highs in the Southern Hemisphere (SH). South-eastern South America would experience an increase in precipitation from the same poleward storm track displacement.

11.6.2 Skill of Models in Simulating Present Climate

In the Central America (CAM) and AMZ regions, most models in the MMD have a cold bias of 0°C to 3°C, except in AMZ in SON (Supplementary Material Table S11.1). In southern South America (SSA) average biases are close to zero. The biases are unevenly geographically distributed (Supplementary Material Figure S11.25). The MMD mean climate shows a warm bias around 30°S (particularly in summer) and in parts of central South America (especially in SON). Over the rest of South America (central and northern Andes, eastern Brazil, Patagonia) the biases tend to be predominantly negative. The SST biases along the western coasts of South America are likely related to weakness in oceanic upwelling.

For the CAM region, the multi-model scatter in precipitation is substantial, but half of the models lie in the range of -15 to 25% in the annual mean. The largest biases occur during the boreal winter and spring seasons, when precipitation is meagre (Supplementary Material Table S11.1). For both AMZ and SSA, the ensemble annual mean climate exhibits drier than observed conditions, with about 60% of the models having a negative bias. Unfortunately, this choice of regions for averaging is particularly misleading for South America since it does not clearly bring out critical regional biases such as those related to rainfall underestimation in the Amazon and La Plata Basins (Supplementary Material Figure S11.26). Simulation of the regional climate is seriously affected by model deficiencies at low latitudes. In particular, the MMD ensemble tends to depict a relatively weak ITCZ, which extends southward of its observed position. The simulations have a systematic bias towards underestimated rainfall over the Amazon Basin. The simulated subtropical climate is typically also adversely affected by a dry bias over most of south-eastern South America and in the South Atlantic Convergence Zone, especially during the rainy season.

In contrast, rainfall along the Andes and in northeast Brazil is excessive in the ensemble mean.

Some aspects of the simulation of tropical climate with AOGCMs have improved. However, in general, the largest errors are found where the annual cycle is weakest, such as over tropical South America (see, e.g., Section 8.3). Atmospheric GCMs approximate the spatial distribution of precipitation over the tropical Americas, but they do not correctly reproduce the temporal evolution of the annual cycle in precipitation, specifically the mid-summer drought (Magaña and Caetano, 2005). Tropical cyclones are important contributors to precipitation in the region. If close to the continent, they will produce large amounts of precipitation over land, and if far from the coast, moisture divergence over the continental region enhances drier conditions.

Zhou and Lau (2002) analyse the precipitation and circulation biases in a set of six AGCMs provided by the Climate Variability and Predictability Programme (CLIVAR) Asian-Australian Monsoon AGCM Intercomparison Project (Kang et al., 2002). This model ensemble captures some large-scale features of the South American monsoon system reasonably well, including the seasonal migration of monsoon rainfall and the rainfall associated with the South America Convergence Zone. However, the South Atlantic subtropical high and the Amazonia low are too strong, whereas low-level flow tends to be too strong during austral summer and too weak during austral winter. The model ensemble captures the Pacific-South American pattern quite well, but its amplitude is generally underestimated.

Regional models are still being tested and developed for this region. Relatively few studies using RCMs for Central and South America exist, and those that do are constrained by short simulation length. Some studies (Chou et al., 2000; Nobre et al., 2001; Druyan et al., 2002) examine the skill of experimental dynamic downscaling of seasonal predictions over Brazil. Results suggest that both more realistic GCM forcing and improvements in the RCMs are needed. Seth and Rojas (2003) performed seasonal integrations driven by reanalyses, with emphasis on tropical South America. The model was able to simulate the different rainfall anomalies and large-scale circulations but, as a result of weak low-level moisture transport from the Atlantic, rainfall over the western Amazon was underestimated. Vernekar et al. (2003) follow a similar approach to study the low-level jets and report that the RCM produces better regional circulation details than does the reanalysis. However, an ensemble of four RCMs did not provide a noticeable improvement in precipitation over the driving large-scale reanalyses (Roads et al., 2003).

Other studies (Misra et al., 2003; Rojas and Seth, 2003) analyse seasonal RCM simulations driven by AGCM simulations. Relative to the AGCMs, regional models generally improve the rainfall simulation and the tropospheric circulation over both tropical and subtropical South America. However, AGCM-driven RCMs degrade compared with the reanalyses-driven integrations and they could even exacerbate the dry bias over sectors of AMZ and perpetuate the erroneous ITCZ over

the neighbouring ocean basins from the AGCMs. Menéndez et al. (2001) used a RCM driven by a stretched-grid AGCM with higher resolution over the southern mid-latitudes to simulate the winter climatology of SSA. They find that both the AGCM and the regional model have similar systematic errors but the biases are reduced in the RCM. Analogously, other RCM simulations for SSA give too little precipitation over the subtropical plains and too much over elevated terrain (e.g., Nicolini et al., 2002; Menéndez et al., 2004).

11.6.3 Climate Projections

11.6.3.1 Temperature

The warming as simulated by the MMD-A1B projections increases approximately linearly with time during this century, but the magnitude of the change and the inter-model range are greater over CAM and AMZ than over SSA (Figure 11.14). The annual mean warming under the A1B scenario between 1980 to 1999 and 2080 to 2099 varies in the CAM region from 1.8°C to 5.0°C, with half of the models within 2.6°C to 3.6°C and a median of 3.2°C. The corresponding numbers for AMZ are 1.8°C to 5.1°C, 2.6°C to 3.7°C and 3.3°C, and those for SSA 1.7°C to 3.9°C, 2.3°C to 3.1°C and 2.5°C (Table 11.1). The median warming is close to the global ensemble mean in SSA but about 30% above the global mean in the other two regions. As in the rest of the tropics, the signal-to-noise ratio is large for temperature, and it requires only 10 years for a 20-year mean temperature, growing at the rate of the median A1B response, to be clearly discernible above the models' internal variability.

The simulated warming is generally largest in the most continental regions, such as inner Amazonia and northern Mexico (Figure 11.15). Seasonal variation in the regional area mean warming is relatively modest, except in CAM where there is a difference of 1°C in median values between DJF and MAM (Table 11.1). The warming in central Amazonia tends to be larger in JJA than in DJF, while the reverse is true over the Altiplano where, in other words, the seasonal cycle of temperature is projected to increase (Figure 11.15). Similar results were found by Boulanger et al. (2006), who studied the regional thermal response over South America by applying a statistical method based on neural networks and Bayesian statistics to find optimal weights for a linear combination of MMD models.

For the variation of seasonal warming between the individual models, see Table 11.1. As an alternative approach to estimating uncertainty in the magnitude of the warming, the 5th and 95th percentiles for temperature change at the end of the 21st century, assessed using the method of Tebaldi et al. (2004a), are typically within $\pm 1^\circ\text{C}$ of the median value in all three of these regions (Supplementary Material Table S11.2).

11.6.3.2 Precipitation

The MMD models suggest a general decrease in precipitation over most of Central America, consistent with Neelin et al. (2006), where the median annual change by the end of the 21st

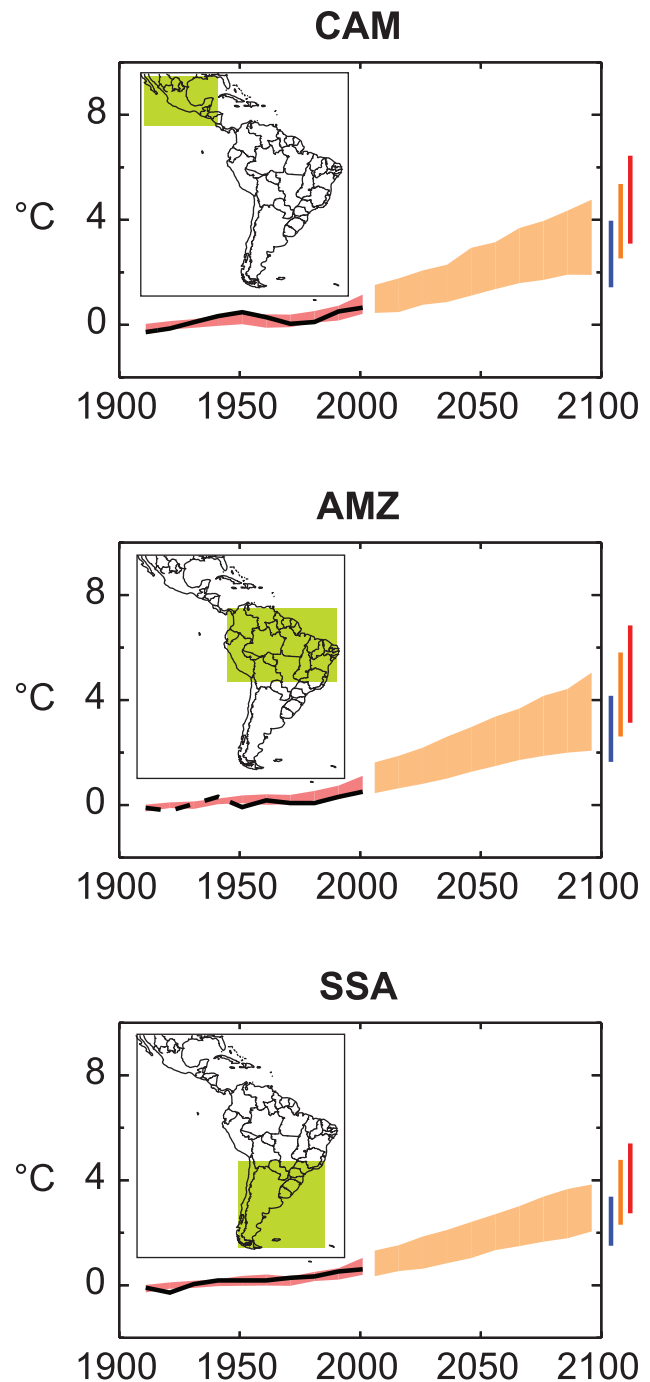


Figure 11.14. Temperature anomalies with respect to 1901 to 1950 for three Central and South American land regions for 1906 to 2005 (black line) and as simulated (red envelope) by MMD models incorporating known forcings; and as projected for 2001 to 2100 by MMD models for the A1B scenario (orange envelope). The bars at the end of the orange envelope represent the range of projected changes for 2091 to 2100 for the B1 scenario (blue), the A1B scenario (orange) and the A2 scenario (red). The black line is dashed where observations are present for less than 50% of the area in the decade concerned. More details on the construction of these figures are given in Box 11.1 and Section 11.1.2.

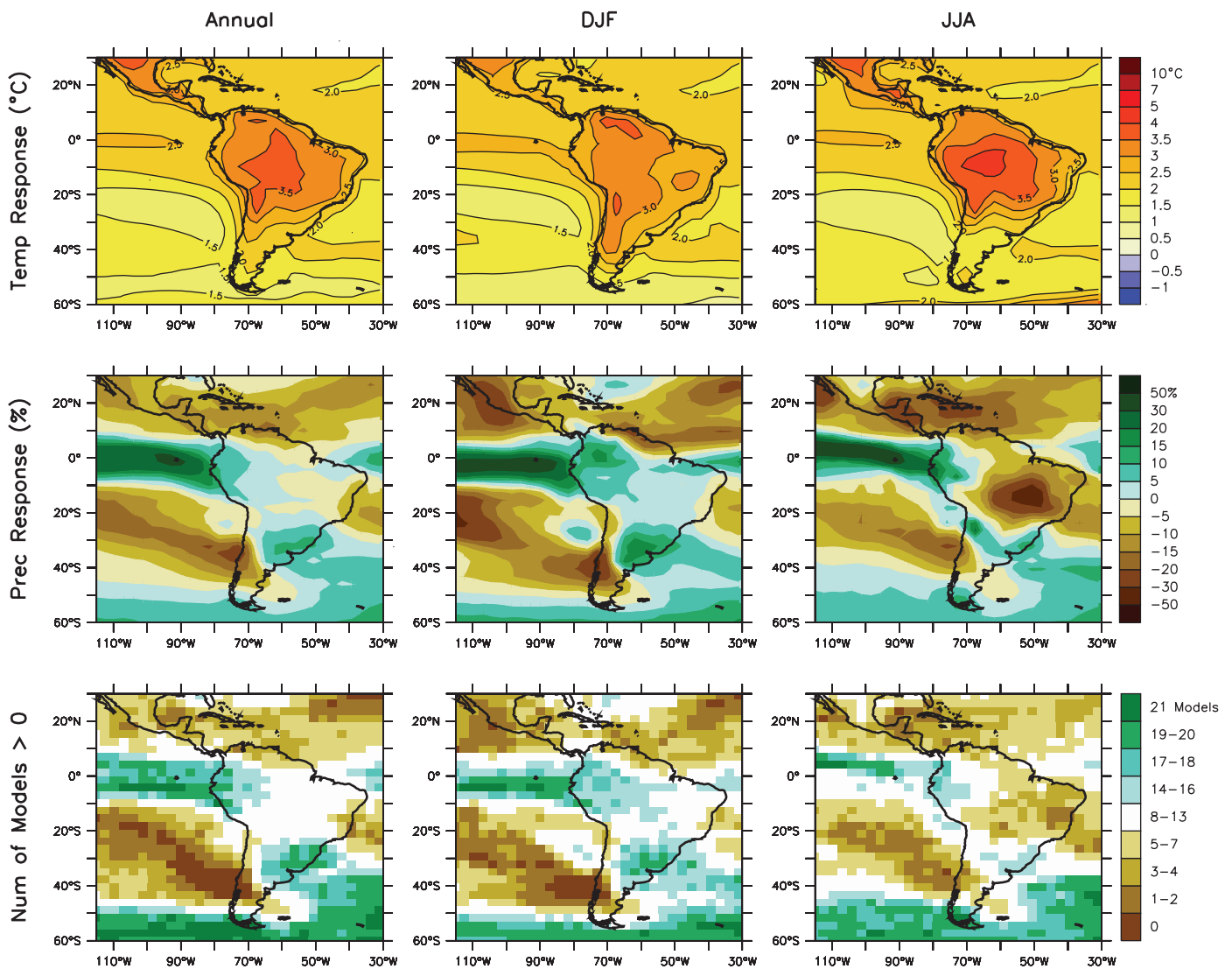


Figure 11.15. Temperature and precipitation changes over Central and South America from the MMD-A1B simulations. Top row: Annual mean, DJF and JJA temperature change between 1980 to 1999 and 2080 to 2099, averaged over 21 models. Middle row: same as top, but for fractional change in precipitation. Bottom row: number of models out of 21 that project increases in precipitation.

century is -9% under the A1B scenario, and half of the models project area mean changes from -16 to -5% , although the full range of the projections extends from -48 to 9% . Median changes in area mean precipitation in Amazonia and southern South America are small and the variation between the models is also more modest than in Central America, but the area means hide marked regional differences (Table 11.1, Figure 11.15).

Area mean precipitation in Central America decreases in most models in all seasons. It is only in some parts of northeastern Mexico and over the eastern Pacific, where the ITCZ forms during JJA, that increases in summer precipitation are projected (Figure 11.15). However, since tropical storms can contribute a significant fraction of the rainfall in the hurricane season in this region, these conclusions might be modified by the possibility of increased rainfall in storms not well captured by these global models. In particular, if the number of storms

does not change, Knutson and Tuleya (2004) estimate nearly a 20% increase in average precipitation rate within 100 km of the storm centre at the time of atmospheric carbon dioxide (CO_2) doubling.

For South America, the multi-model mean precipitation response (Figure 11.15) indicates marked regional variations. The annual mean precipitation is projected to decrease over northern South America near the Caribbean coasts, as well as over large parts of northern Brazil, Chile and Patagonia, while it is projected to increase in Colombia, Ecuador and Peru, around the equator and in south-eastern South America. The seasonal cycle modulates this mean change, especially over the Amazon Basin where monsoon precipitation increases in DJF and decreases in JJA. In other regions (e.g., Pacific coasts of northern South America, a region centered over Uruguay, Patagonia) the sign of the response is preserved throughout the seasonal cycle.

As seen in the bottom panels of Figure 11.15, most models project a wetter climate near the Rio de la Plata and drier conditions along much of the southern Andes, especially in DJF. However, when estimating the likelihood of this response, the qualitative consensus within this set of models should be weighed against the fact that most models show considerable biases in regional precipitation patterns in their control simulations.

The poleward shift of the South Pacific and South Atlantic subtropical anticyclones is a robust response across the models. Parts of Chile and Patagonia are influenced by the polar boundary of the subtropical anticyclone in the South Pacific and experience particularly strong drying because of the combination of the poleward shift in circulation and increase in moisture divergence. The strength and position of the subtropical anticyclone in the South Atlantic is known to influence the climate of south-eastern South America and the South Atlantic Convergence Zone (Robertson et al., 2003; Liebmann et al., 2004). The increase in rainfall in south-eastern South America is related to a corresponding poleward shift in the Atlantic storm track (Yin, 2005).

Some projected changes in precipitation (such as the drying over east-central Amazonia and northeast Brazil and the wetter conditions over south-eastern South America) could be a partial consequence of the El-Niño like response projected by the models (Section 10.3). The accompanying shift and alterations in the Walker Circulation would directly affect tropical South America (Cazes Boezio et al., 2003) and affect southern South America through extratropical teleconnections (Mo and Nogués-Paegle, 2001).

Although feedbacks from carbon cycle and dynamic vegetation are not included in MMD models, a number of coupled carbon cycle-climate projections have been performed since the TAR (see Sections 7.2 and 10.4.1). The initial carbon-climate simulations suggest that drying of the Amazon potentially contributes to acceleration of the rate of anthropogenic global warming by increasing atmospheric CO₂ (Cox et al., 2000; Friedlingstein et al., 2001; Dufresne et al., 2002; Jones et al., 2003). These models display large uncertainty in climate projections and differ in the timing and sharpness of the changes (Friedlingstein et al., 2003). Changes in CO₂ are related to precipitation changes in regions such as the northern Amazon (Zeng et al., 2004). In a version of the HadCM3 model with dynamic vegetation and an interactive global carbon cycle (Betts et al., 2004), a tendency to a more El Niño-like state contributes to reduced rainfall and vegetation dieback in the Amazon (Cox et al., 2004). But the version of HadCM3 participating in the MMD projects by far the largest reduction in annual rainfall over AMZ (–21% for the A1B scenario). This stresses the necessity of being very cautious in interpreting carbon cycle impacts on the regional climate and ecosystem change until there is more convergence among models on rainfall projections for the Amazon with fixed vegetation. Box 11.4 summarises some of the major issues related to regional land use/land changes in the context of climate change.

11.6.4 Extremes

Little research is available on extremes of temperature and precipitation for this region. Table 11.1 provides estimates on how frequently the seasonal temperature and precipitation extremes as simulated in 1980 to 1999 are exceeded in model projections using the A1B scenario. Essentially all seasons and regions are extremely warm by this criterion by the end of the century. In Central America, the projected time mean precipitation decrease is accompanied by more frequent dry extremes in all seasons. In AMZ, models project extremely wet seasons in about 27% (18%) of all DJF (MAM) seasons in the period 2080 to 2099. Significant changes are not projected in the frequency of extremely wet or dry seasons over SSA.

On the daily time scale, Hegerl et al. (2004) analyse an ensemble of simulations from two AOGCMs and find that both models simulate a temperature increase in the warmest night of the year larger than the mean response over the Amazon Basin but smaller than the mean response over parts of SSA. Concerning extreme precipitation, both models project more intense wet days per year over large parts of south-eastern South America and central Amazonia and weaker precipitation extremes over the coasts of northeast Brazil. Intensification of the rainfall amounts are consistent, given the agreement between the MMD model simulations over parts of south-eastern South America and most of AMZ but with longer periods between rainfall events, except in north-western South America, where the models project that it will rain more frequently (Meehl et al., 2005; Tebaldi et al., 2006).

11.7 Australia – New Zealand

Assessment of projected climate change for Australia and New Zealand:

All of Australia and New Zealand are very likely to warm during this century, with amplitude somewhat larger than that of the surrounding oceans, but comparable overall to the global mean warming. The warming is smaller in the south, especially in winter, with the warming in the South Island of New Zealand likely to remain smaller than the global mean. Increased frequency of extreme high daily temperatures in Australia and New Zealand, and decrease in the frequency of cold extremes is very likely.

Precipitation is likely to decrease in southern Australia in winter and spring. Precipitation is very likely to decrease in south-western Australia in winter. Precipitation is likely to increase in the west of the South Island of New Zealand. Changes in rainfall in northern and central Australia are uncertain. Extremes of daily precipitation are very likely to increase. The effect may be offset or reversed in areas of significant decrease in

Box 11.4: Land Use and Land Cover Change Experiments Related to Climate Change

Land use and land cover change significantly affect climate at the regional and local scales (e.g., Hansen et al., 1998; Bonan, 2001; Kabat et al., 2002; Foley et al., 2005). Recent modelling studies also show that in some instances these effects can extend beyond the areas where the land cover changes occur, through climate teleconnection processes (e.g., Gaertner et al., 2001; Pielke et al., 2002; Marland et al., 2003). Changes in vegetation result in alteration of surface properties, such as albedo and roughness length, and alter the efficiency of ecosystem exchange of water, energy and CO₂ with the atmosphere (for more details see Section 7.2). The effects differ widely based on the type and location of the altered ecosystem. The effects of land use and land cover change on climate can also be divided into biogeochemical and biophysical effects (Brovkin et al., 1999; see Sections 7.2 and 2.5 for discussion of these effects).

The net effect of human land cover activities increases the concentration of greenhouse gases in the atmosphere, thus increasing warming (see Sections 7.2 and 10.4 for further discussion); it has been suggested that these land cover emissions have been underestimated in the future climate projections used in the SRES scenarios (Sitch, 2005). Climate models assessed in this report incorporate various aspects of the effects of land cover change including representation of the biogeochemical flux, inclusion of dynamic land use where natural vegetation shifts as climate changes, and explicit human land cover forcing. In all cases, these efforts should be considered at early stages of development (see Chapters 2 and 7, and Table 10.1 for more details on many of these aspects).

One important impact of land cover conversion, generally not simulated in GCMs, is urbanisation. Although small in aerial extent, conversion to urban land cover creates urban heat islands associated with considerable warming (Arnfield, 2003). Since much of the world population lives in urban environments (and this proportion may increase, thus expanding urban areas), many people will be exposed to climates that combine expanded urban heat island effects and increased temperature from greenhouse gas forcing (see Box 7.2 for more details on urban land use effects).

One major shift in land use, relevant historically and in the future, is conversion of forest to agriculture and agriculture back to forest. Most areas well suited to large-scale agriculture have already been converted to this land use/cover type. Yet land cover conversion to agriculture may continue in the future, especially in parts of western North America, tropical areas of south and central America and arable regions in Africa and south and central Asia (IPCC, 2001; RIVM, 2002). In the future, mid-latitude agricultural areal expansion (especially into forested areas) could possibly result in cooling that would offset a portion of the expected warming due to greenhouse gas effects alone. In contrast, reforestation may occur in eastern North America and the eastern portion of Europe. In these areas, climate effects may include local warming associated with reforestation due to decreased albedo values (Feddema et al., 2005).

Tropical land cover change results in a very different climate response compared to mid-latitude areas. Changes in plant cover and the reduced ability of the vegetation to transpire water to the atmosphere lead to temperatures that are warmer by as much as 2°C in regions of deforestation (Costa and Foley, 2000; Gedney and Valdes, 2000; De Fries et al., 2002). The decrease in transpiration acts to reduce precipitation, but this effect may be modified by changes in atmospheric moisture convergence. Most model simulations of Amazonian deforestation suggest reduced moisture convergence, which would amplify the decrease in precipitation (e.g., McGuffie et al., 1995; Costa and Foley, 2000; Avissar and Worth, 2005). However, increased precipitation and moisture convergence in Amazonia during the last few decades contrast with this expectation, suggesting that deforestation has not been the dominant driver of the observed changes (see Section 11.6).

Tropical regions also have the potential to affect climates beyond their immediate areal extent (Chase et al., 2000; Delire et al., 2001; Voltaire and Royer, 2004; Avissar and Werth, 2005; Feddema et al., 2005; Snyder, 2006). For example, changes in convection patterns can affect the Hadley Circulation and thus propagate climate perturbations into the mid-latitudes. In addition, tropical deforestation in the Amazon has been found to affect SSTs in nearby ocean locations, further amplifying teleconnections (Avissar and Werth, 2005; Feddema et al., 2005; Neelin and Su, 2005; Voltaire and Royer, 2005). However, studies also indicate that there are significantly different responses to similar land use changes in other tropical regions and that responses are typically linked to dry season conditions (Voltaire and Royer, 2004a; Feddema et al., 2005). However, tropical land cover change in Africa and southeast Asia appears to have weaker local impacts largely due to influences of the Asian and African monsoon circulation systems (Mabuchi et al., 2005a,b; Voltaire and Royer, 2005).

Several land cover change studies have explicitly assessed the potential impacts (limited to biophysical effects) associated with specific future SRES land cover change scenarios, and the interaction between land cover change and greenhouse gas forcings (De Fries et al., 2002; Maynard and Royer, 2004a; Feddema et al., 2005; Sitch et al., 2005; Voltaire, 2006). In the A2 scenario, large-scale Amazon deforestation could double the expected warming in the region (De Fries et al., 2002; Feddema et al., 2005). Lesser local impacts are expected in tropical Africa and south Asia, in part because of the difference in regional circulation patterns (Delire et al., 2001; Maynard and Royer, 2004a,b; Feddema et al., 2005; Mabuchi et al., 2005a,b). In mid-latitude regions, land-cover induced cooling could offset some of the greenhouse-gas induced warming. Feddema et al. (2005) suggest that in the B1 scenario (where reforestation occurs in many areas and there are other low-impact tropical land cover changes) there are few local tropical climate or teleconnection effects. However, in this scenario, mid-latitude reforestation could lead to additional local warming compared to greenhouse-gas forcing scenarios alone.

(continued)

These simulations suggest that the effects of future land cover change will be a complex interaction of local land cover change impacts combined with teleconnection effects due to land cover change elsewhere, in particular the Amazon, and areas surrounding the Indian Ocean. However, projecting the potential outcomes of future climate effects due to land cover change is difficult for two reasons. First, there is considerable uncertainty regarding how land cover will change in the future. In this context, the past may not be a good indicator of the types of land transformation that may occur in the future. For example, if land cover change becomes a part of climate change mitigation (e.g., carbon trading) then a number of additional factors that include carbon sequestration in soils and additional land cover change processes will need to be incorporated in scenario development schemes. Second, current land process models cannot simulate all the potential impacts of human land cover transformation. Such processes as adequate simulation of urban systems, agricultural systems, ecosystem disturbance regimes (e.g., fire) and soil impacts are not yet well represented.

mean rainfall (southern Australian in winter and spring). An increase in potential evaporation is likely. Increased risk of drought in southern areas of Australia is likely.

Increased mean wind speed across the Southern Island of New Zealand, particularly in winter, is likely.

Significant factors contribute to uncertainty in projected climate change for the region. The El Niño-Southern Oscillation significantly influences rainfall, drought and tropical cyclone behaviour in the region and it is uncertain how ENSO will change in the future. Monsoon rainfall simulations and projections vary substantially from model to model, thus we have little confidence in model precipitation projections for northern Australia. More broadly, across the continent summer rainfall projections vary substantially from model to model, reducing confidence in their reliability. In addition, no detailed assessment of MMD model performance over Australia or New Zealand is available, which hinders efforts to establish the reliability of projections from these models. Finally, downscaling of MMD model projections are not yet available for New Zealand but are much needed because of the strong topographical control of New Zealand rainfall.

11.7.1 Key Processes

Key climate processes affecting the Australian region include the Australian monsoon (the SH counterpart of the Asian monsoon), the Southeast trade wind circulation, the subtropical high-pressure belt and the mid-latitude westerly wind circulation with its embedded disturbances. The latter two systems also predominate over New Zealand. Climatic variability in Australia and New Zealand is also strongly affected by the ENSO system (McBride and Nicholls, 1983; Mullan, 1995) modulated by the Inter-decadal Pacific Oscillation (IPO; Power et al., 1999; Salinger et al., 2001). Tropical cyclones occur in the region, and are a major source of extreme rainfall and wind events in northern coastal Australia, and, more rarely, on the North Island of New Zealand (Sinclair, 2002). Rainfall patterns in New Zealand are also strongly influenced by the interaction of the predominantly westerly circulation with its very mountainous topography.

Apart from the general increase in temperature that the region will share with most other parts of the globe, details of anthropogenic climate change in the Australia-New Zealand

region will depend on the response of the Australian monsoon, tropical cyclones, the strength and latitude of the mid-latitude westerlies, and ENSO.

11.7.2 Skill of Models in Simulating Present Climate

There are relatively few studies of the quality of the MMD global model simulations in the Australia-New Zealand area. The ensemble mean of the MMD model simulations has a systematic low-pressure bias near 50°S at all longitudes in the SH, including the Australia-New Zealand sector, corresponding to an equatorward displacement of the mid-latitude westerlies (see Chapter 8). On average, mid-latitude storm track eddies are displaced equatorward (Yin, 2005) and deep winter troughs over southwest Western Australia are over-represented (Hope 2006a,b). How this bias might affect climate change simulations is unclear. It can be hypothesised that by spreading the effects of mid-latitude depressions too far inland, the consequences of a poleward displacement of the westerlies and the storm track might be exaggerated, but the studies needed to test this hypothesis are not yet available.

The simulated surface temperatures in the surrounding oceans are typically warmer than observed, but at most by 1°C in the composite. Despite this slight warm bias, the ensemble mean temperatures are biased cold over land, especially in winter in the southeast and southwest of the Australian continent, where the cold bias is larger than 2°C. At large scales, the precipitation also has some systematic biases (see Supplementary Material Table S11.1). Averaged across northern Australia, the median model error is 20% more precipitation than observed, but the range of biases in individual models is large (−71 to +131%). This is discouraging with regard to confidence in many of the individual models. Consistent with this, Moise et al. (2005) identify simulation of Australian monsoon rainfall as a major deficiency of many of the AOGCM simulations included in Phase 2 of the Coupled Model Intercomparison Project (CMIP2). The median annual bias in the southern Australian region is −6%, and the range of biases −59 to +36%. In most models, the northwest is too wet and the northeast and east coast too dry, and the central arid zone is insufficiently arid.

The Australasian simulations in the AOGCMs utilised in the TAR have recently been scrutinised more closely, in part as a component of a series of national and state-based climate change

projection studies (e.g., Whetton et al., 2001; Cai et al., 2003b; McInnes et al., 2003; Hennessy et al., 2004a,b; McInnes et al., 2004). Some high-resolution regional simulations were also considered in this process. The general conclusion is that large-scale features of Australian climate were quite well simulated. In winter, temperature patterns were more poorly simulated in the south where topographic variations have a stronger influence, although this was alleviated in the higher-resolution simulations. A set of the TAR AOGCM simulations was also assessed for the New Zealand region by Mullan et al. (2001a) with similar conclusions. The models were able to represent ENSO-related variability in the Pacific and the temperature and rainfall teleconnection patterns at the Pacific-wide scale, but there was considerable variation in model performance at finer scales (such as over the New Zealand region).

Decadal-scale variability patterns in the Australian region as simulated by the CSIRO AOGCM were considered by Walland et al. (2000) and found 'broadly consistent' with the observational studies of Power et al. (1998). At smaller scales, Suppiah et al. (2004) directly assessed rainfall-producing processes by comparing the simulated correlation between rainfall anomalies and pressure anomalies in Victoria against observations. They find that this link was simulated well by most models in winter and autumn, but less well in spring and summer. As a result of this, they warn that the spring and summer projected rainfall changes should be viewed as less reliable.

Pitman and McAvaney (2004) examine the sensitivity of GCM simulations of Australian climate to methods of representation of the surface energy balance. They find that the quality of the simulation of variability is strongly affected by the land surface model, but that simulation of climate means, and the changes in those means in global warming simulations, is less sensitive to the scheme employed.

Statistical downscaling methods have been employed in the Australian region and have demonstrated good performance at representing means, variability and extremes of station temperature and rainfall (Timbal and McAvaney, 2001; Charles et al., 2004; Timbal, 2004) based on broad-scale observational or climate model predictor fields. The method of Charles et al. (2004) is able to represent spatial coherence at the daily time scale in station rainfall, thus enhancing its relevance to hydrological applications.

11.7.3 Climate Projections

In addition to the MMD models, numerous studies have been conducted with earlier models. Recent regional average projections are provided in Giorgi et al. (2001b) and Ruosteenoja et al. (2003). The most recent national climate change projections of CSIRO (2001) were based on the results of eight AOGCMs and one higher-resolution regional simulation. The methodology (and simulations) used in these projections is described in Whetton et al. (2005) and follows closely that described for earlier projections in Whetton et al. (1996). More detailed projections for individual states and other regions have also been prepared in recent years (Whetton

et al., 2001; Cai et al., 2003b; McInnes et al., 2003, 2004; Hennessy et al., 2004a,b; IOCI, 2005). This work has focused on temperature and precipitation, with additional variables such as potential evaporation and winds being included in the more recent assessments.

A range of dynamically downscaled projections have been undertaken for Australia using the DARLAM regional model (Whetton et al., 2001) and the CCAM stretched grid model (McGregor and Dix, 2001) at resolutions of 60 km across Australia and down to 14 km for Tasmania (McGregor, 2004). These projections use forcing from recent CSIRO AOGCM projections. Downscaled projected climate change using statistical methods has also been recently undertaken for parts of Australia (e.g., Timbal and McAvaney, 2001; Charles et al., 2004; Timbal, 2004) and New Zealand (Mullan et al., 2001a; Ministry for the Environment, 2004).

11.7.3.1 Mean Temperature

In both the southern and northern Australia regions, the projected MMD-A1B warming in the 21st century represents a significant acceleration of warming over that observed in the 20th century (Figure 11.16). The warming is larger than over the surrounding oceans, but only comparable to, or slightly larger than the global mean warming. Averaging over the region south of 30°S (SAU), the median 2100 warming among all of the models is 2.6°C (with an inter-quartile range of 2.4°C to 2.9°C) whereas the median warming averaged over the region north of 30°S (NAU) is 3.0°C (range of 2.8°C to 3.5°C). The seasonal cycle in the warming is weak, but with larger values (and larger spread among model projections) in summer (DJF). Across the MMD models, the warming is well correlated with the global mean warming, with a correlation coefficient of 0.79, so that more than half of the variance among models is controlled by global rather than local factors, as in many other regions. The range of responses is comparable but slightly smaller than the range in global mean temperature responses, and warming over equivalent time periods under the B1, A1B, and A2 scenarios is close to the ratios of the global mean responses. The warming varies sub-regionally, with less warming in coastal regions, Tasmania and the South Island of New Zealand, and greater warming in central and northwest Australia (see Figure 10.8).

These results are broadly (and in many details) similar to those described in earlier studies, so other aspects of these earlier studies can be assumed to remain relevant. For the CSIRO (2001) projections, pattern-scaling methods were used to provide patterns of change rescaled by the range of global warming given by IPCC (2001) for 2030 and 2070 based on the SRES scenarios. By 2030, the warming is 0.4°C to 2°C over most of Australia, with slightly less warming in some coastal areas and Tasmania, and slightly more warming in the northwest. By 2070, annual average temperatures increase by 1°C to 6°C over most of Australia with spatial variations similar to those for 2030. Dynamically downscaled mean temperature change typically does not differ very significantly from the picture based on AOGCMs (e.g., see Whetton et al., 2002).

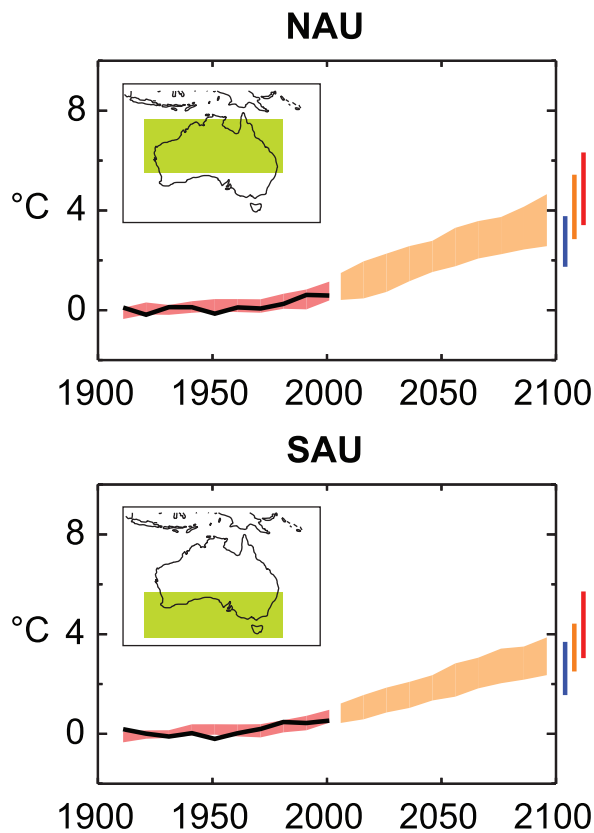


Figure 11.16. Temperature anomalies with respect to 1901 to 1950 for two Australian land regions for 1906 to 2005 (black line) and as simulated (red envelope) by MMD models incorporating known forcings; and as projected for 2001 to 2100 by MMD models for the A1B scenario (orange envelope). The bars at the end of the orange envelope represent the range of projected changes for 2091 to 2100 for the B1 scenario (blue), the A1B scenario (orange) and the A2 scenario (red). More details on the construction of these figures are given in Box 11.1 and Section 11.1.2.

Projected warming over New Zealand (allowing for the IPCC (2001) range of global warming and differences in the regional results of six GCMs used for downscaling) is 0.2°C to 1.3°C by the 2030s and 0.5°C to 3.5°C by the 2080s (Ministry for the Environment, 2004).

11.7.3.2 Mean Precipitation

A summary of projected precipitation changes from the MMD models is presented in Figure 11.17 and Table 11.1. The most robust feature is the reduction in rainfall along the south coast in JJA (not including Tasmania) and in the annual mean, and a decrease is also strongly evident in SON. The percentage JJA change in 2100 under the A1B scenario for southern Australia has an inter-quartile range of –26 to –7% and by comparison the same range using the probabilistic method of Tebaldi et al. (2004b) is –13 to –6% (Supplemental Material Table S11.2). There are large reductions to the south of the continent in all seasons, due to the poleward movement of the westerlies and embedded depressions (Cai et al., 2003a; Yin, 2005; Chapter 10), but this reduction extends over land during

winter when the storm track is placed furthest equatorward. Due to poleward drift of the storm track as it crosses Australian longitudes, the strongest effect is in the southwest, where the ensemble mean drying is in the 15 to 20% range. Hope (2006a,b) shows a southward or longitudinal shift in storms away from south-western Australia in the MMD simulations. To the east of Australia and over New Zealand, the primary storm track is more equatorward, and the north/south drying/moistening pattern associated with the poleward displacement is shifted equatorward as well. The result is a robust projection of increased rainfall on the South Island (especially its southern half), possibly accompanied by a decrease in the north part of the North Island. The South Island increase is likely to be modulated by the strong topography (see Box 11.3) and to appear mainly upwind of the main mountain range.

Other aspects of simulated precipitation change appear less robust. On the east coast of Australia, there is a tendency in the models for an increase in rain in the summer and a decrease in winter, with a slight annual decrease. However, consistency among the models on these features is weak.

These results are broadly consistent with results based on earlier GCM simulations. In the CSIRO (2001) projections based on a range of nine simulations, projected ranges of annual average rainfall change tend towards a decrease in the southwest and south but show more mixed results elsewhere (Whetton et al., 2005). Seasonal results showed that rainfall tended to decrease in southern and eastern Australia in winter and spring, increase inland in autumn and increase along the east coast in summer. Moise et al. (2005) also find a tendency for winter rainfall decreases across southern Australia and a slight tendency for rainfall increases in eastern Australia in 18 CMIP2 simulations under a 1% yr⁻¹ atmospheric CO₂ increase.

Whetton et al. (2001) demonstrate that inclusion of high-resolution topography could reverse the simulated direction of rainfall change in parts of Victoria (see Box 11.3). In a region of strong rainfall decrease as simulated directly by the GCMs, two different downscaling methods (Charles et al., 2004; Timbal, 2004) have been applied to obtain the characteristics of rainfall change at stations (IOCI, 2002, 2005; Timbal, 2004). The downscaled results continued to show the simulated decrease, although the magnitude of the changes was moderated relative to the GCM in the Timbal (2004) study. Downscaled rainfall projections for New Zealand (incorporating differing results from some six GCMs) showed a strong variation across the islands (Ministry for the Environment, 2004). The picture that emerges is that the pattern of precipitation changes described above in the global simulations is still present, but with the precipitation changes focused on the upwind sides of the islands, with the increase in rainfall in the south concentrated in the west, and the decrease in the north concentrated in the east.

11.7.3.3 Snow Cover

The likelihood that precipitation will fall as snow will decrease as temperature rises. Hennessy et al. (2003) modelled snowfall and snow cover in the Australian Alps under the

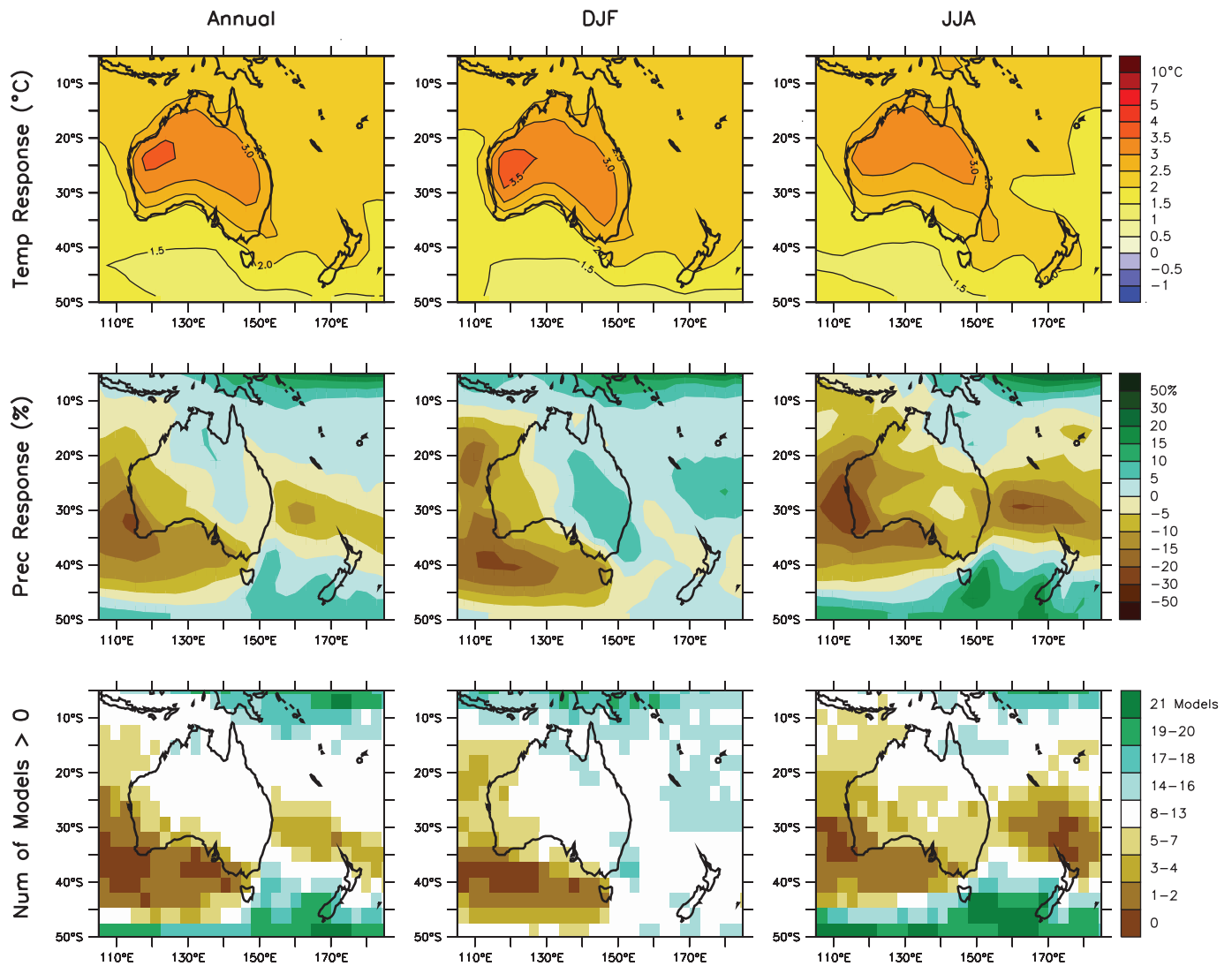


Figure 11.17. Temperature and precipitation changes over Australia and New Zealand from the MMD-A1B simulations. Top row: Annual mean, DJF and JJA temperature change between 1980 to 1999 and 2080 to 2099, averaged over 21 models. Middle row: same as top, but for fractional change in precipitation. Bottom row: number of models out of 21 that project increases in precipitation.

CSIRO (2001) projected temperature and precipitation changes and obtained very marked reductions in snow. The total alpine area with at least 30 days of snow cover decreases 14 to 54% by 2020, and 30 to 93% by 2050. Because of projected increased winter precipitation over the southern Alps, it is less clear that mountain snow will be reduced in New Zealand (Ministry for the Environment, 2004; see also Box 11.3). However, marked decreases in average snow water over New Zealand (60% by 2040 under the A1B scenario) have been simulated by Ghan and Shippert (2006) using a high-resolution sub-grid scale orography in a global model that simulates little change in precipitation.

11.7.3.4 Potential Evaporation

Using the method of Walsh et al. (1999), changes in potential evaporation in the Australian region have been calculated for

a range of enhanced greenhouse climate model simulations (Whetton et al., 2002; Cai et al., 2003b; McInnes et al., 2003, 2004; Hennessy et al., 2004a,b). In all cases, increases in potential evaporation were simulated, and in almost all cases, the moisture balance deficit became larger. This has provided a strong indication of the Australian environment becoming drier under enhanced greenhouse conditions.

11.7.3.5 Temperature and Precipitation Extremes

Where the analysis has been done for Australia (e.g., Whetton et al., 2002), the effect on changes in extreme temperature due to simulated changes in variability is small relative to the effect of the change in the mean. Therefore, most regional assessments of changes in extreme temperatures have been based on adding a projected mean temperature change to each day of a

station-observed data set. Based on the CSIRO (2001) projected mean temperature change scenarios, the average number of days over 35°C each summer in Melbourne would increase from 8 at present to 9 to 12 by 2030 and 10 to 20 by 2070 (CSIRO, 2001). In Perth, such hot days would rise from 15 at present to 16 to 22 by 2030 and 18 to 39 by 2070 (CSIRO, 2001). On the other hand, cold days become much less frequent. For example, Canberra's current 44 winter days of minimum temperature below 0°C is projected to be 30 to 42 by 2030 and 6 to 38 by 2070 (CSIRO, 2001).

Changes in extremes in New Zealand have been assessed using a similar methodology and simulations (Mullan et al., 2001b). Decreases in the annual frequency of days below 0°C of 5 to 30 days by 2100 are projected for New Zealand, particularly for the lower North Island and the South Island. Increases in the annual number of days above 25°C of 10 to 50 days by 2100 are projected.

A range of GCM and regional modelling studies in recent years have identified a tendency for daily rainfall extremes to increase under enhanced greenhouse conditions in the Australian region (e.g., Hennessy et al., 1997; Whetton et al., 2002; McInnes et al., 2003; Watterson and Dix, 2003; Hennessy et al., 2004b; Suppiah et al., 2004; Kharin and Zwiers, 2005). Commonly, return periods of extreme rainfall events halve in late 21st-century simulations. This tendency can apply even when average rainfall is simulated to decrease, but not necessarily when this decrease is marked (see Timbal, 2004). Recently, Abbs (2004) dynamically downscaled to a resolution of 7 km current and enhanced greenhouse cases of extreme daily rainfall occurrence in northern New South Wales and southern Queensland as simulated by the CSIRO GCM. The downscaled extreme events for a range of return periods compared well with observations and the enhanced greenhouse simulations for 2040 showed increases of around 30% in magnitude, with the 1-in-40 year event becoming the 1-in-15 year event. Less work has been done on projected changes in rainfall extremes in New Zealand, although the recent analysis of Ministry for the Environment (2004) based on Semenov and Bengtsson (2002) indicates the potential for extreme winter rainfall (95th percentile) to change by between -6% and +40%.

Where GCMs simulate a decrease in average rainfall, it may be expected that there would be an increase in the frequency of dry extremes (droughts). Whetton and Suppiah (2003) examine simulated monthly frequencies of serious rainfall deficiency for Victoria, which show strong average rainfall decreases in most simulations considered. There is a marked increase in the frequency of rainfall deficiencies in most simulations, with doubling in some cases by 2050. Using a slightly different approach, likely increases in the frequency of drought have also been established for the states of South Australia, New South Wales and Queensland (Walsh et al., 2002; McInnes et al., 2003; Hennessy et al., 2004c). Mullan et al. (2005) show that by the 2080s in New Zealand there may be significant increases in drought frequency in the east of both islands.

11.7.3.6 Tropical Cyclones

A number of recent regional model-based studies of changes in tropical cyclone behaviour in the Australian region have examined aspects of number, tracks and intensities under enhanced greenhouse conditions (e.g., Walsh and Katzfey, 2000; Walsh and Ryan, 2000; Walsh et al., 2004). There is no clear picture with respect to regional changes in frequency and movement, but increases in intensity are indicated. For example, Walsh et al. (2004) obtained, under tripled CO₂ conditions, a 56% increase in storms with a maximum wind speed greater than 30 m s⁻¹. It should also be noted that ENSO fluctuations have a strong impact on patterns of tropical cyclone occurrence in the region, and therefore uncertainty with respect to future ENSO behaviour (see Section 10.3) contributes to uncertainty with respect to tropical cyclone behaviour (Walsh, 2004). See Section 10.3.6.3 for a global assessment of changes in tropical cyclone characteristics.

11.7.3.7 Winds

The MMD ensemble mean projected change in winter sea level pressure is shown in Figure 10.9. Much of Australia lies to the north of the centre of the high-pressure anomaly. With the mean latitude of maximum pressure near 30°S at this season, this corresponds to a modest strengthening of the mean wind over inland and northern areas and a slight weakening of the mean westerlies on the southern coast, consistent with Hennessy et al. (2004b). Studies of daily extreme winds in the region using high-resolution model output (McInnes et al., 2003) indicate increases of up to 10% across much of the northern half of Australia and the adjacent oceans during summer by 2030. In winter, the pressure gradient is projected to increase over the South Island of New Zealand (see Figure 10.9), implying increased windiness. This increase is present in all of the MMD-A1B projections.

11.8 Polar Regions

Assessment of projected climate change for the polar regions:

The Arctic is very likely to warm during this century in most areas, and the annual mean warming is very likely to exceed the global mean warming. Warming is projected to be largest in winter and smallest in summer.

Annual arctic precipitation is very likely to increase. It is very likely that the relative precipitation increase will be largest in the winter and smallest in summer.

Arctic sea ice is very likely to decrease in extent and thickness. It is uncertain how the Arctic Ocean circulation will change.

It is likely that the Antarctic will be warmer and that precipitation will increase over the continent.

It is uncertain to what extent the frequency of extreme temperature and precipitation events will change in the polar regions.

Polar climate involves large natural variability on interannual, decadal and longer time scales, which is an important source of uncertainty. The projections of the trends in the underlying teleconnections, such as the Northern Annular Mode (NAM) or ENSO, contain substantial uncertainty (see Chapter 10). Further, understanding of the polar climate system is still incomplete due to its complex atmosphere-land-cryosphere-ocean-ecosystem interactions involving a variety of distinctive feedbacks. Processes that are not particularly well represented in the models are clouds, planetary boundary layer processes and sea ice. Additionally, the resolution of global models is still not adequate to resolve important processes in the polar seas. All this contributes to a rather large range of present-day and future simulations, which may reduce confidence in the future projections. A serious problem is the lack of observations against which to assess models, and for developing process knowledge, particularly over Antarctica.

11.8.1 Arctic

11.8.1.1 Key Processes

Arctic climate is characterised by a distinctive complexity due to numerous nonlinear interactions between and within the atmosphere, cryosphere, ocean, land and ecosystems. Sea ice plays a crucial role in the arctic climate, particularly through its albedo. Reduction of ice extent leads to warming due to increased absorption of solar radiation at the surface. Substantial low-frequency variability is evident in various atmosphere and ice parameters (Polyakov et al., 2003a,b), complicating the detection and attribution of arctic changes. Natural multi-decadal variability has been suggested as partly responsible for the large warming in the 1920s to 1940s (Bengtsson et al., 2004; Johannessen et al., 2004) followed by cooling until the 1960s. In both models and observations, the interannual variability of monthly temperatures is at a maximum at high latitudes (Räsänen, 2002). Natural atmospheric patterns of variability on annual and decadal time scales play an important role in the arctic climate. Such patterns include the NAM, the NAO, the Pacific-North American (PNA) pattern and the Pacific Decadal Oscillation (PDO), which are associated with prominent arctic regional precipitation and temperature anomalies (see Box 3.4 and Section 3.6). For instance, the positive NAM/NAO phase is associated with warmer, wetter winters in Siberia and colder, drier winters in western Greenland and north-eastern Canada. The NAM/NAO showed a trend towards its positive phase over the last three to four decades, although it returned to near its long-term mean state in the last five years (see Section 3.6). In the future, global models project a positive trend in the NAO/NAM during the 21st century (see Section 10.3). There was

substantial decadal-to-inter-decadal atmospheric variability in the North Pacific over the 20th century, associated with fluctuations in the strength of the winter Aleutian Low that covary with North Pacific SST in the PDO (see Section 3.6). A deeper and eastward-shifted Aleutian Low advects warmer and moister air into Alaska. While some studies have suggested that the Brooks Range effectively isolates arctic Alaska from much of the variability associated with North Pacific teleconnection patterns (e.g., L'Heureux et al., 2004), other studies find relationships between the Alaskan and Beaufort-Chukchi region's climate and North Pacific variability (Stone, 1997; Curtis et al., 1998; Lynch et al., 2004). Patterns of variability in the North Pacific, and their implications for climate change, are especially difficult to sort out due to the presence of several patterns (NAM, PDO, PNA) with potentially different underlying mechanisms (see Chapter 3).

11.8.1.2 Skill of Models in Simulating Present Climate

Many processes are still poorly understood and thus continue to pose a challenge for climate models (ACIA, 2005). In addition, evaluating simulations of the Arctic is difficult because of the uncertainty in the observations. The few available observations are sparsely distributed in space and time and different data sets often differ considerably (Serreze and Hurst, 2000; ACIA, 2005; Liu et al., 2005; Wyser and Jones, 2005). This holds especially for precipitation measurements, which are problematic in cold environments (Goodison et al., 1998; Bogdanova et al., 2002).

Few pan-arctic atmospheric RCMs are in use. When driven by analysed lateral and sea ice boundary conditions, RCMs tend to show smaller temperature and precipitation biases in the Arctic compared to GCMs, indicating that sea ice simulation biases and biases originating from lower latitudes contribute substantially to the contamination of GCM results in the Arctic (e.g., Dethloff et al., 2001; Wei et al., 2002; Lynch et al., 2003; Semmler et al., 2005). However, even under a very constrained experimental design, there can be considerable across-model scatter in RCM simulations (Tjernström et al., 2005; Rinke et al., 2006). The construction of coupled atmosphere-ice-ocean RCMs for the Arctic is a recent development (Maslanik et al., 2000; Debernard et al., 2003; Rinke et al., 2003; Mikolajewicz et al., 2005).

Temperature

The simulated spatial patterns of the MMD ensemble mean temperatures agree closely with those of the observations throughout the annual cycle. Generally, the simulations are 1°C to 2°C colder than the European Centre for Medium-Range Weather Forecasts 40-year (ERA40) reanalyses with the exception of a cold bias maximum of 6°C to 8°C in the Barents Sea (particularly in winter/spring) caused by overestimated sea ice in this region (Chapman and Walsh, 2007; see also Section 8.3). Compared with earlier model versions, the annual temperature simulations improved in the Barents and Norwegian Seas and Sea of Okhotsk, but some deterioration is noted in the central Arctic Ocean and the high terrain areas

of Alaska and northwest Canada (Chapman and Walsh, 2007). The mean model ensemble bias is relatively small compared to the across-model scatter of temperatures. The annual mean root-mean-squared error in the individual MMD models ranges from 2°C to 7°C (Chapman and Walsh, 2007). Compared with previous models, the MMD-simulated temperatures are more consistent across the models in winter, but somewhat less so in summer. There is considerable agreement between the modelled and observed interannual variability both in magnitude and spatial pattern.

Precipitation

The AOGCM-simulated monthly precipitation varies substantially among the models throughout the year but the MMD ensemble mean monthly means are within the range of different observational data sets. This is an improvement compared to earlier simulations (Walsh et al., 2002; ACIA, 2005), particularly from autumn to spring (Kattsov et al., 2007). The ensemble mean bias varies with season and remains greatest in spring and smallest in summer. The annual bias pattern (positive over most parts of the Arctic) can be partly attributed to coarse orography and to biased atmospheric storm tracks and sea ice cover (see Chapter 8). The MMD models capture the observed increase in the annual precipitation through the 20th century (see Section 3.3).

Sea Ice and Ocean

Arctic sea ice biases in present-day MMD simulations are discussed in Section 8.3. Arctic ocean-sea ice RCMs under realistic atmospheric forcing are increasingly capable of reproducing the known features of the Arctic Ocean circulation and observed sea ice drift patterns. The inflow of the two branches of Atlantic origin via the Fram Strait and the Barents Sea and their subsequent passage at mid-depths in several cyclonic circulation cells are present in most recent simulations (Karcher et al., 2003; Maslowski et al., 2004; Steiner et al., 2004). Most of the models are biased towards overly salty values in the Beaufort Gyre and thus too little freshwater storage in the arctic halocline. Several potential causes have been identified, among them a biased simulation of arctic shelf processes and wind forcing. Most hindcast simulations with these RCMs show a reduction in the arctic ice volume over recent decades (Holloway and Sou, 2002).

11.8.1.3 Climate Projections

Temperature

A northern high-latitude maximum in the warming ('polar amplification') is consistently found in all AOGCM simulations (see Section 10.3). The simulated annual mean arctic warming exceeds the global mean warming by roughly a factor of two in the MMD models, while the winter warming in the central arctic is a factor of four larger than the global annual mean when averaged over the models. These magnitudes are comparable to those obtained in previous studies (Holland and Bitz, 2003;

ACIA, 2005). The consistency between observations and the ensemble mean 20th-century simulations (Figure 11.18), combined with the fact that the near-future projections (2010–2029) continue the late 20th-century trends in temperature, ice extent and thickness with little modification (Serreze and Francis, 2006), increases confidence in this basic polar-amplified warming pattern, despite the inter-model differences in the amount of polar amplification.

At the end of the 21st century, the projected annual warming in the Arctic is 5°C, estimated by the MMD-A1B ensemble mean projection (Section 11.8.2.3, Figure 11.21). There is a considerable across-model range of 2.8°C to 7.8°C (Table 11.1). Larger (smaller) mean warming is found for the A2 (B1) scenario of 5.9°C (3.4°C), with a proportional across-model range. The across-model and across-scenario variability in the projected temperatures are both considerable and of comparable amplitude (Chapman and Walsh, 2007).

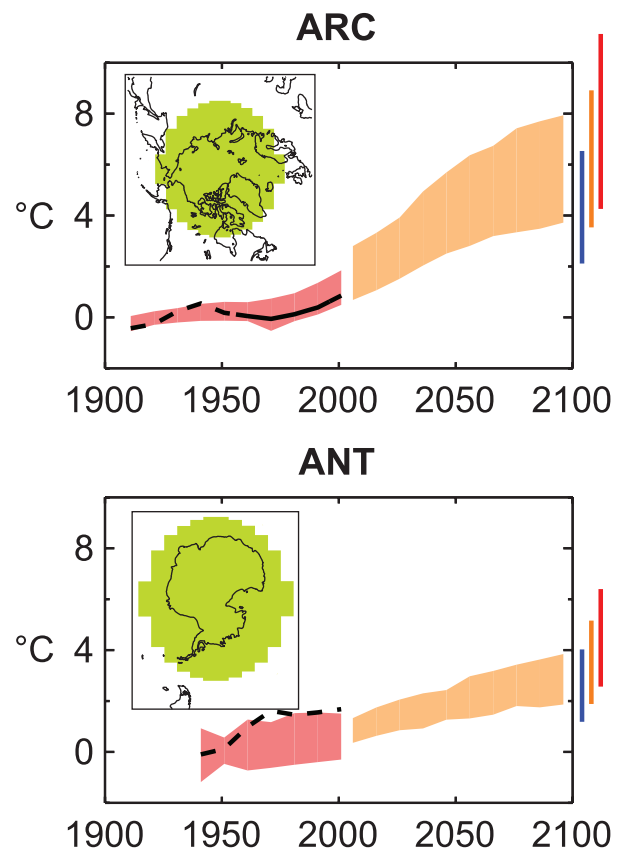


Figure 11.18. Top panels: Temperature anomalies with respect to 1901 to 1950 for the whole Arctic for 1906 to 2005 (black line) as simulated (red envelope) by MMD models incorporating known forcings; and as projected for 2001 to 2100 by MMD models for the A1B scenario (orange envelope). The bars at the end of the orange envelope represent the range of projected changes for 2091 to 2100 for the B1 scenario (blue), the A1B scenario (orange) and the A2 scenario (red). The black line is dashed where observations are present for less than 50% of the area in the decade concerned. Bottom panels: The same for Antarctic land, but with observations for 1936 to 2005 and anomalies calculated with respect to 1951 to 2000. More details on the construction of these figures are given in Box 11.1 and Section 11.1.2.

Over both ocean and land, the largest (smallest) warming is projected in winter (summer) (Table 11.1, Figure 11.19). But the seasonal amplitude of the temperature change is much larger over ocean than over land due to the presence of melting sea ice in summer keeping the temperatures close to the freezing point. The surface air temperature over the Arctic Ocean region is generally warmed more than over arctic land areas (except in summer). The range between the individual simulated changes remains large (Figure 11.19, Table 11.1). By the end of the century, the mean warming ranges from 4.3°C to 11.4°C in winter, and from 1.2°C to 5.3°C in summer under the A1B scenario. The corresponding 5 to 95% confidence intervals are given in Supplementary Material Table S11.2. In addition to the overall differences in global warming, difficulties in simulating sea ice, partly related to biases in the surface wind fields, as well as deficiencies in cloud schemes, are likely responsible for much of the inter-model scatter. Internal variability plays a secondary role when examining these late-21st century responses.

The annual mean temperature response pattern at the end of the 21st century under the A1B scenario (Supplementary Material Figures S11.27 and S11.11) is characterised by a robust and large warming over the central Arctic Ocean (5°C to 7°C), dominated by the warming in winter/autumn associated with the reduced sea ice. The maximum warming is projected over the Barents Sea, although this could result from an overestimated albedo feedback caused by removal of the present-day simulations' excessive sea ice cover. A region of reduced warming (<2°C, even slight cooling in several models) is projected over the northern North Atlantic, which is consistent among the models. This is due to weakening of the MOC (see Section 10.3).

While the natural variability in arctic temperatures is large compared to other regions, the signals are still large enough

to emerge quickly from the noise (Table 11.1). Looking more locally, as described by Chapman and Walsh (2007), Alaska is perhaps the land region with the smallest signal-to-noise ratio, and is the only arctic region in which the 20-year mean 2010 to 2029 temperature is not clearly discernible from the 1981 to 2000 mean in the MMD models. But even here the signal is clear by mid-century in all three scenarios.

The regional temperature responses are modified by changes in circulation patterns (Chapter 10). In winter, shifts in NAO phase can induce inter-decadal temperature variations of up to 5°C in the eastern Arctic (Dorn et al., 2003). The MMD models project winter circulation changes consistent with an increasingly positive NAM/NAO (see Section 10.3), which acts to enhance the warming in Eurasia and western North America. In summer, circulation changes are projected to favour warm anomalies north of Scandinavia and extending into the eastern Arctic, with cold anomalies over much of Alaska (Cassano et al., 2006). However, deficiencies in the arctic summer synoptic activity in these models reduce confidence in the detailed spatial structure. In addition, these circulation-induced temperature changes are not large enough to change the relatively uniform summer warming seen in the MMD models.

The patterns of temperature changes simulated by RCMs are quite similar to those simulated by GCMs. However, they show an increased warming along the sea ice margin possibly due to a better description of the mesoscale weather systems and air-sea fluxes associated with the ice edge (ACIA, 2005). The warming over most of the central Arctic and Siberia, particularly in summer, tends to be lower in RCM simulations (by up to 2°C) probably due to more realistic present-day snowpack simulations (ACIA, 2005). The warming is modulated by the topographical height, snow cover and associated albedo feedback as shown for the region of northern Canada and Alaska (see Section 11.5.3).

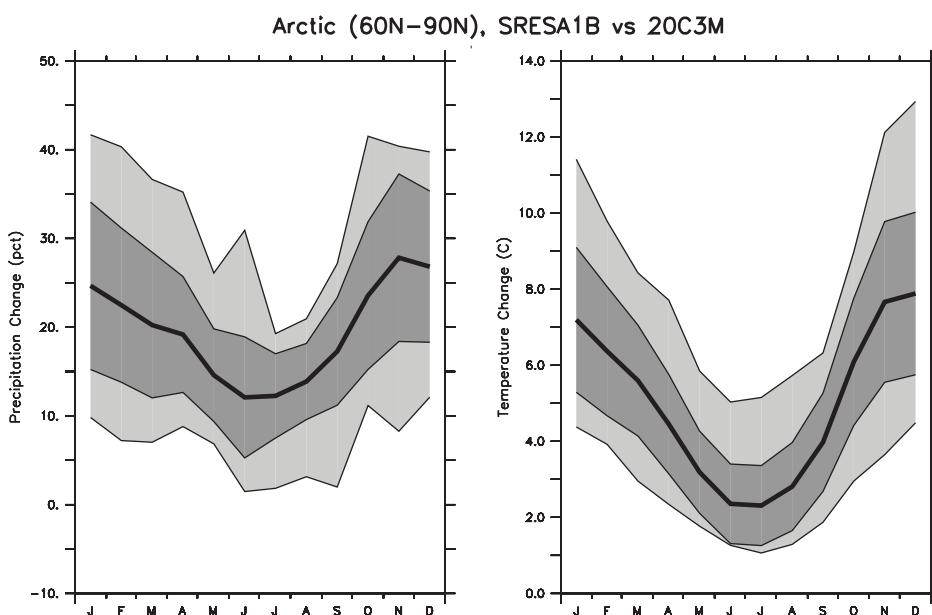


Figure 11.19. Annual cycle of arctic area mean temperature and percentage precipitation changes (averaged over the area north of 60°N) for 2080 to 2099 minus 1980 to 1999, under the A1B scenario. Thick lines represent the ensemble median of the 21 MMD models. The dark grey area represents the 25 and 75% quartile values among the 21 models, while the light grey area shows the total range of the models.

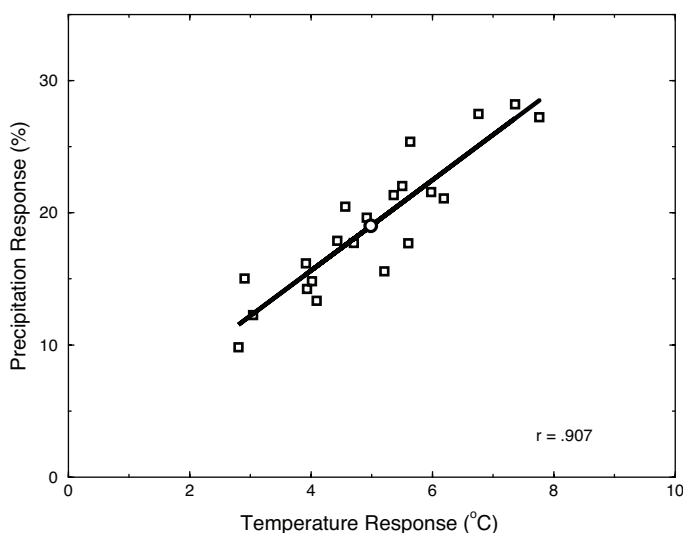


Figure 11.20. Relationship between the change in annual precipitation (%) and temperature (°C) (2080–2099 minus 1980–1999) in the Arctic (averaged over the area north of 60°N) in the MMD-A1B projections. Each point represents one model. The model ensemble mean response is indicated by the circle.

Precipitation

The MMD simulations show a general increase in precipitation over the Arctic at the end of the 21st century (Table 11.1; Supplementary Material Figure S11.28). The precipitation increase is robust among the models (Table 11.1; Supplementary Material Figure S11.19) and qualitatively well understood, attributed to the projected warming and related increased moisture convergence (Section 10.3). The very strong correlation between the temperature and precipitation changes (approximately a 5% precipitation increase per degree Celsius warming) across the model ensemble is worth noting (Figure 11.20). Thus, both the sign and the magnitude (per degree warming) of the percentage precipitation change are robust among the models.

The spatial pattern of the projected change (Supplementary Material Figure S11.28) shows the greatest percentage increase over the Arctic Ocean (30 to 40%) and smallest (and even slight decrease) over the northern North Atlantic (<5%). By the end of the 21st century, the projected change in the annual mean arctic precipitation varies from 10 to 28%, with an MMD-A1B ensemble median of 18% (Table 11.1). Larger (smaller) mean precipitation increases are found for the A2 (B1) scenario with 22% (13%). The percentage precipitation increase is largest in winter and smallest in summer, consistent with the projected warming (Figure 11.19; Table 11.1). The across-model scatter of the precipitation projections is substantial (Figure 11.19; Table 11.1). The Tebaldi et al. (2004a) 5th to 95th percentile confidence interval of percentage precipitation change in winter is 13 to 36% and in summer 5 to 19% (Supplementary Material Table S11.2).

Differences between the projections for different scenarios are small in the first half of the 21st century but increase later.

Differences among the models increase rapidly as the spatial domain becomes smaller (ACIA, 2005). The geographical variation of precipitation changes is determined largely by changes in the synoptic circulation patterns. During winter, the MMD models project a decreased (increased) frequency of strong Arctic high (Icelandic low) pressure patterns that favour precipitation increases along the Canadian west coast, southeast Alaska and North Atlantic extending into Scandinavia (Cassano et al., 2006). Projections with RCMs support the broad-scale messages while adding expected local and regional detail (ACIA, 2005).

By the end of the 21st century, the MMD-A1B ensemble-projected precipitation increase is significant (Table 11.1), particularly the annual and cold season (winter/autumn) precipitation. However, local precipitation changes in some regions and seasons (particularly in the Atlantic sector and generally in summer) remain difficult to discern from natural variability (ACIA, 2005).

Extremes of Temperature and Precipitation

Very little work has been done in analysing future changes in extreme events in the Arctic. However, the MMD simulations indicate that the increase in mean temperature and precipitation will be combined with an increase in the frequency of very warm and wet winters and summers. Using the definition of extreme season in Section 11.1.2, every DJF and JJA season, in all model projections, is ‘extremely’ warm in the period 2080 to 2099 (Table 11.1). The corresponding numbers for extremely wet seasons are 90 and 85% for DJF and JJA. For the other scenarios, the frequency of extremes is very similar, except that for the wet seasons under B1, which is smaller (~63%).

Cryosphere

Northern Hemisphere sea ice, snow and permafrost projections are discussed in Section 10.3; projected changes in the surface mass balance of arctic glaciers and of the Greenland Ice Sheet are discussed in Sections 10.3 and 10.7.

Arctic Ocean

A systematic analysis of future projections for the Arctic Ocean circulation is still lacking. Coarse resolution in global models prevents the proper representation of local processes that are of global importance (such as the convection in the Greenland Sea that affects the deep waters in the Arctic Ocean and the intermediate waters that form overflow waters). The MMD models project a reduction in the MOC in the Atlantic Ocean (see Section 10.3). Correspondingly, the northward oceanic heat transport decreases south of 60°N in the Atlantic. However, the CMIP2 model assessment showed a projected increase in the oceanic heat transport at higher latitudes, associated with a stronger subarctic gyre circulation in the models (Holland and Bitz, 2003). The Atlantic Ocean north of 60°N freshens during the 21st century, in pronounced contrast to the observed development in the late 20th century (Wu et al., 2003).

11.8.2 Antarctic

11.8.2.1 Key Processes

Over Antarctica, there is special interest in changes in snow accumulation expected to accompany global climate change as well as the pattern of temperature change, particularly any differences in warming over the peninsula and the interior of the ice sheet. As in the Arctic, warming of the troposphere is expected to increase precipitation. However, circulation changes in both ocean and atmosphere can alter the pattern of air masses, which would modify both precipitation and temperature patterns substantially over the region.

The dominant patterns controlling the atmospheric seasonal-to-interannual variability of the SH extratropics are the Southern Annular Mode (SAM) and ENSO (see Section 3.6). Signatures of these patterns in the Antarctic have been revealed in many studies (reviews by Carleton, 2003 and Turner, 2004). The positive phase of the SAM is associated with cold anomalies over most of Antarctica and warm anomalies over the Antarctic Peninsula (Kwok and Comiso, 2002a). Over recent decades, a drift towards the positive phase in the SAM is evident (see Section 3.6). Observational studies have presented evidence of pronounced warming over the Antarctic Peninsula, but little change over the rest of the continent during the last half of the 20th century (see Sections 3.6 and 4.6). The response of the SAM in transient warming simulations is a robust positive trend, but the response to the ozone hole in the late 20th century, which is also a positive perturbation to the SAM, makes any simple extrapolation of current trends into the future uncertain (see Section 10.3).

Compared to the SAM, the Southern Oscillation (SO) shows weaker association with surface temperature over Antarctica but the correlation with SST and sea ice variability in the Pacific sector of the Southern Ocean is significant (e.g., Kwok and Comiso, 2002b; Renwick, 2002; Bertler et al., 2004; Yuan, 2004). Correlation between the SO index and antarctic precipitation and accumulation has also been studied but the persistence of the signal is not clear (Bromwich et al., 2000, 2004a; Genthon and Cosme, 2003; Guo et al., 2004; Genthon et al., 2005). Recent work suggests that this intermittence is due to nonlinear interactions between ENSO and SAM that vary on decadal time scales (Fogt and Bromwich, 2006; L'Heureux and Thompson, 2006). The SO index has a negative trend over recent decades (corresponding to a tendency towards more El Niño-like conditions in the equatorial Pacific; see Section 3.6) associated with sea ice cover anomalies in the Pacific sector, namely negative (positive) anomalies in the Ross and Amundsen Seas (Bellingshausen and Weddell Seas) (Kwok and Comiso, 2002a). However, a definitive assessment of ENSO amplitude and frequency changes in the 21st century cannot be made (see Chapter 10).

11.8.2.2 Skill of Models in Simulating Present Climate

Evaluating temperature and precipitation simulations over Antarctica is difficult due to sparse observations and often relies on numerical weather prediction (re)analyses. However, significant differences between those have been found, and comparisons with station observations show that the surface temperature can be subject to considerable biases (Connolley and Harangozo, 2001; Bromwich and Fogt, 2004). Marked improvement in the bias is seen after the satellite era (~1978) (Simmons et al., 2004), and parts of the bias are explained by the reanalyses' smoothing of the sharp changes in the terrain near coastal stations. Satellite-derived monthly surface temperatures agree with antarctic station data with an accuracy of 3°C (Comiso, 2000). Precipitation evaluation is even more challenging and the different (re)analyses differ significantly (Connolley and Harangozo, 2001; Zou et al., 2004). Very few direct precipitation gauge and detailed snow accumulation data are available, and these are uncertain to varying degrees (see Section 4.6).

Major challenges face the simulation of the atmospheric conditions and precipitation patterns of the polar desert in the high interior of East Antarctica (Guo et al., 2003; Bromwich et al., 2004a; Pavolonis et al., 2004; Van de Berg et al., 2005). Driven by analysed boundary conditions, RCMs tend to show smaller temperature and precipitation biases in the Antarctic compared to the GCMs (Bailey and Lynch, 2000; Van Lipzig et al., 2002a,b; Van den Broeke and Van Lipzig, 2003; Bromwich et al., 2004b; Monaghan et al., 2006). Krinner et al. (1997) show the value of a stretched model grid with higher horizontal resolution over the Antarctic as compared to standard GCM formulations. Despite these promising developments, since the TAR there has been no coordinated comparison of the performance of GCMs, RCMs and other alternatives to global GCMs over Antarctica.

Temperature

Compared to National Centers for Environmental Prediction (NCEP) reanalyses, the MMD ensemble annual surface temperatures are in general slightly warmer in the Southern Ocean to the north of the sea ice region. The mean bias is predominantly less than 2°C (Carril et al., 2005), which may indicate a slight improvement compared to previous models due to better simulation of the position and depth of the Antarctic trough (Carril et al., 2005; Raphael and Holland, 2006). The temperature bias over sea ice is larger. Biases over the continent are several degrees where the model topography is erroneous (Turner et al., 2006). However, as emphasized above, the biases have to be viewed in the context of the uncertainty in the observations. Changes in cloud and radiation parametrizations have been shown to change the temperature simulation significantly (Hines et al., 2004). A lateral nudging of a stretched-grid GCM (imposing the correct synoptic cyclones from 60°S and lower latitudes) brings the model in better agreement with observations but significant biases remain (Genthon et al., 2002).

The spread in the individual MMD-simulated patterns of surface temperature trends over the past 50 years is very large, but in contrast to previous models, the multi-model composite of the MMD models qualitatively captures the observed enhanced warming trend over the Antarctic Peninsula (Chapman and Walsh, 2006). The general improvements in resolution, sea ice models and cloud-radiation packages have evidently contributed to improved simulations. The ensemble-mean temperature trends show similarity to the observed spatial pattern of the warming, for both annual and seasonal trends. For the annual trend, this includes the warming of the peninsula and near-coastal Antarctica and neutral or slight cooling over the sea-ice covered regions of the Southern Ocean. While the large spread among the models is not encouraging, this level of agreement suggests that some confidence in the ensemble mean 21st-century projection is appropriate.

Precipitation

The MMD models simulate the position of the storm tracks reasonably well but nearly all show some deficiency in the distribution and level of cyclone activity compared to reanalyses (see Section 8.3). Regional Climate Models generally capture the cyclonic events affecting the coast and the associated synoptic variability of precipitation with more fidelity (Adams, 2004; Bromwich et al., 2004a). Over the 20th century, the MMD models simulate changes in storm track position that are generally consistent with observed changes (i.e., poleward displacement of the storm tracks; see Sections 9.5 and 10.3).

The precipitation simulations by both GCMs and RCMs contain uncertainty, on all time scales (Covey et al., 2003; Bromwich et al., 2004a,b; Van de Berg et al., 2005), as a result of model physics limitations. All atmospheric models, including the models underlying the reanalyses, have incomplete parametrizations of polar cloud microphysics and ice crystal precipitation. The simulated precipitation depends, among other things, on the simulated sea ice concentrations, and is strongly affected by biases in the sea ice simulations (Weatherly, 2004). Recent RCM simulations driven by observed sea ice conditions demonstrate good precipitation skill (Van de Berg et al., 2005; Monaghan et al., 2006). However, as emphasized above, the observational uncertainty contributes to uncertainty in the differences between observations and simulations.

Sea Ice

The performance biases of SH sea ice conditions in present-day MMD simulations are discussed in Section 8.3.

11.8.2.3 Climate Projections

Very little effort has been spent to model the future climate of Antarctica at a spatial scale finer than that of GCMs.

Temperature

At the end of the 21st century, the annual warming over the Antarctic continent is moderate but significant (Figure 11.21;

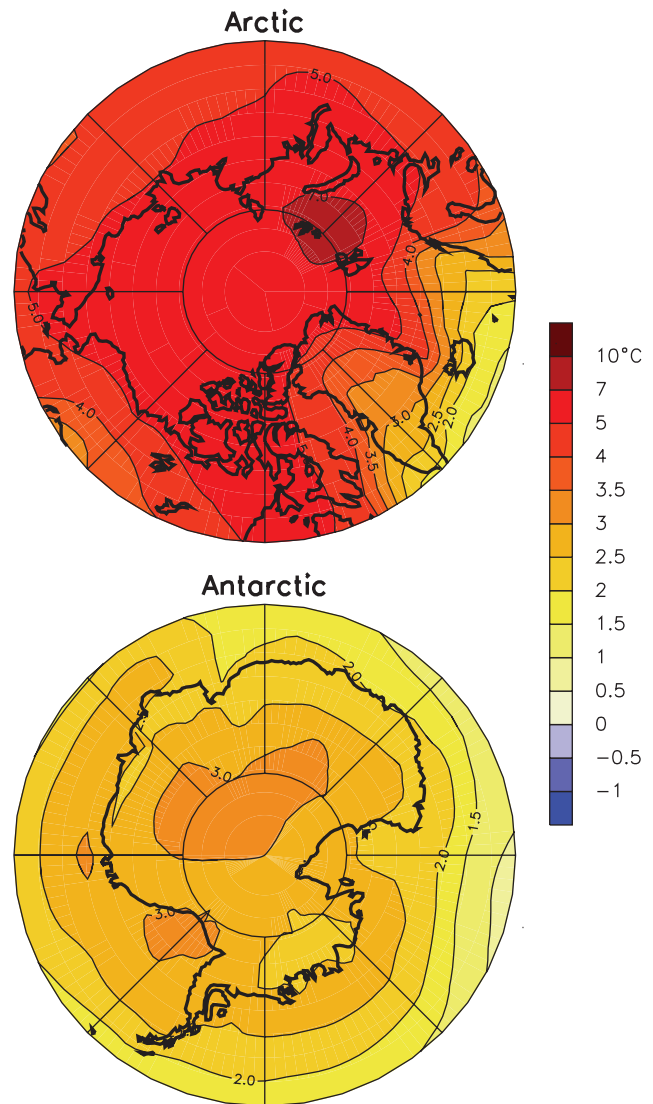


Figure 11.21. Annual surface temperature change between 1980 to 1999 and 2080 to 2099 in the Arctic and Antarctic from the MMD-A1B projections.

Table 11.1; Chapman and Walsh, 2006). It is estimated to be 2.6°C by the median of the MMD-A1B models with a range from 1.4°C to 5.0°C across the models (Table 11.1). Larger (smaller) warming is found for the A2 (B1) scenario with mean value of 3.1°C (1.8°C). These warming magnitudes are similar to previous estimates (Covey et al., 2003). The annual mean MMD model projections show a relatively uniform warming over the entire continent (with a maximum in the Weddell Sea) (Figure 11.21; Carril et al., 2005; Chapman and Walsh, 2006). They do not show a local maximum warming over the Antarctic Peninsula. This is a robust feature among the individual models (Supplementary Material Figure S11.12). Thus, the pattern of observed temperature trends in the last half of the 20th century (warming over the Antarctic Peninsula, little change over the rest of the continent) is not projected to continue throughout the 21st century, despite a projected positive SAM trend (see

Section 10.3). It has been argued that two distinct factors have contributed to the observed SAM trend: greenhouse gas forcing and the ozone hole formation (Stone et al., 2001; Shindell and Schmidt, 2004). Their relative importance for the peninsular warming is not readily understood (see Chapter 10).

The mean antarctic temperature change does not show a strong seasonal dependency; the MMD-A1B ensemble mean winter (summer) warming is 2.8°C (2.6°C) (Table 11.1; Supplementary Material Figure S11.29; Chapman and Walsh, 2006). This is also illustrated by how close the Tebaldi et al. (2004a) 5 to 95% confidence interval for the two seasons is: 0.1°C to 5.7°C in summer and 1.0°C to 4.8°C in winter (Supplementary Material Table S11.2). However, over the Southern Oceans, the temperature change is larger in winter/autumn than in summer/spring, which can primarily be attributed to the sea ice retreat (see Section 10.3).

Precipitation

Almost all MMD models simulate a robust precipitation increase in the 21st century (Supplementary Material Figures S11.29 and S11.30; Table 11.1). However, the scatter among the individual models is considerable. By the end of the 21st century, the projected change in the annual precipitation over the Antarctic continent varies from –2% to 35%, with a MMD-A1B ensemble median of 14% (Table 11.1). Similar (smaller) mean precipitation increase is found for the A2 (B1) scenario, with values of 15% (10%). The spatial pattern of the annual change is rather uniform (Supplementary Material Figure S11.30). The projected relative precipitation change shows a seasonal dependency, and is larger in winter than in summer (Supplementary Material Figure S11.29). The Tebaldi et al. (2004a) 5 to 95% confidence interval for winter is –1 to 34% and in summer –6 to 22% (Supplementary Material Table S11.2). The projected increase in precipitation over Antarctica and thus greater accumulation of snow, without substantial surface melting, will contribute negatively to sea level rise relative to the present day (see Section 10.6). It is notable that the most recent model studies of antarctic precipitation show no significant contemporary trends (Van de Berg et al., 2005; Monaghan et al., 2006; Van den Broeke et al., 2006; see Section 4.6).

The moisture transport to the continent by synoptic activity represents a large fraction of net precipitation (Noone and Simmonds, 2002; Massom et al., 2004). During summer and winter, a systematic shift towards strong cyclonic events is projected by the MMD models (see Section 10.3). In particular, the frequency of occurrence of deep cyclones in the Ross Sea to Bellingshausen Sea sector is projected to increase by 20 to 40% (63%) in summer (winter) by the middle of the 21st century (Lynch et al., 2006). Related to this, the precipitation over the sub-antarctic seas and Antarctic Peninsula is projected to increase.

Extremes of Temperature and Precipitation

Very little work has been done in analysing future changes in extreme events in the Antarctic. However, the MMD simulations indicate that the increase in mean temperature and precipitation

will be combined with an increase in the frequency of very warm and wet winters and summers. Using the definition of ‘extreme’ seasons provided in Section 11.1.2, the MMD models predict extremely warm seasons in about 85% of all DJF and 83% of all JJA seasons in the period 2080 to 2099, as averaged over all models (Table 11.1). The corresponding numbers for extremely wet seasons are 34% and 59%. For the B1 scenario, the frequency of extremes is smaller, with little difference between A1B and A2.

Sea Ice and Antarctic Ice Sheet

Southern Hemisphere sea ice projections are discussed in Section 10.3. The projections of the Antarctic Ice Sheet surface mass balance are discussed in Section 10.6.

11.9 Small Islands

Assessment of projected climate change for Small Islands regions:

Sea levels are likely to continue to rise on average during the century around the small islands of the Caribbean Sea, Indian Ocean and Northern and Southern Pacific Oceans. Models indicate that the rise will not be geographically uniform but large deviations among models make regional estimates across the Caribbean, Indian and Pacific Oceans uncertain.

All Caribbean, Indian Ocean and North and South Pacific islands are very likely to warm during this century. The warming is likely to be somewhat smaller than the global annual mean warming in all seasons.

Summer rainfall in the Caribbean is likely to decrease in the vicinity of the Greater Antilles but changes elsewhere and in winter are uncertain. Annual rainfall is likely to increase in the northern Indian Ocean with increases likely in the vicinity of the Seychelles in DJF, and in the vicinity of the Maldives in JJA while decreases are likely in the vicinity of Mauritius in JJA. Annual rainfall is likely to increase in the equatorial Pacific, while most models project decreases just east of French Polynesia in DJF.

Since AOGCMs do not have sufficiently fine resolution to see the islands, the projections are given over ocean surfaces rather than over land and very little work has been done in downscaling these projections to individual islands. Assessments are also difficult because some climatic processes are still not well understood, such as the midsummer drought in the Caribbean and the ocean-atmosphere interaction in the Indian Ocean. Furthermore, there is insufficient information on future SST changes to determine the regional distribution of cyclone changes. Large deviations among models make the regional distribution of sea level rise uncertain and the number of models addressing storm surges is very limited.

11.9.1 Key Processes

Climate change scenarios for small islands of the Caribbean Sea, Indian Ocean and Pacific Ocean are included in the AR4 for a number of reasons. Ocean-atmosphere interactions play a major role in determining the climate of the islands and including their climate in the projections for neighbours with larger landmasses would miss features peculiar to the islands themselves. Many small islands are sufficiently removed from large landmasses so that atmospheric circulation may be different over the smaller islands compared to their larger neighbours (e.g., in the Pacific Ocean). For the Caribbean, which is close to large landmasses in Central America and northern South America, some islands partly share climate features of one, while others partly share features of the other. At the same time, the Caribbean islands share many common features that are more important than are those shared with the larger landmasses, such as the strong relationship of their climate to SST.

11.9.1.1 Caribbean

The Caribbean region spans roughly the area between 10°N to 25°N and 85°W to 60°W. Its climate can be broadly characterised as dry winter/wet summer with orography and elevation being significant modifiers at the sub-regional scale (Taylor and Alfero, 2005). The dominant synoptic influence is the North Atlantic subtropical high (NAH). During the winter, the NAH is southernmost and the region is generally at its driest. With the onset of the spring, the NAH moves northward, the trade wind intensity decreases and the equatorial flank of the NAH becomes convergent. Concurrently, easterly waves traverse the Atlantic from the coast of Africa into the Caribbean. These waves frequently mature into storms and hurricanes under warm SSTs and low vertical wind shear, generally within a 10°N to 20°N latitudinal band. They represent the primary rainfall source and their onset in June and demise in November roughly coincide with the mean Caribbean rainy season. In the coastal zones of Venezuela and Columbia, the wet season occurs later, from October to January (Martis et al., 2002). Interannual variability of the rainfall is influenced mainly by ENSO events through their effect on SSTs in the Atlantic and Caribbean Basins. The late rainfall season tends to be drier in El Niño years and wetter in La Niña years (Giannini et al., 2000, Martis et al., 2002, M. Taylor et al., 2002) and tropical cyclone activity diminishes over the Caribbean during El Niño summers (Gray, 1984). However, the early rainfall season in the central and southern Caribbean tends to be wetter in the year after an El Niño and drier in a La Niña year (Chen and Taylor, 2002). The phase of the NAO modulates the behaviour of warm ENSO events (Giannini et al., 2001). A positive NAO phase implies a stronger than normal NAH and amplifies the drying during a warm ENSO. On the other hand, a negative NAO phase amplifies the precipitation in the early rainfall season in the year after an El Niño.

11.9.1.2 Indian Ocean

The Indian Ocean region refers to the area between 35°S to 17.5°N and 50°E to 100°E. The climate of the region is influenced primarily by the Asian monsoons (see Section 11.4.1 for processes influencing monsoons). During January, the ITCZ is located primarily in the SH. The region north of the ITCZ then experiences north-easterly trade winds (northeast monsoons) and the region to the south, the south-easterly trades. During northern summer, the ITCZ is located in the north and virtually covers the entire Bay of Bengal, the surrounding lands and the eastern Arabian Sea. The winds in the north turn into strong south-westerlies (southwest monsoons), while the south-easterlies persist in the south. Precipitation and wind stress bring about a response that is distinctly different in the northern and southern parts of the Indian Ocean (International CLIVAR Project Office, 2006). The wet (dry) season in the Maldives occurs during the southwest (northeast) monsoons. From May to October, the southeast trades dominate in the Seychelles and the climate is relatively cool and dry, and December to March is the principal wet season with winds mainly from west to northwest.

While the monsoons recur each year, their irregularity at a range of time scales from weeks to years depends on feedback from the ocean in ways that are not fully understood. Intra-seasonal variability is associated with the Monsoon Intra-Seasonal Oscillation (MISO) and the Madden-Julian Oscillation (MJO), which are long-lasting weather patterns that evolve in a systematic way for periods of four to eight weeks. On an interannual and decadal scale, statistical methods have shown that while there are periods of high correlation between ENSO and monsoon variation, there are decades where there appears to be little or no association (International CLIVAR Project Office, 2006; see also Section 10.3.5.4). A modulating factor is the Indian Ocean Dipole or Indian Ocean Zonal Mode (IOZM), a large interannual variation in zonal SST gradient (see Section 3.6). The magnitude of the secondary rainfall maximum from October to December in East Africa is strongly correlated with IOZM events, and the positive phase of IOZM, with higher SSTs in the west, counters the drying effect that ENSO has on monsoon rainfall (Ashok et al., 2001).

11.9.1.3 Pacific

The Pacific region refers to equatorial, tropical and subtropical region of the Pacific in which there is a high density of inhabited small islands. Broadly, it is the region between 20°N and 30°S and 120°E to 120°W. The major climatic processes that play a key role in the climate of this region are the easterly trade winds (both north and south of the equator), the SH high pressure belt, the ITCZ and the South Pacific Convergence Zone (SPCZ; see Vincent, 1994), which extends from the ITCZ near the equator due north of New Zealand south-eastward to at least 21°S, 130°W. The region has a warm, highly maritime climate and rainfall is abundant. The highest rainfall follows the seasonal migration of the ITCZ and SPCZ.

Year-to-year climatic variability in the region is very strongly affected by ENSO events. During El Niño conditions, rainfall increases in the zone northeast of the SPCZ (Vincent, 1994). Tropical cyclones are also a feature of the climate of the region, except within 10 degrees of the equator, and are associated with extreme rainfall, strong winds and storm surge. Many islands in the region are very low lying, but there are also many with strong topographical variations. In the case of the latter, orographic effects on rainfall amount and seasonal distribution can be strong.

11.9.2 Skill of Models in Simulating Present Climate

The ability of the MMD models to simulate present climate in the Caribbean, Indian Ocean and North and South Pacific Ocean is summarised in Supplementary Material Table S11.1. In general, the biases in about half of the temperature simulations are less than 1°C in all seasons, so that the model performances are, on the whole, satisfactory. There are, however, large spreads in precipitation simulations. During the last decade, steady progress has been made in simulating and predicting ENSO using coupled GCMs. However, serious systematic errors in both the simulated mean climate and the natural variability persist (see Section 8.4.7)

11.9.2.1 Caribbean

Simulations of the annual Caribbean temperature in the 20th century (1980–1999) by the MMD models give an average that agrees closely with climatology, differing by less than 0.1°C. The inter-quartile range difference between individual models and climatology ranged from –0.3°C to +0.3°C. Thus, the models have good skill in simulating annual temperature. The average of the MMD simulations of precipitation, however, underestimates the observed precipitation by approximately 30%. The deviations in individual models range from –64 to +20%, a much greater range than the deviations in temperature simulations. Recently the Parallel Climate Model (at T42 resolution – about 3.75 degrees), a fully coupled global climate model, was found to be capable of simulating the main climate features over the Caribbean region (Angeles et al., 2007), but it also underestimated the area average precipitation across the Caribbean. Martinez-Castro et al. (2006), in a sensitivity experiment, conclude that the Regional Climate Model (RegCM3), using the Anthes-Kuo cumulus parametrization scheme, can be used for long-term area-averaged climatology.

11.9.2.2 Indian Ocean

For annual temperature in the Indian Ocean in the 20th century (1980–1999), the mean value of the MMD outputs overestimated the climatology by 0.6°C, with 50% of deviations ranging from 0.2°C to 1.0°C. For rainfall, the multi-model ensemble average was only slightly below the mean precipitation by 3%, and the model deviations ranged from –22 to +20%. There are, however, problems with the simulation of

year-to-year variation. Many of the important climatic effects of the MJO, including its impacts on rainfall variability in the monsoons, are still poorly simulated by contemporary climate models (see Section 8.4).

11.9.2.3 Pacific

Climate model simulations of current-climate means of temperature and precipitation were investigated by Jones et al. (2000, 2002) and Lal et al. (2002) for the South Pacific. The AOGCMs available at the time of these studies simulated well the broad-scale patterns of temperature and precipitation across the region, with the precipitation patterns more variable than for temperature in the models considered, and with some significantly underestimating or overestimating of the intensity of rainfall in the high-rainfall zones. All models simulated a broad rainfall maximum stretching across the SPCZ and ITCZ, but not all models resolved a rainfall minimum between these two regions. A problem of simulating the spatial structure of the MJO resulting in tendencies for the convective anomaly to split into double ITCZs in the Pacific is also discussed in Section 8.4.8.

Analysis of the MMD simulations shows that the average model value overestimated the annual mean temperature from 1980 to 1999 by 0.9°C over a southern Pacific region, with 50% of the deviations varying from 0.6°C to 1.2°C. Over the North Pacific, the simulated ensemble average temperature for the same period was only 0.7°C above the climatology, with half of the model deviations from the climatology ranging from 0.2°C to 1.0°C. Average precipitation was overestimated by 10%, but individual model values varied from –7 to 31% in the southern Pacific region, whereas in the northern Pacific the mean model output for precipitation almost agreed with the climatology, while the individual models deviated from –13 to 13%. Thus, the models are better at simulating rainfall in the northern Pacific than in the southern Pacific and the quality of the simulations, both north and south, were not much different from those for the Indian Ocean.

11.9.3 Temperature and Precipitation Projections

Scenarios of temperature change and percentage precipitation change between 1980 to 1999 and 2080 to 2099 are summarised in Table 11.1 (described in Section 11.1.3). A small value of T implies a large signal-to-noise ratio and it can be seen that, in general, the signal-to-noise ratio is greater for temperature than for precipitation change. The probability of extreme warm seasons is 100% in all cases for the small islands and the scenarios of warming are all very significant by the end of the century. Approximate results for the A2 and B1 scenarios and for other future times in this century can be obtained by scaling the A1B values, as described in Section 11.1.3.

The temporal evolution of temperature as simulated by the MMD models for the 20th and 21st centuries is also shown in Figure 11.22 for oceanic regions including the Caribbean (CAR), Indian Ocean (IND), North Pacific Ocean (NPA) and South

Pacific Ocean (SPA). In general, it can be seen, by comparison with Box 11.1, Figure 1, that the temperature increases for the small islands are less than for the continental regions. The almost linear nature of the evolution is also apparent in the figure. Temperature and precipitation projections for the small island regions are discussed below in the context of Table 11.1.

11.9.3.1 Caribbean

The MMD-simulated annual temperature increases at the end of the 21st century range from 1.4°C to 3.2°C with a median of 2.0°C, somewhat below the global average. Fifty percent of the models give values differing from the median by only $\pm 0.4^\circ\text{C}$. Statistical downscaling of HadCM3 results using the A2 and B2 emission scenarios gives around a 2°C rise in temperature by the 2080s, approximately the same as the HadCM3 model. The agreement between the AOGCMs and the downscaling analysis gives a high level of confidence in the temperature simulations. The downscaling was performed with the use of the Statistical DownScaling Model (SDSM) developed by Wilby et al. (2002) as part of an Assessments of Impacts and Adaptations to Climate Change in Multiple Regions and Sectors (AIACC) Small Island States SIS06 project (<http://www.aiaccproject.org>). Angeles et al. (2007) also simulate an approximately 1°C rise in SST up to the 2050s using the IS92a scenario. There were no noticeable differences in monthly changes (see Supplementary Material Figure S11.31). Observations suggest that warming is ongoing (Peterson et al., 2002).

According to Table 11.1, most models project decreases in annual precipitation and a few increases, varying from -39 to $+11\%$, with a median of -12% . Figure 11.23 shows that the annual mean decrease is spread across the entire region. In DJF,

some areas of increases are noted and in JJA, the region-wide decrease is enhanced, especially in the region of the Greater Antilles, where the model consensus is also strong. Monthly changes in the Caribbean are shown in Supplementary Material Figure S11.32, which also shows that the simulations for the Caribbean have a greater spread compared to the other oceanic regions (IND, NPA and SPA in S11.32). Results from HadCM3 downscaled for the A2 and B2 emission scenarios using the SDSM also show a near-linear decrease in summer precipitation to the 2080s for a station in Jamaica. Downscaled results from the SDSM for stations in Barbados and Trinidad, however, show increases rather than decreases. Thus, there is consensus between the MMD results and the downscaled results for the Greater Antilles in JJA but not for the other islands, and also not on an annual basis. Angeles et al. (2007) also simulate decreases up to the middle of the century in the vicinity of the Greater Antilles but not in the other islands in the late rainfall season. Table 11.1 shows that the decrease in JJA has the largest signal-to-noise ratio. The decrease is in agreement with the expected drying in the subtropics discussed in Sections 9.5 and 11.1. In the multi-model analysis, most models show shift to a more positive phase of the NAO (see Section 10.3), and consensus on temperature changes in the Pacific indicates an El Niño-like pattern with higher temperatures in the eastern Pacific (see Section 10.3). These conditions are associated with drying in the Caribbean. Observed trends in precipitation are unclear. While Peterson et al. (2002) find no statistically significant trends in mean precipitation amounts from the 1950s to 2000, Neelin et al. (2006) note a modest but statistically significant summer drying trend over recent decades in the Caribbean in several observational data sets.

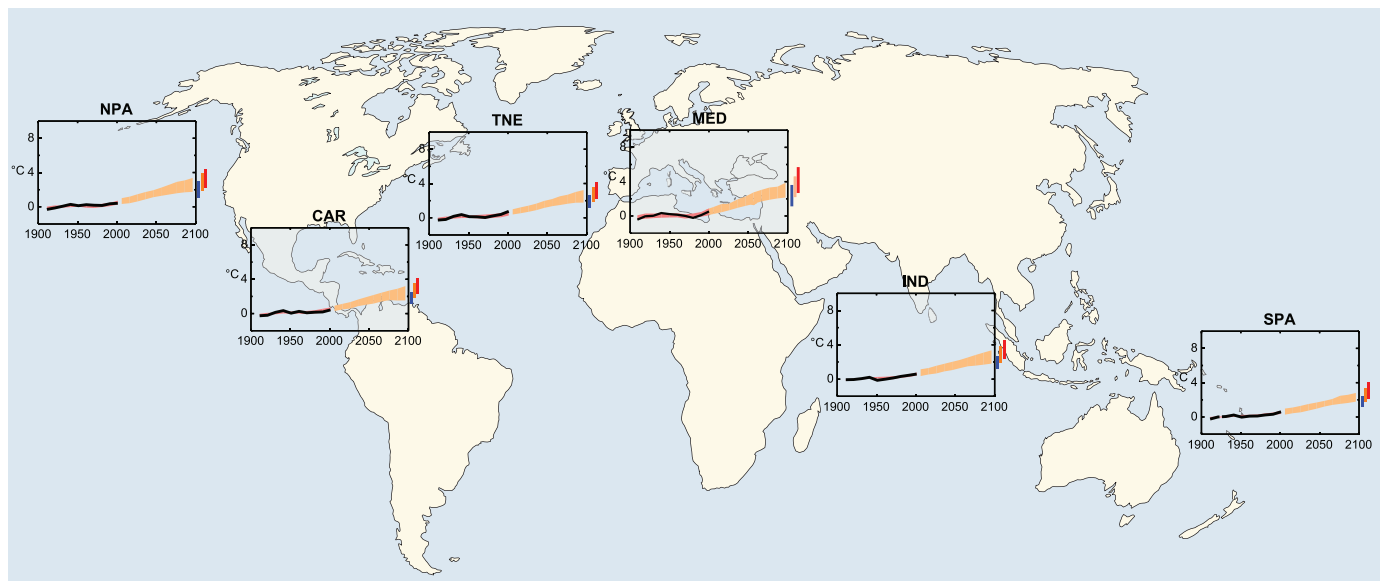


Figure 11.22. Temperature anomalies with respect to 1901 to 1950 for six oceanic regions for 1906 to 2005 (black line) and as simulated (red envelope) by MMD models incorporating known forcings; and as projected for 2001 to 2100 by MMD models for the A1B scenario (orange envelope). The bars at the end of the orange envelope represent the range of projected changes for 2091 to 2100 for the B1 scenario (blue), the A1B scenario (orange) and the A2 scenario (red). The black line is dashed where observations are present for less than 50% of the area in the decade concerned. More details on the construction of these figures are given in Box 11.1 and Section 11.1.2.

11.9.3.2 Indian Ocean

Based on the MMD ensemble mean the annual temperature is projected to increase by about 2.1°C, somewhat below the global average, with individual models ranging from 1.4°C to 3.7°C and at least half of the models giving values quite close to the mean. All models show temperature increases in all months with no significant seasonal variation (Supplementary Material Figure S11.31). Evidence of temperature increases from 1961 to 1990 in the Seychelles is provided by Easterling et al. (2003), who find that the percentage of time when the minimum temperature is below the 10th percentile is decreasing, and the percentage of time where the minimum temperature exceeds the 90th percentile is increasing. Similar results were obtained for the maximum temperatures. This is consistent with general patterns of warming elsewhere (see Chapter 3).

The annual precipitation changes projected by individual MMD models varied from -2 to 20% with a median of 4% and 50% of the models projecting changes between 3 and 5%. Thus, there is some level of confidence in the precipitation results although not as high as for temperature. Figure 11.24 shows that the annual increase is restricted mainly to the north Indian Ocean, where the model consensus is greatest, especially in the vicinity of the Maldives. In DJF, some increases are noted in the south. Model agreement on increases is greatest for the Seychelles in DJF and for the Maldives in JJA. There is also strong agreement on decreases in the vicinity of Mauritius in

JJA. Sections 10.3.5 and 11.4 discuss changes in monsoon behaviour in a warmer climate. There is an emerging consensus that the effect of enhanced moisture convergence in a warmer atmosphere will dominate over possible weaker monsoonal flows and tropical large-scale circulation in global warming simulations, resulting in increased monsoonal precipitation. Easterling et al. (2003) find evidence that extreme rainfall tended to increase from 1961 to 1990 (see also Section 11.4.3, South Asia projections).

11.9.3.3 Pacific

Projected regional temperature changes in the South Pacific from a range of AOGCMs have been prepared by Lal et al. (2002), Lal (2004) and Ruosteenoja et al. (2003). Jones et al. (2000, 2002) and Whetton and Suppiah (2003) also consider patterns of change. Broadly, simulated warming in the South Pacific closely follows the global average warming rate. However, there is a tendency in many models for the warming to be a little stronger in the central equatorial Pacific (North Polynesia) and a little weaker to the south (South Polynesia).

The MMD-A1B projections for the period 2080 to 2099 show an increase in annual temperature of 1.8°C, somewhat below the global average over the South Pacific (Table 11.1). The individual model values vary from 1.4°C to 3.1°C and at least half of the models project values very close to the mean. All models show increases, slightly less in the second half of

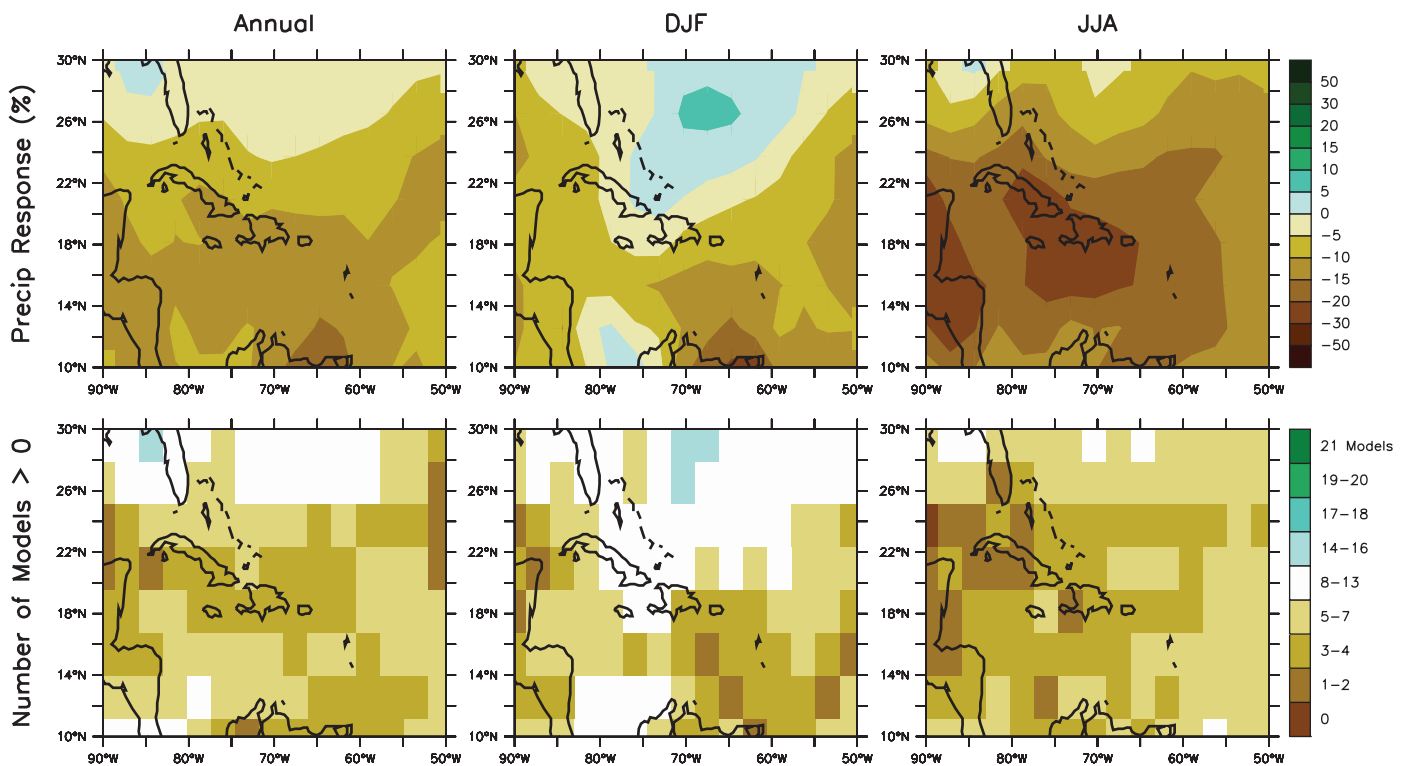


Figure 11.23. Precipitation changes over the Caribbean from the MMD-A1B simulations. Top row: Annual mean, DJF and JJA fractional precipitation change between 1980 to 1999 and 2080 to 2099, averaged over 21 models. Bottom row: number of models out of 21 that project increases in precipitation.

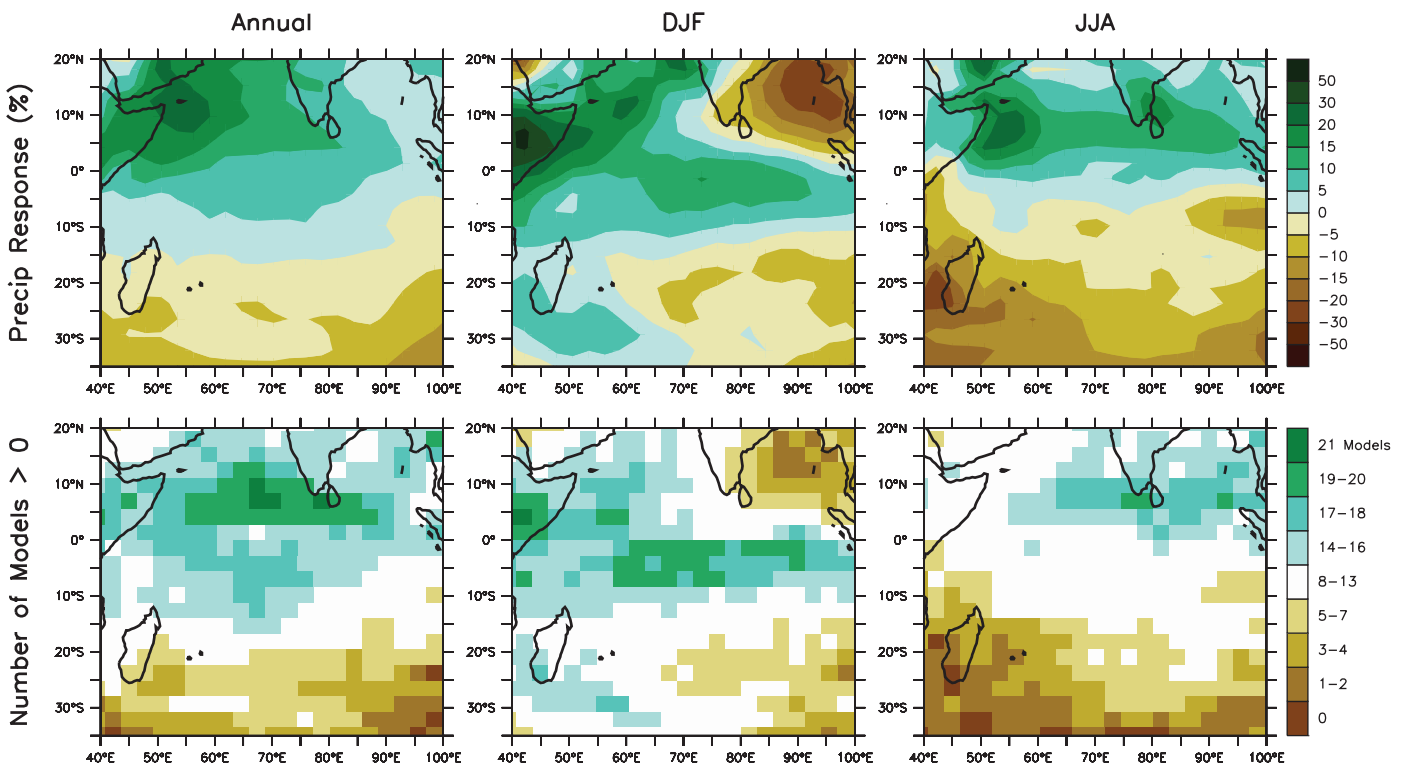


Figure 11.24. As for Figure 11.23 but for the Indian Ocean.

the year compared to the first (Supplementary Material Figure S11.31). Over the North Pacific, the models simulate an increase in temperature of 2.3°C, slightly below the global average, with values ranging from 1.5°C to 3.7°C and 50% of the models within $\pm 0.4^\circ\text{C}$ of the mean. All models show increases, more in the second half of the year compared to the first (Supplementary Material Figure S11.31).

For the same period, 2080 to 2099, annual precipitation increases over the southern Pacific when averaged over all MMD models are close to 3%, with individual models projecting values from -4 to $+11\%$ and 50% of the models showing increases between 3 and 6%. The time to reach a discernible signal is relatively short. (Table 11.1). Most of these increases were in the first half of the year (Supplementary Material Figure S11.32). For precipitation in the northern Pacific, an increase of 5% is found, with individual models projecting values from 0 to 19% and at least half of the models within -2 to $+5\%$ of the median. The time to reach a discernible signal is relatively long. Most of these increases were in the latter half of the year (Supplementary Material Figure S11.32). Figure 11.25 illustrates the spatial distribution of annual, DJF and JJA rainfall changes and inter-model consistency. The figure shows that the tendency for precipitation increase in the Pacific is strongest in the region of the ITCZ due to increased moisture transport described in Section 11.1.3.1. Griffiths et al. (2003) find an increasing trend from 1961 to 2000 in mean rainfall in and northeast of the SPCZ in the southern Pacific. As for the Indian Ocean, there is some level of confidence in the

precipitation results for the Pacific, but not as high as for the temperature results.

Changes in rainfall variability in the South Pacific were analysed by Jones et al. (2000) using IPCC (1996) scenarios, but more recent simulations have not been examined. These changes will be strongly driven by changes in ENSO, and this is not well understood (see Section 10.3).

11.9.4 Sea Level Rise

Sea level is projected to rise between the present (1980–1999) and the end of this century (2090–2099) by 0.35 m (0.23 to 0.47 m) for the A1B scenario (see Section 10.6). Due to ocean density and circulation changes, the distribution will not be uniform and Figure 10.32 shows a distribution of local sea level change based on ensemble mean of 14 AOGCMs. A lower-than-average rise in the Southern Ocean can be seen, possibly due to increased wind stress. Also obvious is a narrow band of pronounced sea level rise stretching across the southern Atlantic and Indian Oceans at about 40°S. This is also seen in the southern Pacific at about 30°S. However, large deviations among models make estimates of distribution across the Caribbean, Indian and Pacific Oceans uncertain. Extreme sea level changes, including storm surges, are discussed in Box 11.5 in a broader context. The range of uncertainty cannot be reliably quantified due to the limited set of models addressing the problem.

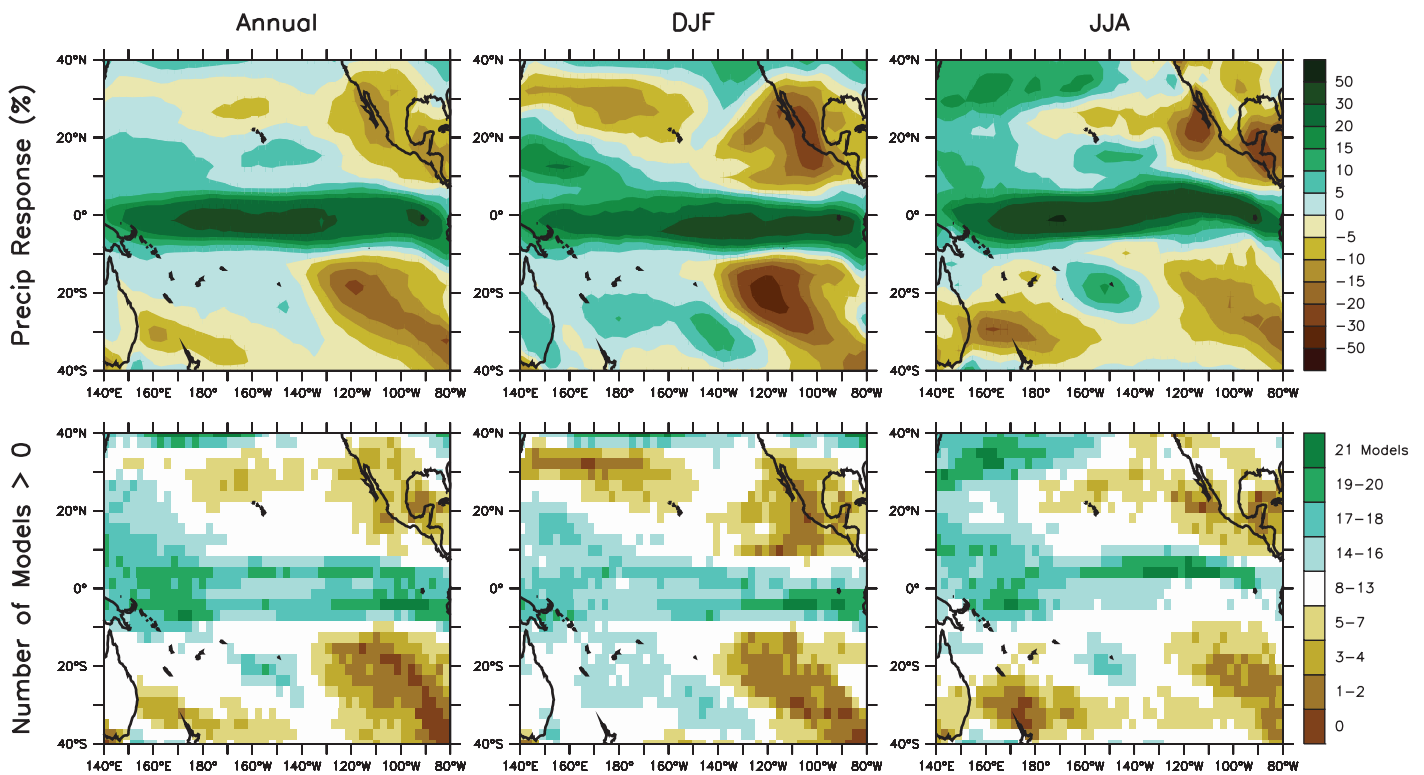


Figure 11.25. As for Figure 11.23 but for the northern and southern Pacific Ocean.

Global sea level rise over the 20th century is discussed in Section 5.5; the best estimate is 0.17 ± 0.05 m. From estimates of observed sea level rise from 1950 to 2000 by Church et al. (2004), the rise in the Caribbean appeared to be near the global mean. Church et al. (2006) also estimate the average rise in the region of the Indian and Pacific Ocean to be close to the global average. There have been large observed variations in sea level rise in the Pacific Ocean mainly due to ocean circulation changes associated with ENSO events. From 1993 to 2001, all the data show large rates of sea level rise over the western Pacific and eastern Indian Ocean and sea level falls in the eastern Pacific and western Indian Ocean (Church et al., 2006). Observed sea level rise in the Pacific and Indian Oceans is discussed in Chapter 5.

11.9.5 Tropical Cyclones

Fewer models have simulated tropical cyclones in the context of climate change than those simulating temperature and precipitation changes and sea level rise, mainly because of the computational burden associated with the high resolution needed to capture the characteristics of tropical cyclones. Accordingly, there is less certainty about the changes in frequency and intensity of tropical cyclones on a regional basis than for temperature and precipitation changes. An assessment of results for projected changes in tropical cyclones is presented in Section 10.3.6.3, and a synthesis is given at the end of the section. Regional model-based studies of changes in tropical cyclone behaviour in the southwest Pacific include works by Nguyen and Walsh (2001) and Walsh (2004). Walsh concludes that in general there is no clear picture with respect to regional changes in frequency and movement, but increases in intensity are indicated. It should also be noted that ENSO fluctuations have a strong impact on patterns of tropical cyclone occurrence in the southern Pacific, and that therefore uncertainty with respect to future ENSO behaviour (see Section 10.3) contributes to uncertainty with respect to tropical cyclone behaviour (Walsh, 2004).

Box 11.5: Coastal Zone Climate Change

Introduction

Climate change has the potential to interact with the coastal zone in a number of ways including inundation, erosion and salt water intrusion into the water table. Inundation and intrusion will clearly be affected by the relatively slow increases in mean sea level over the next century and beyond. Mean sea level is addressed in Chapter 10; this box concentrates on changes in extreme sea level that have the potential to significantly affect the coastal zone. There is insufficient information on changes in waves or near-coastal currents to provide an assessment of the effects of climate change on erosion.

The characteristics of extreme sea level events are dependent on the atmospheric storm intensity and movement and coastal geometry. In many locations, the risk of extreme sea levels is poorly defined under current climate conditions because of sparse tide gauge networks and relatively short temporal records. This gives a poor baseline for assessing future changes and detecting changes in observed records. Using results from 141 sites worldwide for the last four decades, Woodworth and Blackman (2004) find that at some locations extreme sea levels have increased and that the relative contribution from changes in mean sea level and atmospheric storminess depends on location.

Methods of simulating extreme sea levels

Climate-driven changes in extreme sea level will come about because of the increases in mean sea level and changes in the track, frequency or intensity of atmospheric storms. (From the perspective of coastal flooding, the vertical movement of land, for instance due to post glacial rebound, is also important when considering the contribution from mean sea level change.) To provide the large-scale context for these changes, global climate models are required, although their resolution (typically 150 to 300 km horizontally) is too coarse to represent the details of tropical cyclones or even the extreme winds associated with mid-latitude cyclones. However, some studies have used global climate model forcing to drive storm surge models in order to provide estimates of changes in extreme sea level (e.g., Flather and Williams, 2000). To obtain more realistic simulations from the large-scale drivers, three approaches are used: dynamical and statistical downscaling and a stochastic method (see Section 11.10 for general details).

As few RCMs currently have an ocean component, these are used to provide high-resolution (typically 25 to 50 km horizontally) surface winds and pressure to drive a storm surge model (e.g., Lowe et al., 2001). This sequence of one-way coupled models is usually carried out for a present-day (Debenard et al., 2003) or historical baseline (e.g., Flather et al., 1998) and a period in the future (e.g., Lowe et al., 2001; Debenard et al., 2003). In the statistical approach, relationships between large-scale synoptic conditions and local extreme sea levels are constructed. These relationships can be developed either by using analyses from weather prediction models and observed extreme sea levels, or by using global climate models and present-day simulations of extreme water level generated using the dynamic methods described above. Simulations of future extreme sea level are then derived from applying the statistical relationships to the future large-scale atmospheric synoptic conditions simulated by a global climate model (e.g., von Storch and Reichardt, 1997). The statistical and dynamical approach can be combined, using a statistical model to produce the high-resolution wind fields forcing the wave and storm surge dynamical models (Lionello et al., 2003). Similarly, the stochastic sampling method identifies the key characteristics of synoptic weather events responsible for extreme sea levels (intensity and movement) and represents these by frequency distributions. For each event, simple models are used to generate the surface wind and pressure fields and these are applied to the storm surge model (e.g., Hubbert and McInnes, 1999). Modifications to the frequency distributions of the weather events to represent changes under enhanced greenhouse conditions are derived from global climate models and then used to infer a future storm surge climatology.

Extreme sea level changes – sample projections from three regions

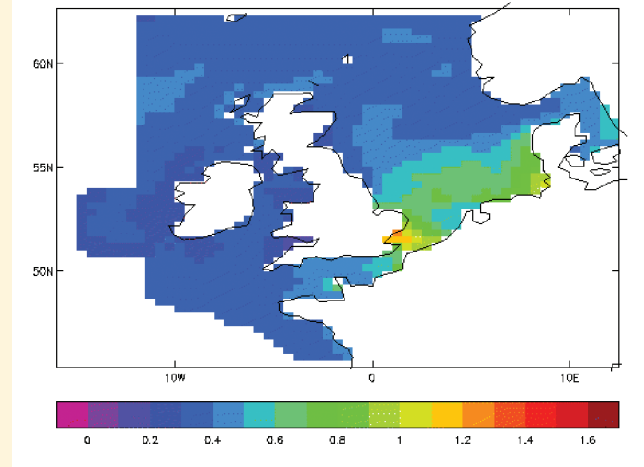
1. Australia

In a study of storm surge impacts in northern Australia, a region with only a few short sea level records, McInnes et al. (2005) used stochastic sampling and dynamical modelling to investigate the implications of climate change on extreme storm surges and inundation. Cyclones occurring in the Cairns region from 1907 to 1997 were used to develop probability distribution functions governing the cyclone characteristics of speed and direction with an extreme value distribution fitted to the cyclone intensity. Cyclone intensity distribution was then modified for enhanced greenhouse conditions based on Walsh and Ryan (2000), in which cyclones off northeast Australia were found to increase in intensity by about 10%. No changes were imposed upon cyclone frequency or direction since no reliable information is available on the future behaviour of the main influences on these, respectively ENSO or mid-level winds. Analysis of the surges resulting from 1,000 randomly selected cyclones with current and future intensities shows that the increased intensity leads to an increase in the height of the 1-in-100 year event from 2.6 m to 2.9 m with the 1-in-100 year event becoming the 1-in-70 year event. This also results in the areal extent of inundation more than doubling (from approximately 32 to 71 km²). Similar increases for Cairns and other coastal locations were found by Hardy et al. (2004). *(continued)*

2. Europe

Several dynamically downscaled projections of climate-driven changes in extreme water levels in the European shelf region have been carried out. Woth (2005) explored the effect of two different GCMs and their projected climate changes due to two different emissions scenarios (SRES A2 and B2) on storm surges along the North Sea coast. She used data from one RCM downscaling the four GCM simulations (Woth et al., 2006) (using data from four RCMs driven by one GCM produced indistinguishable results) and demonstrates significant increases in the top 1% of events (10 to 20 cm above average sea level change) over the continental European North Sea coast. The changes projected by the different experiments were statistically indistinguishable, although those from the models incorporating the A2 emissions scenario were consistently larger. When including the effects of global mean sea level rise and vertical land movements, Lowe and Gregory (2005) find that increases in extreme sea level are projected for the entire UK coastline, using a storm surge model driven by one of the RCMs analysed by Woth et al. (2006) (Box 11.5, Figure 1). Using a Baltic Sea model driven by data from four RCM simulations, Meier (2006) finds that the changes in storm surges vary strongly between the simulations but with some tendency for larger increases in the 100-year surges than in the mean sea level.

Lionello et al. (2003) estimate the effect of atmospheric CO₂ doubling on the frequency and intensity of high wind waves and storm surge events in the Adriatic Sea. The regional surface wind fields were derived from the sea level pressure field in a 30-year long ECHAM4 high-resolution (about 1.5 degrees) time slice experiment by statistical downscaling and then used to force a wave and an ocean model. They find no statistically significant changes in the extreme surge level and a decrease in the extreme wave height with increased atmospheric CO₂. An underestimation of the observed wave heights and surge levels calls for caution in the interpretation of these results. Using AOGCM projections, X.L. Wang et al. (2004) infer an increase in winter and autumn seasonal mean and extreme wave heights in the northeast and southwest North Atlantic, but a decrease in the mid-latitudes of the North Atlantic. Not all changes were significant and in some regions (e.g., the North Sea), their sign was found to depend on the emissions scenario.



Box 11.5, Figure 1. The change with respect to 1961-1990 in the 50-year return period extreme water level (m) in the North Sea due to changes in atmospheric storminess, mean sea level and vertical land movements for the period 2071 to 2100 under the A2 scenario (from Lowe and Gregory, 2005).

3. Bay of Bengal

Several dynamic simulations of storm surges have been carried out for the region but these have often involved using results from a small set of historical storms with simple adjustments (such as adding on a mean sea level or increasing wind speeds by 10%) to account for future climate change (e.g., Flather and Khandker, 1993). This technique has the disadvantage that by taking a relatively small and potentially biased set of storms it may lead to a biased distribution of water levels with an unrealistic count of extreme events. In one study using dynamical models driven by RCM simulations of current and future climates, Unnikrishnan et al. (2006) show that despite no significant change in the frequency of cyclones there are large increases in the frequency of the highest storm surges.

Uncertainty

Changes in storm surges and wave heights have been addressed for only a limited set of models. Thus, we cannot reliably quantify the range of uncertainty in estimates of future coastal flooding and can only make crude estimates of the minimum values (Lowe and Gregory, 2005). There is some evidence that the dynamical downscaling step in providing data for storm surge modelling is robust (i.e., does not add to the uncertainty). However, the general low level of confidence in projected circulation changes from AOGCMs implies a substantial uncertainty in these projections.

11.10 Assessment of Regional Climate Projection Methods

The assessment of methods recognises the challenges posed by the complex interactions that occur at many spatial and temporal scales, involving the general circulation, cross-scale feedbacks and regional-scale forcing.

11.10.1 Methods for Generating Regional Climate Information

Atmosphere-Ocean General Circulation Models constitute the primary tool for capturing the global climate system behaviour. They are used to investigate the processes responsible for maintaining the general circulation and its natural and forced variability (Chapter 8), to assess the role of various forcing factors in observed climate change (Chapter 9) and to provide projections of the response of the system to scenarios of future external forcing (Chapter 10). As AOGCMs seek to represent the whole climate system, clearly they provide information on regional climate and climate change and relevant processes directly. For example, the skill in simulating the climate of the last century when accounting for all known forcings demonstrates the causes of recent climate change (Chapter 9) and this information can be used to constrain the likelihood of future regional climate change (Stott et al., 2006; see also Section 11.10.2). AOGCM projections provide plausible future regional climate scenarios, although methods to establish the reliability of the regional AOGCM scales have yet to mature. The spread within an ensemble of AOGCMs is often used to characterise the uncertainty in projected future climate changes. Some regional responses are consistent across AOGCM simulations, although for other regions the spread remains large (see Sections 11.2 to 11.9).

Because of their significant complexity and the need to provide multi-century integrations, horizontal resolutions of the atmospheric components of the AOGCMs in the MMD range from 400 to 125 km. Generating information below the grid scale of AOGCMs is referred to as downscaling. There are two main approaches, dynamical and statistical. Dynamical downscaling uses high-resolution climate models to represent global or regional sub-domains, and uses either observed or lower-resolution AOGCM data as their boundary conditions. Dynamical downscaling has the potential for capturing mesoscale nonlinear effects and providing coherent information among multiple climate variables. These models are formulated using physical principles and they can credibly reproduce a broad range of climates around the world, which increases confidence in their ability to downscale realistically future climates. The main drawbacks of dynamical models are their computational cost and that in future climates the parametrization schemes they use to represent sub-grid scale processes may be operating outside the range for which they were designed.

Empirical SD methods use cross-scale relationships that have been derived from observed data, and apply these to climate model data. Statistical downscaling methods have the advantage of being computationally inexpensive, able to access finer scales than dynamical methods and applicable to parameters that cannot be directly obtained from the RCM outputs. They require observational data at the desired scale for a long enough period to allow the method to be well trained and validated. The main drawbacks of SD methods are that they assume that the derived cross-scale relationships remain stable when the climate is perturbed, they cannot effectively accommodate regional feedbacks and, in some methods, can lack coherency among multiple climate variables.

11.10.1.1 High-Resolution Atmosphere-Only GCMs

Atmosphere-only GCMs (AGCMs) include interactive land surface schemes as in an AOGCM but require information on SST and sea ice as a lower boundary condition. Given the short time scales associated with the atmosphere and land surface components compared to those in the ocean, relatively short time slices (a few decades) can be run at high resolution. The SST and sea ice information required can be derived from observations or AOGCMs. The use of observations can improve simulations of current climate but combining these with AOGCM-derived changes for the future climate (e.g., Rowell, 2005) increases the risk of inconsistency in the projected climate. The absence of two-way feedback between the atmosphere and ocean in AGCMs can cause a significant distortion of the climatic variability (Bretherton and Battisti, 2000), as documented over regions such as the Indian Ocean and the South Asian monsoon (Douville, 2005; Inatsu and Kimoto, 2005). The large-scale climate responses of AGCMs and AOGCMs appear to be similar in many regions; when and where they differ, the consistency of the oceanic surface boundary condition may be questioned (May and Roeckner, 2001; Govindasamy et al., 2003). Further research is required to determine if the similarity is sufficient for the time-slice approach with AGCMs to be considered a robust downscaling technique.

Model grids of 100 km and finer have become feasible and 50 km will likely be the norm in the near future (Bengtsson, 1996; May and Roeckner, 2001; Déqué and Gibelin, 2002; Govindaswamy, 2003). High-performance computer systems now allow global computations at 20 km (e.g., May, 2004a; Mizuta et al., 2006), although for short time slices only. Evaluated on the scale typical of current AOGCMs, nearly all quantities simulated by high-resolution AGCMs agree better with observations, but the improvements vary significantly for different regions (Duffy et al., 2003) and specific variables, and extensive recalibration of parametrizations is often required. Notable improvements occur in orographic precipitation and dynamics of mid-latitude weather systems (see Chapter 10). The highest resolution offers the prospect of credible simulations of the climatology of tropical cyclones (e.g., May, 2004a; Mizuta et al., 2006). Coordinated multi-model experiments are needed,

however, to optimise the value of these high-resolution studies for general assessment.

An alternative to uniform high-resolution AGCMs is Variable-Resolution AGCMs (VRGCMs; e.g., Déqué and Piedelievre, 1995; Krinner et al., 1997; Fox-Rabinovitz et al., 2001; McGregor et al., 2002; GIBELIN and Déqué, 2003). The VRGCM approach is attractive as it permits, within a unified modelling framework, a regional increase in resolution while retaining the interaction of all regions of the atmosphere. Numerical artefacts due to stretching have been shown to be small when using modest stretching factors (e.g., Lorant and Royer, 2001). The results from VRGCMs capture, over the high-resolution region, finer-scale details than uniform-resolution models while retaining global skill similar to uniform-resolution simulations with the same number of grid points.

11.10.1.2 *Nested Regional Climate Models*

The principle behind nested modelling is that, consistent with the large-scale atmospheric circulation, realistic regional climate information can be generated by integrating an RCM if the following premises are satisfied: time-varying large-scale atmospheric fields (winds, temperature and moisture) are supplied as lateral boundary conditions (LBCs) and SST and sea ice as lower boundary conditions; the control from the LBCs keeps the interior solution of the RCM consistent with the driving atmospheric circulation; and sub-grid scale physical processes are suitably parametrized, including fine-scale surface forcing such as orography, land-sea contrast and land use.

A typical RCM grid for climate change projections is around 50 km, although some climate simulations have been performed using grids of 15 or 20 km (e.g., Leung et al., 2003, 2004; Christensen and Christensen, 2004; Kleinn et al., 2005). Recently, projections of climate changes for East Asia were completed with a 5-km non-hydrostatic RCM (Kanada et al., 2005; Yoshizaki et al., 2005; Yasunaga et al., 2006), but only for short simulations. Following the trend in global modelling, RCMs are increasingly coupled interactively with other components of the climate system, such as regional ocean and sea ice (e.g., Bailey and Lynch 2000; Döscher et al., 2002; Rinke et al., 2003; Bailey et al., 2004; Meier et al., 2004; Sasaki et al., 2006a), hydrology, and with interactive vegetation (Gao and Yu, 1998; Xue et al., 2000).

Multi-decadal RCM experiments are becoming standard (e.g., Whetton et al., 2000; Kwon et al., 2003; Leung et al., 2004; Kjellström et al., 2007; Plummer et al., 2006), including the use of ensembles (Christensen et al., 2002), enabling a more thorough validation and exploration of projected changes. In multi-year ensemble simulations driven by reanalyses of atmospheric observations, Vidale et al. (2003) show that RCMs have skill in reproducing interannual variability in precipitation and surface air temperature. The use of ensemble simulations has enabled quantitative estimates regarding the sources of uncertainty in projections of regional climate changes (Rowell, 2005; Déqué et al., 2005, 2007; Beniston et al., 2007; Frei et al.,

2006; Graham et al., 2007). Combining information from four RCM simulations, Christensen et al. (2001) and Rummukainen et al. (2003) demonstrate that it is feasible to explore not only uncertainties related to projections in the mean climate state, but also for higher-order statistics.

The difficulties associated with the implementation of LBCs in nested models are well documented (e.g., Davies, 1976; Warner et al., 1997). As time progresses in a climate simulation, the RCM solution gradually turns from an initial-value problem more into a boundary value problem. The mathematical interpretation is that nested models represent a fundamentally ill-posed boundary value problem (Staniforth, 1997; Laprise, 2003). The control exerted by LBCs on the internal solution generated by RCMs appears to vary with the size of the computational domain (e.g., Rinke and Dethloff, 2000), as well as location and season (e.g., Caya and Biner, 2004). In some applications, the flow developing within the RCM domain may become inconsistent with the driving LBC. This may (Jones et al., 1997) or may not (Caya and Biner, 2004) affect climate statistics. Normally, RCMs are only driven by LBCs with high time resolution to capture the temporal variations of large-scale flow. Some RCMs also use nudging or relaxation of large scales in the interior of the domain (e.g., Kida et al., 1991; Biner et al., 2000; von Storch et al., 2000). This has proved useful to minimise the distortion of the large scales in RCMs (von Storch et al., 2000; Mabuchi et al., 2002; Miguez-Macho et al., 2004), although it can also hide model biases. One-way RCM-GCM coupling is mostly used, although recently a two-way nested RCM has been developed (Lorenz and Jacob, 2005) thus achieving interaction with the global atmosphere as with variable-resolution AGCMs.

The ability of RCMs to simulate the regional climate depends strongly on the realism of the large-scale circulation that is provided by the LBCs (e.g., Pan et al., 2001). Latif et al. (2001) and Davey et al. (2002) show that strong biases in the tropical climatology of AOGCMs can negatively affect downscaling studies for several regions of the world. Nonetheless, the reliability of nested models, that is, their ability to generate meaningful fine-scale structures that are absent in the LBCs, is clear. A number of studies have shown that the climate statistics of atmospheric small scales can be re-created with the right amplitude and spatial distribution, even if these small scales are absent in the LBCs (Denis et al., 2002, 2003; Antic et al., 2005; Dimitrijevic and Laprise, 2005). This implies that RCMs can add value at small scales to climate statistics when driven by AOGCMs with accurate large scales. Overall, the skill at simulating current climate has improved with the MMD AOGCMs (Chapter 8), which will lead to higher quality LBCs for RCMs.

11.10.1.3 *Empirical and Statistical Downscaling Methods*

A complementary technique to RCMs is to use derived relationships linking large-scale atmospheric variables (predictors) and local/regional climate variables (predictands).

The local/regional-scale climate change information is then obtained by applying the relationships to equivalent predictors from AOGCM simulations. The guidance document (Wilby et al., 2004) from the IPCC Task Group on Data and Scenario Support for Impact and Climate Analysis (TGICA) provides a comprehensive background on this approach and covers important issues in using SD applications. Statistical downscaling methods cover regression-type models including both linear and nonlinear relationships, unconditional or conditional weather generators for generating synthetic sequences of local variables, techniques based on weather classification that draw on the more skilful attributes of models to simulate circulation patterns, and analogue methods that seek equivalent weather states from the historical record; a combination of these techniques possibly being most appropriate. An extension to SD is the statistical-dynamical downscaling technique (e.g., Fuentes and Heimann, 2000), which combines weather classification with RCM simulations. A further development is the application of SD to high-resolution climate model output (Lionello et al., 2003; Imbert and Benestad, 2005).

Research on SD has shown an extensive growth in application, and includes an increased availability of generic tools for the impact community (e.g., SDSM, Wilby et al., 2002; the clim.pact package, Benestad, 2004b; the pyclimate package, Fernández and Sáenz, 2003); applications in new regions (e.g., Asia, Chen and Chen, 2003); the use of techniques to address exotic variables such as phenological series (Matulla et al., 2003), extreme heat-related mortality (Hayhoe et al., 2004), ski season (Scott et al., 2003), land use (Solecki and Oliveri, 2004), streamflow or aquatic ecosystems (Cannon and Whitfield, 2002; Blenckner and Chen, 2003); the treatment of climate extremes (e.g., Katz et al., 2002; Seem, 2004; X.L. Wang et al., 2004; Cairns et al., 2006); intercomparison studies evaluating methods (e.g., STATistical and Regional dynamical Downscaling of EXtremes for European regions (STARDEX), Haylock et al., 2006; Schmidli et al., 2006); application to multi-model and multi-ensemble simulations in order to express model uncertainty alongside other key uncertainties (e.g., Benestad, 2002a,b; Hewitson and Crane, 2006; Wang and Swail, 2006b); assessing non-stationarity in climate relationships (Hewitson and Crane, 2006); and spatial interpolation using geographical dependencies (Benestad, 2005). In some cases SD methods have been used to project statistical attributes instead of raw values of the predictand, for example, the probability of rainfall occurrence, precipitation, wind or wave height distribution parameters and extreme event frequency (e.g., Beckmann and Buishand, 2002; Buishand et al., 2004; Busuioc and von Storch, 2003; Abaurrea and Asin, 2005; Diaz-Nieto and Wilby, 2005; Pryor et al., 2005a,b; Wang and Swail, 2006a,b).

Evaluation of SD is done most commonly through cross-validation with observational data for a period that represents an independent or different 'climate regime' (e.g., Busuioc et al. 2001; Trigo and Palutikof, 2001; Bartman et al., 2003; Hanssen-Bauer et al., 2003). Stationarity, that is, whether the statistical relationships are valid under future climate regimes, remains a

concern with SD methods. This is only weakly assessed through cross-validation tests because future changes in climate are likely to be substantially larger than observed historical changes. This issue was assessed in Hewitson and Crane (2006) where, within the SD method used, the non-stationarity was shown to result in an underestimation of the magnitude of the change. In general, the most effective SD methods are those that combine elements of deterministic transfer functions and stochastic components (e.g., Hansen and Mavromatis, 2001; Palutikof et al., 2002; Beersma and Buishand, 2003; Busuioc and von Storch, 2003; Katz et al., 2003; Lionello et al., 2003; Wilby et al., 2003; X.L. Wang et al., 2004; Hewitson and Crane, 2006). Regarding the predictors, the best choice appears to combine dynamical and moisture variables, especially in cases where precipitation is the predictand (e.g., Wilby et al., 2003).

Pattern scaling is a simple statistical method for projecting regional climate change, which involves normalising AOGCM response patterns according to the global mean temperature. These normalised patterns are then rescaled using global mean temperature responses estimated for different emissions scenarios from a simple climate model (see Chapter 10). Some developments were made using various versions of scaling techniques (e.g., Christensen et al., 2001; Mitchell, 2003; Salathé, 2005; Ruosteenoja et al., 2007). For example, Ruosteenoja et al. (2007) developed a pattern-scaling method using linear regression to represent the relationship between the local AOGCM-simulated temperature and precipitation response and the global mean temperature change. Another simple statistical technique is to use the GCM output for the variable of interest (i.e., the predictand) as the predictor and then apply a simple local change factor/scaling procedure (e.g., Chapter 13 of IPCC, 2001; Hanssen-Bauer et al., 2003; Widmann et al., 2003; Diaz-Nieto and Wilby, 2005).

Many studies have been performed since the TAR comparing various SD methods. In general, conclusions about one method compared to another are dependent on region and the criteria used for comparison, and on the inherent attributes of each method. For example, Diaz-Nieto and Wilby (2005) downscale river flow and find that while two methods give comparable results, they differ in responses as a function of how the methods treat multi-decadal variability.

When comparing the merits of SD methods based on daily and monthly downscaling models, in terms of their ability to predict monthly means, daily models are better (e.g., Buishand et al., 2004). In terms of nonlinearity in downscaling relationships, Trigo and Palutikof (2001) note that complex nonlinear models may not be better than simpler linear/slightly nonlinear approaches for some applications. However, Haylock et al. (2006) find that SD methods based on nonlinear artificial neural networks are best at modelling the interannual variability of heavy precipitation but they underestimate extremes. Much downscaling work remains unreported, as SD activities are often implemented pragmatically for serving specific project needs, rather than for use by a broader scientific community; this is especially the case in developing nations. In some cases, this

work is only found within the “grey” literature, for example, the AIACC project (<http://www.aiaccproject.org/>), which supports impact studies in developing nations.

11.10.1.4 Intercomparison of Downscaling Methods

At the time of the TAR, SD methods were viewed as a complementary technique to RCMs for downscaling regional climate, each approach having distinctive strengths and weaknesses. The conclusion of the TAR that SD methods and RCMs are comparable for simulating current climate still holds.

Since the TAR, a few additional studies have systematically compared the SD and RCM approaches (e.g., Huth et al., 2001; Hanssen-Bauer et al., 2003, 2005; Wood et al., 2004; Busuioc et al., 2006; Haylock et al., 2006; Schmidli et al., 2006). These related mainly to the similarity of the climate change signal (e.g., Hanssen-Bauer et al., 2003). A more complex study considered additional information about the RCM skill in simulating the current regional climate features and reproducing the connection between large- and regional-scale patterns used for fitting the SD method (Busuioc et al., 2006). Other studies following the STARDEX project (e.g., Haylock et al., 2006; Schmidli et al., 2006) compared the two approaches in terms of their skill in reproducing current climate features, as well as in terms of the climate change signal derived from their outputs, focusing on climate extremes and complex topography processes over Europe.

11.10.2 Quantifying Uncertainties

11.10.2.1 Sources of Regional Uncertainty

Most sources of uncertainty at regional scales are similar to those at the global scale (Section 10.5 and Box 10.2), but there are both changes in emphasis and new issues that arise in the regional context. Spatial inhomogeneity of both land use and land cover change (De Fries et al., 2002; Chapter 2, Section 7.2 and Box 11.4) and aerosol forcing adds to regional uncertainty. When analysing studies involving models to add local detail, the full cascade of uncertainty through the chain of models has to be considered. The degree to which these uncertainties influence the regional projections of different climate variables is not uniform. An indication of this is, for example, that models agree more readily on the sign and magnitude of temperature changes than of precipitation changes.

The regional impact of these uncertainties in climate projections has been illustrated by several authors. For example, incorporating a model of the carbon cycle into a coupled AOGCM gave a dramatically enhanced response to climate change over the Amazon Basin (Cox et al., 2000; Jones et al., 2003) and Borneo (Kumagi et al., 2004). Further, the scale of the resolved processes in a climate model can significantly affect its simulation of climate over large regional scales (Pope and Stratton, 2002; Lorenz and Jacob, 2005). Frei et al. (2003) show that models with the same representation of resolved

processes but different representations of sub-grid scale processes can represent the climate differently. The regional impact of changes in the representation of the land surface feedback is demonstrated by, for example, Oleson et al. (2004) and Feddema et al. (2005) (see also Box 11.4).

Evaluation of uncertainties at regional and local scales is complicated by the smaller ratio of the signal to the internal variability, especially for precipitation, which makes the detection of a response more difficult. In addition, the climate may itself be poorly known on regional scales in many data-sparse regions. Thus, evaluation of model performance as a component of an analysis of uncertainty can itself be problematic.

11.10.2.2 Characterising and Quantifying Regional Uncertainty

11.10.2.2.1 Review of regional uncertainty portrayed in the TAR

In the TAR, uncertainties in regional climate projections were discussed, but methods for quantifying them were relatively primitive. For example, in the TAR chapter on regional projections (Giorgi et al., 2001a), uncertainties in regional projections of climate change (e.g., large or small increases/decreases in precipitation) from different GCMs were qualitatively portrayed based only on simple agreement heuristics (e.g., seven of the nine models showed increases). Early examples of quantitative estimates of regional uncertainty include portraying the median and inter-model range of a variable (e.g., temperature) across a series of model projections and attaching probabilities to a group of scenarios on a regional scale (Jones, 2000; New and Hulme, 2000).

11.10.2.2.2 Using multi-model ensembles

A number of studies have taken advantage of multi-model ensembles formed by GCMs that have been driven by the same forcing scenarios to generate quantitative measures of uncertainty, particularly probabilistic information at a regional scale. Table 11.3 summarises aspects of the methods reviewed in this section and in Section 11.10.2.2.3. The results highlighted in Section 10.5 and Box 10.2 on climate sensitivity demonstrate that multi-model ensembles explore only a limited range of the uncertainty. In addition, the distribution of GCM sensitivities is not by construction a representative sample from those probability distributions and thus the regional probabilities generated using multi-model ensembles will not represent the full spread of possible regional changes.

Räisänen and Palmer (2001) used 17 GCMs forced with an idealised annual increase in atmospheric CO₂ of 1% to calculate the probability of exceedance of thresholds of temperature increase (e.g., >1°C) and precipitation change (e.g., <-10%). These were used to demonstrate that a probabilistic approach has advantages over conventional deterministic estimates by demonstrating the economic value of a probabilistic assessment of future climate change. Giorgi and Mearns (2002) developed measures of uncertainty for regional temperature

Table 11.3. Methods for generating probabilistic information from future climate simulations at continental and sub-continental scales, SRES-scenario specific. Results from the methods of Greene et al. (2006) and Tebaldi et al. (2004a,b) are displayed in Figure 11.26.

Reference	Experiment	Input Type Spatial Scale	Time Resolution	Synthesis Method and Results	Methodological Assumptions	Model Performance Evaluation
Furrer et al. (2007)	Multi-model Ensemble	Grid points (after interpolation to common grid)	Seasonal multi-decadal averages	Bayesian approach. AOGCMs are assumed independent. Large-scale patterns projected on basis functions, small-scale modelled as an isotropic Gaussian process. Spatial dependence fully accounted for by spatial model. PDFs at grid point level, jointly derived accounting for spatial dependence		Model performance not explicitly brought to bear.
Giorgi and Mearns (2003)	Multi-model Ensemble	Regional averages (Giorgi and Francisco, 2000)	Seasonal multi-decadal averages	Cumulative Distribution Functions (CDFs) derived by counting threshold exceedances among members, and weighing the counts by the REA method. Stepwise CDFs at the regional levels		Model performance (bias and convergence) explicitly quantified in each AOGCMs' weight. Observable at same spatial scale and time resolution, for period 1961 to 1990.
Greene et al. (2006)	Multi-model Ensemble	Regional averages (Giorgi and Francisco, 2000)	Seasonal and annual averages	Bayesian approach. AOGCMs dependence is modelled. Linear regression of observed values on model's values (similar to Model-Output-Statistics approach used in weather forecasting and seasonal forecasting) with coefficients estimates applied to future simulations. PDFs at regional level		Model performance measured on 1902 to 1998 historical trend reproduction at same spatial scale and time resolution.
Harris et al. (2006)	Perturbed Physics Ensemble (PPE)	Grid points	Seasonal multi-annual averages	Scaled equilibrium response patterns from a large slab-model Perturbed Physics Ensemble (PPE), using transient responses of an Energy Balance Model driven by PPE climate feedbacks. Quantifying scaling error, against a smaller PPE of transient simulations, to include in PDFs. PDFs at arbitrary level of aggregation		All model versions assumed equally likely.
Stott et al. (2006a)	Single Model (HadCM3)	Continental averages	Annual decadal averages	Linear scaling factor estimated through optimal fingerprinting approach at continental scales or at global scale and applied to future projections, with estimated uncertainty. Natural variability estimated from control run added as additional uncertainty component. PDFs at the continental-scale level		Not applicable
Tebaldi et al. (2004a,b)	Multi-model Ensemble	Regional averages (Giorgi and Francisco, 2000)	Seasonal multi-decadal averages	Bayesian approach. AOGCMs are assumed independent. Normal likelihood for their projections, with AOGCM-specific variability. PDFs at the regional level		Model performance (bias and convergence) implicitly brought to bear through likelihood assumptions. Observable at same spatial scale and time resolution, for period 1961 to 1990 in original papers, for period 1980 to 1999 for results displayed in this report.

and precipitation change by weighting model results according to biases in their simulation of present-day climate and convergence of their projections to the ensemble's mean. Their Reliability Ensemble Average (REA) method was applied to the nine GCMs assessed in the TAR to provide uncertainty estimates separately for the SRES A2 and B2 emission scenarios for 22 large sub-continental regions.

Tebaldi et al. (2004a,b) used a Bayesian approach to define a formal statistical model for deriving probabilities from an ensemble of projections forced by a given SRES scenario. Using the Giorgi and Mearns (2002, 2003) approach, model bias and convergence criteria determine the shape and width of the posterior probability density functions (PDFs) of temperature and precipitation change signals. Expert judgement can be incorporated in the form of prior distributions that have the effect of assigning different relative weights to the two criteria (Tebaldi et al., 2004b; Lopez et al., 2006). The method developed by Furrer et al. (2007) to combine GCM output at the grid point scale into probabilistic projections is described in detail in Chapter 10. By straightforward area averaging, PDFs of climate change at the regional scale can be obtained. When this is done for the Giorgi and Francisco (2000) regions, the regional PDFs from Furrer et al. (2007) agree overall with the

empirical histogram of the ensemble projections and the Tebaldi et al. (2004b) PDFs, with relatively small differences in spread and generally no clear difference in location.

Greene et al. (2006) used a Bayesian framework to model an ensemble of GCM projections under individual SRES scenarios by an extension of methods used for seasonal ensemble forecasting. The set of GCM simulations of the observed period 1902 to 1998 are individually aggregated in area-averaged annual or seasonal time series and jointly calibrated through a linear model to the corresponding observed regional trend. The calibration coefficients and their uncertainty are estimated and then applied to the future projections to provide probabilistic forecasts of future trends. Two critical assumptions are responsible for this method's results being so different from the ensemble projections or the PDFs produced by Tebaldi et al. (2004a,b) (see Figure 11.26 and Supplementary Material Figures S11.33 to S11.35). Firstly, the method attributes large uncertainty to models that are unable to reproduce historical trends despite the uncertainty in the relatively weak forcings in the historical period and the large natural variability at regional scales. Second, a strong stationarity assumption is required to extrapolate the relationship derived over the historical record to future trends, which involve a different combination of and

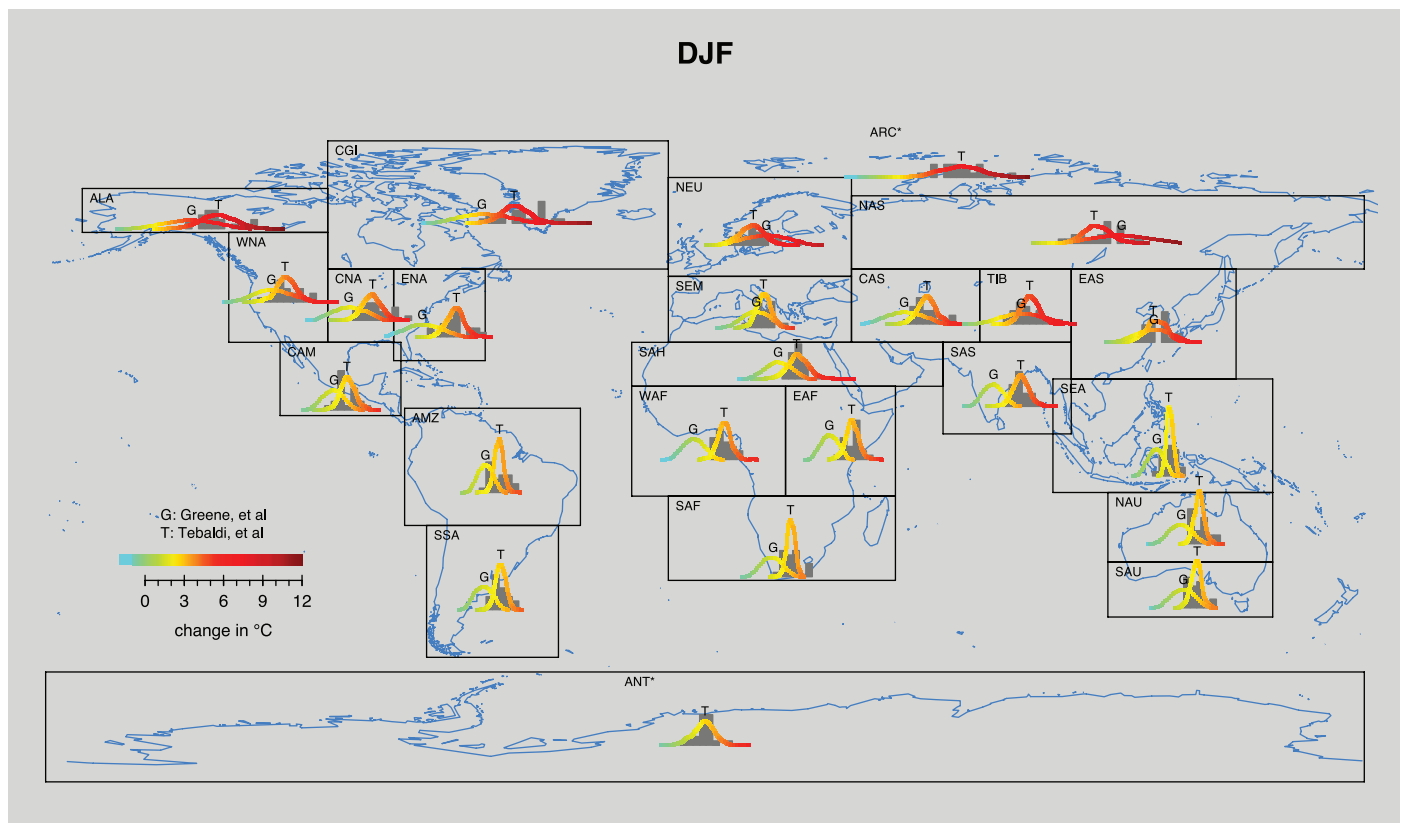


Figure 11.26. Map comparing PDFs of change in temperature (2080 to 2099 compared to 1980 to 1999) from Tebaldi et al. (2004a,b) and Greene et al. (2006) as well as the raw model projections (represented by shaded histograms) for the Giorgi and Francisco (2000) regions. Areas under the curves and areas covered by the histograms have been scaled to equal unity. The scenario is SRES A1B and the season is NH winter (DJF). Asterisks adjacent to ARC and ANT regions indicate that only the Tebaldi et al. results were available.

some significantly stronger forcings. The significantly smaller warming and the large width of the PDFs (at times including negative values) labelled by a 'G' in Figure 11.26 are then interpretable as a result of this stationarity constraint and the large uncertainty in the fitting of the trends. They contrast starkly with the larger warming represented in the histograms of model projections and their synthesis in the Tebaldi et al. (2004a,b) and in the Furrer et al. (2007, not shown) PDFs. This is particularly so in the lower-latitude regions of Africa, South Asia and the SH, possibly as a consequence of particularly weak trends in the observations and/or relatively worse performance of the GCMs.

Dessai et al. (2005) apply the idea of simple pattern scaling (Santer et al., 1990) to a multi-model ensemble of AOGCMs. They 'modulate' the normalised regional patterns of change by the global mean temperature changes generated under many SRES scenarios and climate sensitivities through the Model for the Assessment of Greenhouse-Gas Induced Climate Change (MAGICC), a simple probabilistic energy balance model (Wigley and Raper, 2001). Their work focuses on measuring the changes in PDFs as a function of different sources of uncertainty. In this analysis, the impact of the SRES scenarios turns out to be the most relevant for temperature changes, particularly in the upper tail of the distributions, while the GCM weighting does not produce substantial differences. This result is probably dependent on the long horizon of the projections considered (late 21st century). Arguably, the emission scenario would be less important in the short to mid-term. Climate sensitivity has an impact mainly in the lower tail of the distributions. For precipitation changes, all sources of uncertainty seem relevant but the results are very region-specific and thus difficult to generalise. More work to test the robustness of these conclusions is needed, especially when these are obviously not consistent with the results in Figure 10.29. For example, the use of pattern scaling is likely to underestimate the range of projections that would be obtained by running a larger ensemble of GCMs (Murphy et al., 2004).

The work described above has involved either large-area averages of temperature and precipitation change or statistical modelling at the grid box scale. Good and Lowe (2006) show that trends in large-area and grid-box average projections of precipitation are often very different from the local trends within the area. This demonstrates the inadequacy of inferring the behaviour at fine scales from that of large-area averages.

11.10.2.2.3 *Using perturbed physics ensembles*

Another method for exploring uncertainties in regional climate projections is the use of large perturbed physics ensembles (described in detail in Chapter 10). These allow a characterisation of the uncertainty due to poorly constrained parameters within the formulation of a model. Harris et al. (2006) combined the results from a 17-member ensemble (Collins et al., 2006) with a larger perturbed physics ensemble, investigating the equilibrium climate response to a doubling of atmospheric CO₂ (Webb et al., 2006). They developed a

bridge between spatial patterns of the transient and equilibrium climate response by way of simple pattern scaling (Santer et al., 1990), allowing results from the large ensemble to be translated into PDFs of time-dependent regional changes. Uncertainties in surface temperature and precipitation changes are derived (Supplementary Material Figures S11.36 and S11.37), which arise from the poorly constrained atmospheric model parameters, internal variability and pattern scaling errors. The latter are quantified by comparing the scaled equilibrium response with the transient response for 17 model versions with identical parameter settings. Errors introduced by the pattern-scaling technique are largest when the transient response varies nonlinearly with global temperature, as is the case for precipitation in certain regions.

11.10.2.2.4 *Other approaches to quantifying regional uncertainty*

As described in Chapter 10, Stott and Kettleborough (2002) provide PDFs of future change in climate by making use of the robust observational constraints on a climate model's response to greenhouse gas and sulphate aerosol forcings that underpin the attribution of recent climate change to anthropogenic sources. The study by Stott et al. (2006a) is the first to adapt this method for continental scales. It considers two methods of constraining future continental temperature projections, one based on using observed historical changes only over the region of interest and one based on using observed changes in global temperature patterns. The first approach produces wider PDFs, since the uncertainty of detection at the regional scale is larger. The second approach incorporates more information, hence reducing the uncertainty, but assumes that the GCM represents correctly the relationship between global mean and regional temperature change. In contrast to the studies of Section 11.10.2.2.2, this work uses projections from a single GCM (HadCM3), although Stott et al. (2006b) have confirmed the results of this methodology for other models.

In general, the regional sections of this chapter assess the uncertainty in regional changes based on expert understanding of the relevant processes, rather than by formal probabilistic methods, which are still in their infancy and currently do not provide definitive results. An approach to a process-based assessment of the reliability of modelled climate change responses and thus uncertainties in its future projections has been proposed by Rowell and Jones (2006). They perform an assessment of the physical and dynamical mechanisms responsible for a specific future outcome, in their case European summer drying. Their analysis isolates the contribution of the four major mechanisms analysed: the spatial pattern of warming, other large-scale changes, reduced spring soil moisture and summer soil moisture feedbacks. In certain regions, the second process makes a minor contribution with the first and third dominating. This leads to the conclusion that the sign of the change is robust as confidence in the processes underlying these mechanisms is high.

11.10.2.2.5 *Combined uncertainties: General Circulation Models, emissions and downscaling techniques*

It is important to quantify the relative importance of the uncertainty arising from the downscaling step (from the RCM formulation or the assumptions underlying an empirical SD method) against the other sources of uncertainty. For example, in the application of SD methods to probabilistic scenarios, Benestad (2002b, 2004a) used a multi-model ensemble coupled to SD to derive tentative probabilistic scenarios at a regional scale for northern Europe.

The PRUDENCE project (Box 11.2) provided the first opportunity to weigh these various sources of uncertainty for simulations over Europe. Rowell (2005) evaluated a four-dimensional matrix of climate modelling experiments that included two different emissions scenarios, four different GCM experiments, multiple ensemble members within the latter to assess internal variability, and nine different RCMs, for the area of the British Isles. He found that the dynamical downscaling added a small amount of uncertainty compared to the other sources for temperature evaluated as monthly/seasonal averages. For precipitation, the relative contributions of the four sources of uncertainty are more balanced. Déqué et al. (2005, 2007) show similar results for the whole of Europe, as do Ruosteenoja et al. (2007) for subsections of Europe. Kjellström et al. (2007) find that the differences among different RCMs driven by the same GCM become comparable to those among the same RCM driven by different GCMs when evaluating daily maximum and minimum temperatures. However, mean responses in the PRUDENCE RCMs were often quite different from that of the driving GCM. This suggests that some of the spread in RCM responses may be unrealistic due to model inconsistency (Jones et al., 1997). However, it should be noted that only a few of the RCMs in PRUDENCE were driven by more than one GCM, which adds further uncertainty regarding these conclusions. Other programs similar to PRUDENCE have begun for other regions of the world, such as NARCCAP over North America (Mearns et al., 2005), Regional Climate Change Scenarios for South America (CREAS; Marengo and Ambrizzi, 2006), and the Europe-South America Network for Climate Change Assessment and Impact Studies (CLARIS; <http://www.claris-eu.org>) over South America.

References

- Abaurrea, J., and J. Asin, 2005: Forecasting local daily precipitation patterns in a climate change scenario. *Clim. Res.*, **28**, 183–197.
- Abbs, D.J., 2004: A high resolution modelling study of the effect of climate change on the intensity of extreme rainfall events. In: *Staying Afloat: Floodplain Management Authorities of NSW 44th Annual Conference: Conference Proceedings, Coffs Harbour, NSW*. Floodplain Management Authorities of New South Wales, Tamworth, pp. 17–24.
- ACIA, 2005: *Arctic Climate Impact Assessment*. Cambridge University Press, New York, 1042 pp.
- Adam, J.C., and D.P. Lettenmeier, 2003: Adjustment of global gridded precipitation for systematic bias. *J. Geophys. Res.*, **108**, 4257–4272.
- Adams, N., 2004: A numerical modelling study of the weather in East Antarctica and the surrounding Southern Ocean. *Weather Forecasting*, **19**, 653–672.
- AIACC (Assessments of Impacts and Adaptations to Climate Change in Multiple Regions and Sectors), 2004: *AIACC Regional Study AS07: Southeast Asia Regional Vulnerability to Changing Water Resource and Extreme Hydrological Events due to Climate Change. Progress Report: Period Year-end 2003*. 8 pp., http://sedac.ciesin.columbia.edu/aiacc/progress/AS07_Jan04.pdf.
- Aldrian, E., and R. Dwi Susanto, 2003: Identification of three dominant rainfall regions within Indonesia and their relationship to sea surface temperature. *Int. J. Climatol.*, **23**(12), 1435–1452.
- Aldrian, E., et al., 2004a: Long term simulation of the Indonesian rainfall with the MPI Regional Model. *Clim. Dyn.*, **22**(8), 794–814, doi:10.1007/s00382-004-0418-9.
- Aldrian, E., et al., 2004b: Modelling Indonesian rainfall with a coupled regional model. *Clim. Dyn.*, **25**(1), 1–17, doi:10.1007/s00382-004-0483-0.
- Anderson, C.J., et al., 2003: Hydrological processes in regional climate model simulations of the Central United States flood of June–July 1993. *J. Hydrometeorol.*, **4**, 584–598.
- Angeles, M.E., J.E. Gonzalez, D.J. Erickson, and J.L. Hernández, 2007: Predictions of future climate change in the Caribbean region using global general circulation models. *Int. J. Climatol.*, **27**, 555–569, doi:10.1002/joc.1416.
- Antic, S., R. Laprise, B. Denis, and R. de Elia, 2005: Testing the downscaling ability of a one-way nested regional climate model in regions of complex topography. *Clim. Dyn.*, **23**, 473–493.
- Anyah, R., and F. Semazzi, 2004: Simulation of the sensitivity of Lake Victoria basin climate to lake surface temperatures. *Theor. Appl. Climatol.*, **79**(1–2), 55–69.
- Arakawa, O., and A. Kitoh, 2005: Rainfall diurnal variation over the Indonesian Maritime Continent simulated by 20km-mesh GCM. *Scientific Online Letters on the Atmosphere*, **1**, 109–112.
- Arnell, N., D. Hudson, and R. Jones, 2003: Climate change scenarios from a regional climate model: Estimating change in runoff in southern Africa. *J. Geophys. Res.*, **108**(D16), 4519, doi:10.1029/2002JD002782.
- Arnfield, A.J., 2003: Two decades of urban climate research: a review of turbulence, exchanges of energy and water, and the urban heat island. *Int. J. Climatol.*, **23**, 1–26.
- Ashok, K., Z.Y. Guan, and T. Yamagata, 2001: Impact of the Indian Ocean Dipole on the relationship between the Indian monsoon rainfall and ENSO. *Geophys. Res. Lett.*, **28**, 4499–4502.
- Ashrit, R.G., K. Rupa Kumar, and K. Krishna Kumar, 2001: ENSO-monsoon relationships in a greenhouse warming scenario. *Geophys. Res. Lett.*, **29**, 1727–1730.
- Ashrit, R.G., H. Douville, and K. Rupa Kumar, 2003: Response of the Indian monsoon and ENSO-monsoon teleconnection to enhanced greenhouse effect in the CNRM coupled model. *J. Meteorol. Soc. Japan*, **81**, 779–803.
- Augustine, J.A., and F. Caracena, 1994: Lower-tropospheric precursors to nocturnal MCS development over central United States. *Weather Forecasting*, **9**, 116–135.
- Avisar, R., and D. Werth, 2005: Global hydroclimatological teleconnections resulting from tropical deforestation. *J. Hydrometeorol.*, **6**, 134–145.
- Bader, J., and M. Latif, 2003: The impact of decadal-scale Indian Ocean sea surface temperature anomalies on Sahelian rainfall and the North Atlantic Oscillation. *Geophys. Res. Lett.*, **30**(22), 2166–2169, doi:10.1029/2003GL018426.
- Bailey, D.A., and A.H. Lynch, 2000: Development of an Antarctic regional climate system model: Part 2. Station validation and surface energy balance. *J. Clim.*, **13**, 1351–1361.
- Bailey, D.A., A.H. Lynch, and T.E. Arbetter, 2004: The relationship between synoptic forcing and polynya formation in the Cosmonaut Sea, II: Polynya simulation. *J. Geophys. Res.*, **109**, doi:10.1029/2003JC001838.
- Barnett, D.N., et al., 2006: Quantifying uncertainty in changes in extreme event frequency in response to doubled CO₂ using a large ensemble of GCM simulations. *Clim. Dyn.*, **26**, 489–511.
- Barnett, T.P., J.C. Adam, and D.P. Lettenmeier, 2005: Potential impacts of a warming climate on water availability in snow-dominated regions. *Nature*, **438**, 303–309, doi:10.1038/nature04141.825111-825179.
- Bartman, A.G., W.A. Landman, and C.J. de W. Ratenbach, 2003: Recalibration of general circulation model output to Austral summer rainfall over Southern Africa. *Int. J. Climatol.*, **23**, 1407–1419.
- Becker, A., and H. Bugmann (eds.), 1997: *Predicting Global Change Impacts on Mountain Hydrology and Ecology: Integrated Catchment Hydrology/Altitudinal Gradient Studies*. IGBP Report 43, International Geosphere-Biosphere Programme, Stockholm.
- Beckmann, B.R., and T.A. Buishand, 2002: Statistical downscaling relationship for precipitation in the Netherlands and North Germany. *Int. J. Climatol.*, **22**, 15–32.
- Beersma, J.J., and T.A. Buishand, 2003: Multi-site simulation of daily precipitation and temperature conditional on atmospheric circulation. *Clim. Res.*, **25**, 121–133.
- Bell, J.L., L.C. Sloan, and M.A. Snyder, 2004: Changes in extreme climatic events: A future climate scenario. *J. Clim.*, **17**(1), 81–87.
- Benestad, R.E., 2002a: Empirically downscaled temperature scenarios for Northern Europe based on a multi-model ensemble. *Clim. Res.*, **21**(2), 105–125.
- Benestad, R.E., 2002b: Empirically downscaled multimodel ensemble temperature and precipitation scenarios for Norway. *J. Clim.*, **15**, 3008–3027.
- Benestad, R.E., 2004a: Tentative probabilistic temperature scenarios for Northern Europe. *Tellus*, **56A**(2), 89–101.
- Benestad, R.E., 2004b: Empirical-statistical downscaling in climate modeling. *Eos*, **85**(42), 417.
- Benestad, R.E., 2005: Climate change scenarios for northern Europe from multi-model IPCC AR4 climate simulations. *Geophys. Res. Lett.*, **32**, L17704, doi:10.1029/2005GL023401.
- Bengtsson, L., 1996: The climate response to the changing greenhouse gas concentration in the atmosphere. In: *Decadal Climate Variability, Dynamics And Variability* [Anderson, D.L.T., and J. Willebrand (eds.)]. NATO ASI Series 44, Springer, Berlin, 493 pp.
- Bengtsson, L., V.A. Semenov, and O.M. Johannessen, 2004: The early twentieth-century warming in the Arctic - a possible mechanism. *J. Clim.*, **17**, 4045–4057.
- Beniston, M., and P. Junco, 2001: Shifts in the distributions of pressure, temperature and moisture in the alpine region in response to the behavior of the North Atlantic Oscillation. *Theor. Appl. Climatol.*, **71**, 29–42.
- Beniston, M., F. Keller, B. Koffi, and S. Goyette, 2003: Estimates of snow accumulation and volume in the Swiss Alps under changing climatic conditions. *Theor. Appl. Climatol.*, **76**, 125–140.
- Beniston, M., et al., 2007: Future extreme events in European climate: An exploration of regional climate model projections. *Clim. Change*, doi:10.1007/s10584-006-9226-z.

- Bertler, N.A.N., P.J. Barrett, P.A. Mayewski, and R.L. Fogt, 2004: El Niño suppresses Antarctic warming. *Geophys. Res. Lett.*, **31**, L15207, doi:10.1029/2004GL020749.
- Betts, A.K., 1998: Climate-convection feedbacks: Some further issues. *Clim. Dyn.*, **39**(1), 35–38.
- Betts, R.A., et al., 2004: The role of ecosystem-atmosphere interactions in simulated Amazonian precipitation decrease and forest dieback under global climate warming. *Theor. Appl. Climatol.*, **78**, 157–175.
- Biasutti, M., and A. Giannini, 2006: Robust Sahel drying in response to late 20th century forcings. *Geophys. Res. Lett.*, **33**, L11706, doi:10.1029/2006GRL026067.
- Biner, S., D. Caya, R. Laprise and L. Spacek, 2000: Nesting of RCMs by imposing large scales. In: *Research Activities in Atmospheric and Oceanic Modelling*. WMO/TD No. 987, Report No. 30, World Meteorological Organization, Geneva, pp. 7.3–7.4.
- Black, E., et al., 2004: Factors contributing to the summer 2003 European heatwave. *Weather*, **59**, 217–223.
- Blenckner, T. and D. Chen, 2003: Comparison of the impact of regional and North-Atlantic atmospheric circulation on an aquatic ecosystem. *Clim. Res.*, **23**, 131–136.
- Boer, R., and A. Faqih, 2004: *Current and Future Rainfall Variability in Indonesia*. AIACC Technical Report 021, http://sedac.ciesin.columbia.edu/aiacc/progress/AS21_Jan04.pdf.
- Bogdanova, E.G, B.M. Ilyin, and I.V. Dragomilova, 2002: Application of a comprehensive bias correction model to application of a comprehensive bias correction model to stations. *J. Hydrometeorol.*, **3**, 700–713.
- Bojariu, R., and F. Giorgi, 2005: The North Atlantic Oscillation signal in a regional climate simulation for the European region. *Tellus*, **57A**(4), 641–653.
- Bonan, G.B., 2001: Observational evidence for reduction of daily maximum temperature by croplands in the Midwest United States. *J. Clim.*, **14**, 2430–2442.
- Boo, K.-O., W.-T. Kwon, and J.-K. Kim, 2005: Vegetation changes in the regional surface climate over East Asia due to global warming using BIOME4. *Il Nuovo Cimento*, **27**(4), 317–327.
- Boo, K.-O., W.-T. Kwon, and H.-J. Baek, 2006: Change of extreme events of temperature and precipitation over Korea using regional projection of future climate change. *Geophys. Res. Lett.*, **33**(1), L01701, doi:10.1029/2005GL023378.
- Booij, M.J., 2002: Extreme daily precipitation in western Europe with climate change at appropriate spatial scales. *Int. J. Climatol.*, **22**, 69–85.
- Bordoni, S., et al., 2004: The low-level circulation of the North American Monsoon as revealed by QuikSCAT. *Geophys. Res. Lett.*, **31**, L10109, doi:10.1029/2004GL020009.
- Boulanger, J.P., F. Martinez, and E.C. Segura, 2006: Projection of future climate change conditions using IPCC simulations, neural networks and Bayesian statistics. Part I: Temperature mean state and seasonal cycle in South America. *Clim. Dyn.*, **27**, 233–259.
- Bretherton, C.S., and D.S. Battisti, 2000: An interpretation of the results from atmospheric general circulation models forced by the time history of the observed sea surface temperature distribution. *Geophys. Res. Lett.*, **27**, 767–770.
- Bromwich, D.H., and R.L. Fogt, 2004: Strong trends in the skill of the ERA-40 and NCEP/NCAR Reanalyses in the high and middle latitudes of the Southern Hemisphere, 1958–2001. *J. Clim.*, **17**, 4603–4619.
- Bromwich, D.H., A.J. Monaghan, and Z. Guo, 2004a: Modeling the ENSO modulation of Antarctic climate in the late 1990s with the Polar MM5. *J. Clim.*, **17**, 109–132.
- Bromwich, D.H., A.J. Monaghan, K.W. Manning, and J.G. Powers, 2004b: Real-time forecasting for the Antarctic: An evaluation of the Antarctic Mesoscale Prediction System (AMPS). *Mon. Weather Rev.*, **133**, 579–603.
- Bromwich, D.H., et al., 2000: ECMWF analyses and reanalyses depiction of ENSO signal in Antarctic precipitation. *J. Clim.*, **13**, 1406–1420.
- Brovkin, V., et al., 1999: Modelling climate response to historical land cover change. *Global Ecol. Biogeogr.*, **8**, 509–517.
- Buishand, T.A., M.V. Shabalova, and T. Brandsma, 2004: On the choice of the temporal aggregation level for statistical downscaling of precipitation. *J. Clim.*, **17**, 1816–1827.
- Busuioc, A., and H. von Storch, 2003: Conditional stochastic model for generating daily precipitation time series. *Clim. Res.*, **24**, 181–195.
- Busuioc, A., D. Chen, and C. Hellström, 2001: Performance of statistical downscaling models in GCM validation and regional climate change estimates: application for Swedish precipitation. *Int. J. Climatol.*, **21**(5), 557–578.
- Busuioc, A., F. Giorgi, X. Bi, and M. Ionita, 2006: Comparison of regional climate model and statistical downscaling simulations of different winter precipitation change scenarios over Romania. *Theor. Appl. Climatol.*, **86**, 101–120.
- Cai, W., P.H. Whetton, and D.J. Karoly, 2003a: The response of the Antarctic Oscillation to increasing and stabilized atmospheric CO₂. *J. Clim.*, **16**, 1525–1538.
- Cai, W., et al., 2003b: *Climate Change in Queensland under Enhanced Greenhouse Conditions. Annual Report, 2003*. CSIRO Atmospheric Research, Aspendale, Vic., 74 pp. <http://www.longpaddock.qld.gov.au/ClimateChanges/pub/CSIRO2003.html#end>.
- Caires, S., V.R. Swail, and X.L. Wang, 2006: Projection and analysis of extreme wave climate. *J. Clim.*, **19**, 5581–5605.
- Caminade, C., L. Teray, and E. Maisonnave, 2006: West African monsoon system response to greenhouse gas and sulphate aerosol forcing under two emission scenarios. *Clim. Dyn.*, **26**, 531–547.
- Cannon, A., and P. Whitfield, 2002: Downscaling recent streamflow conditions in British Columbia, Canada using ensemble neural network models. *J. Hydrol.*, **259**(1–4), 136–151.
- Carleton, A.M., 2003: Atmospheric teleconnections involving the Southern Ocean. *J. Geophys. Res.*, **108**, 8080, doi:10.1029/2000JC000379.
- Carril, A.F., C.G. Menéndez, and A. Navarra, 2005: Climate response associated with the Southern Annular Mode in the surroundings of the Antarctic Peninsula: a multi-model ensemble analysis. *Geophys. Res. Lett.*, **32**, L16713, doi:10.1029/2005GL023581.
- Cassano, J.J., P. Uotila, and A. Lynch, 2006: Changes in synoptic weather patterns in the polar regions in the 20th and 21st centuries. Part I: Arctic. *Int. J. Climatol.*, **26**, 1027–1049, doi:10.1002/joc.1306.
- Caya, D., and S. Biner, 2004: Internal variability of RCM simulations over an annual cycle. *Clim. Dyn.*, **22**, 33–46.
- Cayan, D.R., et al., 2001: Changes in the onset of spring in the western United States. *Bull. Am. Meteorol. Soc.*, **82**, 399–415.
- Cazes Boezio, G., A.W. Robertson, and C.R. Mechoso, 2003: Seasonal dependence of ENSO teleconnections over South America and relationships with precipitation in Uruguay. *J. Clim.*, **16**(8), 1159–1176.
- Chaboureaud, J.P., F. Guichard, J.L. Redelsperger, and J.P. Lafore, 2004: The role of stability and moisture in the diurnal cycle of convection over land. *Q. J. R. Meteorol. Soc.*, **130**, 3105–3117.
- Chapman, W.L., and J.E. Walsh, 2006: A synthesis of Antarctic temperatures. *J. Clim.*, **26**, 1181–2119, doi:10.1002/joc.1305.
- Chapman, W.L., and J.E. Walsh, 2007: Simulations of Arctic temperature and pressure by global coupled models. *J. Clim.*, **20**, 609–632, doi:10.1175/JCLI4026.1.
- Charles, S.P., B.C. Bates, I.N. Smith, and J.P. Hughes, 2004: Statistical downscaling of daily precipitation from observed and modelled atmospheric fields. *Hydrolog. Process.*, **18**(8), 1373–1394.
- Chase, T.N., et al., 2000: Simulated impacts of historical land cover changes on global climate in northern winter. *Clim. Dyn.*, **16**, 93–105.
- Chen, A.A., and M.A. Taylor, 2002: Investigating the link between early season Caribbean rainfall and the El Niño +1 year. *Int. J. Climatol.*, **22**, 87–106.
- Chen, D.L., and Y.M. Chen, 2003: Association between winter temperature in China and upper air circulation over East Asia revealed by canonical correlation analysis. *Global Planet. Change*, **37**, 315–325.
- Chen, M., D. Pollard, and E.J. Barron, 2003: Comparison of future climate change over North America simulated by two regional climate models. *J. Geophys. Res.*, **108**(D12), 4348, doi:10.1029/2002JD002738.

- Chen, T.-C., J.-H. Yoon, K.J. St. Croix, and E.S. Takle, 2001: Suppressing impacts of the Amazonian deforestation by the global circulation change. *Bull. Am. Meteorol. Soc.*, **82**, 2209–2216.
- Chen, T.-C., S.-Y. Wang, W.-R. Huang, and M.-C. Yen, 2004: Variation of the East Asian summer monsoon rainfall. *J. Clim.*, **17**, 744–762.
- Chou, C., and J.D. Neelin, 2004: Mechanisms of global warming impacts of regional tropical precipitation. *J. Clim.*, **17**, 2688–2701.
- Chou, C., J.D. Neelin, J.-Y. Tu, and C.-T. Chen, 2007: Regional tropical precipitation change mechanisms in ECHAM4/OPYC3 under global warming. *J. Clim.*, **19**, 4207–4223.
- Chou, S.C., A.M.B. Nunes, and I.F.A. Cavalcanti, 2000: Extended range forecasts over South America using the regional eta model. *J. Geophys. Res.*, **105**, 10147–10160.
- Christensen, J.H., and O.B. Christensen, 2003: Severe summertime flooding in Europe. *Nature*, **421**, 805–806.
- Christensen, J.H., T. Carter, and F. Giorgi, 2002: PRUDENCE employs new methods to assess European climate change. *Eos*, **83**, 147.
- Christensen, J.H., T.R. Carter, M. Rummukainen, and G. Amanatidis, 2007: Evaluating the performance and utility of regional climate models: the PRUDENCE project. *Clim. Change*, doi:10.1007/s10584-006-9211-6.
- Christensen, J.H., et al., 2001: A synthesis of regional climate change simulations – A Scandinavian perspective. *Geophys. Res. Lett.*, **28**(6), 1003–1006.
- Christensen, O.B., and J.H. Christensen, 2004: Intensification of extreme European summer precipitation in a warmer climate. *Global Planet. Change*, **44**, 107–117.
- Church, J.A., N.J. White, and J.R. Hunter, 2006: Sea level rise at tropical Pacific and Indian Ocean islands. *Global Planet. Change*, **53**(3), 155–168.
- Church, J.A., et al., 2004: Estimates of regional distribution of sea level rise over the 1950–2000 period. *J. Clim.*, **17**, 2609–2625.
- Clark, R., S. Brown, and J. Murphy, 2006: Modelling Northern Hemisphere summer heat extreme changes and their uncertainties using a physics ensemble of climate sensitivity experiments. *J. Clim.*, **19**, 4418–4435.
- Claussen, M., C. Kutzbacki, V. Brovkin, and A. Ganapolski, 1999: Simulation of an abrupt change in Saharan vegetation in the mid-Holocene. *Geophys. Res. Lett.*, **26**, 2037–2040.
- Collier, J.C., K.P. Bowman, and G.R. North, 2004: A comparison of tropical precipitation simulated by the community climate model with that measured by the tropical rainfall measuring mission satellite. *J. Clim.*, **17**, 3319–3333.
- Collins, M., et al., 2006: Towards quantifying uncertainty in transient climate change. *Clim. Dyn.*, **27**, 127–147.
- Comiso, J.C., 2000: Variability and trends in Antarctic surface temperatures from in situ and satellite infrared measurements. *J. Clim.*, **13**, 1674–1696.
- Connolley, W.M., and S.A. Harangozo, 2001: A comparison of five numerical weather prediction analysis climatologies in southern high latitudes. *J. Clim.*, **14**, 30–44.
- Cook, K.H., and E.K. Vizy, 2006: Coupled model simulations of the West African monsoon system: twentieth-century simulations and twenty-first-century predictions. *J. Clim.*, **19**, 3681–3703.
- Coppola, E., and F. Giorgi, 2005: Climate change in tropical regions from high-resolution time-slice AGCM experiments. *Q. J. R. Meteorol. Soc.*, **131**(612), 3123–3145.
- Costa, M.H., and J.A. Foley, 2000: Combined effects of deforestation and doubled atmospheric CO₂ concentrations on the climate of Amazonia. *J. Clim.*, **13**, 35–58.
- Covey, C., et al., 2003: An overview of results from the Coupled Model Intercomparison Project (CMIP). *Global Planet. Change*, **37**, 103–133, doi:10.1016/S0921-8181(02)00193-5.
- Cox, P.M., et al., 2000: Acceleration of global warming due to carbon-cycle feedbacks in a coupled climate model. *Nature*, **408**, 184–187.
- Cox, P.M., et al., 2004: Amazonian forest dieback under climate-carbon cycle projections for the 21st century. *Theor. Appl. Clim.*, **78**, 137–156.
- CSIRO (Commonwealth Scientific and Industrial Research Organisation), 2001: *Climate Projections for Australia*. CSIRO Atmospheric Research, Melbourne, 8 pp., <http://www.dar.csiro.au/publications/projections2001.pdf>.
- Curtis, J., G. Wendler, R. Stone, and E. Dutton, 1998: Precipitation decrease in the western Arctic, with special emphasis on Barrow and Barter Island, Alaska. *Int. J. Climatol.*, **18**, 1687–1707.
- Dairaku, K., and S. Emori, 2006: Dynamic and thermodynamic influences on intensified daily rainfall during the Asian summer monsoon under doubled atmospheric CO₂ conditions. *Geophys. Res. Lett.*, **33**, L01704, doi:10.1029/2005GL024754.
- Davey, M.K., et al., 2002: STOIC: A study of coupled model climatology and variability in tropical ocean regions. *Clim. Dyn.*, **18**, 403–420.
- Davies, H.C., 1976: A lateral boundary formulation for multi-levels prediction models. *Q. J. R. Meteorol. Soc.*, **102**, 405–418.
- Debernard, J., M.Ø. Køltzow, J.E. Haugen, and L.P. Røed, 2003: Improvements in the sea-ice module of the regional coupled atmosphere-ocean model and the strategy for the coupling of the three spheres. In: *RegClim General Technical Report No. 7* [Iversen, T., and M. Lystad (eds)]. Norwegian Meteorological Institute, Oslo, pp. 59–69.
- DeFries, R.S., L. Bounoua, and G.J. Collatz, 2002: Human modification of the landscape and surface climate in the next fifty years. *Global Change Biol.*, **8**, 438–458.
- Delire, C., et al., 2001: Simulated response of the atmosphere-ocean system to deforestation in the Indonesian Archipelago. *Geophys Res Lett*, **28**(10), 2081–2084.
- Denis, B., R. Laprise, and D. Caya, 2003: Sensitivity of a regional climate model to the spatial resolution and temporal updating frequency of the lateral boundary conditions. *Clim. Dyn.*, **20**, 107–126.
- Denis, B., R. Laprise, D. Caya, and J. Côté, 2002: Downscaling ability of one-way-nested regional climate models: The big-brother experiment. *Clim. Dyn.*, **18**, 627–646.
- Déqué, M., and J.P. Piedelievre, 1995: High resolution climate simulation over Europe. *Clim. Dyn.*, **11**, 321–339.
- Déqué, M., and A.L. Gibelin, 2002: High versus variable resolution in climate modelling. In: *Research Activities in Atmospheric and Oceanic Modelling* [Ritchie, H. (ed.)]. WMO/TD No. 1105, Report No. 32, World Meteorological Organization, Geneva, pp. 74–75.
- Déqué, M., et al., 2005: Global high resolution versus Limited Area Model climate change scenarios over Europe: results from the PRUDENCE project. *Clim. Dyn.*, **25**, 653–670, 10.1007/s00382-005-0052-1.
- Déqué, M., et al., 2007: An intercomparison of regional climate simulations for Europe: assessing uncertainties in model projections. *Clim. Change*, doi:10.1007/s10584-006-9228-x.
- Derbyshire, S.H., et al., 2004: Sensitivity of moist convection to environmental humidity. *Q. J. R. Meteorol. Soc.*, **130**, 3055–3079.
- Dessai, S., X. Lu, and M. Hulme, 2005: Limited sensitivity analysis of regional climate change probabilities for the 21st century. *J. Geophys. Res.*, **110**, D19108, doi:10.1029/2005JD005919.
- Dethloff, K., et al., 2001: Sensitivity of Arctic climate simulations to different boundary layer parameterizations in a regional climate model. *Tellus*, **53**, 1–26.
- Diaz-Nieto, J., and R.L. Wilby, 2005: A comparison of statistical downscaling and climate change factor methods: impacts on low flows in the River Thames, United Kingdom. *Clim. Change*, **69**, 245–268.
- Dibike, Y.B., and P. Coulibaly, 2005: Hydrologic impact of climate change in the Saguenay watershed: Comparison of downscaling methods and hydrologic models. *J. Hydrol.*, **307**, 145–163.
- Diffenbaugh, N.S., J.S. Pal, R.J. Trapp, and F. Giorgi, 2005: Fine-scale processes regulate the response of extreme events to global climate change. *Proc. Natl. Acad. Sci. U.S.A.*, **102**(44), 15774–15778, doi:10.1073/pnas.0506042102.
- Dimitrijevic, M., and R. Laprise, 2005: Validation of the nesting technique in a regional climate model through sensitivity tests to spatial resolution and the time interval of lateral boundary conditions during summer. *Clim. Dyn.*, **25**, 555–580.

- Ding, Y.H., Y.M. Liu, X.L. Shi, and Q.Q. Li, 2003: The experimental use of the regional climate model in the seasonal prediction in China National Climate Center. In: *Proceedings of the 2nd Workshop on Regional Climate Model, March 3-6, 2003, Yokohama, Japan*, GAME Publication No. 39, pp. 9–14.
- Ding, Y.H., et al., 2006: Multi-year simulations and experimental seasonal predictions for rainy seasons in China by using a nested regional climate model (RegCM_NCC). Part I: Sensitivity study. *Adv. Atmos. Sci.*, **23**(3), 323–341.
- Dorn, W., K. Dethloff, and A. Rinke, 2003: Competition of NAO regime changes and increasing greenhouse gases and aerosols with respect to Arctic climate estimate. *Clim. Dyn.*, **21**(5–6), 447–458, doi:10.1007/s00382-003-0344-2.
- Döscher, R., et al., 2002: The development of the coupled ocean-atmosphere model RCAO. *Boreal Environ. Res.*, **7**, 183–192.
- Douville, H., 2005: Limitations of time-slice experiments for predicting regional climate change over South Asia. *Clim. Dyn.*, **24**(4), 373–391.
- Douville, H., et al., 2000: Impact of CO₂ doubling on the Asian summer monsoon: Robust versus model dependent responses. *J. Meteorol. Soc. Japan*, **78**, 1–19.
- Douville, H., et al., 2002: Sensitivity of the hydrological cycle to increasing amounts of greenhouse gases and aerosols. *Clim. Dyn.*, **20**, 45–68.
- Druryan, L.M., M. Fulakeza, and P. Lonergan, 2002: Dynamic downscaling of seasonal climate predictions over Brazil. *J. Clim.*, **15**, 3411–3426.
- Duffy, P.B., et al., 2003: High-resolution simulations of global climate, part 1: Present climate. *Clim. Dyn.*, **21**, 371–390.
- Dufresne, J.-L., et al., 2002: On the magnitude of positive feedback between future climate change and the carbon cycle. *Geophys. Res. Lett.*, **29**(10), 1405, doi:10.1029/2001GL013777.
- Easterling, D.R., L.V. Alexander, A. Mokssit, and V. Detemmerman, 2003: CCI/Clivar workshop to develop priority climate indices. *Bull. Am. Meteorol. Soc.*, **84**, 1403–1407.
- Ekström, M., H.J. Fowler, C.G. Kilsby, and P.D. Jones, 2005: New estimates of future changes in extreme rainfall across the UK using regional climate model integrations. 2. Future estimates and use in impact studies. *J. Hydrol.*, **300**, 234–251.
- Elguindi, N., and F. Giorgi, 2006: Simulating multi-decadal variability of Caspian Sea level changes using regional climate model outputs. *Clim. Dyn.*, **26**: 167–181.
- Engelbrecht, F., C. Rautenbach, J. McGregor, and J. Katzfey, 2002: January and July climate simulations over the SADC region using the limited-area model DARLAM. *Water SA*, **28**(4), 361–374.
- Feddema, J.J., et al., 2005: A comparison of a GCM response to historical anthropogenic land cover change and model sensitivity to uncertainty in present-day land cover representations. *Clim. Dyn.*, **25**, 581–609.
- Fernández, J., and J. Sáenz, 2003: Improved field reconstruction with the analog method: searching the CCA space. *Clim. Res.*, **24**, 199–213.
- Fernandez, J., J. Sáenz, and E. Zorita, 2003: Analysis of wintertime atmospheric moisture transport and its variability over southern Europe in the NCEP reanalyses. *Clim. Res.*, **23**, 195–215.
- Fink, A.H., et al., 2004: The 2003 European summer heatwaves and drought – synoptic diagnostics and impacts. *Weather*, **59**, 209–216.
- Flather, R.A., and H. Khandker, 1993: The storm surge problem and possible effects of sea level changes on coastal flooding in the Bay of Bengal. In: *Climate and Sea Level Change* [Warrick, R.A., E.M. Barrow, and T. Wigley (eds)]. Cambridge University Press, Cambridge, UK, pp. 229–245.
- Flather, R.A., and J.A. Williams, 2000: Climate change effects on storm surges: methodologies and results. In: *Climate Scenarios for Water-Related and Coastal Impacts* [Beersma, J., M. Agnew, D. Viner, and M. Hulme (eds.)]. ECLAT-2 Workshop Report No. 3, KNMI, The Netherlands, pp. 66–78.
- Flather, R.A., et al., 1998: Direct estimates of extreme storm surge elevations from a 40-year numerical model simulation and from observations. *Global Atmos. Ocean System*, **6**, 165–176.
- Fogt, R.L., and D.H. Bromwich, 2006: Decadal variability of the ENSO teleconnection to the high latitude South Pacific governed by coupling with the Southern Annular Mode. *J. Clim.*, **19**, 979–997.
- Foley, J.A., M.T. Coe, M. Scheffer, and G. Wang., 2003: Regime shifts in the Sahara and Sahel: Interactions between ecological systems in Southern Africa. *Ecosystems*, **6**, 524–539.
- Foley, J.A., et al., 2005: Global consequences of land use. *Science*, **309**, 570–574.
- Fowler, H.J., M. Ekström, C.G. Kilsby, and P.D. Jones, 2005: New estimates of future changes in extreme rainfall across the UK using regional climate model integrations. 1. Assessment of control climate. *J. Hydrol.*, **300**, 212–233.
- Fox-Rabinovitz, M.S., L.L. Takacs, R.C. Govindaraju, and M.J. Suarez, 2001: A variable-resolution stretched-grid general circulation model: Regional climate simulation. *Mon. Weather Rev.*, **129**(3), 453–469.
- Frei, C., et al., 2003: Daily precipitation statistics in regional climate models: Evaluation and intercomparison for the European Alps. *J. Geophys. Res.*, **108**(D3), 4124, doi:10.1029/2002JD002287.
- Frei, C., et al., 2006: Future change of precipitation extremes in Europe: Intercomparison of scenarios from regional climate models. *J. Geophys. Res.*, **111**, D06105, doi:10.1029/2005JD005965.
- Freiman, M., and P. Tyson, 2000: The thermodynamic structure of the atmosphere over South Africa: Implications for water vapour transport. *Water SA*, **26**(2), 153–158.
- Friedlingstein, P., J.-L. Dufresne, P.M. Cox, and P. Rayner, 2003: How positive is the feedback between climate change and the carbon cycle? *Tellus*, **55B**, 692–700.
- Friedlingstein, P., et al., 2001: Positive feedback between future climate change and the carbon cycle. *Geophys. Res. Lett.*, **28**, 1543–1546.
- Fu, C.B., et al., 2005: Regional Climate Model Intercomparison project for Asia. *Bull. Am. Meteorol. Soc.*, **86**(2), 257–266, doi:10.11/BAMS-86-2-257.
- Fuentes, U., and D. Heimann, 2000: An improved statistical-dynamical downscaling scheme and its application to the alpine precipitation climatology. *Theor. Appl. Climatol.*, **65**, 119–135.
- Fujibé, F., N. Yamazaki, M. Katsuyama, and K. Kobayashi, 2005: The increasing trend of intense precipitation in Japan based on four-hourly data for a hundred years. *Scientific Online Letters on the Atmosphere*, **1**, 41–44.
- Furrer, R., S.R. Sain, D.W. Nychka, and G.A. Meehl, 2007: Multivariate Bayesian analysis of atmosphere-ocean general circulation models. *Environ. Ecol. Stat.*, in press.
- Gaertner, M.A., et al., 2001: The impact of deforestation on the hydrological cycle in the western Mediterranean: an ensemble study with two regional climate models. *Clim. Dyn.*, **17**, 857–873.
- Gao, Q., and M. Yu, 1998: A model of regional vegetation dynamics and its application to the study of Northeast China Transect (NECT) responses to global change. *Global Biogeochem. Cycles*, **12**(2), 329–344.
- Gao, X.J., Z.C. Zhao, and F. Giorgi, 2002: Changes of extreme events in regional climate simulations over East Asia. *Adv. Atmos. Sci.*, **19**, 927–942.
- Gao, X.J., Z.C. Zhao, and Y.H. Ding, 2003a: Climate change due to greenhouse effects in Northwest China as simulated by a regional climate model. *J. Glaciol. Geocryol.*, **25**(2), 165–169.
- Gao, X.J., J.S. Pal, and F. Giorgi, 2006a: Projected changes in mean and extreme precipitation over the Mediterranean region from a high resolution double nested RCM simulation. *Geophys. Res. Lett.*, **33**, L03706, doi:10.1029/2005GL024954.
- Gao, X.J., D.L. Li, Z.C. Zhao, and F. Giorgi, 2003b: Climate change due to greenhouse effects in Qinghai-Xizang Plateau and along the Qianghai-Tibet Railway. *Plateau Meteorol.*, **22**(5), 458–463.
- Gao, X.J., W.T. Lin, Z.C. Zhao, and F. Kucharsky, 2004: Simulation of climate and short-term climate prediction in China by CCM3 driven by observed SST. *Chin. J. Atmos. Sci.*, **28**, 63–76.
- Gao, X.J., et al., 2001: Climate change due to greenhouse effects in China as simulated by a regional climate model. *Adv. Atmos. Sci.*, **18**, 1224–1230.

- Gao, X.J., et al., 2006b: Impacts of horizontal resolution and topography on the numerical simulation of East Asia precipitation. *Chin. J. Atmos. Sci.*, **30**, 185–192.
- Gedney, N., and P.J. Valdes, 2000: The effect of Amazonian deforestation on the Northern Hemisphere circulation and climate. *Geophys. Res. Lett.*, **27**(19), 3053–3056.
- Genthon, C., and E. Cosme, 2003: Intermittent signature of ENSO in west-Antarctic precipitation. *Geophys. Res. Lett.*, **30**, 2081, doi:10.1029/2003GL018280.
- Genthon, C., G. Krinner, and E. Cosme, 2002: Free and laterally-nudged Antarctic climate of an atmospheric general circulation model. *Mon. Weather Rev.*, **130**, 1601–1616.
- Genthon, C., S. Kapari, and P.A. Mayewski, 2005: Interannual variability of the surface mass balance of West Antarctica from ITASE cores and ERA40 reanalyses. *Clim. Dyn.*, **24**, 759–770.
- Gerbaux, M., et al., 2005: Surface mass balance of glaciers in the French Alps: distributed modeling and sensitivity to climate change. *J. Glaciol.*, **51**(175), 561–572.
- Ghan, S.J., and T. Shippert, 2006: Physically-based global downscaling climate change projections for a full century. *J. Clim.*, **19**, 1589–1604.
- Giannini, A., Y. Kushnir, and M.A. Cane, 2000: Interannual variability of Caribbean rainfall, ENSO and the Atlantic Ocean. *J. Clim.*, **13**, 297–311.
- Giannini, A., M.A. Cane, and Y. Kushnir, 2001: Interdecadal changes in the ENSO teleconnection to the Caribbean region and North Atlantic Oscillation. *J. Clim.*, **14**, 2867–2879.
- Giannini, A., R. Saravanan, and P. Chang, 2003: Oceanic forcing of Sahel rainfall on interannual to interdecadal time scales. *Science*, **302**, 1027–1030.
- Gibelin, A.L., and Déqué, M., 2003: Anthropogenic climate change over the Mediterranean region simulated by a global variable resolution model. *Clim. Dyn.*, **20**, 327–339.
- Giorgi, F., and R. Francesco, 2000: Evaluating uncertainties in the prediction of regional climate change. *Geophys. Res. Lett.*, **27**, 1295–1298.
- Giorgi, F., and L.O. Mearns, 2002: Calculation of average, uncertainty range, and reliability of regional climate changes from AOGCM simulations via the reliability ensemble averaging (REA) method. *J. Clim.*, **15**, 1141–1158.
- Giorgi, F., and L.O. Mearns, 2003: Probability of regional climate change based on the Reliability Ensemble Averaging (REA) method. *Geophys. Res. Lett.*, **30**(12), 1629, doi:10.1029/2003GL017130.
- Giorgi, F., and X. Bi, 2005: Regional changes in surface climate interannual variability for the 21st century from ensembles of global model simulations. *Geophys. Res. Lett.*, **32**, L13701, doi:10.1029/2005GL023002.
- Giorgi, F., X. Bi, and J.S. Pal, 2004: Mean, interannual variability and trends in a regional climate change experiment over Europe. II: climate change scenarios (2071–2100). *Clim. Dyn.*, **23**, 839–858.
- Giorgi, F., J.W. Hurrell, M.R. Marinucci, and M. Beniston, 1997: Elevation signal in surface climate change: A model study. *J. Clim.*, **10**, 288–296.
- Giorgi, F., et al., 2001a: Regional climate information – Evaluation and projections. In: *Climate Change 2001: The Scientific Basis. Contribution of Working Group I to the Third Assessment Report of the Intergovernmental Panel on Climate Change* [Houghton, J.T., et al. (eds.)]. Cambridge University Press, Cambridge, United Kingdom and New York, NY, USA, pp. 583–638.
- Giorgi, F., et al., 2001b: Emerging patterns of simulated regional climatic changes for the 21st century due to anthropogenic forcings. *Geophys. Res. Lett.*, **28**(17), 3317–3320.
- Good, P., and J. Lowe, 2006: Emergent behavior and uncertainty in multi-model climate projections of precipitation trends at small spatial scales. *J. Clim.*, **27**(4), 357–375.
- Goodison, B.E., P.Y.T. Louie, and D. Yang, 1998: *WMO Solid Precipitation Measurement Intercomparison, Final Report*. WMO/TD No.872, World Meteorological Organization, Geneva, 212 pp.
- Govindasamy, B., P.B. Duffy, and J. Coquard, 2003: High resolution simulations of global climate, part 2: Effects of increased greenhouse gases. *Clim. Dyn.*, **21**, 391–404.
- Goyette, S., O. Brasseur, and M. Beniston, 2003: Application of a new wind gust parameterisation: multi-scale case studies performed with the Canadian RCM. *J. Geophys. Res.*, **108**, 4371–4389.
- Graham, L.P., S. Hagemann, S. Jaun, and M. Beniston, 2007: On interpreting hydrological change from regional climate models. *Clim. Change*, doi:10.1007/s10584-006-9217-0.
- Gray, W.M., 1984: Atlantic seasonal hurricane frequency. Part I: El Niño and 30 mb quasi-biennial oscillation influences. *Mon. Weather Rev.*, **112**, 1649–1668.
- Greene, A.M., L. Goddard, and U. Lall, 2006: Probabilistic multimodel regional temperature change projections. *J. Clim.*, **19**, 4326–4343.
- Gregory, J.M., and J.F.B. Mitchell, 1995: Simulation of daily variability of surface temperature and precipitation over Europe in the current and 2×CO₂ climate using the UKMO climate model. *Q. J. R. Meteorol. Soc.*, **121**, 1451–1476.
- Griffiths, G.M., M.J. Salinger, and I. Leleu, 2003: Trends in extreme daily rainfall across the South Pacific and relationship to the South Pacific convergence zone. *Int. J. Climatol.*, **23**, 847–869.
- Groisman, P.Y., et al., 2005: Trends in intense precipitation in the climate record. *J. Clim.*, **18**, 1326–1350.
- Guo, Z., D.H. Bromwich, and J.J. Cassano, 2003: Evaluation of Polar MM5 simulations of Antarctic atmospheric circulation. *Mon. Weather Rev.*, **131**, 384–411.
- Guo, Z., D.H. Bromwich, and K.M. Hines, 2004: Modeled Antarctic precipitation. Part II: ENSO modulation over West Antarctica. *J. Clim.*, **17**, 448–465.
- Gutowski, W.J., et al., 2004: Diagnosis and attribution of a seasonal precipitation deficit in a U.S. regional climate simulation. *J. Hydrometeorol.*, **5**(1), 230–242.
- Haapala, J., H.E.M. Meier, and J. Rinne, 2001: Numerical investigations of future ice conditions in the Baltic Sea. *Ambio*, **30**, 237–244.
- Haarsma, R.J., F. Selten, S. Weber, and M. Kliphuis, 2005: Sahel rainfall variability and response to greenhouse warming. *Geophys. Res. Lett.*, **32**, L17702, doi:10.1029/2005GL023232.
- Hagemann, S., et al., 2004: Evaluation of water and energy budgets in regional climate models applied over Europe. *Clim. Dyn.*, **23**, 547–607.
- Han, J., and J. Roads, 2004: US climate sensitivity simulated with the NCEP Regional Spectral Model. *Clim. Change*, **62**, 115–154, doi:10.1023/B:CLIM.0000013675.66917.15.
- Hansen, J.E., et al., 1998: Climate forcings in the industrial era. *Proc. Natl. Acad. Sci. U.S.A.*, **95**, 12753–12758.
- Hansen, J.W., and T. Mavromatis, 2001: Correcting low-frequency variability bias in stochastic weather generators. *Agr. For. Meteorol.*, **109**, 297–310.
- Hanssen-Bauer, I., E.J. Førland, J.E. Haugen, and O.E. Tveito, 2003: Temperature and precipitation scenarios for Norway: comparison of results from dynamical and empirical downscaling. *Clim. Res.*, **25**(1), 15–27.
- Hanssen-Bauer, I., et al., 2005: Statistical downscaling of climate scenarios over Scandinavia: A review. *Clim. Res.*, **29**, 255–268.
- Hardy, T., L. Mason, A. Astorquia, and B. Harper 2004: *Queensland Climate Change and Community Vulnerability to Tropical Cyclones: Ocean Hazards Assessment*. Report to Queensland Government, 45 pp. +7 appendices, <http://www.longpaddock.qld.gov.au/ClimateChanges/pub/OceanHazards/Stage2LowRes.pdf>.
- Harris, G.R., et al., 2006: Frequency distributions of transient regional climate change from perturbed physics ensembles of general circulation model simulations. *Clim. Dyn.*, **27**, 357–375.
- Hasegawa, A., and S. Emori, 2005: Tropical cyclones and associated precipitation over the Western North Pacific: T106 atmospheric GCM simulation for present-day and doubled CO₂ climates. *Scientific Online Letters on the Atmosphere*, **1**, 145–148.
- Hayhoe, K., et al., 2004: Emissions pathways, climate change, and impacts on California. *Proc. Natl. Acad. Sci. U.S.A.*, **101**, 12422–12427.

- Haylock, M.R., et al., 2006: Downscaling heavy precipitation over the UK: A comparison of dynamical and statistical methods and their future scenarios. *Int. J. Climatol.*, **26**(10), 1397–1415, doi:10.1002/joc.1318.
- Hegerl, G.C., F.W. Zwiers, P.A. Stott, and V.V. Kharin, 2004: Detectability of anthropogenic changes in annual temperature and precipitation extremes. *J. Clim.*, **17**, 3683–3700.
- Held, I.M., et al., 2005: Simulation of Sahel drought in the 20th and 21st centuries. *Proc. Natl. Acad. Sci. U.S.A.*, **102**(50), 17891–17896.
- Hellström, C., D. Chen, C. Achberger, and J. Räisänen, 2001: A comparison of climate change scenarios for Sweden based on statistical and dynamical downscaling of monthly precipitation. *Clim. Res.*, **19**, 45–55.
- Hennessy, K.J., J.M. Gregory, and J.F.B. Mitchell, 1997: Changes in daily precipitation under enhanced greenhouse conditions. *Clim. Dyn.*, **13**, 667–680.
- Hennessy, K.J., et al., 2003: *The Impact of Climate Change on Snow Conditions in Mainland Australia*. CSIRO Atmospheric Research, Aspendale, 47 pp., http://www.cmar.csiro.au/e-print/open/hennessy_2003a.pdf.
- Hennessy, K.J., et al., 2004a: *Climate Change in the Northern Territory*. Consultancy report for the Northern Territory Department of Infrastructure, Planning and Environment by CSIRO Atmospheric Research Climate Impact Group and Melbourne University School of Earth Sciences, Northern Territory Government, Darwin, 65 pp.
- Hennessy, K.J., et al., 2004b: *Climate Change in New South Wales – Part 1: Past Climate Variability and Projected Changes in Average Climate*. Consultancy report for the New South Wales Greenhouse Office by CSIRO Atmospheric Research and Australian Government Bureau of Meteorology, 46 pp., http://www.dar.csiro.au/publications/hennessy_2004b.pdf.
- Hennessy, K.J., et al., 2004c: *Climate Change in New South Wales– Part 2, Projected Changes in Climate Extremes*. Consultancy report for the New South Wales Greenhouse Office. CSIRO Atmospheric Research, Aspendale, 79 pp.
- Hewitson, B.C., and R.G. Crane, 2005: Gridded area-averaged daily precipitation via conditional interpolation. *J. Clim.*, **18**, 41–51.
- Hewitson, B.C., and R.G. Crane, 2006: Consensus between GCM climate change projections with empirical downscaling: precipitation downscaling over South Africa. *Int. J. Climatol.*, **26**, 1315–1337.
- Hewitson, B.C., et al., 2004: *Dynamical Modelling of the Present and Future Climate System*. Technical Report to the Water Research Commission, Report No. 1154/1/04, Pretoria, South Africa.
- Higgins, R.W., and K.C. Mo, 1997: Persistent North Pacific circulation anomalies and the tropical intraseasonal oscillation. *J. Clim.*, **10**, 223–244.
- Hines, K.M., D.H. Bromwich, P.J. Rasch, and M.J. Iacono, 2004: Antarctic clouds and radiation within the NCAR climate models. *J. Clim.*, **17**, 1198–1212.
- Ho, C.-H., J.-J. Baik, J.-H. Kim, and D.Y. Gong, 2004: Interdecadal changes in summertime typhoon tracks. *J. Clim.*, **17**, 1767–1776.
- Hoerling, M.P., J.W. Hurrell, and J. Eischeid, 2006: Detection and attribution of 20th century Northern and Southern African monsoon change. *J. Clim.* **19**(16), 3989–4008.
- Holland, M.M., and C.M. Bitz, 2003: Polar amplification of climate change in the coupled model intercomparison project. *Clim. Dyn.*, **21**, 221–232.
- Holloway, G., and T. Sou, 2002: Has Arctic sea ice rapidly thinned? *J. Clim.*, **15**, 1691–1701.
- Hope, P.K., 2006a: Shifts in synoptic systems influencing southwest Western Australia. *Clim. Dyn.*, **26**, 751–764.
- Hope, P.K., 2006b: Future changes in synoptic systems influencing southwest Western Australia. *Clim. Dyn.*, **26**, 765–780.
- Hori, M.E., and H. Ueda, 2006: Impact of global warming on the East Asian winter monsoon as revealed by nine coupled atmosphere-ocean GCMs. *Geophys. Res. Lett.*, **33**, L03713, doi:10.1029/2005GL024961.
- Hu, Z.Z., L. Bengtsson, and K. Arpe, 2000: Impact of global warming on the Asian winter monsoon in a coupled GCM. *J. Geophys. Res.*, **105**(D4), 4607–4624.
- Hu, Z.Z., S. Yang, and R. Wu, 2003: Long-term climate variations in China and global warming signals. *J. Geophys. Res.*, **108**(D19), 4614, doi:10.1029/2003JD003651.
- Hubbert, G.D., and K.L. McInnes, 1999: A storm surge inundation model for coastal planning and impact studies. *J. Coastal Res.*, **15**, 168–185.
- Huffman, G.J., et al., 2001: Global precipitation at one-degree daily resolution from multisatellite observations. *J. Hydrometeorol.*, **2**, 36–50.
- Hulme, M., and N. Sheard, 1999a: *Climate Change Scenarios for Indonesia*. Climatic Research Unit, Norwich, UK, 6 pp.
- Hulme, M., and N. Sheard, 1999b: *Climate Change Scenarios for the Philippines*. Climatic Research Unit, Norwich, UK, 6 pp.
- Hulme, M., R. Doherty, and T. Ngara, 2001: African climate change: 1900–2100. *Clim. Res.*, **17**, 145–168.
- Hulme, M., et al., 1999: Relative impacts of human-induced climate change and natural variability. *Nature*, **397**, 688–691.
- Huntingford, C., et al., 2003: Regional climate-model predictions of extreme rainfall for a changing climate. *Q. J. R. Meteorol. Soc.*, **129**, 1607–1621.
- Hurrell, J.W., and H. van Loon, 1997: Decadal variations in climate associated with the North Atlantic Oscillation. *Clim. Change*, **36**, 301–326.
- Huth, R., J. Kysely, and M. Dubrovsky, 2001: Time structure of observed, GCM-simulated, downscaled, and stochastically generated daily temperature series. *J. Clim.*, **14**, 4047–4061.
- Im, E.S., E.-H. Park, W.-T. Kwon, and F. Giorgi, 2006: Present climate simulation over Korea with a regional climate model using a one-way double-nested system. *Theor. Appl. Climatol.* **86**, 183–196.
- Imbert, A., and R.E. Benestad, 2005: An improvement of analog model strategy for more reliable local climate change scenarios. *Theor. Appl. Climatol.*, **82**, 245–255.
- Inatsu, M., and M. Kimoto, 2005: Difference of boreal summer climate between coupled and atmosphere-only GCMs. *Scientific Online Letters on the Atmosphere*, **1**, 105–108.
- International CLIVAR Project Office, 2006: *Understanding the Role of the Indian Ocean in the Climate System — Implementation Plan for Sustained Observations*. CLIVAR Publication Series No.100, International CLIVAR Project Office, Southampton, UK, 76 pp.
- IOCI, 2002: *Climate Variability and Change in South West Western Australia*. Technical Report, Indian Ocean Climate Initiative Panel, Perth, Australia, 34 pp.
- IOCI, 2005: *Indian Ocean Climate Initiative Stage 2: Report of Phase 1 Activity*. Indian Ocean Climate Initiative Panel, Perth, Australia, 42 pp., <http://www.ioci.org.au/publications/pdf/2005202-IOCI%20reportvis2.pdf>.
- IPCC, 1996: Technical summary. In: *Climate Change 1995: The Science of Climate Change. Contribution of Working Group I to the Second Assessment Report of the Intergovernmental Panel on Climate Change* [Houghton, J.T., et al. (eds.)]. Cambridge University Press, Cambridge, United Kingdom and New York, NY, USA, pp. 9–49.
- IPCC, 2001: *Climate Change 2001: The Scientific Basis. Contribution of Working Group I to the Third Assessment Report of the Intergovernmental Panel on Climate Change* [Houghton, J.T., et al. (eds.)]. Cambridge University Press, Cambridge, United Kingdom and New York, NY, USA, 881 pp.
- Jacob, D., et al., 2007: An intercomparison of regional climate models for Europe: design of the experiments and model performance. *Clim. Change*, doi: 10.1007/s10584-006-9213-4.
- Jenkins, G.S., G. Adamou, and S. Fongang, 2002: The challenges of modeling climate variability and change in West Africa. *Clim. Change*, **52**, 263–286.

- Jiang, Y.D., 2005: *The Northward Shift of Climatic Belts in China during the Last 50 Years, and the Possible Future Changes*. PhD Thesis, Institute of Atmospheric Physics, China Academy of Science, Beijing, 137 pp.
- Jiao, Y., and D. Caya, 2006: An investigation of summer precipitation simulated by the Canadian regional climate model. *Mon. Weather Rev.*, **134**, 919–932.
- Johannessen, O.M., et al., 2004: Arctic climate change: observed and modelled temperature and sea-ice variability. *Tellus*, **56A**(4), 328.
- Jolly, D., S.P. Harrison, B. Damnati, and E. Bonnefille, 1996: Simulated climate and biomes of Africa during the late Quaternary: comparison with pollen and lake status data. *Quat. Sci. Rev.*, **17**, 629–657.
- Jones, C.D., et al., 2003: Strong carbon cycle feedbacks in a climate model with interactive CO₂ and sulphate aerosols. *Geophys. Res. Lett.*, **30**(9), 1479, doi:10.1029/2003GL016867.
- Jones, P.D., and P.A. Reid, 2001: Assessing future changes in extreme precipitation over Britain using regional climate model integrations. *Int. J. Climatol.*, **21**, 1337–1356.
- Jones, R.G., J.M. Murphy, M. Noguer, and A.B. Keen, 1997: Simulation of climate change over Europe using a nested regional climate model. II: Comparison of driving and regional model responses to a doubling of carbon dioxide. *Q. J. R. Meteorol. Soc.*, **123**, 265–292.
- Jones, R.N., 2000: Managing uncertainty in climate change projections – issues for impact assessment. *Clim. Change*, **45**, 403–419.
- Jones, R.N., et al., 2000: *An Analysis of the Effects of The Kyoto Protocol on Pacific Island Countries, Part Two: Regional Climate Change Scenarios and Risk Assessment Methods*. South Pacific Regional Environment Programme, Apia, Samoa, 68 pp., available from spre@sprep.org.ws.
- Jones, R.N., et al., 2002: Scenarios and projected ranges of change for mean climate and climate variability for the South Pacific. *Asia Pac. J. Environ. Dev.*, **9**(1–2), 1–42.
- Juang, H.M.H., and S.Y. Hong, 2001: Sensitivity of the NCEP regional spectral model to domain size and nesting strategy. *Mon. Weather Rev.*, **129**, 2904–2922.
- Kabat, P., et al., 2002: *Vegetation, Water, Humans and the Climate Change: A New Perspective on an Interactive System*. Springer, Heidelberg, Germany, 566 pp.
- Kamga, A.F., et al., 2005: Evaluating the National Center for Atmospheric Research climate system model over West Africa: Present-day and the 21st century A1 scenario. *J. Geophys. Res.*, **110**(D03106), doi:10.1029/2004JD004689.
- Kanada, S., et al., 2005: Structure of mesoscale convective systems during the late Baiu season in the global warming climate simulated by a non-hydrostatic regional model. *Scientific Online Letters on the Atmosphere*, **1**, 117–120.
- Kang I.-S., et al., 2002: Intercomparison of atmospheric GCM simulated anomalies associated with the 1997/98 El Niño. *J. Clim.*, **15**, 2791–2805.
- Karcher, M.J., R. Gerdes, F. Kauker, and C. Köberle, 2003: Arctic warming: Evolution and spreading of the 1990s warm event in the Nordic seas and the Arctic Ocean. *J. Geophys. Res.*, **108**(C2), 3034, doi:10.1029/2001JC001265.
- Kattsov, V.M., et al., 2007: Simulation and projection of Arctic freshwater budget components by the IPCC AR4 global climate models. *J. Hydrometeorol.*, **8**, in press.
- Katz, R.W., M.B. Parlange, and P. Naveau, 2002: Statistics of extremes in hydrology. *Adv. Water Resour.*, **25**, 1287–1304.
- Katz, R.W., M.B. Parlange, and C. Tebaldi, 2003: Stochastic modelling of the effects of large-scale circulation on daily weather in the southeastern US. *Clim. Change*, **60**, 189–216.
- Keller, F., S. Goyette, and M. Beniston, 2005: Sensitivity analysis of snow cover to climate change scenarios and their impact on plant habitats in alpine terrain. *Clim. Change*, **72**, 299–319.
- Kharin, V.V., and F.W. Zwiers, 2005: Estimating extremes in transient climate change simulations. *J. Clim.*, **18**, 1156–1173.
- Kida, H., T. Koide, H. Sasaki, and M. Chiba, 1991: A new approach for coupling a limited area model to a GCM for regional climate simulations. *J. Meteorol. Soc. Japan.*, **69**, 723–728.
- Kim, J., T.-K. Kim, R.W. Arritt, and N.L. Miller, 2002: Impacts of increased atmospheric CO₂ on the hydroclimate of the Western United States. *J. Clim.*, **15**(14), 1926–1942.
- Kimoto, M., 2005: Simulated change of the east Asian circulation under global warming scenario. *Geophys. Res. Lett.*, **32**, L16701, doi:10.1029/2005GRL023383.
- Kimoto, M., N. Yasutomi, C. Yokoyama, and S. Emori, 2005: Projected changes in precipitation characteristics around Japan under the global warming. *Scientific Online Letters on the Atmosphere*, **1**, 85–88.
- Kitoh, A., and T. Uchiyama, 2006: Changes in onset and withdrawal of the East Asian summer rainy season by multi-model global warming experiments. *J. Meteorol. Soc. Japan*, **84**, 247–258.
- Kitoh, A., M. Hosaka, Y. Adachi and K. Kamiguchi, 2005: Future projections of precipitation characteristics in East Asia simulated by the MRI CGCM2. *Adv. Atmos. Sci.*, **22**(4), 467–478.
- Kjellström, E., et al., 2007: Variability in daily maximum and minimum temperatures: recent and future changes over Europe. *Clim. Change*, doi: 10.1007/s10584-006-9220-5.
- Kleinn, J., et al., 2005: Hydrological simulations in the Rhine basin, driven by a regional climate model. *J. Geophys. Res.*, **110**, D04102, doi:10.1029/2004JD005143.
- Knippertz, P., U. Ulbrich, and P. Speth, 2000: Changing cyclones and surface wind speeds over the North-Atlantic and Europe in a transient GHG experiment. *Clim. Res.*, **15**, 109–122.
- Knutson, T.R., and S. Manabe, 1995: Time-mean response over the tropical Pacific to increased CO₂ in a coupled ocean-atmosphere model. *J. Clim.*, **8**, 2181–2199.
- Knutson, T.R., and R.E. Tuleya, 2004: Impacts of CO₂-induced warming on simulated hurricane intensities and precipitation: sensitivity to the choice of climate model and convective parameterization. *J. Clim.*, **17**, 3477–3495.
- Krinner, G., C. Genthon, Z. Li, and P.L. Van, 1997: Studies of the Antarctic climate with a stretched-grid general circulation model. *J. Geophys. Res.*, **102**, 13731–13745.
- Krishna Kumar, K., B. Rajagopalan, and M.A. Cane, 1999: On the weakening relationship between the Indian monsoon and ENSO. *Science*, **284**, 2156–2159.
- Krishna Kumar, K., et al., 2003: Future scenarios of extreme rainfall and temperature over India. In: *Proceedings of the Workshop on Scenarios and Future Emissions, Indian Institute of Management (IIM), Ahmedabad, July 22, 2003*. NATCOM Project Management Cell, Ministry of Environment and Forests, Government of India, New Delhi, pp. 56–68.
- Kumagi, T., G.G. Katul, and A. Porporato, 2004: Carbon and water cycling in a Bornean tropical rainforest under current and future climate scenarios. *Adv. Water Resour.*, **27**, 1135–1150.
- Kurihara, K., et al., 2005: Projection of climatic change over Japan due to global warming by high-resolution regional climate model in MRI. *Scientific Online Letters on the Atmosphere*, **1**, 97–100.
- Kusunoki, S., et al., 2006: Change of Baiu rain band in global warming projection by an atmospheric general circulation model with a 20-km grid size. *J. Meteorol. Soc. Japan*, **84**(4), 581–611.
- Kutzbach, J.E., G. Bonan, J. Foley, and S. Harrison, 1996: Vegetation and soil feedbacks on the response of the African monsoon to forcing in the early to middle Holocene. *Nature*, **384**, 623–626.
- Kwok, R., and J.C. Comiso, 2002a: Spatial patterns of variability in Antarctic surface temperature: Connections to the Southern Hemisphere annular mode and the Southern Oscillation. *Geophys. Res. Lett.*, **29**(14), 1705, doi:10.1029/2002GL015415.
- Kwok, R., and J.C. Comiso, 2002b: Southern Ocean climate and sea ice anomalies associated with the Southern Oscillation. *J. Clim.*, **15**, 487–501.

- Kwon, W.-T., et al., 2003: *The Development of Regional Climate Change Scenario for the National Climate Change Report (II)*. METRI Technical Report MR030CR09, Meteorological Research Institute, Seoul, Korea, 502 pp (in Korean).
- Kwon, W.-T., et al., 2005: *The Application of Regional Climate Change Scenario of the National Climate Change Report (I)*. METRI Technical Report MR050C03, Meteorological Research Institute, Seoul, Korea, 408 pp (in Korean).
- Lal, M., 2004: Climate change and small island developing countries of the South Pacific. *Fijian Studies*, **2**(1), 1–15.
- Lal, M., and H. Harasawa, 2001: Future climate change scenarios for Asia as inferred from selected coupled atmosphere-ocean global climate models. *J. Meteorol. Soc. Japan*, **79**, 219–227.
- Lal, M., H. Harasawa, and K. Takahashi, 2002: Future climate change and its impacts over small island states. *Clim. Res.*, **19**, 179–192.
- Lal, M., et al., 2001: Future climate change: Implications for Indian summer monsoon and its variability. *Curr. Sci.*, **81**, 1196–1207.
- Lamb, P.J., and R.A. Pepler, 1987: North Atlantic Oscillation: Concept and an application. *Bull. Am. Meteorol. Soc.*, **68**(10), 1218–1225.
- Lambert, S.J., and J.C. Fyfe, 2006: Changes in winter cyclone frequencies and strengths simulated in enhanced greenhouse warming experiments: results from the models participating in the IPCC diagnostic exercise. *J. Clim. Dyn.*, **26**, 713–728.
- Laprise, R., 2003: Resolved scales and nonlinear interactions in limited-area models. *J. Atmos. Sci.*, **60**(5), 768–779.
- Latif, M., et al., 2001: ENSIP: The El Niño Simulation Intercomparison Project. *Clim. Dyn.*, **18**, 255–276.
- Lau, K.M., and J. Zhou, 2003: Responses of the South American Summer Monsoon climate system to ENSO during 1997–99. *Int. J. Climatol.*, **23**, 529–539.
- Leckebusch, G.C., and U. Ulbrich, 2004: On the relationship between cyclones and extreme windstorm events over Europe under climate change. *Global Planet. Change*, **44**, 181–193.
- Leckebusch, G.C., et al., 2007: Analysis of frequency and intensity of winter storm events in Europe on synoptic and regional scales from a multi-model perspective. *Clim. Res.*, **31**, 59–74.
- Lenderink, G., A. van Ulden, B. van den Hurk, and E. van Meijgaard, 2007: Summertime inter-annual temperature variability in an ensemble of regional model simulations: analysis of the surface energy budget. *Clim. Change*, doi: 10.1007/s10584-006-9229-9
- Leung, L.R., L.O. Mearns, F. Giorgi, and R.L. Wilby, 2003: Regional climate research: needs and opportunities. *Bull. Am. Meteorol. Soc.*, **84**, 89–95.
- Leung, L.R., et al., 2004: Mid-century ensemble regional climate change scenarios for the western United States. *Clim. Change*, **62**, 75–113.
- L'Heureux, M.L., and D.W.J. Thompson, 2006: Observed relationships between the El-Niño/Southern Oscillation and the extratropical zonal mean circulation. *J. Clim.*, **19**, 276–287.
- L'Heureux, M.L., et al., 2004: Atmospheric circulation influences on seasonal precipitation patterns in Alaska during the latter 20th century. *J. Geophys. Res.*, **109**(6), D06106, doi:10.1029/2003JD003845.
- Liang, X.Z., et al., 2004: Regional climate model simulation of U.S. precipitation during 1982–2002. Part I: Annual cycle. *J. Clim.*, **17**(18), 3510–3529.
- Liang, X.Z., et al., 2006: Regional climate model downscaling of the U.S. summer climate and future change. *J. Geophys. Res.*, **111**, D10108, doi:10.1029/2005JD006685.
- Liebmann, B., et al., 2004: An observed trend in Central South American precipitation. *J. Clim.*, **17**, 4357–4367.
- Lintner, B.R., and J.C.H. Chiang, 2005: Reorganization of tropical climate during El Niño: a weak temperature gradient approach. *J. Clim.*, **18**(24), 5312–5329.
- Lionello, P., F. Dalan, and E. Elvini, 2002: Cyclones in the Mediterranean region: the present and the doubled CO₂ climate scenarios. *Clim. Res.*, **22**, 147–159.
- Lionello, P., E. Elvini, and A. Nizzero, 2003: Ocean waves and storm surges in the Adriatic Sea: intercomparison between the present and the doubled CO₂ climate scenarios. *Clim. Res.*, **23**, 217–231.
- Liu, J., et al., 2005: Comparison of surface radiative flux data sets over the Arctic Ocean. *J. Geophys. Res.*, **110**, C02015, doi:10.1029/2004JC002381.
- Lopez, A., et al., 2006: Two approaches to quantifying uncertainty in global temperature changes. *J. Clim.*, **19**, 4785–4796.
- Lorant, V., and J-F. Royer, 2001: Sensitivity of equatorial convection to horizontal resolution in aquaplanet simulations with a variable-resolution GCM. *Mon. Weather Rev.*, **129**(11), 2730–2745.
- Lorenz, P., and D. Jacob, 2005: Influence of regional scale information on the global circulation: a two-way nested climate simulation. *Geophys. Res. Lett.*, **32**, L18706, doi:10.1029/2005GL023351.
- Lowe, J.A., and J.M. Gregory, 2005: The effects of climate change on storm surges around the United Kingdom. *Philos. Trans. R. Soc. London Ser. A*, **363**, 1313–1328.
- Lowe, J.A., J.M. Gregory, and R.A. Flather, 2001: Changes in the occurrence of storm surges around the United Kingdom under a future climate scenario using a dynamic storm surge model driven by the Hadley Centre climate models. *Clim. Dyn.*, **18**(3–4), 179–188.
- Lu, J., and T.L. Delworth, 2005: Oceanic forcing of late 20th century Sahel drought. *Geophys. Res. Lett.*, **32**, L22706, doi:10.1029/2005GL023316.
- Lynch, A., P. Uotila, and J.J. Cassano, 2006: Changes in synoptic weather patterns in the polar regions in the 20th and 21st centuries, Part 2: Antarctic. *Int. J. Climatol.*, **26**, 1181–2119.
- Lynch, A.H., E.N. Cassano, J.J. Cassano, and L. Lestak, 2003: Case studies of high wind events in Barrow, Alaska: Climatological context and development processes. *Mon. Weather Rev.*, **131**, 719–732.
- Lynch, A.H., J.A. Curry, R.D. Brunner, and J.A. Maslanik, 2004: Toward an integrated assessment of the impacts of extreme wind events on Barrow, Alaska. *Bull. Am. Meteorol. Soc.*, **85**, 209–221.
- Mabuchi, K., Y. Sato, and H. Kida, 2002: Verification of the climatic features of a regional climate model with BAIM. *J. Meteorol. Soc. Japan*, **80**(4), 621–644.
- Mabuchi, K., Y. Sato, and H. Kida, 2005a: Climatic impact of vegetation change in the Asian tropical region. Part I: Case of the Northern Hemisphere summer. *J. Clim.*, **18**(3), 410–428.
- Mabuchi, K., Y. Sato, and H. Kida, 2005b: Climatic impact of vegetation change in the Asian tropical region. Part II: Case of the Northern Hemisphere winter and impact on the extratropical circulation. *J. Clim.*, **18**(3), 429–446.
- Magaña, V., and E. Caetano, 2005: Temporal evolution of summer convective activity over the Americas warm pools. *Geophys. Res. Lett.*, **32**, L02803, doi:10.1029/2004GL021033.
- Magaña, V., J.A. Amador, and S. Medina, 1999: The mid-summer drought over Mexico and Central America. *J. Clim.*, **12**, 1577–1588.
- Manabe, S., and R.T. Wetherald, 1987: Large-scale changes of soil wetness induced by an increase in atmospheric carbon dioxide. *J. Atmos. Sci.*, **44**, 1211–1235.
- Marengo, J.A., and T. Ambrizzi, 2006: Use of regional climate models in impacts assessments and adaptation studies from continental to regional and local scales. In: *Proceedings of the 8th International Conference on Southern Hemisphere Meteorology and Oceanography (ICSHMO), Foz do Iguaçu, Brazil, 24-28 April 2006*. Brazilian Institute for Space Research (INPE), São José dos Campos, pp. 291–296.
- Marland, G., et al., 2003: The climatic impacts of land surface change and carbon management, and the implications for climate-change mitigation policy. *Clim. Policy*, **3**, 149–157.
- Martin E., E. Brun, and Y. Durand, 1994: Sensitivity of the French Alps snow cover to the variation of climatic variables. *Ann. Geophys.*, **12**, 469–477.
- Martinez-Castro, D., et al., 2006: Sensitivity studies of the RegCM-3 simulation of summer precipitation, temperature and local wind field in the Caribbean region. *Theor. Appl. Climatol.*, **86**, 5–22.

- Martis, A., G.J. van Oldenborgh, and G. Burgers, 2002: Predicting rainfall in the Dutch Caribbean – More than El Niño? *Int. J. Climatol.*, **22**, 1219–1234.
- Maslanik, J.A., A.H. Lynch, M.C. Serreze, and W. Wu, 2000: A case study of regional climate anomalies in the Arctic: performance requirements for a coupled model. *J. Clim.*, **13**, 383–401.
- Maslowski, W., et al., 2004: On climatological mass, heat, and salt transports through the Barents Sea and Fram Strait from a pan-Arctic coupled ice-ocean model simulation. *J. Geophys. Res.*, **109**, C03032, doi:10.1029/2001JC001039.
- Massom, R.A., et al., 2004: Precipitation over the interior East Antarctic ice sheet related to midlatitude blocking-high activity. *J. Clim.*, **17**, 1914–1928.
- Matulla C., H. Scheffinger, A. Menzel, and E. Koch, 2003: Exploring two methods for statistical downscaling of Central European phenological time series. *Int. J. Biometeorol.*, **48**, 56–64.
- May, W., 2004a: Simulation of the variability and extremes of daily rainfall during the Indian summer monsoon for present and future times in a global time-slice experiment. *Clim. Dyn.*, **22**, 183–204.
- May, W., 2004b: Potential of future changes in the Indian summer monsoon due to greenhouse warming: analysis of mechanisms in a global time-slice experiment. *Clim. Dyn.*, **22**, 389–414.
- May, W., and E. Roeckner, 2001: A time-slice experiment with the ECHAM4 AGCM at high resolution: The impact of horizontal resolution on annual mean climate change. *Clim. Dyn.*, **17**, 407–420.
- Maynard, K., and J.-F. Royer, 2004a: Effects of realistic land-cover change on a greenhouse-warmed African climate. *Clim. Dyn.*, **22**(4), 343–358.
- Maynard, K., and J.-F. Royer, 2004b: Sensitivity of a general circulation model to land surface parameters in African tropical deforestation experiments. *Clim. Dyn.*, **22**(6/7), 555–572.
- Maynard, K., J.-F. Royer, and F. Chauvin, 2002: Impact of greenhouse warming on the West African summer monsoon. *Clim. Dyn.*, **19**, 499–514.
- McBride, J.L., and N. Nicholls, 1983: Seasonal relationships between Australian rainfall and the Southern Oscillation. *Mon. Weather Rev.*, **111**, 1998–2004.
- McBride, J.L., M.R. Haylock, and N. Nicholls, 2003: Relationships between the Maritime Continent heat source and the El Niño-Southern Oscillation phenomenon. *J. Clim.*, **16**, 2905–2914.
- McGregor, J.L., 2004: Regional climate modelling activities at CSIRO. In: *Symposium on Water Resource and its Variability in Asia in the 21st Century, 1-2 March 2004, Epochal Tsukuba (International Congress Center), Tsukuba, Ibaraki, Japan*. Meteorological Research Institute, Japan Meteorological Agency, Tsukuba, Japan, pp. 68–71.
- McGregor, J.L., and M.R. Dix, 2001: The CSIRO conformal-cubic atmospheric GCM. In: *IUTAM Symposium on Advances in Mathematical Modelling of Atmosphere and Ocean Dynamics* [Hodnett, P.F. (ed.)]. Kluwer Academic, Dordrecht, pp. 307–315.
- McGregor, J.L., and K.C. Nguyen, 2003: Simulations of the East Asian and Australian monsoons using a variable-resolution model. In: *Proceedings of the 2nd Workshop on Regional Climate Modeling for Monsoon System, Yokohama, Japan*. GAME Publication No. 39, FRSGC and GAME International Science Panel, Yokohama, pp. 117–120.
- McGregor, J.L., J.J. Katzfey, and K.C. Nguyen, 1998: *Fine Resolution Simulations of Climate Change for Southeast Asia*. Final report for a research project commissioned by Southeast Asian Regional Committee for START (SARCS), CSIRO Atmospheric Research, Aspendale, Vic., 35 pp. + 3 CD-ROMs.
- McGregor, J.L., K.C. Nguyen, and J.J. Katzfey, 2002: Regional climate simulations using a stretched-grid global model. In: *Research Activities in Atmospheric and Oceanic Modelling* [Ritchie, H. (ed.)]. Report No. 32, WMO/TD-No. 1105, World Meteorological Organisation, Geneva, pp. 15–16.
- McGuffie, K., et al., 1995: Global climate sensitivity to tropical deforestation. *Global Planet. Change*, **10**, 97–128.
- McInnes, K.L., et al., 2003: *Assessment of climate change, impacts and possible adaptation strategies relevant to South Australia*. Consultancy report undertaken for the South Australian Government by the Climate Impact Group, CSIRO Atmospheric Research, Aspendale, VIC, Australia, 61pp. http://www.cmar.csiro.au/e-print/open/mcInnes_2003a.pdf
- McInnes, K. L., et al. (2004). *Climate change in Tasmania*. A report undertaken for Hydro Tasmania by the Climate Impact GroupC/0919. CSIRO Atmospheric Research, Aspendale, Vic, 49 pp., http://www.cmar.csiro.au/e-print/open/mcInnesskl_2004a.pdf
- McInnes, K. L., et al. (2005). *Climate change in Eastern Victoria: Stage 2 report: the effect of climate change on storm surges*. A project undertaken for the Gippsland Coastal Board. CSIRO Marine and Atmospheric Research, Aspendale, Vic.: 37 pp. http://www.cmar.csiro.au/e-print/open/mcInnes_2005b.pdf
- Mearns, L.O., et al., 2005: NARCCAP, North American Regional Climate Change Assessment Program, A multiple AOGCM and RCM climate scenario project over North America. *Preprints of the American Meteorological Society 16th Conference on Climate Variations and Change. 9-13 January, 2005*. Paper J6.10, American Meteorological Society, Washington, DC, pp. 235–238.
- Meehl, G.A., and C. Tebaldi, 2004: More intense, more frequent, and longer lasting heat waves in the 21st century. *Science*, **305**, 994–997.
- Meehl, G.A., J.M. Arblaster, and C. Tebaldi, 2005: Understanding future patterns of increased precipitation intensity in climate model simulations. *Geophys. Res. Lett.*, **32**, L18719, doi:10.1029/2005GL023680.
- Meehl, G.A., et al., 2006: Climate change in the 20th and 21st centuries and climate change commitment in the CCSM3. *J. Clim.*, **19**, 2597–2616.
- Meier, H.E.M., 2002: Regional ocean climate simulations with a 3D ice-ocean model for the Baltic Sea. Part 2: results for sea ice. *Clim. Dyn.*, **19**, 255–266.
- Meier, H.E.M., 2006: Baltic Sea climate in the late twenty-first century: a dynamical downscaling approach using two global models and two emission scenarios. *Clim. Dyn.*, **27**(1), 39–68, doi:10.1007/s00382-006-0124-x.
- Meier, H.E.M., R. Döscher, and A. Halkka, 2004: Simulated distributions of Baltic sea-ice in warming climate and consequences for the winter habitat of the Baltic Sea ringed seal. *Ambio*, **33**, 249–256.
- Meleshko, V.P., et al., 2004: Anthropogenic climate changes in Northern Eurasia in the 21st century. *Russ. Meteorol. Hydrol.*, **7**, 5–26.
- Menéndez, C.G., A.C. Saulo, and Z.-X. Li, 2001: Simulation of South American wintertime climate with a nesting system. *Clim. Dyn.*, **17**, 219–231.
- Menéndez, C.G., M.F. Cabré, and M.N. Nuñez, 2004: Interannual and diurnal variability of January precipitation over subtropical South America simulated by a regional climate model. *CLIVAR Exchanges*, **29**, 1–3.
- Miguez-Macho, G., G.L. Stenchikov, and A. Robock, 2004: Spectral nudging to eliminate the effects of domain position and geometry in regional climate model simulations. *J. Geophys. Res.*, **109**, D13104, doi:10.1029/2003JD004495.
- Mikolajewicz, U., et al., 2005: Simulating Arctic sea ice variability with a coupled regional atmosphere-ocean-sea ice model. *Meteorol. Z.*, **14**, 793–800.
- Min, S.K., E.H. Park, and W.T. Kwon, 2004: Future projections of East Asian climate change from Multi-AOGCM ensembles of IPCC SRES scenario simulations. *J. Meteorol. Soc. Japan*, **82**(4), 1187–1211.
- Ministry for the Environment, 2004: *Climate Change Effects and Impacts Assessment: A Guidance Manual for Local Government in New Zealand*. New Zealand Climate Change Office, Ministry for the Environment, Wellington, <http://www.climatechange.govt.nz/resources/local-govt/effects-impacts-may04/index.html>.
- Misra, V., P.A. Dirmeyer, and B.P. Kirtman, 2003: Dynamic downscaling of seasonal simulations over South America. *J. Clim.*, **16**, 103–117.
- Mitchell, T.D., 2003: Pattern scaling: an examination of the accuracy of the technique for describing future climates. *Clim. Change*, **60**(3), 217–242.

- Mizuta, R., et al., 2005: Changes in extremes indices over Japan due to global warming projected by a global 20-km-mesh atmospheric model. *Scientific Online Letters on the Atmosphere*, **1**, 153–156.
- Mizuta, R., et al., 2006: 20km-mesh global climate simulations using JMA-GSM model. Mean climate states. *J. Meteorol. Soc. Japan.*, **84**, 165–185.
- Mo, K.C., and J. Nogués-Paegle, 2001: The Pacific-South American modes and their downstream effects. *Int. J. Climatol.*, **21**, 1211–1229.
- Moise, A., R. Colman, and H. Zhang, 2005: Coupled model simulations of current Australian surface climate and its changes under greenhouse warming: An analysis of 18 CMIP2 models. *Aust. Meteorol. Mag.*, **54**, 291–307.
- Monaghan, A.J., D.H. Bromwich, and S.-H. Wang, 2006: Recent trends in Antarctic snow accumulation from Polar MM5 simulations. *Philos. Trans. R. Soc. London Ser. A.*, **364**, 1683–1708.
- Mote, P.W., and N.J. Mantua, 2002: Coastal upwelling in a warmer future. *Geophys. Res. Lett.*, **29**(23), 2138, doi:10.1029/2002GL016086.
- Mullan, A.B., 1995: On the linearity and stability of Southern Oscillation - climate relationships for New Zealand. *Int. J. Climatol.*, **15**, 1365–1386.
- Mullan, A.B., D.S. Wratt, and J.A. Renwick, 2001a: Transient model scenarios of climate changes for New Zealand. *Weather and Climate*, **21**, 3–34.
- Mullan, A.B., M.J. Salinger, C.S. Thompson, and A.S. Porteous, 2001b: The New Zealand climate: present and future. In: *Effects of Climate Change and Variation in New Zealand: An Assessment using the CLIMACTS System* [Warrick, R.A., G.J. Kenny, and J.J. Harman, (eds.)]. International Global Change Institute, University of Waikato, pp. 11–31.
- Mullan, B., A. Porteous, D. Wratt, and M. Hollis, 2005: *Changes in Drought Risk with Climate Change*. NIWA Client Report WLG2005-23, National Institute for Water and Atmosphere Research, Wellington, New Zealand, 68 pp.
- Murphy, J.M., et al., 2004: Quantification of modelling uncertainties in a large ensemble of climate change simulations. *Nature*, **430**, 768–772.
- Neelin, J.D., and H. Su, 2005: Moist teleconnection mechanisms for the tropical South American and Atlantic sector. *J. Clim.*, **18**(18), 3928–3950.
- Neelin, J.D., et al., 2006: Tropical drying trends in global warming models and observations. *Proc. Natl. Acad. Sci. U.S.A.*, **103**, 6110–6115.
- New, M., and M. Hulme, 2000: Representing uncertainty in climate change scenarios: a Monte Carlo approach. *Integr. Assess. J.*, **1**, 203–213.
- New, M., B.C. Hewitson, C. Jack, and R. Washington, 2003: Sensitivity of southern African rainfall to soil moisture. *CLIVAR Exchanges*, **27**, 45–47.
- Nguyen, K.C., and K.J.E. Walsh, 2001: Interannual, decadal, and transient greenhouse simulation of tropical cyclone-like vortices in a regional climate model of the South Pacific. *J. Clim.*, **14**(13), 3043–3054.
- Nicolini, M., et al., 2002: January and July regional climate simulation over South America. *J. Geophys. Res.*, **107**(D22), 4637, doi:10.1029/2001JD000736.
- Nobre, P., A. Moura, and L. Sun, 2001: Dynamic downscaling of seasonal climate prediction over Nordeste Brazil with ECHAM3 and NCEP's regional spectral models at IRI. *Bull. Am. Meteorol. Soc.*, **82**, 2787–2796.
- Noone, D., and I. Simmonds, 2002: Annular variations in moisture transport mechanisms and the abundance of delta O-18 in Antarctic snow. *J. Geophys. Res.*, **107**, 4742, doi:10.1029/2002JD002262.
- Oh, J-H et al., 2004: Regional climate simulation for Korea using dynamic downscaling and statistical adjustment. *J. Meteorol. Soc. Japan*, **82**(6), 1629–1643.
- Oleson, K.W., G.B. Bonan, S. Levis, and M. Vertenstein, 2004: Effects of land use change on U.S. climate: Impact of surface datasets and model biogeophysics. *Clim. Dyn.*, **23**, 117–132.
- Oouchi, K., et al., 2006: Tropical cyclone climatology in a global-warming climate as simulated in a 20 km-mesh global atmospheric model: Frequency and wind intensity analyses. *J. Meteorol. Soc. Japan*, **84**, 259–276.
- Osborn, T.J., et al., 1999: Evaluation of the North Atlantic Oscillation as simulated by a coupled climate model. *Clim. Dyn.*, **15**, 685–702.
- Paeth, H., and A. Hense, 2004: SST versus climate change signals in West African rainfall: 20th-century variations and future projections. *Clim. Change*, **65**(1–2): 179–208.
- Paeth, H., K. Born, D. Jacob, and R. Podzun, 2005: Regional dynamic downscaling over West Africa: model validation and comparison of wet and dry years. *Meteorol. Z.*, **14**(3), 349–367.
- Pal, J.S., F. Giorgi, and X. Bi, 2004: Consistency of recent European summer precipitation trends and extremes with future regional climate projections. *Geophys. Res. Lett.*, **31**, L13202, doi:10.1029/2004GL019836.
- Palmer, T.N., 1986: Influence of the Atlantic, Pacific and Indian Oceans on Sahel rainfall. *Nature*, **322**, 251–253.
- Palutikof, J.P., C.M. Goodess, S.J. Watkins, and T. Holt, 2002: Generating rainfall and temperature scenarios at multiple sites: examples from the Mediterranean. *J. Clim.*, **15**, 3529–3548.
- Pan, Z., E.S. Takle, and F. Otiemo, 2001: Evaluation of uncertainties in regional climate change simulations. *J. Geophys. Res.*, **106**(D16), 17735–17752.
- Pan, Z., M. Segal, R.W. Arritt, and E.S. Takle, 2004: On the potential change in solar radiation over the US due to increases of atmospheric greenhouse gases. *Renew. Energy*, **29**(11), 1923–1928.
- Pant, G.B., and K. Rupa Kumar, 1997: *Climates of South Asia*. John Wiley & Sons, Chichester, 320 pp.
- Pavolonis, M.J., J.R. Key, and J.J. Cassano, 2004: A study of the Antarctic surface energy budget using a polar regional atmospheric model forced with satellite-derived cloud properties. *Mon. Weather Rev.*, **132**, 654–661.
- Peterson, T.C., et al., 2002: Recent changes in climate extremes in the Caribbean region. *J. Geophys. Res.*, **107**(D21), 4601, doi:10.1029/2002JD002251.
- Pielke, R.A. Sr., et al., 2002: The influence of land-use change and landscape dynamics on the climate system – Relevance to climate change policy beyond the radiative effect of greenhouse gases. *Philos. Trans. R. Soc. London Ser. A*, **360**, 1705–1719.
- Pinto, J.G., T. Spanghel, U. Ulbrich, and P. Speth, 2006: Assessment of winter cyclone activity in a transient ECHAM4-OPYC3 GHG experiment. *Meteorol. Z.*, **15**, 279–291.
- Pitman, A.J., and B.J. McAvaney, 2004: Impact of varying the complexity of the land surface energy balance on the sensitivity of the Australian climate to increasing carbon dioxide. *Clim. Res.*, **25**(3), 191–203.
- Plummer, D.A., et al., 2006: Climate and climate change over North America as simulated by the Canadian Regional Climate Model. *J. Clim.*, **19**, 3112–3132.
- Polyakov, I.V., et al., 2003a: Long-term ice variability in Arctic marginal seas. *J. Clim.*, **16**, 2078–2085.
- Polyakov, I.V., et al., 2003b: Variability and trends of air temperature and pressure in the maritime Arctic, 1875–2000. *J. Clim.*, **16**, 2067–2077.
- Pope, V.D., and R.A. Stratton, 2002: The processes governing resolution sensitivity in a climate model. *Clim. Dyn.*, **19**, 211–236.
- Power, S., C. Folland, A. Colman, and V. Mehta, 1999: Inter-decadal modulation of the impact of ENSO on Australia. *Clim. Dyn.*, **15**, 319–324.
- Power, S., et al., 1998: Australian temperature, Australian rainfall, and the Southern Oscillation, 1910–1996: Coherent variability and recent changes. *Aust. Meteorol. Mag.*, **47**, 85–101.
- Pryor, S.C., R.J. Barthelmie, and E. Kjellström, 2005a: Potential climate change impact on wind energy resources in northern Europe: Analyses using a regional climate model. *Clim. Dyn.*, **25**, 815–835.

- Pryor, S.C., J.T. School, and R.J. Barthelmie, 2005b: Potential climate change impacts on wind speeds and wind energy density in northern Europe: Results from empirical downscaling of multiple AOGCMs. *Clim. Res.*, **29**, 183–198.
- Räisänen, J., 2001: Hiilidioksidin lisääntymisen vaikutus Pohjois-Euroopan ilmastoon globaaleissa ilmastomalleissa (The impact of increasing carbon dioxide on the climate of northern Europe in global climate models). *Terra*, **113**, 139–151.
- Räisänen, J., 2002: CO₂-induced changes in interannual temperature and precipitation variability in 19 CMIP2 experiments. *J. Clim.*, **15**, 2395–2411.
- Räisänen, J., 2005: CO₂-induced impact of increasing CO₂ on monthly-to-annual precipitation extremes: analysis of the CMIP2 experiments. *Clim. Dyn.*, **24**, 309–323.
- Räisänen, J., and R. Joellsson, 2001: Changes in average and extreme precipitation in two regional climate model experiments. *Tellus*, **53A**, 547–566.
- Räisänen, J., and T.N. Palmer, 2001: A probability and decision-model analysis of a multi-model ensemble of climate change simulations. *J. Clim.*, **14**, 3212–3226.
- Räisänen, J., and H. Alexandersson, 2003: A probabilistic view on recent and near future climate change in Sweden. *Tellus*, **55A**, 113–125.
- Räisänen, J., et al., 2003: *GCM Driven Simulations of Recent and Future Climate with the Rossby Centre Coupled Atmosphere – Baltic Sea Regional Climate Model RCAO*. Reports Meteorology and Climatology 101, Swedish Meteorological and Hydrological Institute, Norrköping, Sweden, 61 pp.
- Räisänen, J., et al., 2004: European climate in the late 21st century: regional simulations with two driving global models and two forcing scenarios. *Clim. Dyn.*, **22**, 13–31.
- Rajendran, K., A. Kitoh, and S. Yukimoto, 2004: South and East Asian summer monsoon climate and variation in the MRI coupled model (MRI-CGM2). *J. Clim.*, **17**, 763–782.
- Ramanathan, V., et al., 2005: Atmospheric brown clouds: Impacts on South Asian climate and hydrological cycle. *Proc. Natl. Acad. Sci. U.S.A.*, **102**(15), 5326–5333.
- Raphael, M.N., and M.M. Holland, 2006: Twentieth century simulation of the Southern hemisphere climate in coupled models. Part 1: Large-scale circulation variability. *Clim. Dyn.*, **26**, 217–228, doi:10.1007/s00382-005-0082-8.
- Rauthe, M., and H. Paeth, 2004: Relative importance of Northern Hemisphere circulation modes in predicting regional climate change. *J. Clim.*, **17**, 4180–4189.
- Reason, C., and A. Keibel, 2004: Tropical Cyclone Eline and its unusual penetration and impacts over the southern African mainland. *Weather Forecasting*, **19**(5), 789–805.
- Reason, C.J.C., and M. Rouault, 2005: Links between the Antarctic Oscillation and winter rainfall over western South Africa. *Geophys. Res. Lett.*, **32**, L07705, doi:10.1029/2005GL022419.
- Renwick, J.A., 2002: Southern Hemisphere circulation and relations with sea ice and sea surface temperature. *J. Clim.*, **15**, 3058–3068.
- Rinke, A., and K. Dethloff, 2000: On the sensitivity of a regional Arctic climate model to initial and boundary conditions. *Clim. Res.*, **14**(2), 101–113.
- Rinke, A., et al., 2003: A case study of the anomalous Arctic sea ice conditions during 1990: Insights from coupled and uncoupled regional climate model simulations. *J. Geophys. Res.*, **108**, 4275, doi:10.1029/2002JD003146.
- Rinke, A., et al., 2006: Evaluation of an ensemble of Arctic regional climate models: Spatial patterns and height profiles. *Clim. Dyn.*, **26**(5), 459–472, doi:10.1007/s00382-005-0095-3.
- RIVM (Rijks Instituut voor Volksgezondheid en Milieu), 2002: *The IMAGE 2.2 Implementation of the SRES Scenarios: A Comprehensive Analysis of Emissions, Climate Change and Impacts in the 21st Century*. CD-ROM, <http://www.rivm.nl/bibliotheek/rapporten/481508018.html>.
- Roads, J., et al., 2003: International Research Institute/Applied Research Centers (IRI/ARCs) regional model intercomparison over South America. *J. Geophys. Res.*, **108**(D14), 4425, doi:10.1029/2002jd003201.
- Robertson, A.W., J.D. Farrara, and C.R. Mechoso, 2003: Simulations of the atmospheric response to South Atlantic sea surface temperature anomalies. *J. Clim.*, **16**, 2540–2551.
- Rockel, B., and K. Woth, 2007: Future changes in near surface wind speed extremes over Europe from an ensemble of RCM simulations. *Clim. Change*, doi: 10.1007/s10584-006-9227-y.
- Rojas, M., and A. Seth, 2003: Simulation and sensitivity in a nested modeling system for South America. Part II: GCM boundary forcing. *J. Clim.*, **16**, 2454–2471.
- Rotstayn, L.D., and U. Lohmann, 2002: Tropical rainfall trends and the indirect aerosol effect. *J. Clim.*, **15** (15), 2103–2116.
- Rowell, D.P., 2003: The impact of Mediterranean SSTs on the Sahelian rainfall season. *J. Clim.*, **16** (5), 849–862.
- Rowell, D.P., 2005: A scenario of European climate change for the late 21st century: seasonal means and interannual variability. *Clim. Dyn.*, **25**, 837–849.
- Rowell, D.P., and R.G. Jones, 2006: Causes and uncertainty of future summer drying over Europe. *Clim. Dyn.*, **27**, 281–299.
- Rowell, D.P., C.K. Folland, K. Maskell, and N.M. Ward, 1995: Variability of summer rainfall over Tropical North Africa (1906–92): Observations and modelling. *Q. J. R. Meteorol. Soc.*, **121**, 669–704.
- Rummukainen, M., et al., 2003: Regional climate scenarios for use in Nordic water resources studies. *Nord Hydrol.*, **34**(5), 399–412.
- Rummukainen, M., et al., 2004: The Swedish Regional Climate Modelling Programme, SWECLIM: a review. *Ambio*, **33**, 176–182.
- Ruosteenoja, K., H. Tuomenvirta, and K. Jylhä, 2007: GCM-based regional temperature and precipitation change estimates for Europe under four SRES scenarios applying a super-ensemble pattern-scaling method. *Clim. Change*, doi: 10.1007/s10584-006-9222-3.
- Ruosteenoja, K., T.R. Carter, K. Jylhä, and H. Tuomenvirta, 2003: *Future Climate in World Regions: And Intercomparison of Model-Based Projections for the New IPCC Emissions Scenarios*. Finnish Environment Institute, Helsinki, 83 pp.
- Rupa Kumar, K., and R.G. Ashrit, 2001: Regional aspects of global climate change simulations: Validation and assessment of climate response over Indian monsoon region to transient increase of greenhouse gases and sulfate aerosols. *Mausam, Special Issue on Climate Change*, **52**, 229–244.
- Rupa Kumar, K., et al., 2002: Climate change in India: Observations and model projections. In: *Climate Change and India: Issues, Concerns and Opportunities* [Shukla, P.R., et al., (eds.)]. Tata McGraw-Hill Publishing Co. Ltd., New Delhi, pp. 24–75.
- Rupa Kumar, K., et al., 2003: Future climate scenarios. In: *Climate Change and India: Vulnerability Assessment and Adaptation* [Shukla, P.R., et al. (eds.)]. Universities Press, Hyderabad, pp. 69–127.
- Rupa Kumar, K., et al., 2006: High-resolution climate change scenarios for India for the 21st century. *Curr. Sci. India.*, **90**, 334–345.
- Russell, G.L., and D. Rind, 1999: Response to CO₂ transient increase in the GISS model: regional coolings in a warming climate. *J. Clim.*, **12**, 531–539.
- Salathé, E.P., 2005: Downscaling simulations of future global climate with application to hydrologic modelling. *Int. J. Climatol.*, **25**, 419–436.
- Salinger, M.J., J.A. Renwick, and A.B. Mullan, 2001: Interdecadal Pacific Oscillation and South Pacific climate. *Int. J. Climatol.*, **21**, 1705–1721.
- Sánchez, E., C. Gallardo, M.A. Gaertner, A. Arribas and M. Castro, 2004: Future climate extreme events in the Mediterranean simulated by a regional climate model: first approach. *Global Planet. Change*, **44**, 163–180.
- Santer, B.D., T.W.L. Wigley, M.E. Schlesinger, and J.F.B. Mitchell, 1990: *Developing Climate Scenarios from Equilibrium GCM Results*. Report No. 47, Max-Planck Institute for Meteorology, Hamburg, 29 pp.
- Sarkar, S., R.P. Singh, and M. Kafatos, 2004: Further evidences for the weakening relationship of Indian rainfall and ENSO over India. *Geophys. Res. Lett.*, **31**, L13209, doi:10.1029/2004GL020259.

- Sasaki, H., K. Kurihara, and I. Takayabu, 2006a: Comparison of climate reproducibilities between a super-high-resolution atmosphere general circulation model and a Meteorological Institute regional climate model. *Scientific Online Letters on the Atmosphere*, **1**, 81–84.
- Sasaki, H., et al., 2006b: Preliminary results from the coupled atmosphere-ocean regional climate model developed at Meteorological Research Institute. *J. Meteorol. Soc. Japan*, **84**, 389–403.
- Scaife, A., J.R. Knight, G.K. Vallis, and C.K. Folland, 2005: A stratospheric influence on the winter NAO and North Atlantic surface climate. *Geophys. Res. Lett.*, **32**, L18715, doi:10.1029/2005GL023226.
- Schaeffer, M., F.M. Selten, J.D. Opsteegh, and H. Goosse, 2004: The influence of ocean convection patterns on high-latitude climate projections. *J. Clim.*, **17**, 4316–4329.
- Schär, C., et al., 2004: The role of increasing temperature variability in European summer heatwaves. *Nature*, **427**, 332–336.
- Schmidli, J., C. Frei, and P.L. Vidale, 2006: Downscaling from GCM precipitation: A benchmark for dynamical and statistical downscaling. *Int. J. Climatol.*, **26**, 679–689.
- Scott, D., G. McBoyle, and B. Mills, 2003: Climate change and the skiing industry in southern Ontario (Canada): exploring the importance of snowmaking as a technical adaptation. *Clim. Res.*, **23**, 171–181.
- Seem, R., 2004: Forecasting plant disease in a changing climate: a question of scale. *Can. J. Plant Pathol.*, **26**(3), 274–283.
- Semenov, V.A., and L. Bengtsson, 2002: Secular trends in daily precipitation characteristics: greenhouse gas simulation with a coupled AOGCM. *Clim. Dyn.*, **19**, 123–140.
- Semmler, T., and D. Jacob, 2004: Modeling extreme precipitation events – a climate change simulation for Europe. *Global Planet. Change*, **44**, 119–127.
- Semmler, T., D. Jacob, K.H. Schlunzen, and R. Podzun, 2005: The water and energy budget of the Arctic atmosphere. *J. Clim.*, **18**, 2515–2530, doi:10.1175/JCLI3414.1.
- Serreze, M.C., and C.M. Hurst, 2000: Representation of mean Arctic precipitation from NCEP-NCAR and ERA reanalyses. *J. Clim.*, **13**, 182–201.
- Serreze, M.C., and J. Francis, 2006: The Arctic amplification debate. *Clim. Change*, **76**, 241–264, doi:10.1007/s10584-005-9017-y.
- Seth, A., and M. Rojas, 2003: Simulation and sensitivity in a nested modeling system for South America. Part I: Reanalyses boundary forcing. *J. Clim.*, **16**, 2437–2453.
- Shindell, D.T., and G.A. Schmidt, 2004: Southern hemisphere climate response to ozone changes and greenhouse gas increases. *Geophys. Res. Lett.*, **31**, L18209, doi:10.1029/2004GL020724.
- Shkolnik, I.M., V.P. Meleshko, and V.M. Kattsov, 2006: Climate change in the 21st century over the Western Russia: a simulation with the MGO Regional Climate Model. *Russ. Meteorol. Hydrol.*, **3**, 5–17.
- Simmons, A.J., et al., 2004: Comparison of trends and low-frequency variability in CRU, ERA-40, and NCEP/ NCAR analyses of surface air temperature. *J. Geophys. Res.*, **109**, D24115, doi:10.1029/2004JD005306.
- Sinclair, M.R., 2002: Extratropical transition of southwest Pacific tropical cyclones. Part I: Climatology and mean structure changes. *Mon. Weather Rev.*, **130**, 590–609.
- Sitch, S., et al., 2005: Impacts of future land cover changes on atmospheric CO₂ and climate. *Global Biogeochem. Cycles*, **19**(2), GB2013, doi:10.1029/2004GB002311.
- Small, E., F. Giorgi, and L.C. Sloan, 1999: Regional climate model simulation of precipitation in central Asia: Mean and interannual variability. *J. Geophys. Res.*, **104**, 6563–6582.
- Snyder, M.A., L.C. Sloan, N.S. Diffenbaugh, and J.L. Bell, 2003: Future climate change and upwelling in the California Current. *Geophys. Res. Lett.*, **30**(15), 1823, doi:10.1029/2003GL017647.
- Solecki, W.D., and C. Oliveri, 2004: Downscaling climate change scenarios in an urban land use change model. *J. Environ. Manage.*, **72**, 105–115.
- Somot, S., 2005: *Modélisation Climatique du Bassin Méditerranéen: Variabilité et Scénarios de Changement Climatique*. PhD Thesis, Université Paul Sabatier, Toulouse, France, 333 pp.
- Staniforth, A., 1997: Regional modeling: A theoretical discussion. *Meteorol. Atmos. Phys.*, **63**, 15–29.
- Steiner, N., et al., 2004: Comparing modelled streamfunction, heat and freshwater content in the Arctic Ocean. *Ocean Model.*, **6**(3–4), 265–284.
- Stephenson, D.B., H. Douville, and K. Rupa Kumar, 2001: Searching for a fingerprint of global warming in the Asian summer monsoon. *Mausam*, **52**, 213–220.
- Stephenson, D.B., et al., 2006: North Atlantic Oscillation response to transient greenhouse gas forcing and the impact on European winter climate: A CMIP2 multi-model assessment. *Clim. Dyn.*, **27**, 401–420.
- Stone, D.A., A.J. Weaver, and R.J. Stouffer, 2001: Projection of climate change onto modes of atmospheric variability. *J. Clim.*, **14**, 3551–3565.
- Stone, R.S., 1997: Variations in western Arctic temperatures in response to cloud radiative and synoptic-scale influences. *J. Geophys. Res.*, **102**, 21769–21776.
- Stott, P.A., and J.A. Kettleborough, 2002: Origins and estimates of uncertainty in predictions of twenty-first century temperature rise. *Nature*, **416**, 723–726.
- Stott, P.A., J.A. Kettleborough, and M.R. Allen, 2006a: Uncertainty in continental-scale temperature predictions. *Geophys. Res. Lett.*, **33**, L02708, doi:10.1029/2005GL024423.
- Stott, P.A., et al., 2006b: Observational constraints on past attributable warming and predictions of future global warming. *J. Clim.*, **19**, 3055–3069.
- Stouffer, R.J., et al., 2006: Investigating the causes of the response of the thermohaline circulation to past and future climate changes. *J. Clim.*, **19**(8), 1365–1387.
- Sugi, M., A. Noda, and N. Sato, 2002: Influence of the global warming on tropical cyclone climatology: An experiment with the JMA Global Model. *J. Meteorol. Soc. Japan*, **80**, 249–272.
- Suppiah, R., P.H. Whetton, and I.G. Watterson, 2004: *Climate Change in Victoria: Assessment of Climate Change for Victoria: 2001–2002*. Undertaken for Victorian Department of Sustainability and Environment. CSIRO Atmospheric Research, Aspendale, Vic., 33 pp.
- Tadross, M.A., B.C. Hewitson, and M.T. Usman, 2005a: The interannual variability of the onset of the maize growing season over South Africa and Zimbabwe. *J. Clim.*, **18**(16), 3356–3372.
- Tadross, M.A., C. Jack, and B. Hewitson, 2005b: On RCM-based projections of change in southern African summer climate. *Geophys. Res. Lett.*, **32**, L23713, doi:10.1029/2005GL024460.
- Tadross, M.A., et al., 2006: MM5 simulations of interannual change and the diurnal cycle of southern African regional climate. *Theor. Appl. Climatol.*, **86**, 63–80.
- Taylor, C.M., et al., 2002: The influence of land use change on climate in the Sahel. *J. Clim.*, **15**, 3615–3629.
- Taylor, M., and E. Alfaro, 2005: Climate of Central America and the Caribbean. In: *The Encyclopedia of World Climatology* [Oliver, J. (ed.)]. Encyclopedia of Earth Sciences Series, Springer Press, 854 pp.
- Taylor, M., D. Enfield, and A. Chen, 2002: The influence of the tropical Atlantic vs. the tropical Pacific on Caribbean rainfall. *J. Geophys. Res.*, **107** (C9), 3127, doi:10.1029/2001JC001097.
- Tebaldi, C., L.O. Mearns, D. Nychka, and R. Smith, 2004a: Regional probabilities of precipitation change: A Bayesian analysis of multi-model simulations. *Geophys. Res. Lett.*, **31**, L24213, doi:10.1029/2004GL021276.
- Tebaldi, C., R. Smith, D. Nychka, and L.O. Mearns, 2004b: Quantifying uncertainty in projections of regional climate change: A Bayesian Approach. *J. Clim.*, **18**(10), 1524–1540.
- Tebaldi, C., K. Hayhoe, J.M. Arblaster, and G.E. Meehl, 2006: Going to the extremes: an intercomparison of model-simulated historical and future changes in extreme events. *Clim. Change*, **79**, 185–211.
- Tennant, W., 2003: An assessment of intraseasonal variability from 13-yr GCM simulations. *Mon. Weather Rev.*, **131**(9), 1975–1991.
- Timbal, B., 2004: Southwest Australia past and future rainfall trends. *Clim. Res.*, **26**, 233–249.

- Timbal, B., and B.J. McAvaney, 2001: An analogue-based method to downscale surface air temperature: Application for Australia. *Clim. Dyn.*, **17**(12), 947–963.
- Tjernström, M., et al., 2005: Modeling the Arctic boundary layer: An evaluation of six ARCMIP regional-scale models with data from the SHEBA project. *Bound.-Lay. Meteorol.*, **117**, 337–381.
- Todd, M., and R. Washington, 1999: Circulation anomalies associated with tropical-temperate troughs in southern Africa and the south west Indian Ocean. *Clim. Dyn.*, **15**(12), 937–951.
- Trigo, R.M., and J.P. Palutikof, 2001: Precipitation scenarios over Iberia: a comparison between direct GCM output and different downscaling techniques. *J. Clim.*, **14**, 4422–4446.
- Turner, J., 2004: The El Niño–Southern Oscillation and Antarctica. *Int. J. Climatol.*, **24**, 1–31.
- Turner, J., W.M. Connolley, T.A. Lachlan-Cope, and G.J. Marshall, 2006: The performance of the Hadley Centre climate model (HadCM3) in high southern latitudes. *Int. J. Climatol.*, **26**, 91–112.
- Ueda, H., A. Iwai, K. Kuwako, and M.E. Hori, 2006: Impact of anthropogenic forcing on the Asian summer monsoon as simulated by eight GCMs. *Geophys. Res. Lett.*, **33**, L06703, doi:10.1029/2005GL025336.
- Ulbrich, U., et al., 2006: The Mediterranean climate change under global warming. In: *Mediterranean Climate Variability* [Lionello, P., P. Malanotte, and R. Boscolo (eds.)]. Elsevier B.V, pp. 399–415.
- Unnikrishnan, A.S., et al., 2006: Sea level changes along the Indian coast: Observations and projections. *Curr. Sci. India*, **90**, 362–368.
- van de Berg, W.J., M.R. van den Broeke, C.H. Reijmer, and E. van Meijgaard, 2005: Characteristics of the Antarctic surface mass balance (1958–2002) using a regional atmospheric climate model. *Ann. Glaciol.*, **41**, 97–104.
- van den Broeke, M.R., and N.P.M. van Lipzig, 2003: Factors controlling the near-surface wind field in Antarctica. *Mon. Weather Rev.*, **131**, 733–743.
- van den Broeke, M., W.J. van de Berg, and E. van Meijgaard, 2006: Snowfall in coastal West Antarctica much greater than previously assumed. *Geophys. Res. Lett.*, **33**, L02505, doi:10.1029/2005GL025239.
- van den Hurk, B., et al., 2005: Soil control on runoff response to climate change in regional climate model simulations. *J. Clim.*, **18**, 3536–3551.
- van den Hurk, B., et al., 2006: *KNMI Climate Change Scenarios 2006 for the Netherlands*. KNMI WR-2006-01, KNMI, The Netherlands, 82 pp.
- van Lipzig, N.P.M., E.W. van Meijgaard, and J. Oerlemans, 2002a: The spatial and temporal variability of the surface mass balance in Antarctica: results from a regional atmospheric climate model. *Int. J. Climatol.*, **22**, 1197–1217.
- van Lipzig, N.P.M., E.W. van Meijgaard, and J. Oerlemans, 2002b: Temperature sensitivity of the Antarctic surface mass balance in a regional atmospheric climate model. *J. Clim.*, **15**, 2758–2774.
- van Ulden, A.P., and G.J. van Oldenborgh, 2006: Large-scale atmospheric circulation biases and changes in global climate model simulations and their importance for climate change in Central Europe. *Atmos. Chem. Phys.*, **6**, 863–881.
- van Ulden, A., G. Lenderink, B. van den Hurk, and E. van Meijgaard, 2007: Circulation statistics and climate change in Central Europe: Prudence simulations and observations. *Clim. Change*, doi: 10.1007/s10584-006-9212-5.
- Vannitsem, S., and F. Chomé, 2005: One-way nested regional climate simulations and domain size. *J. Clim.*, **18**, 229–233.
- Vera, C., et al., 2006: Towards a unified view of the American monsoon systems. *J. Clim.*, **19**, 4977–5000.
- Vérant, S., 2004: *Etude des Dépressions sur l'Europe de l'Ouest : Climat Actuel et Changement Climatique*. PhD thesis, Université Paris VI, Paris, France, 204 pp.
- Vernekar, A.D., B.P. Kirtman, and M.J. Fennessy, 2003: Low-level jets and their effects on the South American summer climate as simulated by the NCEP Eta model. *J. Clim.*, **16**, 297–311.
- Vidale, P.L., D. Lüthi, R. Wegmann, and C. Schär, 2007: European climate variability in a heterogeneous multi-model ensemble. *Clim. Change*, doi: 10.1007/s10584-006-9218-z.
- Vidale, P.L., et al., 2003: Predictability and uncertainty in a regional climate model. *J. Geophys. Res.*, **108**(D18), 4586, doi:10.1029/2002JD002810.
- Vincent, C., 2002: Influence of climate change over the 20th century on 4 French glacier mass balances. *J. Geophys. Res.*, **107**, 4375, doi:10.1029/2001JD000832.
- Vincent, D.G., 1994: The South Pacific Convergence Zone (SPCZ): A review. *Mon. Weather Rev.*, **122**, 1949–1970.
- Vizy, E.K., and K.H. Cook, 2002: Development and application of a mesoscale climate model for the tropics: Influence of sea surface temperature anomalies on the West African monsoon. *J. Geophys. Res.*, **107**(D3), 4023, doi:10.1029/2001JD000686.
- Voldoire, A., 2006: Quantifying the impact of future land-use changes against increases in GHG concentrations. *Geophys. Res. Lett.*, **33**, L04701, doi:10.1029/2005GL024354.
- Voldoire, A., and J.F. Royer, 2004: Tropical deforestation and climate variability. *Clim. Dyn.*, **22**, 857–874.
- Voldoire, A., and J.F. Royer, 2005: Climate sensitivity to tropical land surface changes with coupled versus prescribed SSTs. *Clim. Dyn.*, **24**, 843–862.
- von Storch, H., and H. Reichardt, 1997: A scenario of storm surge statistics for the German Bight at the expected time of doubled atmospheric carbon dioxide concentration. *J. Clim.*, **10**, 2653–2662.
- von Storch, H., H. Langenberg, and F. Feser, 2000: A spectral nudging technique for dynamical downscaling purposes. *Mon. Weather Rev.*, **128**, 3664–3673.
- Voss, R., W. May, and E. Roeckner, 2002: Enhanced resolution modelling study on anthropogenic climate change: Changes in extremes of the hydrological cycle. *Int. J. Climatol.*, **22**, 755–777.
- Vuille, M., and Bradley, R.S., 2000: Mean annual temperature trends and their vertical structure in the tropical Andes. *Geophys. Res. Lett.*, **27**, 3885–3888.
- Walland, D.J., S.B. Power, and A.C. Hirst, 2000: Decadal climate variability simulated in a coupled general circulation model. *Clim. Dyn.*, **16**(2–3), 201–211.
- Walser, A., and C. Schär, 2004: Convection-resolving precipitation forecasting and its predictability in Alpine river catchments. *J. Hydrol.*, **288**, 57–73.
- Walsh, J.E., et al., 2002: Comparison of Arctic climate simulations by uncoupled and coupled global models. *J. Clim.*, **15**, 1429–1446.
- Walsh, K.J., 2004: Tropical cyclones and climate change: unresolved issues. *Clim. Res.*, **27**, 77–84.
- Walsh, K.J.E., and J.J. Katzfey, 2000: The impact of climate change on the poleward movement of tropical cyclone-like vortices in a regional climate model. *J. Clim.*, **13**(6), 1116–1132.
- Walsh, K.J.E., and B.F. Ryan, 2000: Tropical cyclone intensity increase near Australia as a result of climate change. *J. Clim.*, **13**(16), 3029–3036.
- Walsh, K.J., K.C. Nguyen, and J.L. McGregor, 2004: Fine-resolution regional climate model simulations of the impact of climate change on tropical cyclones near Australia. *Clim. Dyn.*, **22**(1), 47–56.
- Walsh, K., et al., 1999: *Climate Change in Queensland Under Enhanced Greenhouse Conditions: First Annual Report, 1997–1998*. CSIRO Atmospheric Research, Melbourne, 84 pp.
- Wang, B., I.S. Kang, and J.Y. Lee, 2004: Ensemble simulations of Asian–Australian monsoon variability by 11 GCMs. *J. Clim.*, **17**, 803–818.
- Wang, G., 2005: Agricultural drought in a future climate: results from 15 global climate models participating in the IPCC 4th assessment. *Clim. Dyn.*, **25**, 739–753.
- Wang, G., and E.A.B. Eltahir, 2000: Role of vegetation dynamics in enhancing the low-frequency variability of the Sahel rainfall. *Water Resour. Res.*, **36**(4), 1013–1021.
- Wang, X.L., and V.R. Swail, 2006a: Climate change signal and uncertainty in projections of ocean wave heights. *Clim. Dyn.*, **26**, 106–126, doi:10.1007/s00382-005-0080-x.

- Wang, X.L., and V.R. Swail, 2006b: Historical and possible future changes of wave heights in Northern Hemisphere oceans. In: *Atmosphere-Ocean Interactions – Vol. 2* [Perrie, W. (ed.)]. Advances in Fluid Mechanics Series, Vol 39. Wessex Institute of Technology Press, Southampton, UK, 240 pp.
- Wang, X.L., F. Zwiers, and V. Swail, 2004: North Atlantic ocean wave climate change scenarios for the twenty-first century. *J. Clim.*, **17**, 2368–2383.
- Warner, T.T., R.A. Peterson, and R.E. Treadon, 1997: A tutorial on lateral conditions as a basic and potentially serious limitation to regional numerical weather prediction. *Bull. Am. Meteorol. Soc.*, **78**(11), 2599–2617.
- Watterson, I.G., and M.R. Dix, 2003: Simulated changes due to global warming in daily precipitation means and extremes and their interpretation using the gamma distribution. *J. Geophys. Res.*, **108**(D13), 4379, doi:10.1029/2002JD002928.
- Weatherly, J., 2004: Sensitivity of Antarctic precipitation to sea ice concentrations in a general circulation model. *J. Clim.*, **17**, 3214–3223.
- Webb, M., et al., 2006: On the contribution of local feedback mechanisms to the range of climate sensitivity in two GCM ensembles. *Clim. Dyn.*, **27**, 17–38.
- Wehner, M.F., 2004: Predicted twenty-first-century changes in seasonal extreme precipitation events in the Parallel Climate Model. *J. Clim.*, **17**, 4281–4290.
- Wei, H., W.J. Gutowski, C.J. Vorosmarty, and B.M. Fekete, 2002: Calibration and validation of a regional climate model for pan-Arctic hydrologic simulation. *J. Clim.*, **15**, 3222–3236.
- Weisheimer, A., and T. Palmer, 2005: Changing frequency of occurrence of extreme seasonal temperatures under global warming. *Geophys. Res. Lett.*, **32**, L20721, doi:10.1029/2005GL023365.
- Weisman, M.L., W.S. Skamarock, and J.B. Klemp, 1997: The resolution dependence of explicitly modeled convective systems. *Mon. Weather Rev.*, **125**, 527–548.
- Weisse, R., H. von Storch, and F. Feser, 2005: Northeast Atlantic and North Sea storminess as simulated by a regional climate model 1958–2001 and comparison with observations. *J. Clim.*, **18**, 465–479.
- Whetton, P.H., and R. Suppiah, 2003: Climate change projections and drought. In: *Science for Drought. Proceedings of the National Drought Forum, Carlton Crest Hotel, Brisbane* [Stone, R., and I. Partridge (eds.)]. Queensland Department of Primary Industries, Brisbane, Qld., pp. 130–136.
- Whetton, P.H., A.B. Mullan, and A.B. Pittock, 1996: Climate-change scenarios for Australia and New Zealand. In: *Greenhouse: Coping with Climate Change* [Bouma, W.J., G.I. Pearman, and M.R. Manning (eds.)]. CSIRO, Collingwood, Vic., pp. 145–168.
- Whetton, P.H., et al., 2000: *Climate Averages Based on a Doubled CO₂ Simulation*. Victorian Dept. of Natural Resources and Environment, Melbourne, 43 pp.
- Whetton, P.H., et al., 2001: Developing scenarios of climate change for Southeastern Australia: An example using regional climate model output. *Clim. Res.*, **16**(3), 181–201.
- Whetton, P. H., et al. 2002. *Climate change in Victoria : high resolution regional assessment of climate change impacts*. Undertaken for the Victorian Department of Natural Resources and Environment. Dept. of Natural Resources and Environment, East Melbourne, VIC, 44 pp., <http://www.greenhouse.vic.gov.au/climatechange.pdf>
- Whetton, P.H., et al., 2005: *Australian Climate Change Projections for Impact Assessment and Policy Application: A Review*. CSIRO Marine and Atmospheric Research Paper 001, CSIRO Marine and Atmospheric Research, Aspendale, Vic., 34 pp.
- Widmann, M., C.S. Bretherton, and E.P. Salathé Jr., 2003: Statistical precipitation downscaling over the Northwestern United States using numerically simulated precipitation as a predictor. *J. Clim.*, **16**, 799–816.
- Wigley, T.M.L., and S.C.B. Raper, 2001: Interpretation of high projections for global-mean warming. *Science*, **293**, 451–454.
- Wilby, R.L., C.W. Dawson, and E.M. Barrow, 2002: SDSM – A decision support tool for the assessment of regional climate change impacts. *Environ. Model. Software*, **17**, 147–159.
- Wilby, R.L., O.J. Tomlinson, and C.W. Dawson, 2003: Multi-site simulation of precipitation by conditional resampling. *Clim. Res.*, **23**, 183–194.
- Wilby, R.L., et al., 2004: *Guidelines for Use of Climate Scenarios Developed from Statistical Downscaling Methods*. IPCC Task Group on Data and Scenario Support for Impact and Climate Analysis (TGICA), http://ipcc-ddc.cru.uea.ac.uk/guidelines/StatDown_Guide.pdf.
- Wood, A.W., L.R. Leung, V. Sridhar, and D.P. Lettenmaier, 2004: Hydrologic implications of dynamical and statistical approaches to downscaling climate model outputs. *Clim. Change*, **62**, 189–216.
- Woodworth, R., and D.L. Blackman, 2004: Evidence for systematic changes in extreme high waters since the mid-1970s. *J. Clim.*, **17**(6), 1190–1197.
- Woth, K., 2005: North Sea storm surge statistics based on projections in a warmer climate: How important are the driving GCM and the chosen emission scenario? *Geophys. Res. Lett.*, **32**, L22708, doi:10.1029/2005GL023762.
- Woth, K., R. Weisse, and H. von Storch, 2006: Climate change and North Sea storm surge extremes: An ensemble study of storm surge extremes expected in a changed climate projected by four different Regional Climate Models. *Ocean Dyn.*, **56**, 3–15, doi:10.1007/s10236-005-0024-3.
- Wu, B., and B. Wang, 2004: Assessing impacts of global warming on tropical cyclone tracks. *J. Clim.*, **17**(8), 1686–1698.
- Wu, P., R. Wood, and P. Scott, 2003: Does the recent freshening trend in the North Atlantic indicate a weakening thermohaline circulation? *Geophys. Res. Lett.*, **31**, doi:10.1029/2003GL018584.
- Wyser, K., and C.G. Jones, 2005: Modeled and observed clouds during Surface Heat Budget of the Arctic Ocean (SHEBA). *J. Geophys. Res.*, **110**, D09207, doi:10.1029/2004JD004751.
- Xu, Y., Y.H. Ding., and L.D. Li, 2003a: Climate change projection in Qinghai-Xizang Plateau in the future 100 years. *Plateau Meteorol.*, **22**(5), 451–457.
- Xu, Y., Y.H. Ding, and Z.C. Zhao, 2003b: Scenario of temperature and precipitation changes in Northwest China due to effects of human activities in 21st century. *J. Glaciol.*, **25**(3), 327–330.
- Xu, Y., Z.C. Zhao, and L.D. Li, 2005: The simulated result analyses on climate changes over Qinghai-Xizang Plateau and along the Railway in the coming 50 Years. *Plateau Meteorol.*, **24**(5), 700–707.
- Xu, Y.L., et al., 2005: Statistical analyses of climate change scenario over China in the 21st century. *Adv. Clim. Change Res.*, **1**, 80–83.
- Xue, M., K.K. Droegemeier, and V. Wong, 2000: The Advanced Regional Prediction System (ARPS) - A multi-scale nonhydrostatic atmospheric simulation and prediction model. Part I: Model dynamics and verification. *Meteorol. Atmos. Phys.*, **75**(3–4), 161–193.
- Yasunaga, K., et al., 2006: Changes in the Baiu frontal activity in the future climate simulated by super-high-resolution global and cloud-resolving regional climate models. *J. Meteorol. Soc. Japan*, **84**, 199–220.
- Yin, J.H., 2005: A consistent poleward shift of the storm tracks in simulations of 21st century climate. *Geophys. Res. Lett.*, **32**, L18701, doi:10.1029/2005GL023684.
- Yoshizaki, M., et al., 2005: Changes of Baiu (Mei-yu) frontal activity in the global warming climate simulated by a non-hydrostatic regional model. *Scientific Online Letters on the Atmosphere*, **1**, 25–28.
- Yuan, X.J., 2004: ENSO-related impacts on Antarctic sea ice: a synthesis of phenomenon and mechanisms. *Antarct. Sci.*, **16**, 415–425.
- Zeng, N., H. Qian, E. Munoz, and R. Iacono, 2004: How strong is carbon cycle-climate feedback under global warming? *Geophys. Res. Lett.*, **31**, L20203, doi:10.1029/2004GL020904.
- Zhai, P.M., X.B. Zhang, H. Wan, and X.H. Pan, 2005: Trends in total precipitation and frequency of daily precipitation extremes over China. *J. Clim.*, **18**, 1096–1108.
- Zhang, D.F., X.J. Gao, and Z.C. Zhao, 2005a: Simulation of climate in China by RegCM3. *Adv. Clim. Change Res.*, **1**(3), 119–121.

- Zhang, D.F., X.J. Gao, H.Z. Bai, and D.L. Li, 2005b: Simulation of climate over Qinghai-Xizang Plateau utilizing RegCM3. *Plateau Meteorol.*, **24**, 714–720.
- Zhao, Z.C., X.J. Gao, M.C. Tang, and Y. Xu, 2002: Climate change projections. In: *Assessment for Evolution of Environment in Western China, Vol. 2* [Qin, D.H., and Y.D. Ding (eds.)]. Science Press, Beijing, pp.16–46.
- Zhou, J., and K.-M. Lau, 2002: Intercomparison of model simulations of the impact of 1997/98 El Niño on South American Summer Monsoon. *Meteorologica*, **27**(1–2), 99–116.
- Zhou, T.J., and Z.X. Li, 2002: Simulation of the East Asian summer monsoon by using a variable resolution atmospheric GCM. *Clim. Dyn.*, **19**, 167–180.
- Zhou, T.J., and R.C. Yu, 2006: 20th century surface air temperature over China and the globe simulated by coupled climate models. *J. Clim.*, **19**, 5843–5858.
- Zou, C.-Z., M.L. van Woert, C. Xu, and K. Syed, 2004: Assessment of the NCEP–DOE Reanalysis-2 and TOVS pathfinder moisture fields and their use in Antarctic net precipitation estimates. *Mon. Weather Rev.*, **132**, 2463–2476.
- Zwiers, F.W., and V.V. Kharin, 1998: Changes in the extremes of the climate simulated by CCC GCM2 under CO₂ doubling. *J. Clim.*, **11**, 2200–2222.